# High Strain Rate Compression Testing of Polymers:

# PTFE, PCTFE, PVC and PMMA

**by**

**Hsuan-Hsiou Forrester (Chen)**

*A Doctoral Thesis*
*Submitted in partial fulfilment of the requirements*
*for the award of Doctor of Philosophy*
*of*
*Loughborough University*

*April 2013*

*Department of Physics, School of Science*
*Supervisor: Dr. G. M. Swallowe*

# Certificate of Originality

*To*

*Keela and Tullia*

*Believe in yourselves, own your successes.*

*Love,*

*Mum*

# Acknowledgements

I would like to express the deepest appreciation to my supervisor, Dr. Gerry Swallowe, for the useful comments, remarks and engagement through the learning process of this thesis. Without whose guidance, patience and persistent help this thesis would not have been possible.

Furthermore the support received from the staff were vital, my sincere thanks to Mr. Bryan Dennis and Mr. Phil Sutton for the precise making of my polymer samples; Mr. Raj and Ramesh Pancholi for the building of many electrical devices; Mr Ray Owens for his help with DMA; Mrs M. McKenzie for her kindness and all her help.

In addition, a thank you to Dr. David Parry who taught me a great deal about the Split Hopkinson Pressure Bars system and his enthusiasm on the subject; Dr. D. M. Forrester for his assistance with the computer programs, and the valuable knowledge on the modelling of polymer deformation phenomena. I would also like to thank Loughborough University for my student grant and the Mountsorrel United Charities on partially providing childcare funding during the writing up period of this thesis.

Finally, my gratitude to my family and friends who have also contributed in their own ways to encourage me on this long journey, my parents, grandparents, Aunt Carol, Dennis, Simon, June, Derek and in particular my husband , Michael, for his unconditional love.

# Abstract

The mechanically compressive flow stress sensitivities of various polymers are investigated at high strain rates above $10^3$ $s^{-1}$. Temperatures near the glass transition temperature are investigated and the polymer stress-strain responses have been studied from ambient temperature to 100ºC. Previous work has reported peaks in flow stress as a function of strain rate [**Al-Maliky/Parry 1994, Al-Maliky 1997**]. The analyses showed rapid increases of flow stress followed by a sudden drop at elevated strain rates, which is unlike the well known linear relationship documented at the low strain rates. The mechanics and stipulation of what bring about this phenomenon, or the types of polymers influenced are still unclear.

Two fluoropolymers, polytetrafluoroethylene (PTFE) and polychlorotrifluoroethylene (PCTFE), and two vinyl polymers, polyvinylchloride (PVC) and polymethylmethacrylate (PMMA), are chosen for this study. PTFE, PCTFE and PVC are semi-crystalline polymers with different percentage of crystallinity contents, whereas PMMA is an amorphous polymer. The glass transition temperature, $T_g$, is the characteristic of the amorphous content in polymers, which has been suggested to influence the flow stress peaks [**Swallowe/Lee 2003**]. $T_g$ of the semi-crystalline polymers are within the test temperature range.

High strain rate compression tests have been carried out using the split Hopkinson pressure bar (SHPB). This is a well-established method for determining the stress, strain, and strain rate of materials. The strain rate range of interest is $10^3$ $s^{-1}$ to $10^5$ $s^{-1}$ where the strain rate sensitivity has previously been identified [**Al-Maliky/Parry 1994, Al-Maliky 1997, Walley/Field 1994**]. Two thermal analyses techniques are used to quantify the dependency of the viscoelastic behaviour in relation to time and temperature. Differential scanning calorimetry (DSC) measures the enthalpy of the polymers to show how the materials are affected by heat, and Dynamic mechanical analysis (DMA) is used to characterise the time-temperature dependence of the elastic storage and loss moduli of the polymers

A total of 42 PCTFE, 44 PTFE, 45 PVC and 55 PMMA specimens were tested using the SHPB system, with the strain rate varying between 1600 $s^{-1}$ and 6100 $s^{-1}$. Initial results for PMMA have been reported [**Forrester/Swallowe 2009**]. The rate of strain where specimens begin to show crazing is identified. The value of yield stress increases with the increase of strain rate and the decrease in temperature. Large strain hardening can be seen in all three semi-crystalline polymers at higher strain rates. The temperature rise during plastic flow of compression is calculated by the stress-strain rate curves.

In this thesis, the emphasis is on the relation of yield/flow stress to strain rate as the polymers deform under high strain compression. The mechanism behind the cause of high strain rate deformation responses for amorphous to semi-crystalline polymers in ductile state is discussed, with a view to understanding the sensitivity of yield/flow stresses as a function of strain rate. Also, the modelling of the polymers has been carried in order to alleviate doubts about the validity of the real experimental results that may arise due to the nature of the decomposition of the polymers. It has been shown that the strain energy density pulses through the sample in response to the compression wave in various circular intensities.

Keywords: flow stress, polymers, high rate mechanical test, polymer modelling, amorphous polymers, fluoropolymers.

# Table of content

# Chapter One

# Mechanical properties of solid polymers

## 1.1 Introduction to mechanical properties of polymers

Solid polymers are a unique category of materials with a huge variety of properties. The performance of a polymer correlates with the type of loading and the environment influences. In this study the interest lies in the understanding of the high strain rate compression mechanical properties of polymers and the development of these properties as temperature increases from an ambient level.

Polymers are considered as a soft condensed matter, i.e. they are materials in states which are neither simple liquids nor crystalline solids. The conventional thinking about the distinction between a liquid state and a solid state needs to be extended when describing polymers. Thus, we define soft matter as viscoelastic, whereby the material behaves as a liquid or solid depending upon the loading time-scales, or glassy which lacks long range order (like a liquid) with mechanical elastic behaviour (like a solid). This type of material responds to stress in a time dependent manner. If constant stress is applied, in the first instance the polymer responds in an elastic way and at this point strain is constant. At time $\tau$ (relaxation time), the polymer begins to flow like a liquid. If the timescale of the applied stress is shorter than the relaxation time, for example at high strain-rate compression tests, the material will behave like a solid. And vice versa, at stresses applied on a timescale longer than the relaxation time, the polymer exhibits flow properties. Figure 1.1 contains sketches of the three possible responses of a typical viscoelastic material to stress against strain rate. In Figure 1.1a, the Newtonian linear relationship between stress and strain-rate is shown. In contrast to the linearity that is seen in Figure 1.1a, some possible non-linear relations between stress and strain rate can evolve either to be like that of Figure 1.1b where the flow stress becomes less sensitive to strain rate or like in Figure 1.1c where the polymer becomes more sensitive to the rates of strain at high strain rates. That is to say, another possible relationship exists between stress and strain rate at higher

strain rates and the material shows greater resistance in response to stress. The non-Newtonian behaviour could be considered as being the consequence of the rearrangement of the particles in response to the flow. The deformed polymer is in a higher energy state in comparison to the initial unstressed equilibrium state and the polymer tries to relax back into a lower energy state. The reaction of the polymer allows us to define the elastic modulus of the material (if a tensile/compression stress is applied). At the end of the plastic flow, if the polymer is brittle, then it is not possible for it to relax and failure of the sample is observed. If the polymer behaves liquid-like, however, it is possible for the sample to reduce stress without failure. The relaxation time of polymers can be estimated using the Eyring theory [**Eyring 1935**], which can be found in appendix A.

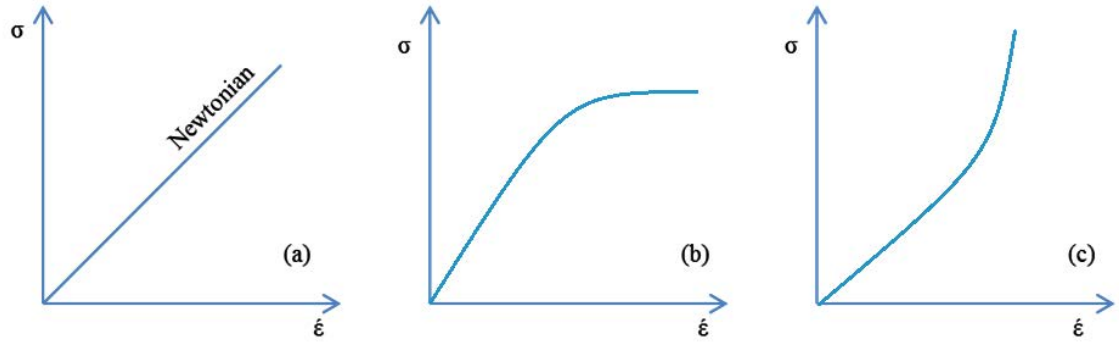


*Figure1.1 The possible stress and strain rate relationships. (a) The stress and strain rate is linear, this is the Newtonian behaviour. (b) The strain rate decreases as stress increases. The polymer is showing more resistance to the stress at higher strain rates. (c) The strain rate progressively increases with increase of stress. The polymer is showing better flow at higher strain rates.*

As almost all polymers do not have perfect crystalline structures, polymers will flow in response to an applied stress. This mode of deformation is creep; it is caused by defects such as dislocations in the polymers which are also due to viscoelasticity, and are primarily due to viscoelastic creep [**Ward/Sweeney 2004**].

The dependency of the amorphous component of polymer mechanical properties on temperature is most significant at the transformation from a glassy into a rubbery state. This range of temperature is called the glass-rubbery transition temperature or just the glass transition temperature, $T_g$. Within this significant range of temperature, the relaxation time becomes comparable to the timescale of the experiment. This means the glass transition temperature of a specific polymer will

depend on the method of measurement, heating rate, and stress if applied. It is not true to state glass as a liquid with a very large viscosity. The change between glassy and rubbery polymer is often sharp followed by a qualitative change of properties. The transition is kinetic in character. The transition of a glass polymer into a rubbery state is defined by the discontinuity in thermodynamic quantities that are second derivatives of a free energy. But the glass transition temperature is not considered as a pure thermodynamic phase transition. This is because the temperature is dependent on the rate of the experiment. Instead, it can be considered as a kinetic transition: in the glass solid state, the polymer forms in one of many possible microstates which are history dependant. The pressure and temperature history of how the microstates are formed then affects the measured glass transition temperature. It is apparent that the mechanical properties of polymers are very much dependent on temperature, rate of load and the amount of strain.

## 1.2 Stress-strain behaviour of a uniaxially compressed polymer

Solid polymers can undergo substantial strains. Thus, the measurements of stress-strain curves are important for studying the mechanical properties of these materials. The basic response of the polymer and the interpretation of the true stress-true strain curves are discussed here.

The polymer stays elastic and returns back to its original dimensions after the removal of the load if it remains within the elastic limit. Most materials, including polymers, are linearly elastic below their yield points where strain $\varepsilon$ is proportional to the applied stress $\sigma$.

$$\sigma = E\varepsilon \tag{1.1}$$

A general polymer deformation stress-strain curve of a polymer is shown in Figure 1.2. Initially the polymer behaves in a viscoelastic, time-dependent manner. For small load, only low strain is reached and the deformation is recoverable and can be described by Equation 1.1. While loading increases, the stress and strain ratio becomes non-linear. Eventually, at the material yield point, the deformation is irrecoverable. This is because the polymer structure has changed due to the increase of stress, resulting in higher resistance to plastic flow and strain softening can be

identified in the stress-strain plot. Finally, with larger strain reached, the polymer molecules become more orientated which gives rise to increase of stress at larger deformation. This is identified as the strain hardening effect on the plot.

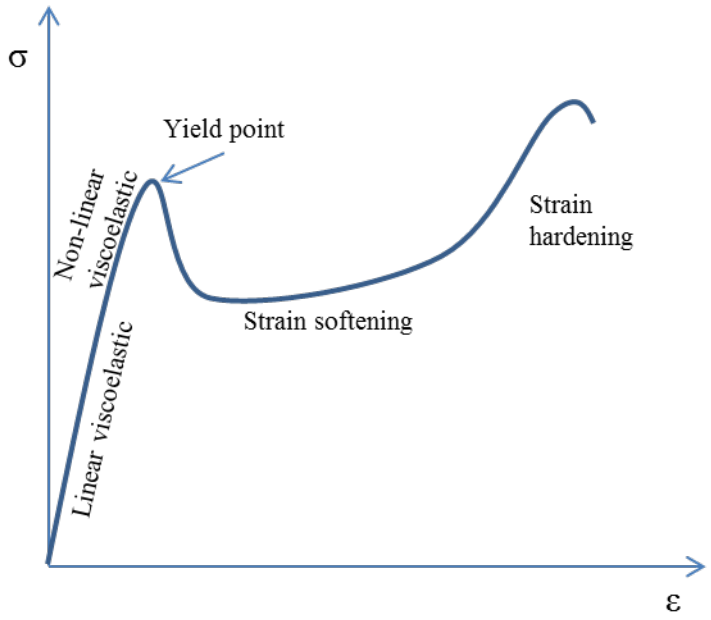


*Figure 1.2 Schematic representation of the general polymer material deformation behaviour.*

Figure 1.2 represents a general polymer true-stress and true-strain response during a homogeneous deformation. Note the details of the true stress-strain curves will differ per material. In a ductile material, the increasing stress continues to strain the material; this is the strain hardening mechanism. The dramatic response of strain hardening in semi-crystalline polymers is a transformation in the microstructure. Initially the crystalline plates are spherulitic. When the induced strain increases the spherulites are deformed in the direction of strain, and then eventually broken. Now the covalent bonds dominate the microstructure; the polymer shows larger strength and stiffness.

Most ductile polymers at large deformation feature strain hardening after yielding and strain softening. It is understood as the mechanical response of long-chains in anisotropic materials. During the plastic deformation the orientation of the covalent chains enhances the mechanical properties in the orientation direction. Experimental evidences show that the strain hardening of polymers, both ductile and semi-crystalline polymers, increases with the increasing of entanglement or crosslink density, while decreases with increasing temperature. It is still in debate as to the

dependency of strain hardening in strain rate. Some studies report strain rate dependent strain hardening, while others do not [**Chu 1973, Rietch and Bouette 1990, Bisilliat et al. 1997**]. It was shown by van Melick that a strong correlation between the amorphous phase and strain hardening in multi-phase systems exists [**van Melick 2003**].

The area under the stress-strain curve during loading is the strain energy received by the polymer. Vice versa, the area under the unloading curve (if there is one) is the energy released by the polymer.

The area under the stress-strain curve is equivalent to the total mechanical energy required per volume gained by the specimen [**Bower 2002**]

$$U = \frac{1}{V}\int F dL = \int_0^L \frac{F}{A_0}\frac{dL}{L_0} = \int_0^\varepsilon \sigma d\varepsilon \tag{1.2}$$

Without considering the energy dissipation mechanics, the energy is stored within the material as strain energy. The unit for stress-strain area is Newton per meter square, which is the same as stress or elasticity modulus which is energy per unit volume. The stress-strain area up to yield point shows how well the material resists loading without permanent deformation, and the area between yield and failure shows the toughness of the material. The higher this energy is, the tougher the polymer.

The focus of this study is the compression mechanical behaviour of PMMA, PTFE, PVC and PCTFE - although, high strain rate mechanical tests are more often investigated in tensile loading. In many materials undergoing small stress loads, when stress and strain are in proportion, tensile and compression stress-strain relations are the same with negative values. Hence, the Young's modulus, E, is the same in both cases. At high strain rates, however, the mechanical properties can be quite different in compression, a planar orientation process, and tension, a uniaxial orientation process. Boyce and Arruda found the large strain rate responses of polycarbonate in tension and compression to be different [**Boyce/Arruda 1990**]. The authors compared the stress-strain rate behaviour and found that in compression the extreme strain hardening occurred at 1.25 strain, but in tensile this occurred earlier at 0.7 strain. This means it is harder to completely plasticise the material under compression; a possible explanation is that the heat produced during high strain rate compression influences the mechanical behaviour of the polymers. This result agrees with the investigation of

tensile and compression loading of PMMA by W. Chen, F. Lu, and M.Cheng [**Chen/Lu/Cheng 2002**]. They found the maximum stress reached by compression is larger than in the tension tests. The authors also reported that stress strain behaviour under tension was significantly different from the dynamic compressive response. Brittle-ductile transition was observed in tensile tests, but not in compression. They suggest this transition could be suppressed by the temperature rise in the specimen from the large inelastic deformation.

## 1.3 Deformation and failure of polymers at high strain rates

Deformation occurring during the loading of polymers is recoverable before the point of yield, after which the post-yield deformation becomes permanent in the specimen. The process of high strain rate impact is complex: the polymer experiences large acceleration and responds with a rapid increase of strain. This usually results in the increase in temperature.

High speed cameras are used in rapid deformation studies to give visual information of the sample while still under impact. A high speed camera at $10^5$ to $10^6$ frames per second was used by Al-Maliky and Parry [**Al-Maliky/Parry 1994**] in the high strain rate expanding ring method experiments. The photography was used to calculate the strain in the deforming process, from which the stress-strain rate properties were determined. At the same time, the authors clearly indicated a specific time (and corresponding strain) at which the polymer specimen showed fracture. The photos also gave evidence to unwanted secondary impacts, which resulted from pieces of the fractured specimens.

The C4-Camera Dropweight was used to film the high impact process of polymers at inter-frame time of 7 μs [**Walley/Field/Pope/Safford 1991; Swallowe/Lee 2003**]. The stress produced by the drop-weight reaches the failure level of the samples; cracking and shattering of the polymers was observed. Walley reported discolouration in polycarbonate (PC), which started off transparent, and nylon, which turned translucent during deformation. In both cases, the discolouration process first started off as a ring roughly commensurate with the original diameter of the specimen. The appearance of the ring was observed after 90 μs in PC and 130 μs in nylon specimens, shown in Figure 1.3. After appearing, the discoloured ring became broader with time,

expanding both inward and outward. The authors ruled out the possibility of a chemical effect due to the film. But no suggestion of the appearance of the ring is given. The discoloured ring was not observed by Lee et al.(shown in Figure 1.4), who studied poly methyl methacrylate (PMMA) and polystyrene (PS). This could be due to the test temperature. Walley et al. cooled the specimens down to -173ºC, whereas Lee et al. heated the specimens above the room temperature.

In high strain rate plastic deformation, most of the deformation energy is transformed into heat. At high rates the heat may not have enough time to dissipate from the deformed area. This induces localised heating which leads to local thermal softening. If the localised plastic work is larger than the heat diffused then adiabatic shear banding occurs. Mention of adiabatic shear bands also appears in the literature under different names such as thermal crosses, heat lines, thermoplastic shear bands or white bands [**Massey 1921, Recht 1963, Bedford et al 1974**]. They develop in the dynamic process due to rapid localised heating from plastic shear strain deformation. Narrow bands usually appear on planes of maximum shear stress, which is observed in the surfaces of loaded specimens, both in metals and polymers.

Rittel observed the evolution of deformation of glassy amorphous polymers and grouped the results into three stages of behaviour according to the pressure applied [**Rittel 2000**]. In the first stage, the polymer specimen sustained the large impact without showing apparent damage. Afterwards, the tested specimen was examined and showed no damage under the light microscope. This demonstrates the deformation energy is not capable of changing the configuration of the polymer before reaching yield point. In the second stage where strain softening is detected after the maximum stress, a network of micro cracks develop in the polymer when the pressure is high enough to cause yield but not enough to fail the specimen. The amplitude of the stress pulse is large enough to initiate the cracks but its duration is too short for final fracture. In the last stage, the specimen shatters into a multitude of small fragments. Here the specimen manifests itself by the decrease in stress with increasing strain. As this stage involves crack frictional effects, Rittel suggests this is the exothermic stage where the increase of temperature occurs [**Rittel 2000**].

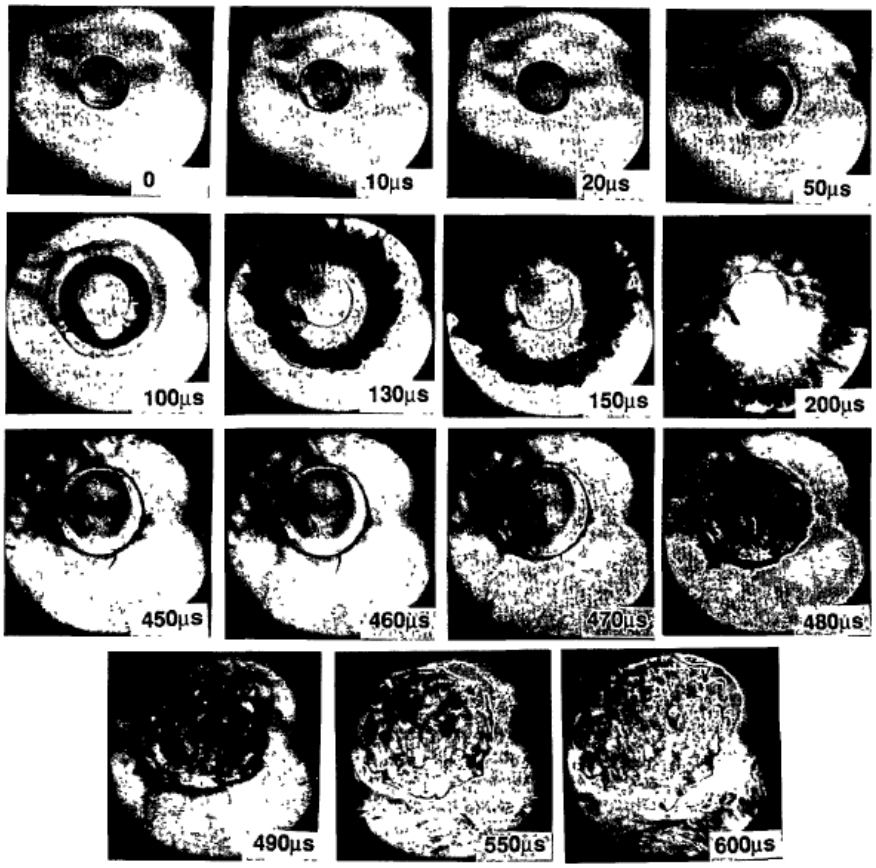


*Figure 1.3 High speed photographic sequence of the deformation of a PC disc at temperature 100K. The fracture strain is 1.0. The appearance of the discoloured ring in PC was observed after 90 µs. [**Walley/Field/Pope/Safford 1991**]*

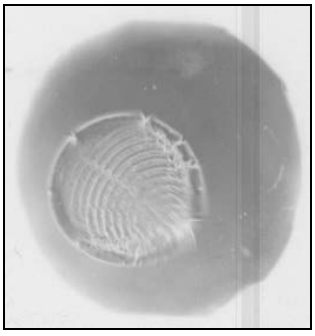

*Figure 1.4 The Deformation of poly methyl methacrylate taken after 1035 µs at 50˚C using the high-speed photographic system. [**Swallowe/Lee 2003**].*

At high strain rates above $10^3$ $s^{-1}$ fracture stress increases with the impact strain rate. This was demonstrated by Parry and is shown in Figure 1.5 [**Parry 1997**]. The stress-strain behaviour of epoxy* (curves a and b) and APC2* (curves c, d and e) composite is plotted with given strain rate. The overlap of Young's modulus is

reasonably linear up to fracture (F), other than curve c where the APC2 recovered elastically. Both materials here show larger fracture stress with increase of strain rate. (*Both epoxy and APC2 are not monopolymers)

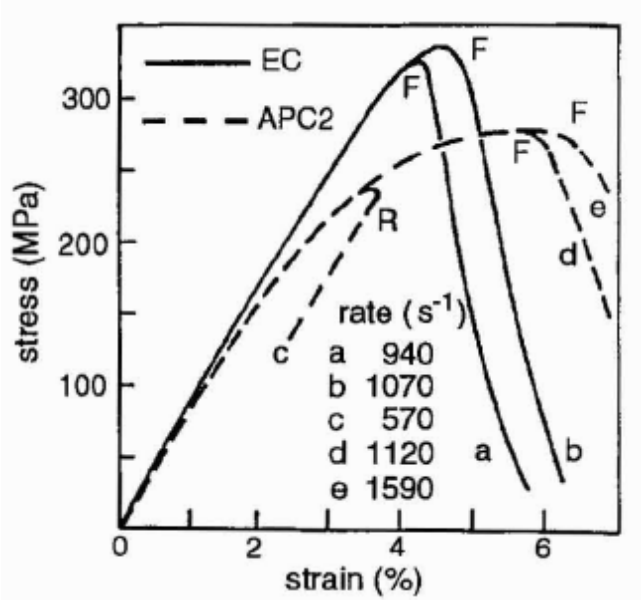


*Figure 1.5 Stress-strain curves for epoxy and APC2 composite under high strain rate compression impact. [**Parry 1997**]*

## 1.4 Phase transitions of polymers

It is not possible to conduct an isothermal rapid deformation of polymers due to the geometrical effects such as inertia or friction. Therefore it is an important part of the high strain rate impact experiments to also take into consideration the phase transitions of polymers before analysing the dynamic mechanical behaviours of the materials.

States and phases of a polymer are determined by the thermal transitions. The primary transition between the solid crystalline and amorphous liquid phase is the melting point, $T_m$. The main thermodynamic properties of the polymer do not change as a sharp transition, but through a range of temperatures. A polymer transition temperature range is related to the molecular weight distribution and also the degree of crystallinity. In essence, the melting transition of a polymer begins as the last crystallite melts. Therefore, a melting point does not exist in amorphous polymers. They soften upon heating and exhibit glass-like solidity at low temperatures. The

glassy phase, which occurs before the glass transition temperature $T_g$, is a significant transition phase.

Amorphous materials are classified as such due to their lack of higher-order structure; in the unstressed state, the main polymer chains are randomly oriented. In general, a microscopic view of amorphous materials may be pictured as a bowl of spaghetti, where chains interact with one another though weak Van der Waals forces, and form a network due to either occasional covalent cross-links or physical entanglements between the chains. This disordered microscopic structure dictates a mechanical response that is very much dependent on the rate at which the polymer is deformed. A semi-crystalline polymer also shows a transition at $T_g$ due to its amorphous component.

The shear and Young's moduli of semi-crystalline polymers not only depend on the amount of crystallinity but also on the micro-crystallites. With very small crystallites the surface energy plays an important role which lowers the melting point [**Hohne 2002**].

The transitions in the glassy region are difficult to determine, because the time needed for such a transition will be very small. These are known as secondary transitions. For that reason general use is made of dynamic mechanical measurements as a function of frequency to elucidate the modulus temperature curves, especially in a glassy region. Another advantage is that elastic and viscous forces are separated in this way of measurement. Figure 1.6 is a schematic logarithmic plot of young's modulus as a function of time for amorphous polymers. The chain interactions related to the secondary transitions are plotted in micro mechanical scale. At the glass transition temperature $T_g$, volume increases as the temperature increases and the polymer main chains have more room to move freely. The $\beta$ transition is usually associated with the side groups of the polymer. Bending and stretching of the main chain is example related to the $\gamma$ transition, and local movement in the polymer chain can contribute to the $\delta$ transition.

The stress-strain curve of amorphous polymers is unique, and well reported. [e.g. **Engels et al. 2010**]. The stress-stain behaviour of amorphous polymers is strongly dependent on strain rate [**Hochstetter et al. 2003**]. This is an important mechanical behaviour when predicting high strain rate properties of amorphous polymers. The temperature dependency of the mechanical behaviour in amorphous polymers is

closely linked to their strain rate dependency, although the reason behind this is still not fully understood.

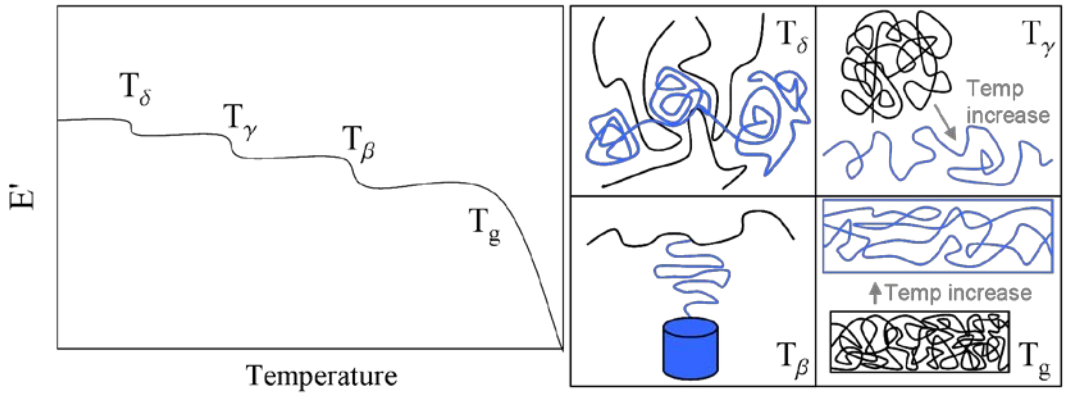


*Figure 1.6 Left: Schematic logarithmic plot of young's modulus against time for an amorphous polymer with glass transition ($T_g$) and secondary transitions ($T_\beta$,$T_\gamma$,$T_\delta$).*

*Right: Chain interactions related to the secondary transitions at micro mechanical level.*

Under rapid deformation many complicated process occur within the system. The polymer experiences quick acceleration and material strain responds rapidly. There are large shock waves and the temperature of the system often rises considerably [**Walley/Field/Pope/Safford 1991**]. The effect of inertia and friction are often more pronounced in a high strain rate test and it is often explained in the literature how this is minimised (i.e. section 2.4.1), or measured so the effect can be quantified. It is impossible to conduct an isothermal high strain rate experiment; the temperature rises during the experiment. The temperatures quoted in the literature are generally the starting temperature. Although it is possible to calculate or measure the rise of temperature, this is not often presented alongside high strain rate experimental results. The strain rate region where the transition from isothermal to adiabatic deformation takes place is around $10^{-1}$ $s^{-1}$ [**Follansbee/Kocks 1988**].

## 1.5 Temperature–time equivalence

### 1.5.1 Willam-Landel-Ferry (WLF) method

The viscoelastic behaviour of polymers is both time t and temperature T dependent. The viscoelastic properties originate from the molecular motions in the

polymer chains. The effect is more pronounced at higher temperatures. This is also true if the time or frequency range is large and the logarithmic scales for t or ω are used. By changing the temperature or the time-scale to obtain the same effect is called time-temperature equivalence. By plotting the viscoelastic behaviour value using the time-temperature effect one can obtain a master curve which is a wider range of strain rates than experimentally possible (due to the limitations of apparatus).

The Willam-Landel-Ferry (WLF) method [**Ward/Sweeney 2004**] is one way of obtaining a master curve. The shift factor $a_T$, for example, in a stress-strain rate curve strain rate should be divided by the shift factor for values gained from different temperature tests. And for stress-logarithmic strain rate curves, a shift of $\pm\log a_T$ along the strain rate axes should be made in order to get superposition for the curve. The shift is the result of a relaxation process, which means if there is more than one important relaxation process, then a shift factor cannot be calculated. More than one shift factor can exist if there are more molecular relaxation processes. Usually the main relaxation is the glass transition temperature in non-crystalline polymers. By using this method, a master curve is relatively simple to obtain, but as the WLF equation is an empirical equation, the results cannot be linked to the structure of the polymers.

### 1.5.2 Temperature dependence of viscoelastic behaviour

With the increase of temperature in a polymer, conformational freedom is achieved in terms of molecular motions. The bonds in the structure begin to rotate, which can be related back to the viscoelastic behaviour. In practice it is possible to have more than one viscoelastic transition corresponding to the change of states (for example from glassy state to rubbery state). The primary transition in an amorphous polymer is the glass transition temperature. But there are usually several secondary transitions involved in small changes in the modulus.

In semi-crystalline polymers, the viscoelastic behaviour still has the characteristics found in the amorphous polymer, but they are much less defined. The fall in modulus for semi-crystalline polymers is of one or two orders of magnitude, and the change in modulus or loss factor with temperature or frequency is more gradual. This means the relaxation times in semi-crystalline polymers are broader.

## 1.6 Strain rate sensitivity of polymers

The properties of polymers are known to depend on the rate of loading rather than strain, and how these differ from one polymer to the next has been investigated by many [**Ward/Sweeney 2004**]. By collecting mechanical compression analysis data of polymers and understanding the microscopic mechanics behind these properties, it is possible to predict the behaviour of polymers and polymer-based systems for specialised tasks.

Yield and flow in polymers are more complicated than metals due to their dependency on time, temperature, strain, strain rate as well as the history of the polymer. It can be visualised as an equilibrium transition state between the elastic and the plastic state. Because of the long carbon chains and bonds between them, this transition period is a longer and more complicated process. The yield/flow state is formed at the potential energy maximum. The higher energy represents an unstable molecular arrangement in which the bonds are still rearranging and with enough energy to reach the next energy minimum state.

The difference between the two is that yield is a homogeneous deformation, whereas plastic flow often occurs faster in localised regions. To investigate large strain polymer deformation, it is important to consider the yield and flow stress. Yield and flow are often described as thermodynamically activated processes that are associated with activation energy and volume [**Walley/Field/Pope/Safford 1991**]. They are connected to the Gibbs free energy, which is needed to characterise the deformation on a molecular scale [**Escaig 1982].**

### 1.6.1 Strain rate sensitivity of yield/flow stress at low strain rate

Walley and Field [**Walley/Field/Pope/Safford 1991, Walley/Field 1994**] investigated seventeen different polymers at room temperature for their uniaxial compressive stress strain response. The thermal characteristics of the polymers were not considered. At low strain rates most polymers exhibit a linear relationship between stress and log strain rate over the strain rate range $10^2$-$10^3$ $s^{-1}$. The aforementioned authors calculated the low strain rate sensitivity increases between 5 and 15 MPa per decade of strain rate up to $10^3$ $s^{-1}$.The results at low strain rates agree with the work by Briscoe and Nosker [**Briscoe/Nosker 1984**] and Dioh [**Dioh et al.**

**1994**]. It is usually possible to estimate the strain rate sensitivity of polymers in this region of strain rate by a few experimental data points. The only polymer found to be the exception to this rule of thumb is polytetraflouroethylene (PTFE). The flow stress as a function of strain rate for PTFE reported by Walley is shown in Figure 1.8. At strain rates lower than $10^3$ $s^{-1}$, PTFE shows a three-fold linear relation to strain rate. The authors suggest PTFE is less sensitive to strain rate and further investigation are needed.

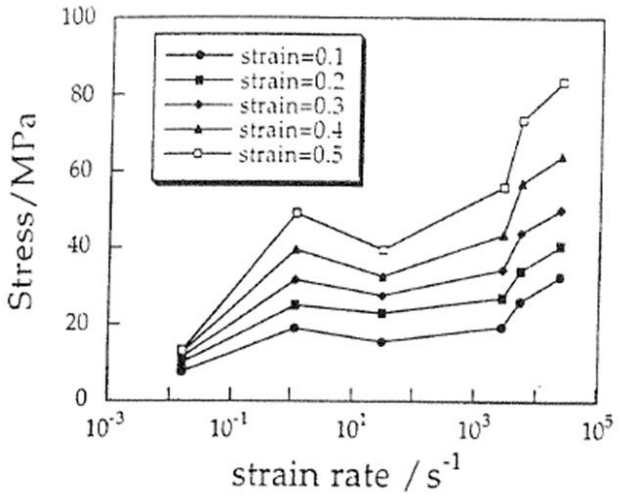


*Figure 1.8 Stress as a function of strain rate for PTFE at five natural strains [**Walley/Field 1994**].*

## 1.6.2 Strain rate sensitivity of yield/flow stress at high strain rate

A sudden increase in the sensitivity of the mechanical properties occurs in a broad range of polymers when the strain rates are above $10^3$ $s^{-1}$. Primary studies of the high strain rate responses of various polymers were reported in the same study by Walley et al. [**Walley/Field/Pope/Safford 1991, Walley/Field 1994**]. The results were inconclusive, with five of the polymers showing a rapid increase around $10^3$ $s^{-1}$, and another five showing a dip near the same strain rate. It was not possible to tell with the rest of the polymers because not enough data was gathered to make clear the trend of yield stress variations. It is clear, however, at high strain rates the sensitivity of yield and flow stress is dominated by a different mechanism to lower strain rates, this was confirmed later by others [e.g. **Lu/Li 2010**]. A more detailed report measuring the high strain rate properties of PEEK, HDPE, ultra high molecular weight polyethylene

(UHMWPE) and Nylatron GS, was reported by Al-Maliky and Parry [**Al-Maliky/Parry 1994, 1997**]. All three materials showed a rapid increase in stress at strain rates at $7\square10^3\ s^{-1}$ for HDPE and UHMWPE, and $4\square10^3\ s^{-1}$ for Nylatron. The increase reached a peak within a very short strain rate and decreased rapidly. For Nylatron the stress dropped to the same value which it had at $4\square10^3\ s^{-1}$. In the experimental evidence of drop in stress at high strain rate only occurred in some of the polymers tested. This could indicate that the drop is governed by a different mechanical response of the polymer structure to the rapid stress increase which takes place before the stress drop. The stress-strain curves shown by Walley et al. are the average of four experiments, and the error quoted for strain rate is the standard deviation. The reason for this method was not made clear. But this could be the reason why clear high strain rate peaks seen in Al-Maliky's work were not found. As illustrated by Al-Maliky and Parry, represented in Figure 1.9, the flow stress peaks only occur at a very narrow strain rate range, and, in hindsight, averaging data in this region would lose the details of strain rate sensitivity. It is also clear that if the strain rate values are too far apart, the flow stress peak could be missed partly or completely, which would result in only identifying a rapid increase or a dip in yield/ flow stress at strain rate range above $10^3\ s^{-1}$. Following the flow stress peak found in Nylatron, Al-Maliky et al. [**Al-Maliky 1997**] reported the same effect in PEEK, illustrated in Figure 1.9b. The rapid stress increase in PEEK begins at $7\square10^3\ s^{-1}$, this was later than in Nylatron. This suggests that maybe the flow stress rapid increase and drop happen at different strain rate values for different polymers. This could be the reason why some investigations into the high strain rate properties of polymers are inconclusive and for the gap in the literature.

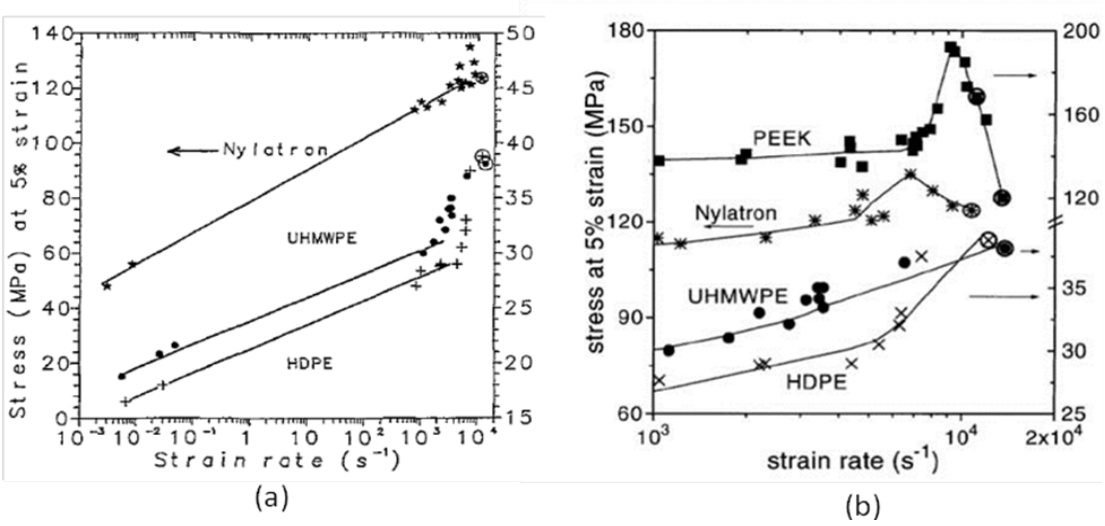


*Figure 1.9 (a) Stress at 5% strain against log strain rate for HDPE, UHMWPE and Nylatron GS. (Al-Maliky and Parry, 1994) (b) Stress at 5% strain against log strain rate for PEEK, HDPE, UHMWPE and Nylatron [**Al-Maliky 1997**].*

Evidence of flow stress peak in the poly methyl methacrylate (PMMA) is illustrated in Figure 1.10, with the peaks detected at 70ºC and 90ºC by Forrester and Swallowe [**Forrester/Swallowe 2009**]. The authors also reported narrowing of a shift in the peaks as the temperature increased, the peaks narrowed and the narrowing became more apparent as temperature was near $T_g$. They suggested this change in the flow stress peak is due to the temperature approaching the glass transition temperature.

The flow stress peak is interpreted as a transition from one or more of a series of thermally activated flow mechanisms [**Gourdin/Lassila 1996**] at low strain rates to a flow process dominated by viscous drag at high rates. Follansbee suggested that this behaviour can be interpreted as a change in the way the structure evolves with strain [**Follansbee/Kocks 1988**]. The deformation velocity, friction and inertia at high strain rate could all be responsible for the increased sensitivity in strain rate [**Gorham 1989**]. A physically based constitutive model based on the same concept as the Ree-Eyring yield theories [**Feck/Stronge/Liu 1990**] was compared with the experimental data for amorphous polymers under large strain rates [**Mulliken/Boyce 2006a/2006b**]. They found the enhanced rate-sensitivity is directly attributable to the restriction of the secondary molecular motions. The primary and secondary processes of the yield strength were predicted separately in addition to the total yield strength of the polymers. Forrester and Swallowe found that the presence of the flow stress peak became more apparent near the glass transition and that the postulated phenomenon

could be a characteristic of the amorphous region, and therefore potentially evident in all amorphous and semi-crystalline polymers [**Forrester/Swallowe 2009**].

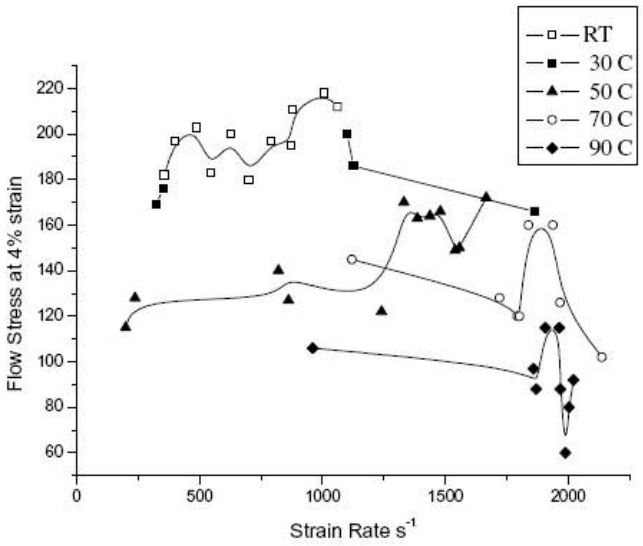


*Figure 1.10 Flow stresses at 4% strain as a function of compressive strain rate of PMMA over a range of temperature [**Forrester/Swallowe 2009**].*

An increase of crystallinity was reported during the high strain rate compression of semi-crystalline polymers [**Swallowe/Lee 2003**]. The mechanical behaviour of several semi-crystalline polymers was studied. Poly ethylene terephthalate yield stress increases with strain rate. Interestingly a sharp increase was found at rates of $10^3$ $s^{-1}$ and above. Increases of up to 40% in crystallinity content were found in recovered samples. The authors concluded this was induced by temperature increase after the impact test, and cannot be accounted for rapid increase of yield and flow stress at the same strain rate. Most of the polymers on which comprehensive tests have been carried out are semi-crystalline polymers. Swallowe and Lee pointed out that the relative contributions of amorphous and crystalline content in the yield and flow stress should be investigated separately [**Swallowe/Lee 2003**]. They concluded that the density variation and changes in the β relaxation temperature or the activation energy for flow are unlikely to be the main contribution factors. The authors speculate that activation volume changes may play a major part in flow stress increases when polymers are tested at high strain rates.

# Chapter Two

# High strain rate experimental technique

## 2.1 Introduction to Split Hopkinson Pressure Bar (SHPB)

The Split Hopkinson Pressure Bar (SHPB) technique is one of the well-established methods for determining properties of solid materials at high strain (up to 15% or more) and high rates of strain ($10^2$ up to $10^5$ $s^{-1}$). The theory for the Split Hopkinson bar has been used for decades, however the diversity of this method means advancements, adjustments and additional aspects are still being developed to accommodate the need to test mechanical properties of a wide variety of solid materials and composites.

A typical compression SHPB system is shown in Figure 2.1. The material of interest is shaped as a cylindrical specimen and it is sandwiched between two long bars, the loading and transmitting bar. The free end of the loading bar is subjected to axial impact, generating a stress pulse which travels along the loading bar to the test specimen. Upon arrival of the specimen, the wave is partly reflecting back to the impact end and the remainder of the wave is transmitting on to the second bar. Provided the stress is large enough this causes plastic deformation in the specimen, which is irreversible. The reflecting and transmitting pulses are proportional to the strain rate and stress of the specimen, respectively, and specimen strain can be calculated from strain rate. Thus the true stress-strain properties of the material can be determined. The use of the SHPB technique can be extended to modify and carry out other loading tests, i.e. tension, shear, bending, indentation as well as combined loading.

The technique was initially developed by J. Hopkinson in 1872 [**Hopkinson J 1872a**]. B. Hopkinson, then developed the pressure bar [**Hopkinson B 1905**]. Then, R.M. Davies in 1948 recorded the wave propagation in the pressure bars [**Davies 1948**] and H. Kolsky determined the dynamic compression stress-strain behaviour of several different materials, developed the 1D pressure bar data analysis and the experimental

procedure [**Kolsky 1959**]. These studies are the foundation of the methods to characterise the high stain rate behaviour of solid materials.

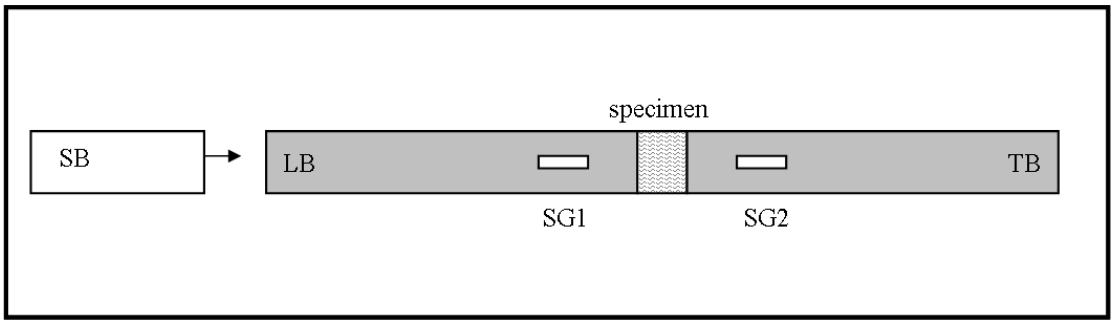


*Figure 2.1 General set up of the SHPB system. Striker bar(SB), loading bar(LB), transmitting bar(TB), strain gauges(SG), and specimen.*

A suitable specimen is placed between the split bars, the loading and transmitting bars. Then the striker bar is fired at the free end of the loading bar producing an impact and compressive stress/strain pulse. The pulse produced is twice the geometric length of the striker bar length, and is in the shape of an approximately flat-topped trapezoidal stress pulse. The amplitude of the stress pulse ($\sigma$) is proportional to the impact velocity of the striker bar ($\upsilon$).

$$\sigma = \rho c \upsilon \tag{2.1}$$

Here $\rho$ is the density of the bar and $c$ the speed of sound travelling in it. The pulse travels though the loading bar, specimen and transmitting bar. The loading and reflecting waves created are recorded by the strain gauges mounted on the loading bar and the transmitting wave from the strain gauges on the transmitting bar. The strain in the loading pulse is denoted as $\frown_L(t)$, reflecting pulse as $\frown_R(t)$, and transmitting pulse as $\frown_T(t)$, as seen in the original recordings in Figure 2.2, the reflecting wave is tensile in nature and is of opposite sign to the loading pulse. Deformation occurs when the specimen material reaches its dynamical limit.

The properties of the bar materials and the specimen dimension are all known prior to the test. The signals are recorded by strain gauges as changes of voltage in the strain gauges against time and can be converted to specimen stress in relation to specimen strain. Then using an analytical model $\frown_L(t)$, $\frown_R(t)$, and $\frown_T(t)$ can be related to the mechanical properties of the tested material. In his paper Kolsky [**1949**],

gave a derivation for both average stress and strain of the specimen as a function of time. The analytical models mostly used can be found in text books [**Bower 2002**].

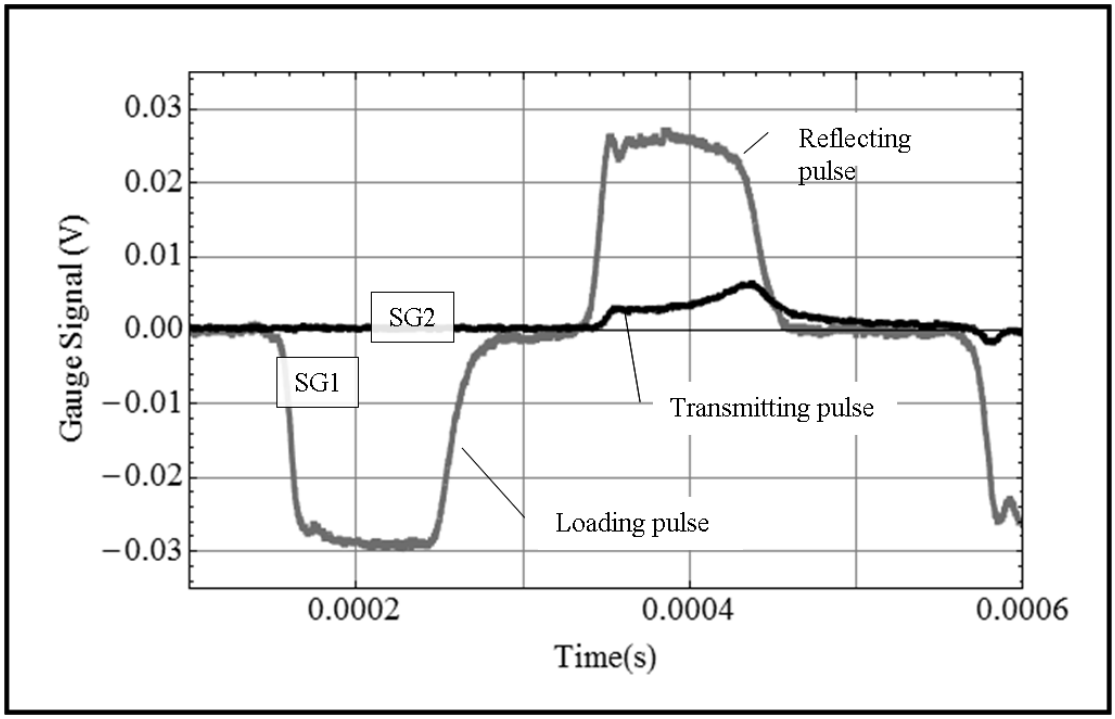


*Figure 2.2 Original pulse traces from experiment using PVC (specimen no. 27) specimen at ambient temperature. The loading $\varepsilon_L(t)$ and reflecting $\varepsilon_R(t)$pulse is detected by strain gauge one (SG1). And the transmitting pulse $\varepsilon_T(t)$detected by strain gauge two (SG2).*

## 2.1.1 Development of the Loughborough University SHPB system

The split Hopkinson Bar system at Loughborough University Physics department has been used to study the dynamic mechanics of a wide range of solid materials. The development and modification of the technique involved many researchers [**Griffiths/Martin 1974, Parry 1979, 1988, 1994b, Ellwood 1981, Ellwood/Griffiths/Parry 1982, , Parry/Walker/Dixon 1995**].

In the early setup the impact was produced from a standard 0.22" calibre bullet, and Griffiths and Martin recorded the sample strain by an optical shutter method. The loading system was modified by Parry and Griffiths. A compact gas gun was developed to fire a short steel projectile at the free end of the loading bar driven by atmospheric pressure. The gas gun could be repeatedly used by firing more consistently than the bullet system, and produced a more uniform stress pulse.

Ellwood introduced a larger gas gun system to produce large amplitude stress pulses by firing a larger projectile. Walker developed an optical fibre system to measure the impact velocity of the projectile to replace the mechanical trigger system introduced by Ellwood. Later Dixon designed an infra-red projectile velocity measuring device, this accurately measures the speed of the projectile as it reaches the free end of the loading bar.

Ellwood, Griffiths and Parry modified the SHPB system apparatus by the addition of a dummy sample, placed between the pre-loading and loading bars [**Ellwood/Griffiths/Parry 1982**]. This modification was to shape the incident pulse in order to produce a constant strain-rate during the test.

The main modification of the modern Loughborough University SHPB system to the typical SHPB compression system is the addition of the pre-loading bar [**Parry/Walker/Dixon 1995**]. The large amplitude of oscillation in the loading pulse in high strain rate tests are a consequence of the short rise time of the loading pulse produced by the impact of a projectile. The authors used this approach to eliminate the Pochhammer-Chree oscillations experimentally, removing the necessity for dispersion corrections.

To analyse the SHPB data, Ellwood introduced software for the Commodore Pet computer. This was expanded by Parry and Walker (1988). In the 1990's Parry replaced the recording system with a digital oscilloscope connected to an IBM PC to store data. This gave more accuracy in capturing the stress pulses and resulted in higher quality plots. Al-Maliky (1992) also developed more options such as smoothing and averaging the results on the software with Swallowe and Parry.

## 2.2 Theory of the SHPB method

Material properties at low rate of strains, up to 10 $s^{-1}$may be investigated by machines such as the Hounsfield Universal Test Machine. Such machines are designed to generate the desired load for compression and tensile tests. Above these rates, resonance and inertia effect must be considered and a wave propagation method must be used.

Expressions for stress and strain in the specimen, in terms of strain recorded on the bars are derived here. The stress pulses are recorded in the Hopkinson bars which are maintained within the elastic limits. Hence the one-dimensional elastic

wave propagation theory is applied. The schematic of the stress pulses acting on the specimen is illustrated in Figure 2.3.

Force = stress × area = (elastic) modulus × strain × area

$$F = \sigma A = E_b A\varepsilon \tag{2.2}$$

and stress is $\sigma = \rho c\dot{u}$, ρ is the density of the bar and c is the speed of the waves travelling though the material. The particle displacement u and particle velocity $\dot{u}$ can be written as

$$\dot{u} = \frac{\sigma}{\rho c_0} \tag{2.3}$$

$$u = \frac{1}{\rho c_0}\int_0^t \sigma(t)dt \tag{2.4}$$

From the one-dimensional wave equation we know the elastic wave velocity in the bar is

$$c_0^2 = \frac{E}{\rho}, c_0 = \sqrt{\frac{E}{\rho}} \tag{2.5}$$

applied to the specimen in contact with the bars. In the following and in Figure 2.3, subscript 1 refers to the incident bar and 2 to the transmitting bar flat face of the specimen.

The forces acting on the specimen can be described as

$$F_1 = E_b A(\varepsilon_L + \varepsilon_R)$$
$$F_2 = E_b A\varepsilon_T$$

The particle velocities are

$$\dot{u}_1 = c_0(\varepsilon_L + \varepsilon_R)$$
$$\dot{u}_2 = c_0\varepsilon_T$$

And the specimen displacements are

$$u_1 = c_0\int_0^t \varepsilon_I dt + (-c_0)\int_0^t \varepsilon_R dt = c_0\int_0^t (\varepsilon_I - \varepsilon_R)dt \quad , \quad u_2 = c_0\int_0^t \varepsilon_T dt$$

$\frown_L(t)$ and $\frown_T(t)$ are travelling in the positive x-direction and $\frown_R(t)$ the negative direction.

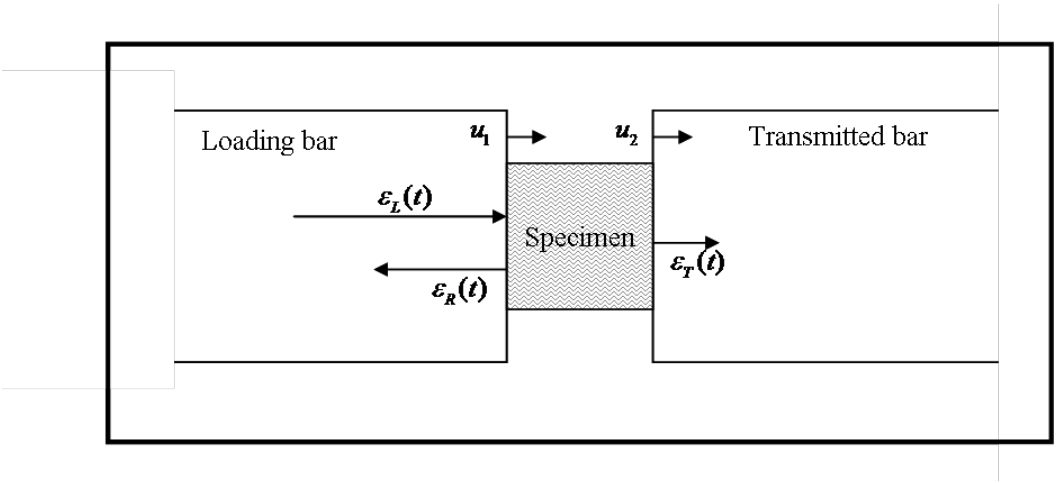


*Figure 2.3 Schematic of stress pulses acting on the specimen. The initial compressive stress pulse propagating down the incident bar is detected by the strain gauge as the incident strain, $\frown_L(t)$. Part of the pulse is then transmitting though the specimen s the transmitting strain $\frown_T(t)$, still as a compressive pulse. At the same time, the rest of the pulse is reflecting back to the loading bar which is detected as the reflecting strain, $\frown_R(t)$, in the form of a tensile pulse.*

The average force acting on the specimen F=(F1+F2)/2, with the average strain as $(u_1-u_2)/l_s$. Thus the specimen engineering stress, strain and strain rate can be expressed in terms of the recorded strain pulses,

$$\sigma_s = \frac{F_1 - F_2}{2A} = \frac{1}{2} E_b(\varepsilon_I + \varepsilon_R + \varepsilon_T) \tag{2.6}$$

$$\dot{\varepsilon}_s = \frac{\dot{u}_1 - \dot{u}_2}{l_s} = \frac{c_0}{l_s}(\varepsilon_I - \varepsilon_R - \varepsilon_T) \tag{2.7}$$

$$\varepsilon_s = \frac{u_1 - u_2}{l_s} = \frac{c_0}{l_s}\int_0^t (\varepsilon_I - \varepsilon_R - \varepsilon_T) \tag{2.8}$$

Then the effect of wave propagation, reflection and transition at both faces of the specimen is neglected, as $l_s$ is small. Then we can assume both faces of the specimen are approximately equal and $F_1 \cong F_2$. Which would translate into

$\overset{\frown}{}_L + \overset{\frown}{}_R \approx \overset{\frown}{}_T$. Then we simplify specimen stress in Equation 2.6, specimen strain rate in Equation 2.7 and specimen strain in Equation 2.8 by approximation into:

$$\sigma_s = E_b \varepsilon_T \tag{2.9}$$

$$\dot{\varepsilon}_S = -\frac{2c_0}{l_s}\varepsilon_R \tag{2.10}$$

$$\dot{\varepsilon}_S = -\frac{2c_0}{l_s}\varepsilon_R \tag{2.11}$$

Once the engineering stress, strain and strain rate derived, the true stress, strain and strain rate can be calculated by a simple conversion formula. The engineering stress is determined by Equation 2.2, where A is the final specimen cross-section area. The engineering values use fixed reference quantities. True stress and strain takes into account for the changes in cross-sectional area, where the instantaneous values are used. True stress is the ratio of the applied force to the instantaneous cross-section area A*

$$\sigma_T = \frac{F}{A^*} \tag{2.12}$$

By assuming that there is no volume change in the specimen, $A^* \cdot l^* = A \cdot l$, so true stress can be written as

$$\sigma_T = \frac{F}{A^*} = \frac{F}{A} \cdot \frac{l^*}{l} = \sigma_S (1 + \varepsilon_S) \tag{2.13}$$

True strain is the sum of all engineering strains, dε=dl/l, so true strain is written as

$$\varepsilon_T = \int d\varepsilon = \int_{l_0}^{l} \frac{dl}{l} = \ln \frac{l}{l_0} \tag{2.14}$$

True strain can be related to the engineering strain by

$$\varepsilon_T = \ln \frac{l}{l_0} = \ln \frac{l_0 + \Delta l}{l_0} = \ln(1 + \varepsilon_S) \tag{2.15}$$

As strain increases during deformation, the cross-sectional area of the specimen also increases (in the case of compression). Then the true stress is smaller than the engineering stress. True strain rate is derived from true strain

$$\dot{\varepsilon}_T = \frac{\dot{\varepsilon}_s}{1-\varepsilon_s} \tag{2.16}$$

## 2.3 Current Loughborough University SHPB system

A schematic diagram of the Loughborough University Physics Department SHPB system used for this study is shown in Figure 2.4. The impact pulse is produced by firing the projectile by the gas gun. The pulse travels though the one meter long pre-loading bar, before the pressure bars and specimen. The loading and transmitting bars are made of high-strength maraging steel half an inch (12.7 mm) in diameter and 1m in length. The 250 mm long projectile bar is made of the same material and diameter as the pressure bars. Elevated temperature experiments are achieved by using the heating system. The strain gauge pairs are located on the pressure bars 400 mm from the specimen. The impact produces a stress pulse of about 100 μs duration; the consequent strain pulses are captured and recorded using a digital storage oscilloscope. The results are transferred to numerical programs developed for the Loughborough SHPB system.

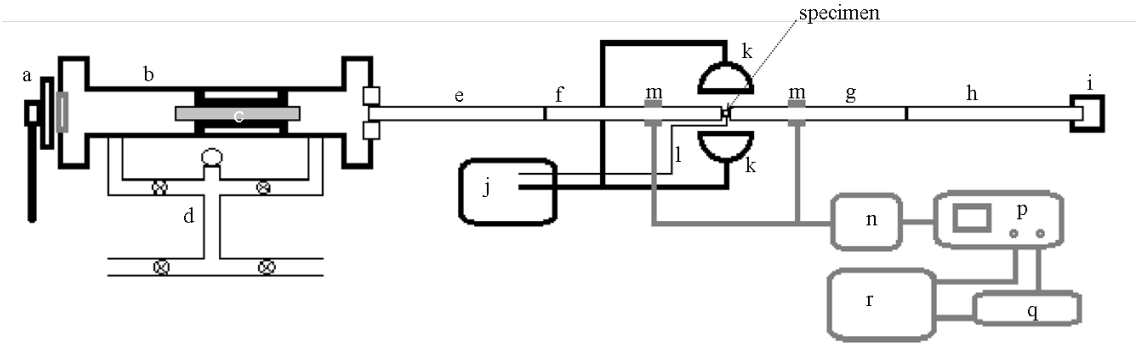


*Figure 2.4 Schematic of the Loughborough University physics department SHPB system. a. valve plate, b. gas gun, c. projectile and guide, d. vacuum system and pressure gauge, e. pre-loading bar, f. loading bar, g. transmitting bar, h. momentum bar, i. trap box, j. heating system, k. lamps, l. thermocouple, m. strain gauge pairs, n. strain gauge bridge circuit, p. digital oscilloscope, q. transmitting signal amplifier, r. stabilised power supply.*

### 2.3.1 The projectile system

A compact gas gun is used and was first described by Parry and Griffiths [**Parry/Griffiths 1979**]. The principle of operation consists of using an evacuated wide-bore acceleration tube of diameter four times that of the projectile rod, which is driven by atmospheric pressure. The acceleration tube is made of stainless steel (type 321) with an internal diameter of 50 mm and wall thickness of 6 mm. The inside wall is polished to remove any burrs. Flanges are screwed on the ends of the tube and flat rubber seals are used to obtain vacuum. The tube is evacuated to lower than 13 Pa (0.1 Torr) using two pumping lines connected to both ends of the tube, this enables the projectile to be brought back to the open end of the gas gun at its starting position after the firing of the projectile, which is enabled by admitting atmospheric air into the evacuated tube though a simple hand-operated sliding valve, constructed of mild steel. The size of the holes in the aperture plate controls the rate of which air enters the tube, and determines the maximum velocity of the projectile.

The projectile consists of a hard stainless steel rod, which is the same material as the pressure bars, of diameter 12.5 mm and length 250 mm. The duration T of a strain pulse caused by the momentum transferred from the projectile is directly proportional to the length of $l_p$.

The projectile bar is mounted axially in a cotton reel shaped PTFE guide to allow the bar to travel centrally though the tube. The guide is shaped in this way to minimise the contact with the inside wall of the tube for a sliding fit. The ends of the rod are polished and ground and the rod is ensured to be perpendicular to the projectile rod axis. There is a 0.5 mm gap between the rod and the guide to minimise radial constraint on the rod in the impact. After firing, the guide slides until its momentum is removed gradually by a hollow rubber cylinder. The rubber cylinder is fitted at the impact end inside the gas gun. This prevents the momentum of the guide being transferred to the pre-loading bar distorting the strain pulse.

In this system the projectile driving force is 16 times greater than would be for a system with the same diameter as the rod. But in practice the weight of the PTFE guide reduces this to around 8 times. The advantage of this design is that it reduces the length of the tube to achieve high projectile velocity and it is also safe to operate. The gas gun is available almost immediately for re-firing. The projectile design gives a stress pulse of ideal shape with duration of 100 μs and maximum stress amplitude

value of 700 MPa. The same projectile, as described above, was used in all the experiments to produce the same length pulse. Strain rate in the work was varied by the projectile velocity rather than using different material/length projectiles. The projectile was kept refrigerated while not in use to avoid thermal expansion and subsequent shape changes. If the projectile is left in ambient temperature too long, the impact bar could possibly swell and stick to the PTFE guide, causing inconsistency in the stress pulse.

### 2.3.2 The pre-loading, split Hopkinson, and momentum bars

The conventional SHPB system shown in Figure 2.4 without the pre-loading bar (noted as e in Figure 2.4) produces large amplitude oscillation pulses at high strain rate tests. The noise is a consequence of the coupling between the axial and radial displacements associated with the propagation of an elastic pulse having high-frequency components of wavelength comparable to the radius of the bars. The high-frequency components are generated by the short rise time (<10 μs) impact of the projectile on the loading bar.

By adding the pre-loading bar, the SHPB system in Loughborough University can experimentally eliminate the oscillations, resulting in a smooth loading pulse and improvement in the interpretation of the stress or strain behaviour. The pre-loading bar is connected to the gas gun though a pair of vacuum tight rings which permit a certain amount of movement of the bar after the impact. The rings reduce vibration generated in the initial stage of the projectile impact onto the pre-loading bar.

The loading and transmitting bars are 12.7 mm in diameter and 1m in length. They are made of stainless steel (431 type) with the yield strength of 700 MPa. The stainless steel bars are especially chosen because they can attenuate the high frequency components which are added on the loading stress pulse by the impact of the projectile, thus providing a clearer and uniformed stress pulse.

Each of the four bars rest on two v-shaped nylon clamps mounted on an optical bench. The stands can be finely adjusted in both vertical and horizontal directions allowing variation in height and transverse distance of the optical bench. This enables precise alignment of the bars. The bars are able to slide freely though the clamps, preventing spurious reflection as the stress pulse passes though.

The axial alignment of the SHPB system must be reasonable: misalignment could cause localised high stresses in the sample, especially during the initial loading stage, and there is also a possibility of bending the bars. In this work, an optical method is used before the experiment of each interface in the system, to close the gap to give good axial alignment. The ends of all bars are sanded down within ±5 μm orthogonal to the axis of the bar to make sure of a good fit in the bar/bar or bar/specimen interfaces.

The momentum bar, 1.5 m in length, is positioned beyond the transmitting bar and is not restrained to the rest of the system. The compression wave propagates though to the momentum bar and the bar then can move away free from the main part of the system preventing reflection of the pulse re-entering the pressure bars and the specimen.

If the momentum bar was not part of the system, the stress pulses would travel forwards and backwards along the specimen, loading and transmitting bars. This would cause multiple loading on the specimen as well as causing possible damage to the system. The momentum bar is used to absorb the unwanted stress energy from the system. Therefore the length of the momentum bar must be greater than half the length of the projectile to avoid the pulse re-entering the system. But the disadvantage of a short momentum bar is it would be travelling at a very high speed which also could cause damage to the system. For this reason most momentum bars are designed to be longer than the projectile but shorter than the transmitting bar.

### 2.3.3 Heating system

A heating system was introduced to the Loughborough University SHPB system to carry out tests above room temperature. To achieve elevated temperature tests, only the specimen and the ends of the loading and transmitting bars touching the specimen are heated. The rest of the system, especially the strain gauges were kept at room temperature. The strain gauges are temperature dependent due to thermal expansion.

The heating of the specimens is done in two steps. First the specimens are left on a heating block until both flat surfaces of the specimen reached the required temperature. Then the specimen is left on the heating block for a further 30 minutes before transferring to the heated pressure bars. Preliminary tests were carried out to

ensure thermal equilibrium between the surface and bulk temperature of the heated specimen. A small hole was drilled though to the centre of a specimen. Then a thermocouple is fitted in the hole to measure the temperature rise in the centre of the specimen, at the same time the surface of the specimen is also recorded during heating. All four polymers were tested this way. The difference in rate of temperature rise on the surface and the centre of the specimens is measured and compared. The results show less than 5% difference for polymers heating up to 100ºC. Also, after the specimen reaches the desired temperature and are left on the heating block for a further 10 minutes, all polymer specimens show no temperature difference between the surface and the centre of the specimens. The whole specimen is equally heated to the same required temperature. The time taken to heat the specimens has been checked to avoid annealing of the polymers. All specimens are stored at ambient temperature. The only occasion the sample would contact a heat source would be during heating before the high temperature experiments.

A type K thermocouple is built into the heating block and the light bulb heating system to measure and feedback specimen temperature to the heating system. hand held infrared thermometer was also used for temperature reading without the need to be attached to the specimen. The infrared thermometer gave instant temperature readings for better accuracy.

The heating system is designed to only heat the tip of the bars in contact with the specimen. The rest of the bar including the strain gauges is still operating under ambient temperature. The analysis of high temperature tests would be the same as described for room temperature tests.

### 2.3.4 Data recording

Measurement of all the pulses is carried out though two pairs of strain gauges mounted on the loading and transmitting bar. The total resistance of each pair is 220 Ω. The strain gauge pairs are in series and forms a simple potential divider bridge circuit. The circuit includes a 2.2 kΩ ballistic resistor ($R_b$) with a constant current of 20 mA and a 50 V dc stabilised power supply (ΔV) maintained across the gauges by a Farnell E350. The polarity of the power supply is configured so when a compressive wave reduces by $R_s$ an output of $V_s$ is produced.

The strain gauges are paired in order to cancel out bending waves which may occur, as well as to double the stress pulse output. The strain recorded by the strain gauge is related to the change in resistance $dR_s$ by

$$\varepsilon = \frac{dR_S}{FR_S} \tag{2.17}$$

where F is the strain gauge factor. (The gauge factor used is 2.12 ± 1%)

Using the potential divider circuit analysis of the gauge circuit, we know the voltage across the strain gauge pair ($V_s$) in terms of the power supplied (E)

$$V_S = \frac{R_S}{R_b + R_S} E = \frac{1}{n+1} E \tag{2.18}$$

where,

$$n = \frac{R_b}{R_S}$$

Differentiating $V_s$ with respect to n we have

$$\frac{dV_S}{dn} = \frac{E}{(n+1)^2} \tag{2.19}$$

and differentiating n with respect to $R_S$ gives

$$\frac{dn}{dR_S} = -\frac{R_b}{R_S{}^2} \tag{2.20}$$

dn can be substituted to Equation 2.19

$$\frac{dV_S}{dR_S} = -\frac{R_b}{R_S}\left[-\frac{E}{(n+1)^2}\right]$$

$$\therefore dR_S = R_S{}^2 \frac{(n+1)^2}{R_b E} dV_S \tag{2.21}$$

Therefore the strain recorded can be presented by the change in the strain gauge electrical resistance as

$$\varepsilon = \frac{(n+1)^2}{nFE} dV_S \tag{2.22}$$

n in terms of voltages can be written as

$$n = \frac{R_b}{R_S} = \frac{IR_b}{IR_S} = \frac{(E - V_S)}{V_S} \tag{2.23}$$

If $(n+1)^2/nFE$ is constant, than the voltages recorded in the gauges are directly in proportion to the strain in the bars. The strain gauge signals are recorded and digitalised by an oscilloscope. The traces are transferred via a floppy disc onto the computer for analyses.

The strain gauges are carefully affixed on the bars. The surface of the bars is first cleaned, sanded and cleaned again using a suitable solvent. Then the strain gauges are attached to the bar with super glue as instructed by the strain gauge manufacturer, Tokyo Sokki Kenkyujo Co., Ltd.

The strain gauge FLA-1-11 type is used on the Loughborough University SHPB system (1 mm long). Different types of strain gauges have been compared by Al-Maliky [**Al-Maliky 1997**], and it was concluded that this type of strain gauge gives better resolution and lasts longer in high strain rate tests. The strain gauge legs are soldered to connect to the bridge circuit (shown in Figure 2.5). The strain gauge legs are protected by plastic electric wire 'sleeves' to protect the solder joints and also to avoid contact between the wires and the bar.

The resolution time, $\Delta t$, of the system can be obtained by the length of the gauges, $L_g$, and the speed of sound in the bars, $c_o$, as

$$\Delta t = \frac{L_g}{c_o} \tag{2.24}$$

hence, the resolution time of the Loughborough SHPB system is 1 (mm)/ 4 (mm/μs)≈0.2μs

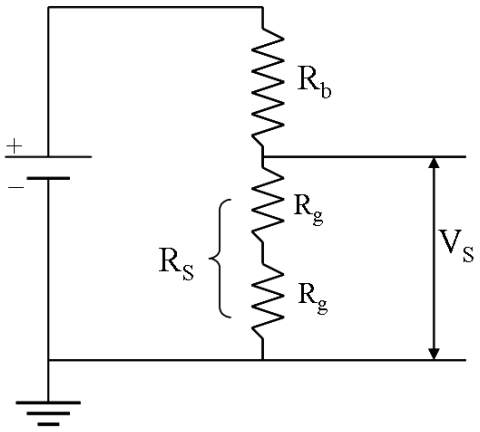


*Figure 2.5 Strain gauge circuit used to monitor voltage deflection $V_S$ across each pair of strain gauges. $R_b$ is the ballistic resistor and $R_g$ is the total resistance of one pair of strain gauges.*

One issue of testing soft materials on a SHPB system is the low mechanical impedance compared to the bar material. This results in a much smaller transmitting force than with metal samples. The transmitting force is relatively small in comparison to the loading and transmitting forces. Small signals are also more sensitive to electrical and other noises creating larger errors. A scope amplifier, SA100 in this case, is used to amplify the transmitting signal by 100 times. At the same time, the noises less than 10 Hz and above 100 Hz were filtered electronically to avoid interference in the transmitting signal. The high frequency is minimised by connecting a 2200 μF capacitor in parallel with the coaxial cable near the inputs of the oscilloscope.

Other methods of improving the transmitting signal are suggested by others [**Siviour 2005**]. The author eliminated the method of increasing the specimen diameter, arguing this would increase the effect of inertia. Instead, the metal split bars were replaced with a set of low impedance bars. This would increase the transmission coefficient between the bar and the soft specimens. Therefore, with the same loading force, the lower impedance bars would produce a greater strain rate. Also the specimen would reach equilibrium faster with closer impedance of specimen and bar [**Yang/Shim 2005**]. However, the disadvantage of lower impedance bars is the limitation in the choices in the range of materials. Dispersion effects in the low impedance bar would also be greater, which would lead to greater challenges producing constant rates of strain [**Pruden 2012**].

The computer programs used to analysis experimental data can be found in Appendix B.

## 2.4 Specimens

### 2.4.1 Inertia and friction effects

One critical part of the SHPB experiment is the design of the specimen. As some assumptions are made during the SHPB experimental method, it is important that the specimen used follows these predetermined rules to obtain correct material properties from the tests. The main assumption during the experiment is the uniform deformation of the specimen, which indicates no inertia within the specimen or friction at the interfaces between the specimen and the pressure bars.

Specimen inertia during the SHPB experiments come from the rapid radial and longitudinal particle acceleration in the specimen [**Lindholm 1964**]. The measured stress becomes greater than the effective stress on the sample. The effective stress is the true elastic-plastic and viscous response of the specimen.

Kolsky proposed a correction for radial inertia [**Kolsky 1959, 1963**],

$$\sigma_S = \sigma_b - \frac{1}{8}\upsilon_S{}^2 d^2 \rho_S \ddot{\varepsilon} \tag{2.25}$$

where $\sigma_S$ is the effective axial stress required to deform specimen in a one-dimensional stress state, $\sigma_b$ is the average stress measured in the two bars, and $\upsilon_S$, $\rho_S$, d, and $\ddot{\varepsilon}$ are correspondingly the Poisson's ratio, density, diameter and axial strain of the specimen. Davies and Hunter and Kolsky introduced the method of a set length-diameter ratio of the specimen to minimise friction and achieve early stress equilibrium in the axial direction [**Davies/Hunter 1963, Kolsky 1963**]. The corrections Davies and Hunter used were from an analysis by Siebel (1923) [**Davies/Hunter 1963**]. This was $(\mu d/3l)\updownarrow 1$, where $\mu$ is the coulomb friction coefficient and l the sample length. They added an axial correction to Kolsky's equation

$$\sigma_S = \sigma_b + \rho_S\left(\frac{l^2}{6} - \frac{\upsilon_S{}^2 d^2}{8}\right)\ddot{\varepsilon} \tag{2.26}$$

Other correction factors were introduced for friction, radical and axial inertia effects by Rand [**Rand 1967**] and Samanta [**Samanta 1971**]. A two-dimensional analysis by Bertholf and Karnes showed by using length-diameter of $\upsilon_S \sqrt{(3/4)} \approx 0.5$ (proposed by [**Davies/Hunter 1963**]) on a lubricated sample, then friction can be ignored [**Bertholf/Karnes 1975**]. For ductile plastically deforming materials, Poisson's ratio can be taken as 0.5. Therefore, the length-diameter ratio of at least 0.5 can be used to correct friction and inertia effects. This is true for both correction equations above, with the exception of the very early period of loading when the specimen has not yet reached stress equilibrium. This was also confirmed by Gorham [**Gorham 1989**]. The author also pointed out the usage of thin specimens for SHPB experiments. A thin sample shortens the time for equilibrium, and the attenuation of a stress wave would be less significant [**Song/Chen 2005**], so the effect of specimen thickness on dynamic stress equilibrium in soft rubber samples leads to the conclusion that a thick soft material may never reach equilibrium during the entire loading history. However, if the specimen is thin, the interfacial friction becomes more significant and potentially complicates the experiment when the rates of strain are high.

To eliminate friction effects in the analysis, a thin layer of grease is applied on the sample/pressure bar interfaces in order to avoid friction during the test. Trautmann et al. investigated several common lubricants and concluded which lubricant to use in order to obtain high quality data from SHPB experiments for the various temperatures and materials of interest [**Trautmann et al. 2005**]. Many experiments have been performed over the years to overcome the effects of friction and inertia in high rate testing, especially in SHPB tests. Without lubrication, friction can cause barrelling in the sample during impact. Also the coefficient of sliding friction for polymers is not a constant. The coefficient of friction decreases as the load is increased. It is also a function of temperature. Both these facts make validation of the resultant data by analytical methods difficult.

Briscoe and Nosker demonstrated a theoretical approximation treatment for the specimen/bar interface friction [**Briscoe/Nosker 1984**]. They first consider the equilibrium equation without body forces and internal stresses in cylindrical co-ordinates, with the z-direction in the cylinder axis,

$$\frac{\partial \sigma_r}{\partial r} + \frac{\partial \tau_{rz}}{\partial z} + \frac{\sigma_r - \sigma_\theta}{r} = 0 \tag{2.27}$$

The Von Mises yield criterion is

$$(\sigma_z - \sigma_r)^2 + (\sigma_r - \sigma_\theta)^2 + (\sigma_\theta - \sigma_z)^2 = 2\sigma_y^2 \tag{2.28}$$

where $\sigma_z$, $\sigma_r$, $\sigma_\theta$ and $\sigma_y$ are the z-direction stress, radical stress, hoop stress and the yield stress in the compressed specimen.

By assuming the friction coefficient $\mu$ is constant we have

$$\frac{\partial \tau_{rz}}{\partial z} = \frac{2\mu\sigma_z}{l_0} \tag{2.29}$$

Also assuming that $\sigma_z$ is a constant, and $\sigma_r = \sigma_\theta$, we can then say

$$\sigma_z - \sigma_r = \sigma_y \tag{2.30}$$

and therefore write Equation 2.27 as

$$\frac{\partial \sigma_z}{\partial r} = \frac{-2\mu\sigma_z}{l_0} \tag{2.31}$$

So stress in the z-direction becomes

$$\sigma_z = -\sigma_y e^{\{\frac{2\mu}{l_0}(a-r)\}} \tag{2.32}$$

The mean applied stress P at yield point is calculated by adding in the boundary condition $\sigma_z = \sigma_y$ at r = a,

$$P = \int_0^a \frac{2\pi\sigma_z dr}{\pi a^2} = \frac{\sigma_y l_0^2}{2\mu^2 a^2}\{e^{\{\frac{2\mu a}{l_0}\}} - \frac{2\mu a}{l_0} - 1\} \tag{2.33}$$

or

$$\frac{P}{\sigma_y} = \frac{l_0^2}{2\mu^2 a^2}\{e^{\{\frac{2\mu a}{l_0}\}} - \frac{2\mu a}{l_0} - 1\} \tag{2.34}$$

The ratio of the applied stress to the yield stress increases with $\mu a/l_0$. This means that with the increase of strain rate in the experiment, the friction becomes larger. If the friction coefficient becomes quite substantial, then $\sigma_z$ can not be considered constant throughout the contact between the bar and the specimen. Therefore, Equation 2.34 will not be valid.

In the experiments conducted in this work, lubricant has been applied at the specimen and bar interface to correct the friction error. Assuming that the coefficient of friction is constant and the lubricant viscosity is $\eta$, then the shear stress generated at the surface of the specimen in Equation 2.29 becomes

$$\tau_{rz} = \frac{\eta V_r}{h} \tag{2.35}$$

where $V_r$ is the radial velocity and h is the thickness of the lubricant.

During the compression, some of the applied lubricant is squeezed outwards, and the diameter of the specimen also increases. Taking into account these two velocities, if we see the specimen or the lubricant as an incompressible disk with total volume of $\pi r^2 b$, with b as the thickness of the disc, then the radical velocity becomes

$$V_r = \frac{r}{2}\frac{db/dt}{b} \tag{2.36}$$

So the maximum radial velocity in the SHPB test happens when the two split bar ends come together. This can be proven using a high speed camera.

The lubricant is considered to be isoviscous and isothermal. The Stefan equation is then applied:

$$\frac{dh/dt}{h} = \frac{2h^2 f}{3\pi\eta a^4} \tag{2.37}$$

where f is the compressive force between the two interface of the specimen and bars.

With polymer specimen thickness $b=h=l_0$, and replacing (db/dt)/b with axial stain rate $\dot{\varepsilon} = (dl_0/d\,t) / l_0$ from the SHPB theory, Equation 2.36 can be rewritten as

$$V_r = \frac{r}{2}\dot{\varepsilon} \tag{2.38}$$

Equation 2.35 as

$$\tau_{rz} = \frac{\eta r \dot{\varepsilon}}{2h} \tag{2.39}$$

and Equation 2.29 as

$$\frac{\partial \tau_{rz}}{\partial z} = \frac{\eta r \dot{\varepsilon}}{h l_0} \tag{2.40}$$

With the same method as above, stress and pressure can be calculated,

$$\sigma_z = \sigma_y + \frac{\eta \dot{\varepsilon}}{2 h l_0}(a^2 - r^2) \tag{2.41}$$

$$P = \sigma_y + \frac{\eta \dot{\varepsilon}}{4 h l_0} a^2 \tag{2.42}$$

In the table below, values of lubricant thickness h, specimen viscosity η, specimen thickness $l_0$, specimen diameter a are given with numbers used in the experiment with the four polymer materials studied. Using the values given, pressure under different strain rates for each material can be calculated using Equation 2.42 to consider the effectiveness when a thin layer of lubricant (h≈10 μm) is applied.

The lubricant effect on the SHPB strain readings, both during the elastic deformation and during viscous flow were also considered by Briscoe and Nosker [**Briscoe/Nosker 1984**]. It is assumed that the lubricant displacement during elastic shear is equal to the displacement as viscous flow with a given time interval

$$\Delta t = \frac{\eta}{G} \tag{2.43}$$

after onset of compression, η is the viscosity and G the shear modulus of the lubricant. An example given by the authors is the petroleum jelly with viscosity of 0.125 Pa.s after initial thinning. The sample compresses by 20% and average radius increased by 10%. This gives an average of 6000% strain into the lubricant. The shear modulus is 1 GPa, so $\Delta t = 1.25 \times 10^4$ μs. Therefore, the elastic shear is not an influence on high strain rate SHPB experiments.

| | η (Pa.s) | $L_0$ (mm) | $\sigma_y$ (MPa) | a (mm) | Strain rate | P |
|---|---|---|---|---|---|---|

| | | | | | $(10^3 s^{-1})$ | $(10^{15} Pa)$ |
|---|---|---|---|---|---|---|
| PMMA | $\sim 10^{10}$ | 5.00 | 346 | 10.00 | 3.92 | ~1.96 |
| PVC | $\sim 10^{10}$ | 3.00 | 115 | 6.00 | 5.79 | ~4.83 |
| PCTFE | $\sim 10^{10}$ | 3.00 | 125 | 6.00 | 3.75 | ~3.13 |
| PTFE | $\sim 10^{10}$ | 4.00 | 21.9 | 8.00 | 4.15 | ~2.6 |

*Table 2-1 Values of the four polymers to determine the pressure under highest strain rate to consider the effectiveness when applying a thin layer of lubricant.*

Note: The strain rate quoted is the largest strain rate tested at ambient temperature.

The next assumption made was that the lubricant displacement due to the elastic compression is equal to displacement during viscous flow over the time interval for h(=10 μm), a(=12.7 mm), η(=0.125 Pa.s) and bulk modulus as 2 GPa

$$\Delta t = \frac{3a^2\eta}{2h^2k} \tag{2.44}$$

Then using values for PCTFE, the time interval would work out to be Δt=151 μs.

In this case during the stress pulse, most lubricant displacement is by bulk rather than viscous flow, so the distribution of force would be uniform across the face of the specimen. The elastic compression of strain due to two sides of lubricant can be obtained by $\sigma_y h / k \approx 0.25$ μm for yield stress around 50 MPa. In a 6 mm thickness sample, the total strain caused by both side of the lubricant works out to be less than 0.01%. The total strain for which the two sides of lubricant are accounted for is small in comparison, and it is safe to conclude that the lubricant does not significantly affect the strain readings during SHPB experiments.

Different sizes of circular disc specimens were used in the experiments. In order to allow for the lateral expansion of the specimens when they were being

compressed, their initial diameters were made less than that of the bar, with the maximum diameter for each material determined by preliminary tests.

### 2.4.2 Equilibrium of specimens during impact

Specimens should achieve equilibrium for the stress-strain curve to represent the bulk properties of the material. To reach mechanical equilibrium is much harder for high strain rate tests than in low strain rates.

Once the compressive stress wave reaches the loading end of the specimen, it splits into reflecting and transmitting parts, depending on the elastic reflection coefficients of the bar and material. The reflecting tensile component travels back into the loading bar and the transmitting part into the specimen. At this point the front of the specimen meets the wave before the rear, and the specimen is not in equilibrium. The moment the wave reaches the rear of the material, the specimen reaches equilibrium state. But this does not last, a new reflection and transmitting wave is formed at the rear boundary. Both reflecting and transmitting components are compressive as the mechanical impedance of the specimen is less than that of the bar. Here the transmitting part forms the beginning of the transmitting wave and the reflecting part joins in with the compression wave travelling from the loading bar. The rear end of the specimen is at a higher stress than the rest of the specimen, and is again not in equilibrium. The schematic of developing stages of the waves along the loading bar , specimen and transmitting bar of equilibrium is illustrated in Figure 2.6.

However, beyond the yield point, the material can no longer take large increases of stress, and the specimen reaches the same stress. As long as the flow stress is a relatively weak function of time, the SHPB results are valid.

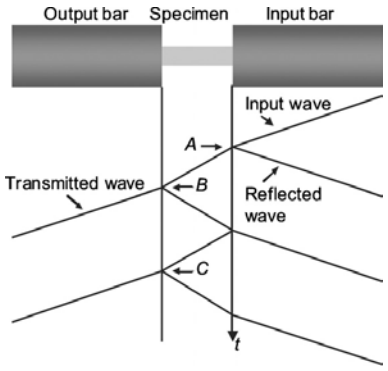


*Figure 2.6 Stages of development of the specimen's equilibrium states* ***[Siviour 2009].***

Calculations of reflecting and transmitting waves in a specimen before reaching yield point were conducted by Al-Maliky [**Al-Maliky 1997**]. The prediction of reflecting and transmitting coefficients at the boundary between bars was first described by Briscoe and Nosker using specimens of the same diameter as the Hopkinson bars [**Briscoe/Nosker 1984**]. More analysis was carried out by Parry et al.[**Parry/Walker/Dixon 1995**] with specimens of different diameters. The authors further applied this to the sharp rising and smooth rising loading pulses. The authors concluded that measurements before the yield point cannot fully give exact representation of what happens in the specimen. The specimen stress increases by the wave travelling away from the specimen bar. At the same time the bar stresses are influenced by the wave travelling towards the boundaries.

### 2.4.3 Specimen thickness

In the original SHPB paper by Kolsky he stressed the test is valid only if 'the thickness of the specimen is small compared with the wavelength of the shortest operative wave in the Fourier spectrum of the pulse' as this would ensure stress equilibrium within the specimen, and therefore the analysis of the SHPB technique would be justified [**Kolsky 1959**]. All specimen are made having length-diameter ratios of 0.5 (as discussed in section 2.4.1). Also the diameter of the specimens must be less than the diameter of the bars, which is less than 12.7 mm.

### 2.4.4 Preparation of specimen

The polymers bought for this study were supplied by Goodfellow™. The polymers came in long rods of different diameters. The specimens were machined on a lathe in the Physics Department mechanical workshop, during which a coolant was applied to ensure the temperature generated from the machine process would not interfere with the internal structure of the polymer specimen. Both flat end surface finishes of the specimens were smoothed. All specimens were treated with the same process to ensure they were identical.

Specimens were produced with the same ratio of diameter-length for data comparison purposes. The PMMA specimens diameters and lengths were 10.00(±0.01) mm×5.0 mm and 6.00 mm×3.00 mm, respectively PTFE specimens were of dimensions 8.00 mm×4.00 mm; PCTFE specimen size were 6.00

mm×3.00 mm; and PVC specimen size were 6.00 mm×3.00 mm. After cutting the specimens were then carefully sanded to ensure smooth parallel flat surfaces.

## 2.5 Other considerations for the SHPB experiment

To obtain valid results from the SHPB technique, some factors must be considered to maximise the accuracy in the stress-strain curves.

### 2.5.1 Specimen/bar interface area variation

The cross sectional area of the specimen increases during the impact, and both the interfaces of the specimen and bar increases. Also, the increase of interface area changes the rate of energy transmitting into the specimen, and increases the amount of wave reflecting back to the loading bar. These effects are taken into account in the SHPB analysis to obtain true stress and true strain of the specimen. It is also important to make sure that the cross sectional area of the specimen does not exceed that of the bar throughout the experiment.

### 2.5.2 Mechanical noise interference

In the SHPB theory, the system is pictured as a one-dimension system and dispersion is not considered. In the experiment dispersion in the longitudinal wave can causes noise within the system. The different frequency wave components travel at different speeds in the bars, with the lower frequencies travelling faster than the higher frequencies. This causes a change in shape of the reflecting and transmitting wave by the time it reaches the strain gauges, and influences the interpretation of the stress and strain representing the material. The rise time of the pulse is also different at the gauge than at the specimen.

### 2.5.3 Temperature rise during testing

At high strain rates the deformation of polymers becomes adiabatic rather than isothermal. The internal heat generated during the inelastic deformation process does not have time to dissipate, therefore the mean temperature of the specimen increases. This temperature rise can affect the stress in properties of the material and needs to be

taken into account when comparison is made with isothermal data. The elastic and plastic deformation region of a stress-strain curve is illustrated in Figure 2.7.

High strain rate deformation in materials such as polymers leads to the conversion of mechanical energy into heat. The converted heat could be localised within crack tips or on shear planes or it could be a uniform temperature rise in the whole sample. Swallowe et al measured the bulk temperature rise with a heat sensitive film [**Swallowe/Field 1982**]. The higher the rate of strain, the higher the temperature rise, which sometimes will be high enough to produce strain, softening. The bulk temperature rise can be estimated by measuring the area under the stress-strain curve.

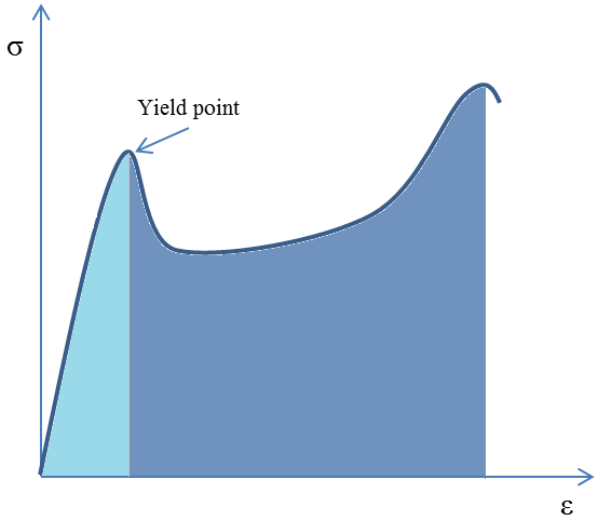


*Figure 2.7 A stress-strain curve showing elastic deformation region, yield point, and plastic flow area.*

Stress and strain is expressed as in section 1.2 as the energy per unit volume due to the plastic deformation in the sample is

$$\therefore \int_C \sigma d\varepsilon = \frac{W_C}{V_S} \tag{2.45}$$

$W_C$ is the work done in the area under the stress-strain curve (work done = force × distance), $V_S$ is the unit volume of the specimen. From the definition of specific heat

$$\Delta Q = mc_p \Delta T \tag{2.46}$$

where ΔQ is the heat supply with in the system, which is also equal

$$\Delta Q = mW_C \tag{2.47}$$

From Equation 2.46 and 2.47 work done can also be related to temperature change as

$$W_C = c_p \Delta T \tag{2.48}$$

$$\therefore \Delta T = \frac{W_C}{c_p} \tag{2.49}$$

Temperature rise in the specimen at plastic flow equals the work done by force divided by the specific heat of the material. As demonstrated in Equation 2.45, the area under the stress-strain curve can also represent the work done to the material per unit volume. Thus,

$$\Delta T = \frac{\int \sigma d\varepsilon}{c_p} \tag{2.50}$$

The specific heat of the polymers is obtained by the DSC method (see chapter four). By calculating the area under a stress-strain curve after yield in increments, this leads to calculation of temperature rise in the plastic flow region of the compression test as a function of strain [**Ward/Sweeney 2004**]. The results are presented and discussed in chapter five and six. To include the stored energy, the real value of the temperature rise is typically 0.8 of the calculated value. In taking account of this, the results obtained from the temperature rise calculation compared to the experimental data for temperature rise agrees with each other.

### 2.5.4 High temperature tests

There are some problems which need to be addressed when testing at non-ambient temperatures with the SHPB. The elasticity of the bars changes with temperature. This would affect the particle velocity at the end of the bar by changing the force given. It would also mean the elastic waves propagating though the heated bar would be distorted differently in comparison to a uniform room temperature rod bar, and part of the input pulse might be reflecting as a result of the temperature gradient. Different methods to overcome these problems have been suggested. Bacon

et al. [**Bacon et al. 1993a**] showed the error in the calculation of the force on a specimen, with rises of 1.5% giving a temperature difference of 125ºC, and 12% for 1000ºC. This was calculated from the temperature distribution and the rod was divided into 80 parts. In this study, with heating up to only 100ºC using steel rods, it is safe to say that the thermal gradient in the bars has a very small distortional effect on the measurement of the stress pulse (which is smaller than the experimental error). Walley et al examined the bar pulses obtained from room temperature to when the tip of the bar was at -155ºC and 550ºC, and reported no visible distortion of the pulses [**Walley/Balzer/Proud/Field 2000**].

Others have considered using specific alloys over a range of temperatures (-200ºC to 600ºC) at which the chosen alloy has low mechanical impedance [**Kandasamy/Brar 1994**]. Walley added a comparison of stainless steel Hopkinson bar to the alloy at room temperature, from which he favoured the stainless steel to the alloy rod at cryogenic temperatures. Another alterative is to heat only the specimen and not the bar. This method has been used by Sizek and Gray III with test temperatures up to 1200ºC [**Sizek/Gray III 1993**]. If the test temperature is above 600ºC, this method might be the best experimental solution as the effect of a temperature gradient in the rods would be too great to dismiss. Many authors have also calculated the effect of temperature gradient on the wave propagation for tests conducted at temperatures above 600ºC. The disadvantage of this method occurs when the specimen is heated (or cooled) rapidly which means the heat flux in the bar would vary from test to test. Thus, how well the approximation of the function of temperature distribution would fit is questionable.

A comparison of the pulses obtained when the whole test was conducted under room temperature with those when the tip of the bars attached to the specimen are heated would be a way to understand whether stress pulses propagated from incident and transmission bars though a temperature gradient without large distortion. The main changes from room temperature testing to tests at 100ºC are that the noise and fluctuations of the pulses are greater at higher temperatures (see chapter five figures for pulses produced at different temperatures), but no obvious pulse dispersion can be recognised.

# Chapter Three

# Materials

The mechanical properties of polymers can be described by a wide range of behaviours. Some behaviour are the result of unique chemical composition and physical structure at the molecular level, while other behaviours are due to the general viscoelastic behaviour shared by this group of materials. The latter was discussed in chapter one. Here, we describe the unique individual microscopic structure of the four polymers and the way this contributes to the mechanical behaviours. The brief background to the materials chosen for analysis and previous investigations of polymers under the same name are also summarised. Nevertheless, polymers which bear the same commercial name are not identical.

## 3.1 Choice of materials

The four materials chosen for investigating the high strain rate mechanical properties of polymers are polychlorotriflouoroethylene (PCTFE), poly-tetrafluoroethylene (PTFE), polyvinylchloride (PVC) and polymethylmethacrylate (PMMA). The four polymers are chosen due to the range of crystallinity, glass transition temperatures, and the basic unit structures of the polymers. The unit chemical composition of the four polymers tested are presented in Figure 3.1. PCTFE, PTFE and PVC all have glass transition temperature in the temperature range of the experiments (ambient temperature to 100ºC). Image of the four materials can be found in Figure 3.2. PMMA is transparent, good evidence of amorphous. Polymers appear transparent or colourless because it absorbs electromagnetic radiation in the infrared and ultraviolet regions, and all visible light travels though the material without alteration. In the case of PCTFE, the light is appreciably scattered, the specimen appears translucent and colourless, somewhat ‘milky’. Higher contents in crystallinity polymers with structures of the size close to the wavelength of light will scatter most light. However, PVC specimens used in this work appears gray due to absorbing light

at most visible wavelengths by the adjacent double bonds in the long chains, not higher crystallinity.

The aim is to give some individual detail of the four chosen polymers. The content of this chapter includes basic chemistry, mechanical properties, processing methods, applications, and recent developments concerning these four materials.

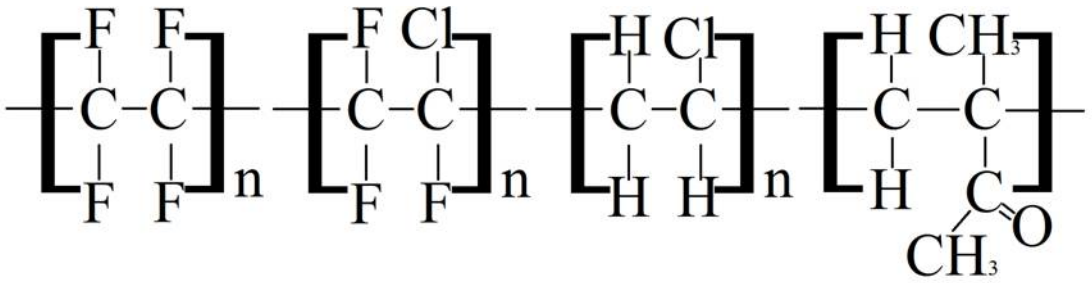

*Figure 3.1 Unit chemical structures of the four polymers chosen for this study. (Left to right) polytetrafluoroethylene (PTFE), polychlorotrifluoroethylene (PCTFE), polyvinylchloride(PVC), and polymethyl methacrylate (PMMA).*

PTFE and PCTFE are in the fluoroplastics group. This is a unique group of plastics which are widely used in industries. Fluoroplastics are defined as a family of thermoplastic resins analogous to polyethylene in which some or all the hydrogen atoms attached to the carbon chain are replaced by fluorine. In general, they exhibit properties of chemical inertness, non-wetting surfaces, low coefficients of friction and resistance to elevated temperatures. Specific properties depend on the structure of the polymer. The main factor for the properties is the very high strength of the C-F bond. The mutual repulsion of fluorine atoms tends to inhibit the bending of the chain backbone, which makes the polymers very stiff. The outer sheath of fluorine atoms protects the carbon backbone which provides the chemical inertness and stability. It lowers the surface energy, hence giving low coefficient of friction. High molecular weight results in high melting point; this suppresses a normal crystal growth and affects the crystallisation rate.

PCTFE contains a chlorine atom in the place of one fluorine atom in PTFE. The chlorine atom promotes the attractive forces between molecular chains, and because of the chlorine atom has a bigger radius it hinders the close packing found in PTFE, as a result PCTFE has a lower melting point and reduced propensity to crystallise.

Mechanical properties of fully fluorinated polymers (in comparison to the fluorinated polymers with hydrogen atom in the structure) exhibit greater elongation and higher working temperature, but are less strong and stiffer. PCTFE has better mechanical properties than PTFE because the presence of the chlorine atom in the molecule promotes the attractive forces between molecular chains. It also exhibits greater hardness, tensile strength and considerably higher resistance to cold flow than PTFE. PTFE exhibits poor optical properties because of its high degree of crystallinity.

*Figure 3.2 Untested cylindrical polymer specimens that have been prepared for high strain rate experiments using the SHPB technique. From left to right the specimen materials are PCTFE, PTFE, PMMA, and PVC.*

PVC and PMMA are both vinyl polymers. This group of polymers have the general formula $(CHX\text{-}CH_2)_n$ where X is a chlorine atom for polyvinylchloride (PVC). A more complicated vinyl polymer is the polymethylmethacrylate (PMMA) with the formula where X is a methyl group and Y is the methacrylate group. Both types of vinyl polymer could have different kinds of irregularity (i.e. the possible ways to join the adjacent monomer units, head-to-tail, head-to-head, and tail-to-tail), and configurational isomerism (isotactic, syndiotactic, atactic). [**Bower 2002**]

The possibility of PVC to be syndiotactic, illustrated in Figure 3.3a, is very low. Commercial PVC are usually atactic (Figure 3.3b), therefore, PVC is usually poor in forming crystallites. PMMA is also atactic, also with the large side group. PMMA cannot form crystallites and is a glassy amorphous polymer. The irregularity of atactic vinyl polymers lead to lowering of crystallinity and melting point.

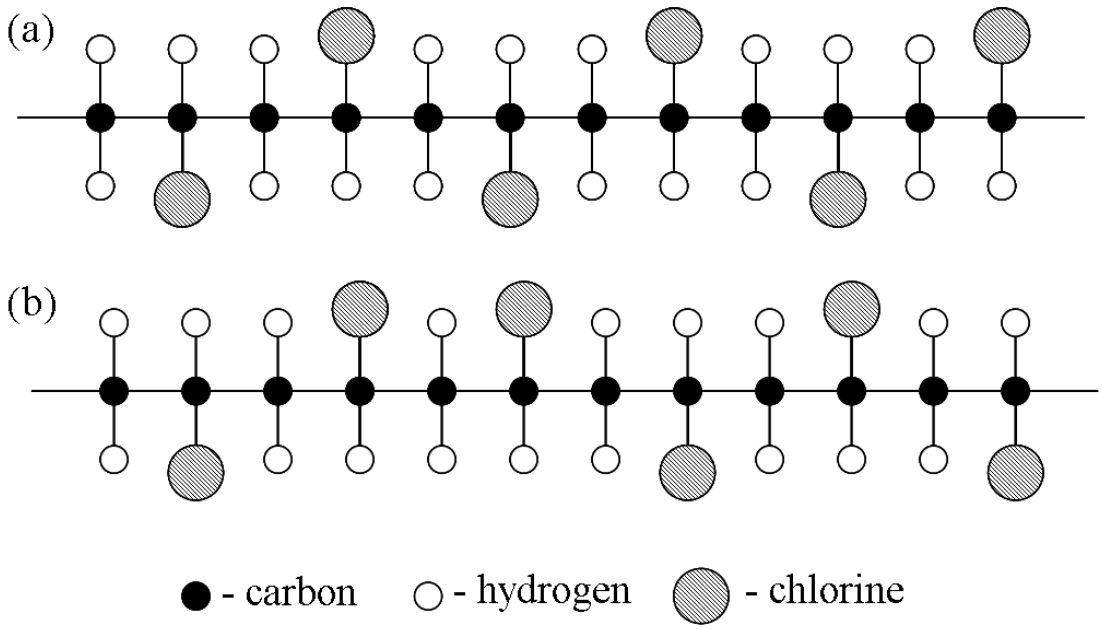


*Figure 3.3 Possible irregularity of vinyl polymer, illustrated by two different configurations. (a) regular syndiotactic, and (b)random atactic.*

The materials used in the experiments are provided by Goodfellow™, The general thermal and mechanical properties of the polymers are given in Table 3-1.

| | $T_M$ (°C) | Commercial names | Density (g $cm^{-3}$) | Specific heat (J $K^{-1}$ $kg^{-1}$) | Elongation at breaking (%) | Tensile modulus (GPa) | Poisson's ratio | Appearance |
|---|---|---|---|---|---|---|---|---|
| **PCTFE** | - | Kel-F Neoflon | 2.10-2.14 | 900 | 80-250 | 1.3 – 1.8 | - | High optical transparency |
| **PTFE** | 327 | Fluon, Hostaflon TF | 2.20 | 1000 | 400` | 0.3 – 0.8 | 0.46 | Semi opaque |
| **PMMA** | - | Diakon, Lucite, Oroglas, Perspex, Plexiglass | 1.19 | 1400 - 1500 | 2.5-4.0 | 2.4 – 3.3 | 0.35 – 0.40 | Transparent, colourless |
| **UPVC** | - | Corvic, Evipol,Geon, Hostalite, Lucorex | 1.40 | 1000 - 1500 | 60 | 2.5 – 4.0 | - | Pigmented (can be transparent) |

*Table 3-1 Properties of the four polymers (polytetrafluoroethylene, polychlorotrifluroethlene, polyvinyl chloride and polymethyl methacrylate) tested in this work.*

## 3.2 PTFE

Polytetrafluoroethylene (PTFE) is a semi-crystalline polymer, better known as Teflon. PTFE can be thought of as a two-phase structure, with rigid crystalline phase in a matrix of a softer amorphous phase, and by increasing the crystallinity of the

sample, the material strengthens. The crystalline phase has been shown to be related to whether PTFE is brittle or ductile. PTFE is chosen in applications for its low coefficient of friction and resistance to wear and chemical corrosion.

The density of PTFE undergoes complicated changes during processing and can be monitored by the values of true specific volume. Discontinuities in such data show transitions at 19ºC and 30ºC and then at crystalline melting point. The coefficient of linear expansion of PTFE has been determined at temperatures ranging from -190 to 300ºC. The transition at 19ºC is of great consequence because it occurs around ambient temperature and significantly affects the behaviour. Above 19ºC, the triclinic pattern changes to a hexagonal unit cell. Around 19 ºC, slight untwisting of the molecule from a 180 degree twist per 13 $CF_2$ groups to a 180 degree per 15 $CF_2$ groups occurs. At the first order transition at 30ºC, the hexagonal unit disappears and the rod-like hexagonal packing of the chains in the lateral direction is retained. Below 19ºC there is almost a perfect three-dimensional order (triclinic). Between 19ºC and 30ºC the chain segments are disordered. And above 30ºC the chain segments are disordered. Above 30ºC the material preferred crystallographic direction is lost and the molecular segments oscillate above their long axes with a random angular orientation. Specific combinations of temperatures and mechanical or electrical vibrations can cause wide fluctuations in the values of the dissipation factor.

The mechanical properties of PTFE at room temperature are similar to those of medium-density polyethylene. Both are relatively soft with high elongation. The mechanical properties remain at useful levels over a wide range of temperatures. The stress strain curves of PTFE are strongly affected by temperature. However, even at 260ºC (recommended upper temperature) its compressive strength is about 34.5 MPa.

Under a sustained load PTFE will creep, which imposes limitations on PTFE applications. This tendency can be greatly reduced by the addition of mineral fillers. The fillers also improve its wear resistance, but have no additional effect on its tensile strength. Fillers can improve impact strength but reduce elongation.

There already exists literature containing studies of the compressive properties of PTFE over a range of strain rates and temperatures [**Rae/Dattelbaum 2004**]. There are two points which the work by did not consider. First the importance of the process history of PTFE samples before testing. The process of sample preparation can make a difference to the crystallinity of the sample, which will change its strength and deformation properties. Second, observing the intense increase in yield stress at high

strain rates. Jordan et al. suggested that annealed PTFE had lower crystallinity and yet showed anomalously higher strength than the extruded, as-received without annealing, PTFE [**Jordan et al. 2007**]. This contributed to the orientation of the polymer chains during the extrusion process.

## 3.3 PCTFE

Polychlorotrifluoroethylene (PCTFE), also known by its trade name Kel-F81, is a semi-crystalline fluoropolymer which has been employed in a wide range of cryogenic components, seals, valve seats, and microelectronics packaging.

For PCTFE the work highlighted in the literature is more focused on the adhesive properties due to its common industrial use. The knowledge of its high strain rate mechanical behaviour is still limited. McCrum et al. investigated the effects and crystallinity on small strain behaviour of PCTFE with a dynamic mechanical analysis (DMA) [**McCrum/Buckley/Bucknall 2003**]. The crystal structure was studied by Mencik [**Mencik 1973**] and the glass transition temperature ($T_g$) has been analysed by a number of authors: Hoffman ($T_g$ = 52ºC), Privalko ($T_g$ = 64ºC), Khanna/Kumar ($T_g$ = 75ºC), and Chang/Bestul ($T_g$ = 47-77ºC depending on crystallinity). [**Hoffman 1952, Privalko 1998, Khanna/Kumar 1991 and Chang/Bestul 1974**]

The influence of temperature and strain rate on the constitutive and damage responses of PCTFE was reported by Brown et al. **[Brown/Rae/Orler 2006**]The compressive yield strength is highly dependent on temperature. Although the loading modulus is higher for lower temperatures, the increase in yield stress is more dominant, leading to associated increases in yield strain. However, for higher rates the data was not complete due to experimental instrument limitations.

Different methods of measuring crystallinity have been compared by Murthy et al. [**Murthy/Grubb 2002**]. The inclusion of the relatively large chlorine molecule into the polymeric chain reduces the tendency to crystallise. As long as the thermally induced crystallisation is avoided, PCTFE exhibits excellent mechanical properties. It also has excellent resistance to creep.

PCTFE is suitable for work under extremely low temperatures. However, at elevated temperatures it is less favourable than most other fluoroplastics, with its relatively low melting temperature of 211ºC, and the material shows thermally induced crystallisation at temperatures below its melting point. This results in

brittleness. PCTFE can be modified by the addition of glass fibres. This improves high temperature properties and increases hardness, but also increases brittleness.

## 3.4 PVC

Poly vinyl chloride (PVC) was discovered by Regnault in 1835, and largely developed in the 1940s. PVC is used as a rigid material for making mouldings. Also when plasticised, giving more flexibility, it also is make into tubing and fake leather. It can be made into syndiotatic PVC (see Figure 3.3a) with a special polymerisation technique, otherwise PVC is very nearly atactic (see Figure 3.3b) therefore would only crystallise very slightly, with crystallinity degree of 0%-10%. [**Bower 2002**]

PVC has limited operational temperature range, becoming brittle at 5ºC (unless modified) and upper continuous use temperature of 50ºC. As additive-free PVC begins to decompose before it melts. Applications of PVC are normally made from plasticised grades or cross-linked PVC. (The cross-lined grade is for minimum flammability.)

## 3.5 PMMA

Perspex, commercial sheeting of poly methyl methacrylate was produced in 1936. In 1959, Kolsky investigated the dynamic elastic properties of various materials using the SHPB, amongst which was PMMA [**Kolsky 1959**]. The stress-strain behaviour was recorded, with overall strain reaching 0.02. By altering the thickness of the cylindrical specimens the author calculated the velocity of the pulse propagating though the PMMA specimen. The velocity reported corresponds to Young's modulus of $6.89\times10^3$ MPa. Another detailed research in the stress-strain properties of PMMA was carried out by Chou et al along side other polymers, over a range of strain rates. The mechanical strength was plotted as a function of strain rate and they reported yield stress increases with increasing strain rate. This was in agreement with the results of Briscoe and Hutchings [**Briscoe/Hutchings 1976**] in HDPE. In his classic paper, Kolsky reported that in the SHBP experiment the transmitting pulse was flatter in shape, longer in duration and much smaller in amplitude than the initial loading pulse.

During the initial loading phase, the material exhibits nonlinear viscoelastic behaviour. At small strains of less then 3%, the elastic behaviour is linear. The elastic region is the result of intermolecular interactions between chains under van der Waals forces, where the chain segments partially rotate and slide with respect to each other. As the stress level increases, more localised regions develop within the bulk material, where the stress is large enough to overcome the secondary intermolecular forces and the chains rotate and slide to a new position. At this point, the response now becomes non-linear as the slope of the stress-strain relationship decreases. Eventually, enough localised events have occurred and percolated through the material such that the entire material yields in plastic deformation, permanently, and flows without a further increase in stress. This is marked in the stress-strain curve as the yield point of the polymer.

Once the polymer reaches yield, the material exhibits strain softening; i.e., the decrease of stress needed to further deform the polymer. At this stage, the intermolecular barriers to chain segments rotation decreases with plastic strain. This means the plastic straining process produces local structural changes in the material. These structural changes, during lower stress, make local chain-segment rotation easier. With the increase of plastic deformation, the chain segments rotates gradually and the network of chain structures move from an initial isotropic random configuration to a molecule oriented network with the chains well aligned in the direction of greater deformation. In the case of compression tests, the chains are equi-biaxial aligned in the plane perpendicular to the compression axis. With increasing plastic straining, entropy of the polymer decreases. Once the segments are aligned the polymer reaches its maximum stretch limit, which is what causes strain hardening in amorphous polymers. This is visible in the stress-strain curve, where the strain hardening takes over and brings the stress above the level of the yield point.

# Chapter Four

# Thermal characterisation of polymers

## 4.1 Introduction to thermal analysis

Thermal analysis is a range of techniques which measures physical properties of materials. The measurements are made as a function of time or temperature. Polymers are viscoelastic materials which display a strong dependency on time and temperature. Thermal analysis of the polymer of interest informs behaviour related to chemical composition and physical structure.

A list of commonly used thermal analysis along with properties measured is presented in Table 4-1. A thermal analysis experimental system can possibly conduct more than one of the techniques. Computer programs used to interpret data into behaviours are most often also provided by the manufacturer. Both dynamic mechanical analysis (DMA) and Thermal mechanical analysis (TMA) techniques measures the mechanical properties of materials. TMA applies a constant static force and measures the change in the material as time or temperature varies. The changes in dimensions are reported. DMA applies an oscillatory force at chosen frequencies and the changes in stiffness and damping is reported. Both identify transitions, but DMA is a more sensitive technique.

DMA measurements are made continuously with heating rate linear to time, although this is not always necessary and the heating rate can be designed to slow down at a temperature range of interest. The result is a characteristic thermal curve. The features of the curve, i.e. peaks, slope, discontinuity, etc., related to the thermal events within the sample. The curve is different in shape for different types of polymers: amorphous (glassy) polymers, semi crystalline polymers and elastomers (cross-linked amorphous polymers).

In this study the DSC and DMA methods are used to analyse the four polymers of interest. DSC will present the transitions of the polymers within the temperature range of the study. The results from the DSC will be temperature

dependent without any dynamic influence. The pressure in the test chamber is kept constant during the experiment. It is useful to scan the untested polymers in the test temperature range before carrying out any mechanical testing to understand how heat affects the samples at different temperatures. DMA will give information of the viscoelastic character of the polymers; this is conducted in two different time bases to detect time dependency of the phase changes.

| Abbreviation | Technique | Properties measured |
|---|---|---|
| DMA | Dynamic mechanical analysis | Mechanical properties |
| DSC | Differential scanning calorimeter | Enthalpy |
| DTA | Differential thermal analysis | Temperature |
| TG | Thermal gravimetry | Mass |
| TMA | Thermomechnical analysis | Mechanical properties |

*Table 4-1 Commonly used thermal analysis methods for soft materials and the particular properties measured.*

The mechanical properties of polymers are described by their elastic parameters (the three moduli) and Poisson's ratio. These parameters are interrelated. Therefore, theoretically if two are known then the other two can be calculated. The nature of the modules, which is the ratio between stress and applied deformation, depends on the nature of deformation. The three elementary modes of deformation are compression, tensile and shear. K, E, G respectively. The definition of the elastic parameters and the mode of deformation are presented in Table 4-2.

In the high strain rate compression tests conducted in this study, the polymers experience deformation in the same manner as the tensile modulus or Young's modulus, E, detected using the DMA method. The Young's modulus can also be measured from the initial slope in a stress-strain diagram. This would be true to both quasi static or dynamic techniques since the extension/compression deformations occur at almost constant volume. The values of moduli for polymers obtained by different techniques do not always agree in the literature for polymers. This is because polymers are not truly elastic, but a viscoelastic material, and therefore do not reach

equilibrium in the high frequency adiabatic techniques. At high frequencies viscoelastic materials behave more elastic and less viscous. Thus, when quoting a transition temperature/ temperature range it is important to also state the strain rate/ frequency of the tested material.

| Mode of deformation | Elastic parameters | | Definition |
|---|---|---|---|
| Isotropic | Bulk modulus | K | $\frac{\text{hydrostatic pressure}}{\text{volume change per unit volume}} = \frac{Pv_0}{\Delta v}$ |
| Shear | Shear modulus | G | $\frac{\text{shear force per unit area}}{\text{shear strain}} = \frac{\tau}{\gamma}$ |
| Uniaxial extension | Young modulus | E | $\lim_{L \to L_0} \frac{\text{force per cross section area}}{\text{strain}} = \lim_{\varepsilon \to 0} \frac{\sigma}{\varepsilon}$ |
| - | Poisson ratio | $\upsilon$ | $\frac{\text{change in width per unit width}}{\text{change in length per unit length}} = \frac{\text{internal contraction}}{\text{axial strain}}$ |

*Table 4-2 The definition of the elastic parameters and mode of deformation for the three elementary modes of deformation compression, tensile and shear ( K, E, G respectively). The definition of Poisson ratio is given.*

## 4.2 Introduction to DSC

The differential scanning calorimetry (DSC) monitors heat effects as a function of temperature. The heat effects in the materials indicate phase transitions and chemical reactions. During the test, the difference in the heat flow between the sample and a known reference is recorded as a function of temperature. The temperature increase/decrease of the sample and reference is kept at a constant rate. Due to the constant pressure of the test, the heat flow measured can be the equivalent of the enthalpy change in the material.

$$(\frac{dq}{dt})_p = \frac{dH}{dt} \tag{4.1}$$

The right hand side of Equation (4.1) is the heat flow measured. The difference in heat flow between the sample and the reference can be described as

$$\Delta \frac{dH}{dt} = (\frac{dH}{dt})_{sample} - (\frac{dH}{dt})_{reference} \tag{4.2}$$

This can both be positive or negative. During most phase transition changes the heat flow to the specimen is lighter than the reference, resulting in a positive difference. On the other hand, the process is exothermic in the case of crystallisation, cross-linking process and oxidation reactions, Δ(dH/dt) is found to be negative.

The setup of DSC consists of two holders; in each is a heater and temperature sensor. The holders are powered separately to hold the sample and reference at the same temperature during the test. A typical DSC scan heat curve is illustrated in Figure 4.1.

Ideally, the DSC scan is done before further mechanical testing studies of the material. This is useful for setting upper temperature limits. For example by obtaining the decomposition temperature of the polymer, one can then calculate, for the SHPB tests, the upper limit of the specimen cylindrical cross section area during the experiment and make sure it is within the cross sectional area of the bars, otherwise the result becomes invalid. Also, it is important to know the melting point of the sample in DMA tests to avoid damaging the set up.

During the DSC test, the peaks with positive and negative Δ(dH/dt) are recorded, and this locates all the heat effects in the test range. The peaks are associated with a specific process in the polymer structure i.e. crystallisation, melting or the glass transition, illustrated in Figure 4.1. The peak temperature is the point at which the maximum reaction rate occurs. By integrating the peak found, the total enthalpy of transition change is known

$$\int \left( \frac{dH}{dt} \right) dt = \Delta H \tag{4.3}$$

The glass transition temperature ($T_g$) is indicated by a change of baseline, as is illustrated in Table 4-1. This is due to the change in heat capacity. The $T_g$ is of great importance in the study of polymer properties, because within a few degrees of $T_g$, the

specific heat, the coefficient of thermal expansion, and the free volume all changes rapidly. Understandably, the mechanical properties of polymers also changes near $T_g$.

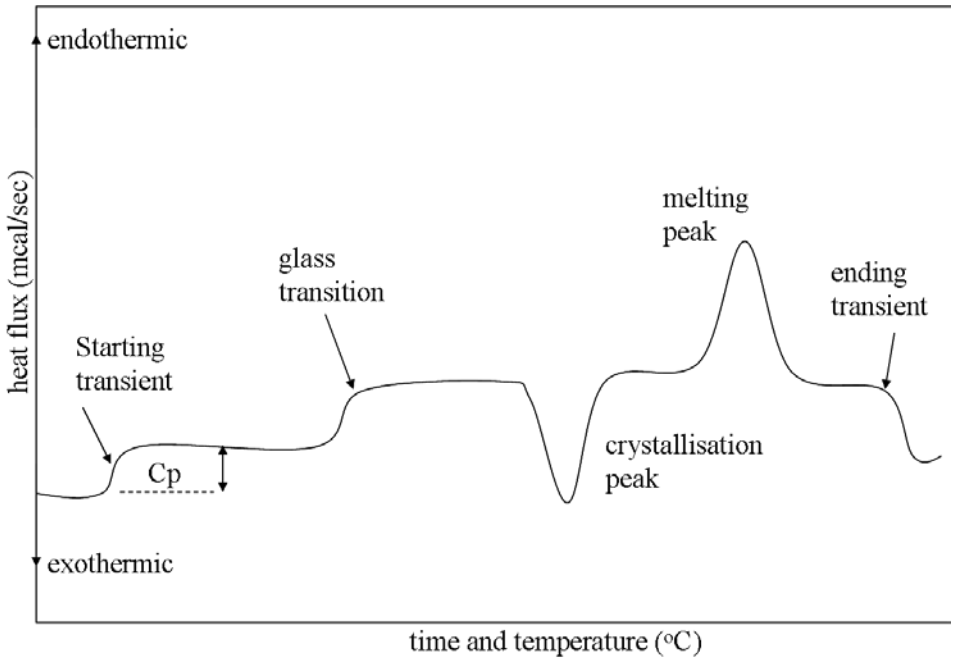


*Figure 4.1 Typical features seen in DSC scans. The baseline shifts at the starting temperature, and the heat capacity of the sample can be calculated. A shift during the test can be interpreted as the glass transition temperature. Crystallisation is an exothermic process while melting is an endothermic process. ΔH is calculated by the area of the peaks. In most cases, not all the feature in this plot can be found in one polymer.*

## 4.3 DSC Experimental procedure and data analysis

The model used to analyse PCTFE, PTFE and PVC is the DSC1 made by Metter-Tolendo. Data collecting and recording is done by the STARe software provided by the same company. The experiment temperature limits are -150ºC to 500ºC. The equipment allows two modes of testing, the dynamic segment heats the sample in the heating rate of choice, and the isothermal segment allows the sample to be held at a certain temperature for a desired period of time.

The samples are prepared by first cutting the polymer weighing between 7.0 and 15.0 mg. The samples are contained in a crucible during the thermal analysis measurement. The material of the crucible needs to have good thermal conductivity, ensuring optimum heat transfer. It should not exhibit any physical transitions in the

temperature range used with high melting point. And the material should not interact with the sample. The crucible used in this analysis is aluminium. The lid of the crucible is cold welded on to the pan containing the sample. Once the sample is sealed inside a hole (approximately 1.0 mm) is punched on the lid so the atmosphere in the pan is the same as the furnace. This allows thermal expansion and gases to escape, thus preventing rupture, at the same time the substance stays in the container. The empty crucible is weighed, and weighed again containing the sample. The reference is weighed and the DSC is calibrated in advance. There is no need to repeat this each time.

The heating curve of the measured sample is evaluated using the software provided by the manufacture. The results and analysis of the heat curve is presented in chapter five. For PCTFE the results and analysis can be found in chapter five, section 5.1.4, PTFE in section 5.2.4, PVC in section 5.3.4, and PMMA in section 5.4.4. Then further discussion is presented in chapter six.

## 4.4 Introduction to DMA

Dynamic mechanical analysis tests the response of a sample by applying small deformation in a cyclic manner. DMA is also called DMTA for dynamic mechanical thermal analysis.

A sinusoidal deformation is applied by the DMA to a sample of known geometry. The amount of sample deformed under a known stress is related to its stiffness. DMA measures the stiffness and damping, which are reported as modulus and loss angle. Because the force applied is sinusoidal, the modulus can be expressed as an in-phase component (the storage modulus) and an out of phase component that is known as the loss modulus.

The storage modulus is the measurement of the sample's elastic behaviour. The ratio of the loss to the storage is the loss angle, also called damping. This measures the energy dissipation of the sample under cyclic load. It illustrates how much energy is lost by the tangent of the phase angle, which shows how well the sample will perform at absorbing energy. Naturally, loss angle varies with temperature and frequency.

Modulus values change with temperature. This allows transitions in the sample to be detected as changes in the modulus and loss angle curves Phase

transitions of the same nature as the glass transition temperature can be detected this way. The moduli of the four polymer samples are plotted in this chapter, section 4.6.

The instrument used was calibrated for both temperature and force, and the sample prepared with even thickness, parallel sides, and right angle to insure a reasonable outcome.

The glass transition temperature is detected in the storage modulus as a large drop in decade (can be more than one). Other than the value of the onset of the storage modulus, the glass transition temperature is more commonly reported as the peak of loss angle. The active energy of the glass transition is usually a decade larger than the next secondary transition energy.

Dynamic mechanical analysis is introduced to investigate the relationship between time and the temperature dependence of the material behaviour. This is done though the measurement of the viscoelastic behaviour and rate-dependent elastic-plastic stress-strain behaviour of polymers. Transitions of the four polymers are measured at moderate and high strain rates to detect the shifts in the transition location in relation to temperature or strain rate.

Viscoelasticity is a combination of viscous and elastic behaviour. The viscoelastic transitions of polymers are usually denoted as $\alpha$, $\beta$, $\gamma$, $\delta$, etc. in the order pertaining to decreasing transition temperature. The transitions in the glassy region are difficult to determine as the time needed for such a transition will be very small. For that reason, use is made of dynamic mechanical measurements as a function of frequency to elucidate the modulus temperature curves, especially in the glassy region. Another advantage of this method is that the elastic and viscous forces are separated. The first transition lower than the melting point is the $\alpha$-transition, which is also known as the glass transition temperature ($T_g$), were the amorphous polymer or the amorphous part of a semi-crystalline polymer changes from a glassy to a rubbery state with the increase of temperature. All other transitions are the secondary transitions, where the change in material is relatively small to that of $T_g$.

Glass transition temperature on a molecular level is related to the cross-linking of the main polymer chain segments, and above this temperature the segments are completely free. Characterisation of other transitions is more dependent on the structure of the polymer molecule. $\beta$-transition, in PMMA, for example has been linked to the rotational freedom of the ester side group **[Swallowe and Lee 2003]**. As

the transitions are dependent on the particular polymer, each transition in the polymer has also shown its own rate-dependency. Therefore, the observed transition temperature depends very much on the strain rate of the experiment.

DMA testing will quantify the shift in transition temperature of the polymers of interest, describing the elastic modulus of the polymers at different rate and temperature.

In general, the DMA instrument applies oscillatory loading in the form of tension, compression, shear or three-point-bending though displacement, strain or force control. The responses of the sample to the loading are two-fold. The elastic, solid-like character of the polymer is in phase with the loading, whereas the viscous, liquid-like character of the polymer is out of phase with the loading. The storage modulus and loss modulus can be calculated from the two phases measured.

A sinusoidal loading under strain control can be described as

$$\varepsilon(t) = \varepsilon_0 \sin \omega t \tag{4.4}$$

where $\widehat{\ }_0$ is the strain amplitude and ω is the oscillation frequency. The stress response to the loading can be split into two components

$$\sigma(t) = \sigma_0 \sin(\omega t + \delta) = \sigma_0 \cos\delta \sin \omega t + \sigma_0 \sin\delta \cos \omega t \tag{4.5}$$

where $\sigma_0$ is the stress amplitude of the oscillation response, and δ is the phase shift of the viscous response. Equation (4.5) can be rewritten to incorporate the storage and loss modulus,

$$\sigma(t) = \varepsilon_0 E' \sin \omega t + \varepsilon_0 E'' \cos \omega t \tag{4.6}$$

where

$$E' = \frac{\sigma_0 \cos\delta}{\varepsilon_0} \tag{4.7}$$

and

$$E'' = \frac{\sigma_0 \sin\delta}{\varepsilon_0} \tag{4.8}$$

E' is the elastic component which is known as the storage modulus, it measures the energy stored during viscoelastic deformation. And E" is the viscous component or the loss modulus, where the energy dissipated during viscoelastic deformation is measured. δ is the phase difference, known as the loss angle. And the loss angle can be calculated from

$$\tan\delta = \frac{E''}{E'} \tag{4.9}$$

The storage modulus, loss modulus and loss angle as a function of temperature is traced at different rates of frequency to show the shift in the polymer transitions. In every dynamic transition region, there is a certain fall of the moduli, in many cases accompanied by a definite peak of the loss angle δ. Figure 1.6 is the schematic of the change in elastic modulus though the transition temperatures in a polymer.

It is common practice to test the specimens on DMA first when studying high strain rate mechanical properties. The DMA results give an insight to the structure of polymer at a particular temperature and frequency. Usually more than one frequency is tested to give an idea of how the transition peaks are detected with a shift in temperature and change in magnitude [e.g. **Siviour 2005**].

## 4.5 DMA experimental methodology

The four polymers studied in this work were all tested with a Dynamic Mechanical Analyser (DMA) for dynamic mechanical and thermal analysis to locate transitions. The polymer samples used in the DMA experiments were machined from the same sample rods which were used in the SHPB experiments. The rods supplied by Goodfellow™ were cut into rectangular rods to fit the dimensions of the DMA material chamber. The final dimensions of the samples used for DMA testing were 35.00 mm × 6.36 mm × 3.95 mm for PCTFE samples, 35.00 mm × 8.26 mm × 4.35 mm for PTFE samples, and 35.00 mm × 6.37 mm × 3.78 mm for PVC samples. For machining convenience, PMMA was shaped into a smaller rod for the DMA experiment; 34.54 mm in length and 4.22 mm in diameter.

DMA testing on PCTFE, PTFE and PVC was performed on a DMA Q800 V7.5, at two frequencies of 1 Hz and 100 Hz. The test temperature range was between -50ºC and 140ºC. PMMA was tested on a Universal V2.5H TA instrument. Testing

was carried out at two frequencies, 0.1 Hz and 100 Hz, at the temperature range of -30ºC to 170ºC. Both machines belong to the Loughborough University Material Department.

In this experiment, the material is heating at a constant rate. While heating, the material is deformed (oscillated) at constant amplitude (strain) over a range of frequencies and the mechanical properties of the material are measured. The moduli were measured as a function of temperature. Another option of the DMA is the multi-frequency method. Opposite to the first method, the sample is deformed at a constant frequency over a range of one or more amplitudes while the mechanical properties are measured. Another option of the DMA test is to heat the sample at a constant rate while the material is deformed at constant amplitude, while the mechanical properties are recorded at one or more frequencies.

The samples were loaded in the DMA on a multi-frequency strain mode. The samples were swept though the temperature range once, during which the data for both frequencies were measured. The dual cantilever clamp was used to hold the sample. The sample is clamped at both ends and flexed by moving one of the clamps. This clamping method is used for evaluations of ridged materials, such as thermoplastics though the glass transition temperature. In this experiment, the amplitude of the moving clamp is 30 μm. The TA Universal analysis computer program operates the DMA machine and extracts data from it.

Before the experiment, the melting temperatures of the samples are known and avoided. This is because of the possibility of the sample melting and sticking to the furnace. Therefore, the curves would not show any melting transition.

## 4.6 Analysis and interpretation of DMA results

The results obtained from the DMA are presented in this section, storage modulus in section 4.6.1 (Figure 4.2, Figure 4.3, Figure 4.4 and Figure 4.5), loss modulus in section 4.6.2 (Figure 4.6, Figure 4.7, Figure 4.8 and Figure 4.9), and loss angle in section 4.6.3 (Figure 4.10, Figure 4.11, Figure 4.12 and Figure 4.13). The figures are presented in the order of PCTFE, PTFE, PVC and PMMA.

### 4.6.1 Storage Modulus

The storage modulus represents the elastic property of the viscoelastic material. When the energy is stored elastically during deformation changes, a change can be identified in the storage modulus curve as a function of temperature. Then transition can be identified. A steep drop in the storage modulus curve is the identification of the glass transition temperature. The transition from bond stretching to long range molecular motion occurs. The increase in crystallinity in a semi-crystalline material increases the elastic response, and the glass transition temperature increases. In an amorphous polymer, the increase in molecular weight increases phase separation and mobility, but decreases glass transition temperature, because less energy is needed.

There is evidence of a drop in the storage curve in PCTFE, in Figure 4.2. But the end of the curve is unclear. This could be due to the semi-crystalline properties of the material. At 1 Hz the curve began to drop at -45ºC until 71ºC for 1840 MPa, and at 100 Hz the curve began near -35ºC and continued till 76ºC for 2250 MPa. The evidence of a transition temperature drop is not clear in this case. This is due to the higher crystallinity in the PCTFE sample. The PTFE storage modulus curve, in Figure 4.3, shows a clear drop near 45ºC of about 900 MPa at 1 Hz and near 55ºC for around 700 MPa at 100 Hz. Less energy is needed to reach transition, even with a small increase in strain.

Both PVC and PMMA have larger storage moduli at ambient temperature than PCTFE and PTFE (values of storage moduli at ambient temperature and other test temperature are compared in Table 4-2). This is because the molecular weights are much higher in PVC and PMMA samples.

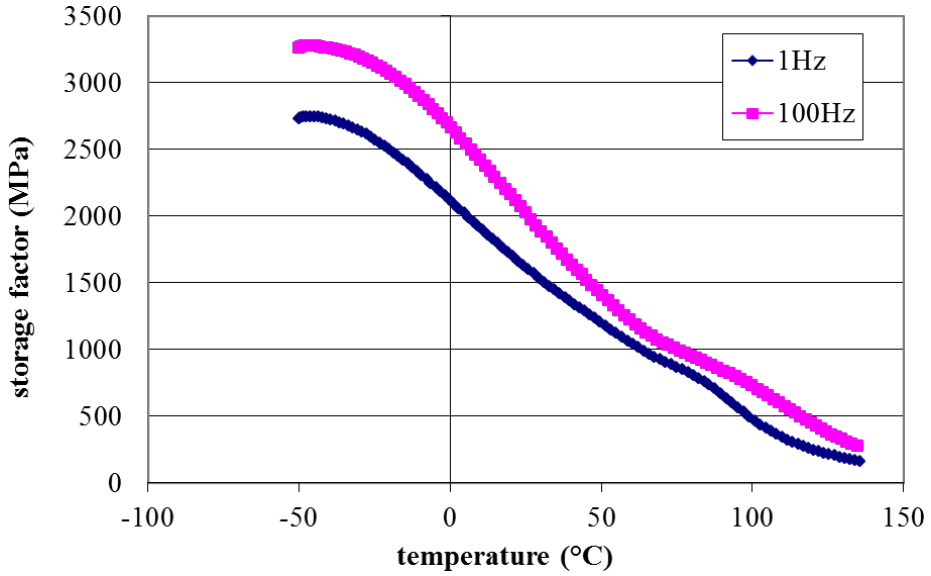


*Figure 4.2 PCTFE storage moduli obtained at two different frequencies. (1 Hz and 100 Hz.)*

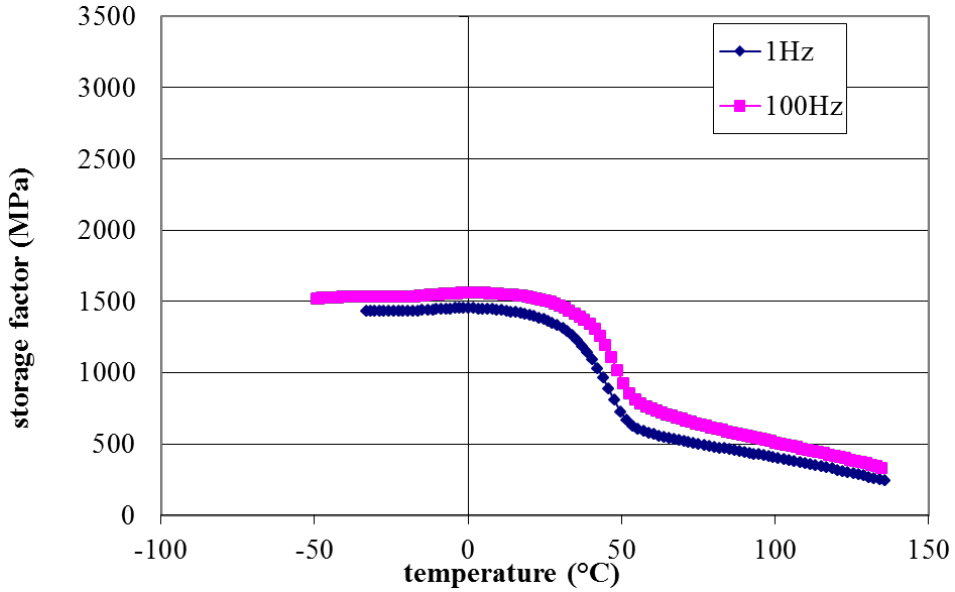


*Figure 4.3 PTFE storage moduli obtained at two different frequencies. (1 Hz and 100 Hz.)*

The drop in storage modulus in PVC is shown in Figure 4.5, the drops in the storage moduli began near 2465 MPa. At the oscillation frequency of 1 Hz the drop indicating the glass transition started at 60ºC and reaches almost 0 MPa just under 100ºC. The rate of change in the modulus is around 60 MPa per degree Celsius. At oscillation frequency of 100 Hz, the glass transition began near 70ºC; the rate of drop in storage modulus during the transition is around 70 MPa per degree Celsius.

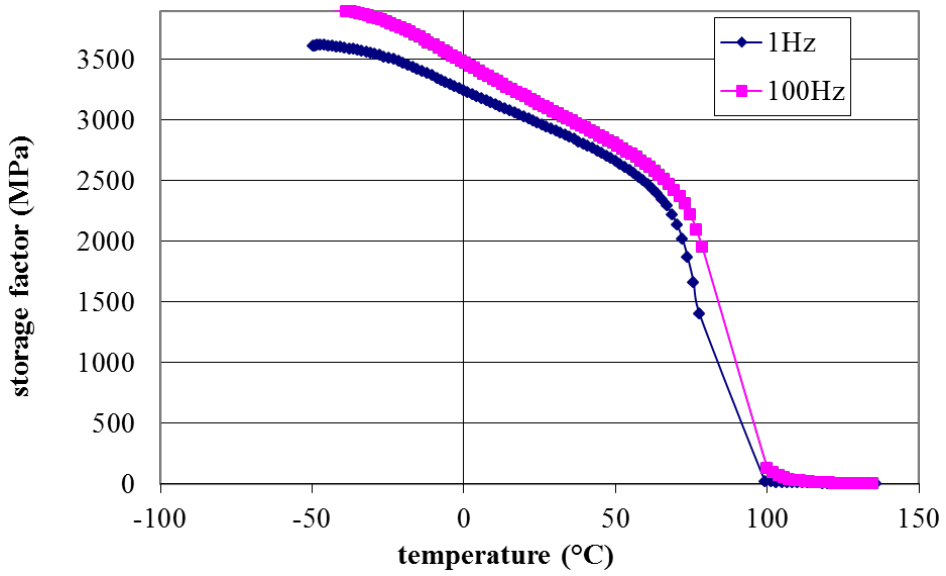


*Figure 4.4 PVC storage moduli obtained at two different frequencies. (1 Hz and 100 Hz.)*

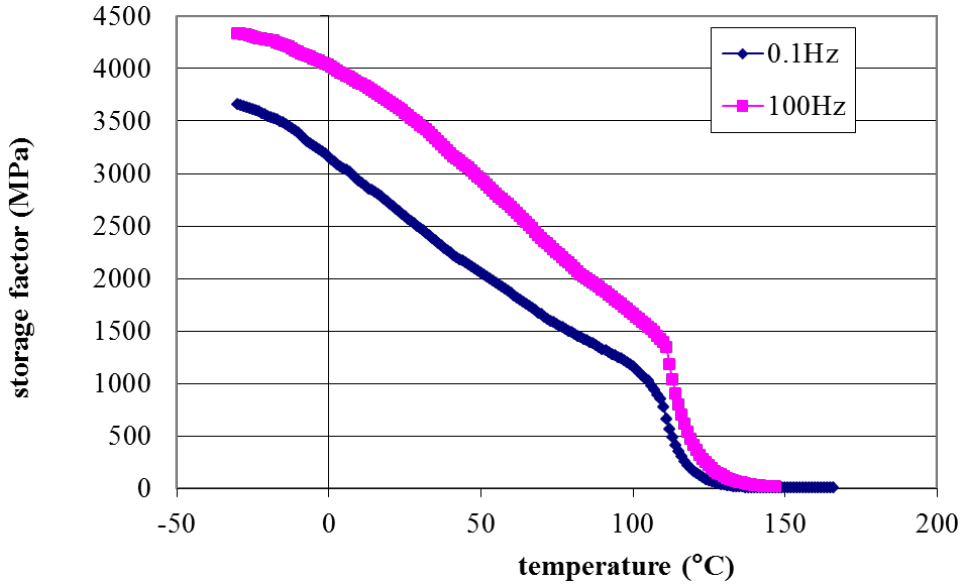


*Figure 4.5 PMMA storage moduli obtained at two different frequencies. (0.1 Hz and 100 Hz.)*

Polymer properties are strongly dependent on temperature and time. The storage modulus under constant load will decrease with time because the molecular structure is trying to minimise the localised stresses by rearrangements. And at higher frequencies, as shown in Figure 4.2, 4.3, 4.4 and 4.5, the moduli will be relatively higher than at lower frequencies.

### 4.6.2 Loss Modulus

The Loss modulus represents the viscosity in a viscoelastic material. It quantifies the energy converted to heat during the deformation.

There are two clear peaks found in the loss moduli of PCTFE, at 1 Hz the peaks correspond to the temperature rate changes seen in storage modulus in Figure 4.3. However, at a high frequency of 100 Hz, the peak in loss modulus is shifted by 60ºC at β-transition and 30ºC in the glass transition. The mechanism that dominates the β-transition is clearly more sensitive to frequency than glass transition in PCTFE samples.

The first loss modulus peak detected in PTFE at 1 Hz and 100 Hz were both detected at 0ºC, this indicates that the β-transition in PTFE is not dominated by the change of frequency. But for the glass transition it is clear that at higher frequency the peak shifted 20ºC higher. The glass transition at lower frequency in PTFE has a higher value than at higher frequency. This could be due to the overlap of the two phase transitions.

The PVC sample also shows two phase transitions in the loss modulus as a function of temperature. At the lower oscillation frequency of 1 Hz, the first peak is not obvious, because the β-transition is slightly lower than the beginning of the test temperature, -50ºC [**Wilkes 2005**]. The main peak in the PVC sample at this frequency is at 77ºC with the loss modulus at 310 MPa. This same peak became broader at 100 Hz, but due to the time setting in the experiment, it was not sufficient to detect the whole peak, the centre of the peak is predicted at 88ºC with loss modulus value greater than 310 MPa. Therefore the shift for the main peak between 1 Hz and 100 Hz is 10ºC.

Loss moduli of PMMA were tested from -30ºC to 170ºC. The β-transition is observed at both 0.1 Hz and 100 Hz oscillation frequencies, at 0ºC and 70ºC respectively. The α-transition is detected at 110ºC at 0.1 Hz, but at oscillation of 100 Hz the α-transition has shifted above the highest test temperature and cannot be recorded. However the beginning of the peak can be seen on the plot in Figure 4.9, it is estimated at around 185ºC.

PMMA shows larger temperature shift in the transition peaks, this is due to the larger gap, three decades instead of two, in the oscillation frequency.

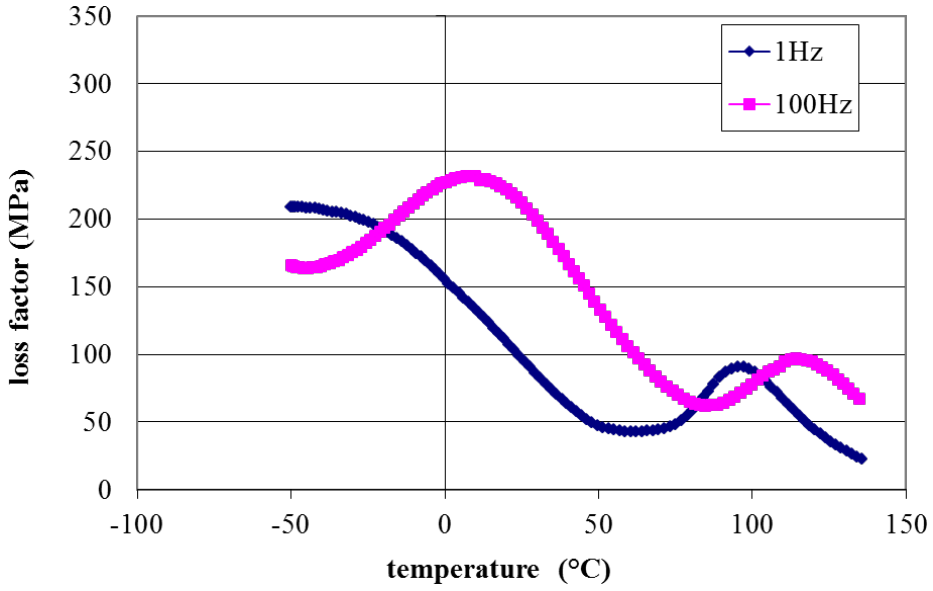


*Figure 4.6 The loss moduli of PCTFE as a function of temperature at 1 Hz and 100 Hz.*

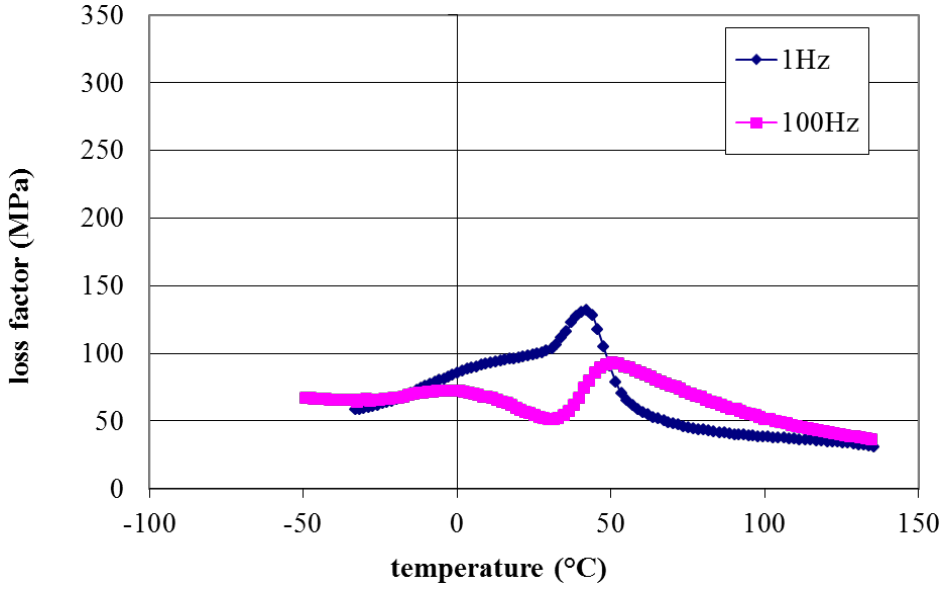


*Figure 4.7 The loss moduli of PTFE as a function of temperature at 1 Hz and 100 Hz.*

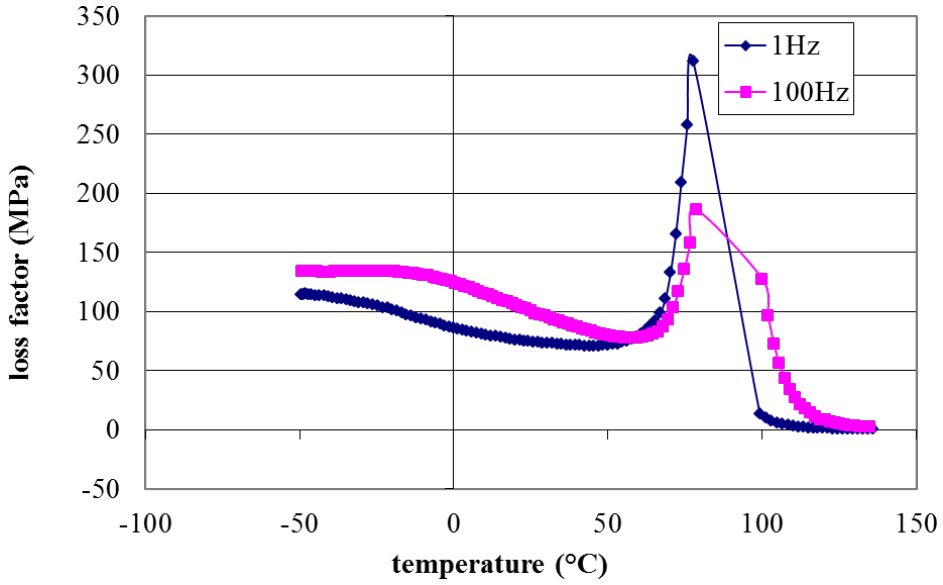


*Figure 4.8 The loss moduli of PVC as a function of temperature at 1 Hz and 100 Hz.*

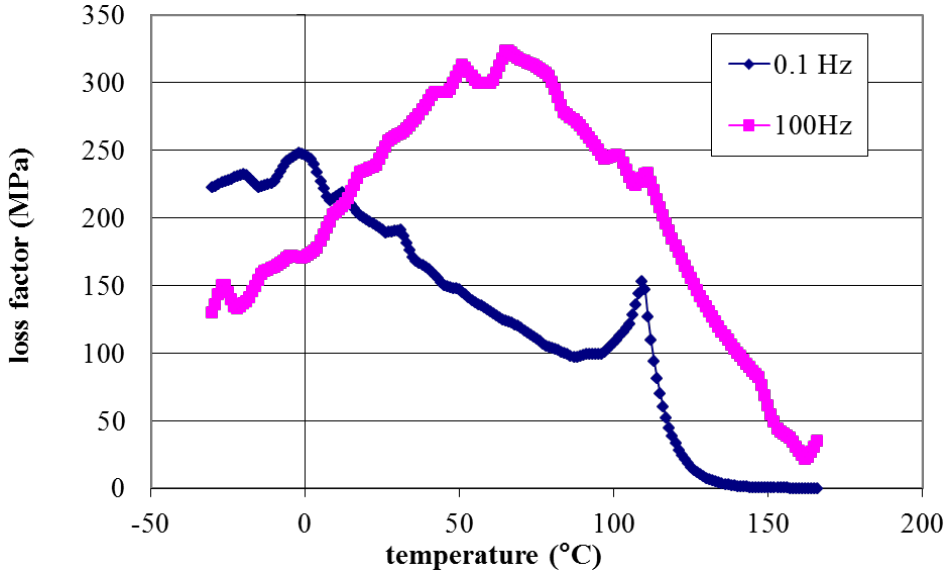


*Figure 4.9 The loss moduli of PMMA as a function of temperature at 0.1 Hz and 100 Hz*

### 4.6.3 Loss angle

Loss angle is the phase lag between the applied stress and the measured stress. It can be calculated by the ratio between the loss and storage modulus. At the glass transition temperature, and also at melting point, a peak can be identified in the loss angle curve; the result gives a clearer temperature than in the storage modulus curve. In this work the glass transition temperature will be quoted from the loss angle curves.

The glass transition temperatures observed at oscillation frequencies of 1 Hz and 100 Hz is at 109ºC and 135ºC in PCTFE samples; at 45ºC and 62ºC in PTFE samples; and at 98ºC and 109ºC in PVC samples. And the glass transition temperature for PMMA is at 130ºC at 0.1 Hz, although this is not observable by the naked eye from Figure 4.13 due to the temperature increasing steps programmed too far apart. The highest point of the peak at 100 Hz was above 150ºC and cannot be detected in this test.

The β-transition temperatures can clearly be observed in PCTFE and PTFE samples, but not so obvious in PVC sample and cannot be seen in PMMA sample. The β-transition for PCTFE sample was at -5ºC at 1Hz and 25ºC at 100 Hz; in the PTFE sample it was observed but at 1 Hz the peak of the curve can not be identified. This is due to the over lapping of the β-transition peak and part of the glass transition peak. It is observed at 50ºC for oscillation frequency of 100 Hz. For the highly amorphous PVC sample the β-transition peak was by two decade of magnitudes smaller than the glass transition temperature. The β-transition in the PVC sample was observed at -6ºC at 1Hz and -48ºC at 100 Hz.

In general, the DMA technique is more sensitive than the DSC to transitions such as glass transition which are weakly energetic but show considerable changes in the mechanical properties.

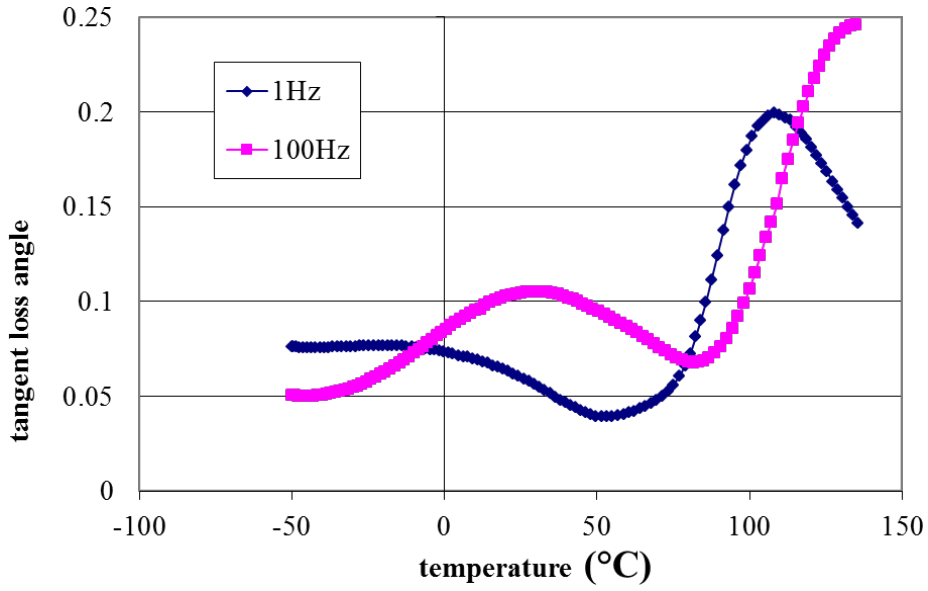


*Figure 4.10 PCTFE tangent of the loss angle as a function of temperature at 1 Hz and 100 Hz.*

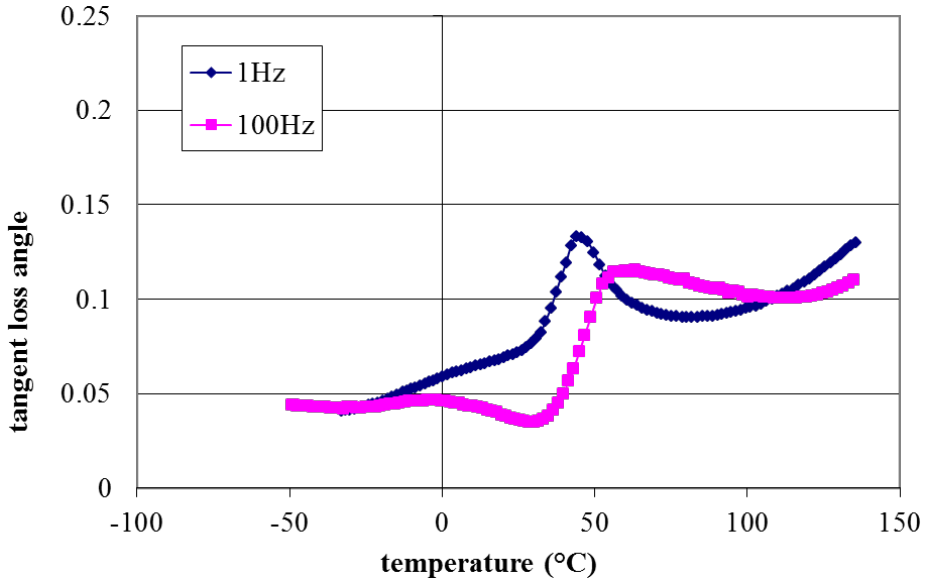


*Figure 4.11 PTFE tangent of the loss angle as a function of temperature at 1 Hz and 100 Hz.*

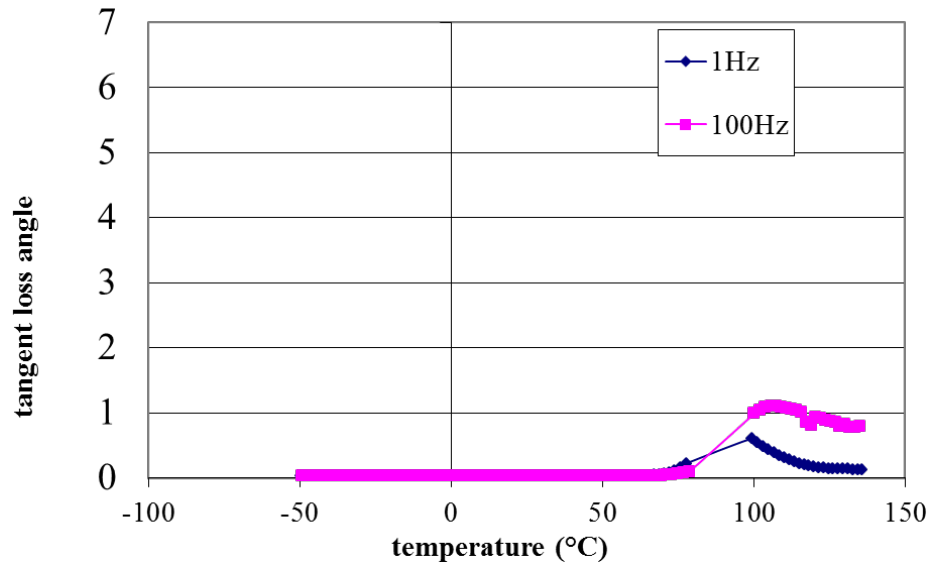


*Figure 4.12 PVC tangent of the loss angle as a function of temperature at 1 Hz and 100 Hz.*

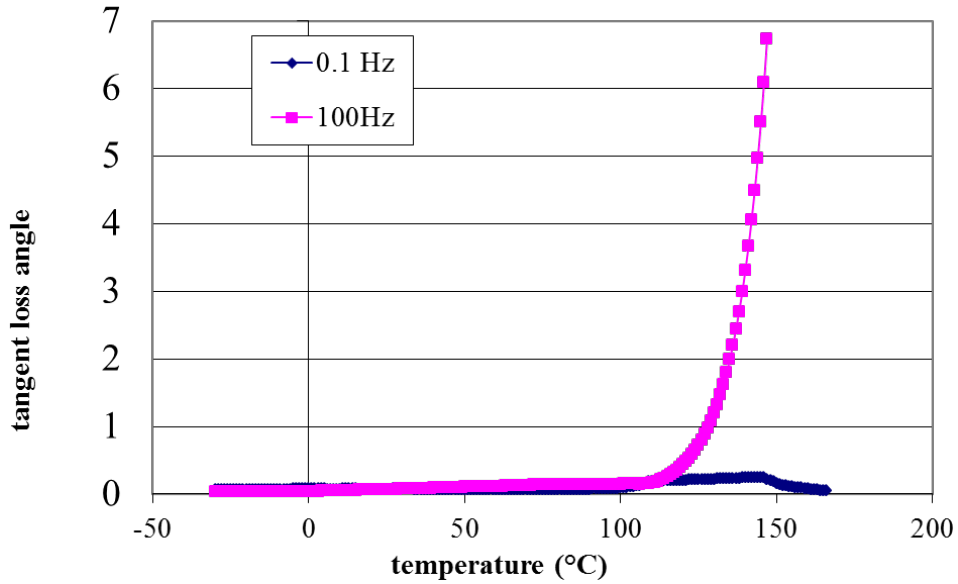


*Figure 4.13 PMMA tangent of the loss angle as a function of temperature at 0.1 Hz and 100 Hz.*

# Chapter Five

# High strain rate experimental results and analysis

Experimental results and analysis of data for the four polymers of interest are presented in this chapter. This includes high strain rate compression experiment results from the split Hopkinson pressure bars (SHPB), as well as the thermal characterisation of polymers from differential scanning calorimetry (DSC) and dynamic mechanical analysis (DMA). The thermal characterisation was made using a Mettler Toledo DSC 1. Both the SHPB and the DSC experimental setup are located in the Loughborough University Physics Department. Elastic moduli of the polymers were obtained by the use of the dynamic mechanical analysis instrument located in the Loughborough University Materials department.

This chapter is divided into four sections. Each section is a collection of the results and analysis describing one particular polymer that is under investigation. More detailed discussion comparing the polymers studied in this work to the work found in the literature is made in the discussion and conclusions chapter.

In each section, three sets of data obtained from the SHPB are first presented. The changes of voltage in the strain gauge signals in the period of the initial pulses, in relation to time, are plotted. The plot is paired with an image of the polymer specimen extracted from the same experiment (Figure 5.2, 5.3, 5.4, 5.12, 5.13, 5.14, 5.22, 5.23, and 5.24). It is important to stress the specimen image is taken after the specimen experiences multiple loadings, as no safe methods were developed to extract the specimen after the desired initial loading was made. Instead, after the initial loading pulse part of the pulse reflects forward and backwards along the bars and the specimen. This creates a series of loading and reflecting pulses within the specimen. Thus, the specimen in the image received more loadings than the data in the strain gauge signal plot shows. The reflection and transmitting stress pulses in the bars are analysed to express the specimen true stress and true strain. The derivation can be found in chapter two, section 2.2. As a result a large collection of stress-strain curves were produced. The range of strain rates is achieved, by changing the speed of the projectile in the SHPB system. Another way to achieve higher strain rate is a change

in specimen size. All specimen ratios of diameter/length remain the same for data compatibility, and reducing specimen inertia effect. Details of specimen design to reduce the errors in the results are discussed in section 2.4 of chapter two. Experiments conducted under the same temperature are collected in the same stress-strain plots for comparison between different temperatures.

The main focus of this study is to verify the existence of the flow stress peak at high strain rates in polymers. After plotting the stress-strain curves from the SHPB data; the yield stress, flow stresses, and strain rates for each individual experiment can be calculated. The flow stresses of 5%-25% strain, depending on the range of strain achieved in the individual experiment are then plotted as a function of temperature at constant strain-rate. The specimen strain is plotted against time to ensure the strain rate used to represent specimen strain in the plastic flow region is constant for validity. The work performed on the specimen during plastic flow is calculated from the stress-strain curve obtained from the SHPB compression experiments. If it is assumed that all the work done in the plastic flow deformation region has been converted to heat and the specimen was experiencing purely adiabatic elastic deformation before the yield point, then the maximum temperature rise during the SHPB high strain rate experiment can be estimated. The discussion and derivation of maximum specimen temperature rise during plastic flow can be found in chapter two, section 2.5.3. The calculated over-all temperature rises with the increase of strain rate, and inverse of temperature and this is true in all four polymers tested.

The specimens for the SHPB experiments were prepared according to the assumptions made for the validity of the experiment; the methods are discussed in chapter two, section 2.4. The data analysis was carried out using several codes written in Wolfram Mathematica 7.0. The details of the method are presented in chapter two, section 2.5.5, and the program codes can be found in the Appendix B.

The work on PMMA was initially studied in 2008 in the strain rate region of $10^2$ to $10^4$ $s^{-1}$ over a range of temperatures from room temperature up to 90ºC. Although not as clearly defined as the sharp peak in flow stress reported by previous workers studying PEEK, there is good evidence of a peak in the flow stress in the strain rate range $10^2$ to $10^3$ $s^{-1}$ which both narrows and moves to a higher strain rate as the temperature approaches the glass transition. Previously reported peaks in flow stress had only been observed in semi-crystalline polymers. The observations in PMMA suggest that this may be a universal phenomenon. More experimental data

has been added to the previous results and is presented in this chapter. PMMA was tested at room temperature, 30ºC, 50ºC, 70ºC and 90ºC.

In total, 42 PCTFE specimens, 44 PTFE specimens, 45 PVC specimens and 55 PMMA specimens were tested using the SHPB system under a range of temperatures and varying strain rates ranging from 1600 to 6100 $s^{-1}$.

Thermal characterisations of the polymers were conducted using the differential scanning calorimeter. The heat flows of the polymer samples were measured and plotted against temperature. Dynamic mechanical analysis was introduced to measure storage modulus, loss modulus, and loss angle of the specimen at the test frequency. DMA measures the viscoelasticity of the sample, showing transition temperatures, and helps elucidate the effect of polymer structure on mechanical behaviour. Viscoelastic materials exhibit both viscous and elastic characteristics; viscosity is the resistance to flow, and this is measured by the loss modulus. Elasticity is the ability to revert back to original shape measured by storage modulus. Delta, loss angle, is the phase lag between applied stress and measured strain, and tangent loss angle is the ratio between storage and loss moduli. More general properties of the four polymers were discussed in chapter three.

All stress, strain, and strain-rates quoted here are true stress, true strain and true strain rates, respectively. The accuracy of the true strain rate is better than ±1% and the error analysis is shown in chapter two, section 2.5.5.

## 5.1 PCTFE results and analysis

High strain rate compression tests at ambient temperature were carried out between 2400 $s^{-1}$ and 3500 $s^{-1}$. Localised crazing at the sample edge randomly occurs with no direct correlation with time or temperature.

Figure 5.1 shows the voltage against time graph collected from the digital oscilloscope for each impact tested on the SHPB. It is clear that after the initial reflecting and transmitting pulse, more impact pulses can be seen traveling forwards and backwards between the bar and specimen. It is important to stress that the images of deformed samples shown later in this chapter have all gone through multiple compression and tensile impact from these pulses. Unfortunately, there was no safe method to extract sample from the impact system without damaging the SHPB system. Therefore, it is unrealistic to relate the deformation of the specimens in the images to the strain rate of the initial loading.

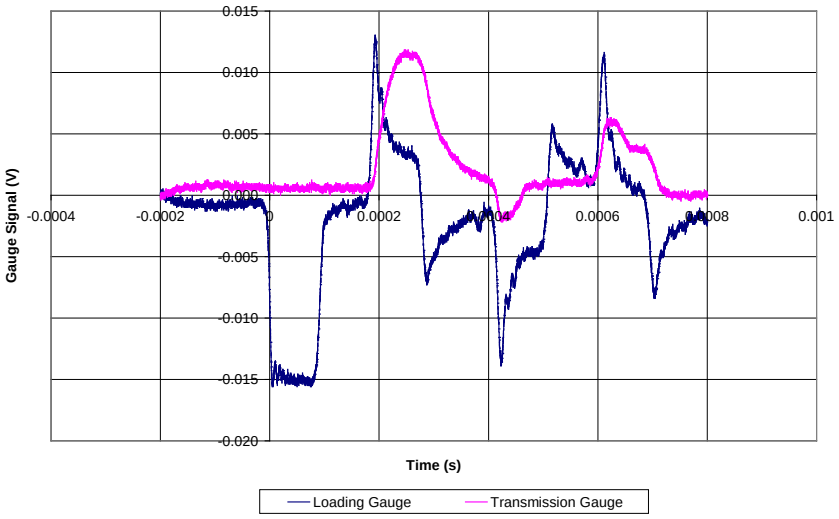


*Figure 5.1 Voltage changes in the loading and transmitting strain gauge against time. Both curves are slightly off set to show the traces. It is clear that after the first reflected pulse (blue line) and transmitting pulse (pink line) at 0.0004 s, the pulses are reflecting forwards and backwards in the loading and transmitting bars. Therefore after the initial impact, the specimen sandwiched between the two bars has experienced multiple loading before been removed from the system.*

In Figure 5.2a, we can see that the beginning of a fracture from the edge of the specimen. PCTFE specimens tested at rates higher than 3530 $s^{-1}$ is observed to

granulate into irregular shapes. This is displayed in Figure 5.2c, where more fractures can be seen within granules of the failed specimen.

At 50ºC, PCTFE specimens were tested at the strain rate range of 2185 $s^{-1}$ to 4340 $s^{-1}$. Three examples are shown in Figure 5.3. Up to the strain rate of 3000 $s^{-1}$ the specimen thins into a flatter disk, as is shown in Figure 5.3d with crazing covering a larger area of the specimen than at the ambient temperature. Above this rate, the specimens scattered into irregular granules 3-5 mm wide and ~2.5 mm thickness. The granules in general were smaller than those at ambient temperature. Another observation of PCTFE tested at 50ºC is the lowering of transparency of the specimens after the impact. This can be related to stress whitening, which is crazing at a large size and concentration, as discussed in chapter one.

The specimens and results from Figure 5.4 are tested at 100ºC with the rate of strain being between 2950 $s^{-1}$ and 5795 $s^{-1}$. Every specimen tested at this temperature completely fractured after the impacts. With the increase of the strain rate, a higher degree of crazing appeared. Some of the specimens deformed into a ring shape, where the centre of the specimen was compressed into a thin layer of flakes.

For similar strain rates at a higher temperature, the specimens are observed to be even more deformed. This can be seen by comparing images of Figure 5.2b, 5.3d and 5.4g. At ambient temperature the specimen was tested at a strain rate of 2900 $s^{-1}$, as shown in Figure 5.2b, here the specimen length parallel to the compression wave decreases by 1.34 ± 0.01 mm as the diameter of the disc increases with no signs of fracture; whereas in Figure 5.3d tested at strain rate of 2800 $s^{-1}$, the length of the 50ºC specimen decreased by 1.46 ± 0.01 mm and failure of the material can be seen at the edge of the specimen. In Figure 5.4g the 100ºC specimen was tested at the strain rate of 2950 $s^{-1}$. The specimen fractured into sharp granules.

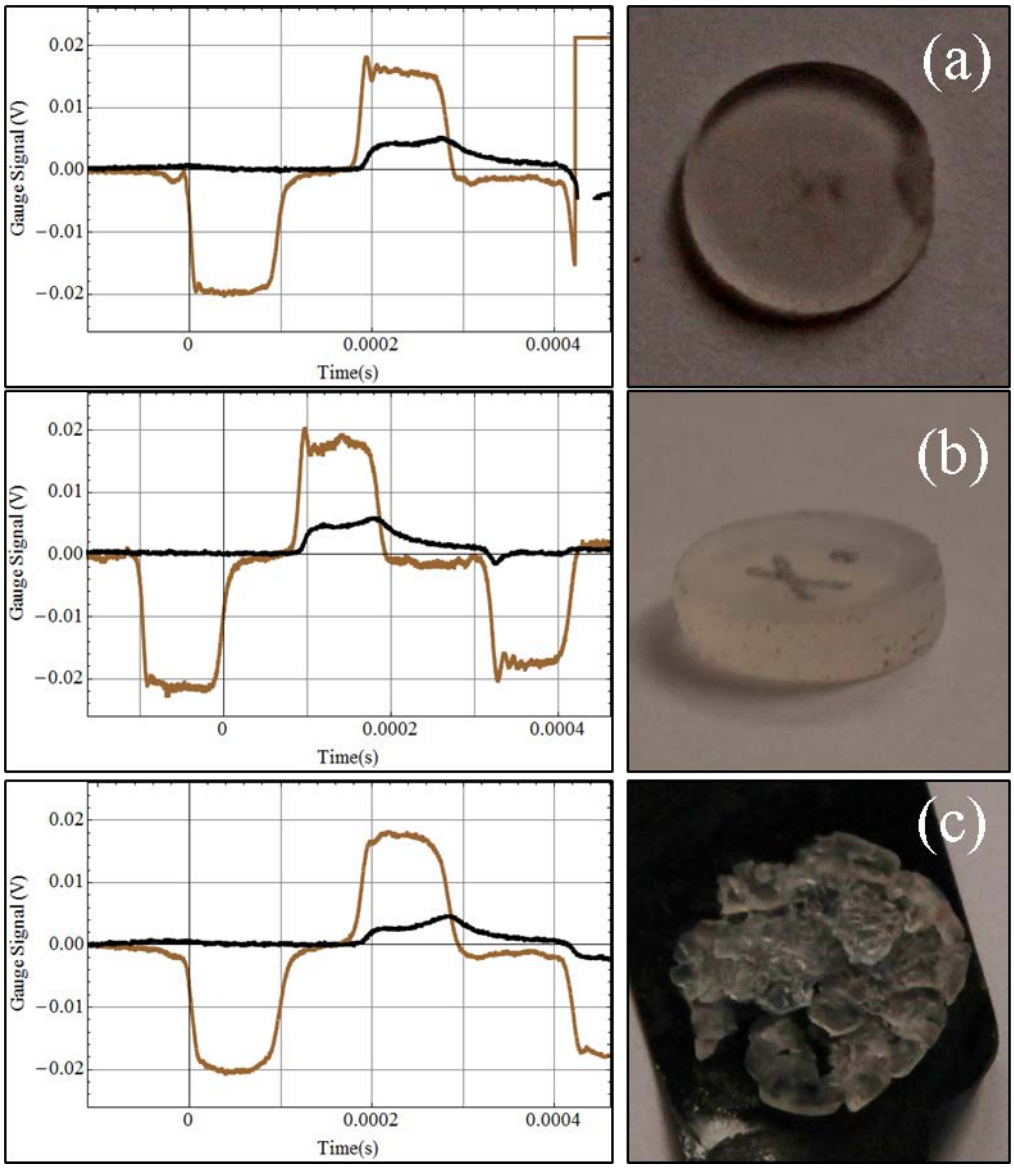


*Figure 5.2 (Graph) Voltage change in strain gauge signals as a function of time. Brown line shows loading and reflecting signals and black line shows the transmitting signal from the impact. (Image) Corresponding image of the PCTFE specimen after SHPB compression testing at ambient temperature under the strain rates of (a) 2475 $s^{-1}$, (b) 2900 $s^{-1}$ and (c) 3530 $s^{-1}$ .Note that the deformed specimen in the image has gone through multiple loading,(i.e. Figure 5.1). Whereas, only the first set of reflecting and transmitting pluses are shown here.*

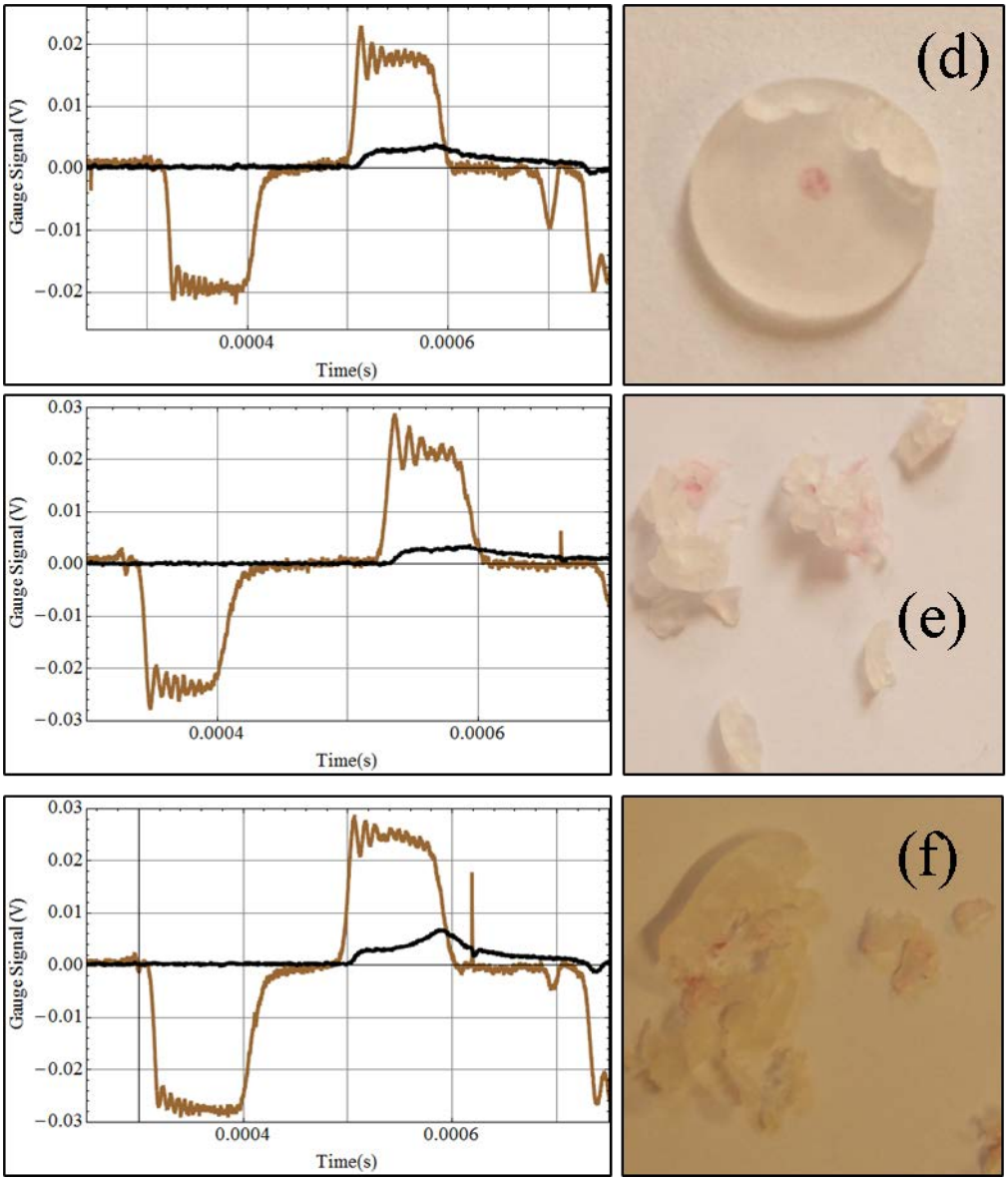


*Figure 5.3 (Graph) Voltage change in strain gauge signals as a function of time. Brown line shows loading and reflecting signals and black line shows the transmitting signal from the impact. (Image) Corresponding image of the PCTFE specimen after SHPB compression testing at 50ºC under the strain rates of (d) 2800 $s^{-1}$, (e) 3375 $s^{-1}$ and (f) 3860 $s^{-1}$. Note that the deformed specimen in the image has gone through multiple loading, (i.e. Figure 5.1). Whereas, only the first set of reflecting and transmitting pluses are shown here.*

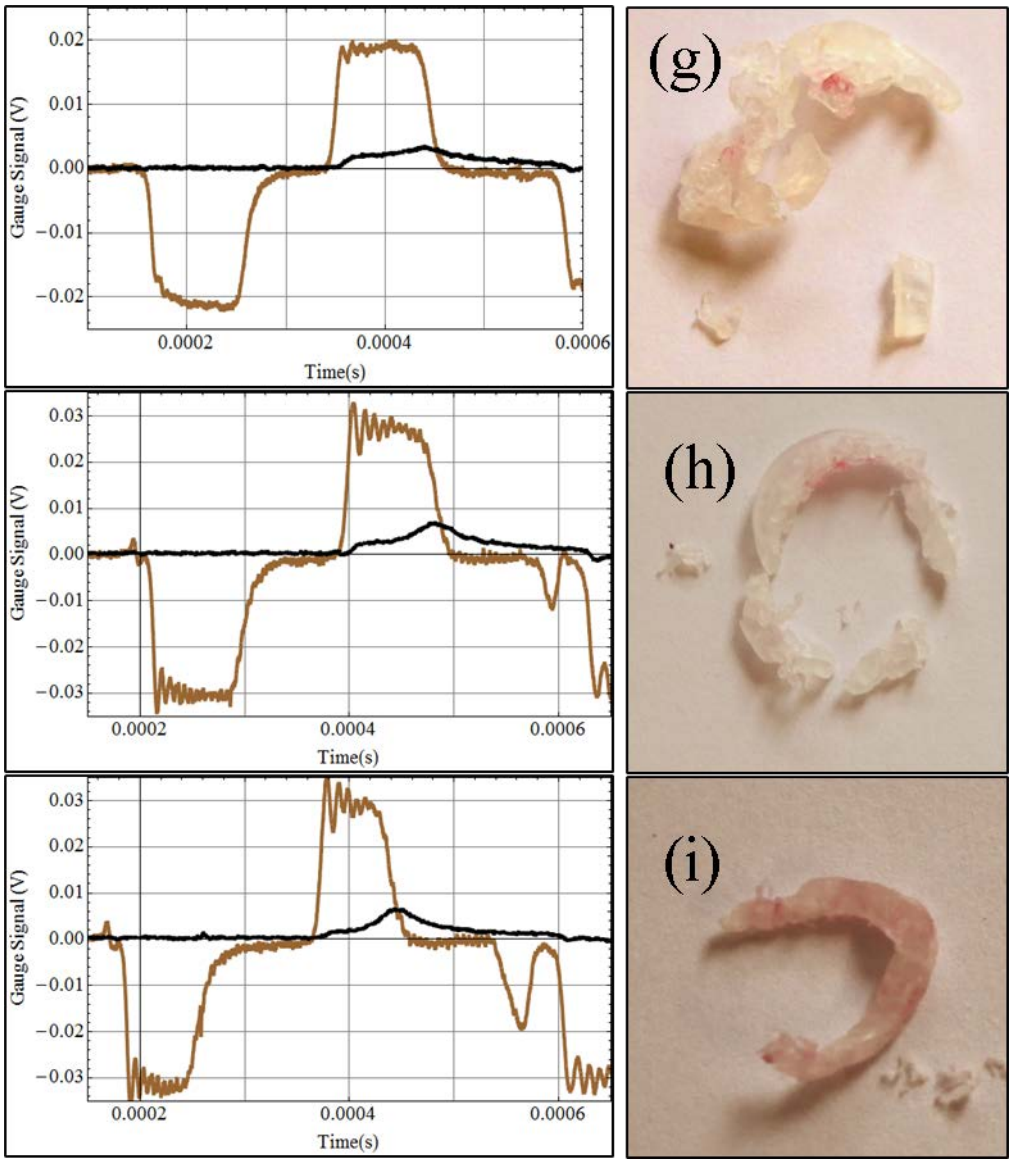


*Figure 5.4 (Graph) Voltage change in strain gauge signals as a function of time. Brown line shows loading and reflecting signals and black line shows the transmitting signal from the impact. (Image) Corresponding image of the PCTFE specimen after SHPB compression testing at 100ºC under the strain rates of (g) 2950 $s^{-1}$, (h) 4370 $s^{-1}$ and (i) 5795 $s^{-1}$. Note that the deformed specimen in the image has gone through multiple loading, (i.e. Figure 5.1). Whereas, only the first set of reflecting and transmitting pluses are shown here.*

### 5.1.1 Stress-strain curves

The stress-strain curves of the PCTFE specimens are plotted in Appendix D. Ambient temperature, 50ºC and 100ºC in Figure C-1, C-2 and C-3 respectively. The stress-strain curves of the nine specimens shown in Figure 5.2, 5.3 and 5.4 can be found in Figure 5.5. The stress-strain curve of PCTFE under compression, tested at ambient temperature, shows yield stress between 112 MPa at 2475 $s^{-1}$ and 128 MPa at 2680 $s^{-1}$. The specimen first appears to show strain softening for 5% strain after yield point then strain hardens again. The yield stress decreases with the increase of temperature. The same effect is found in maximum stress, with the exception of samples showing large strain hardening. At large strain hardening, the maximum stress reached is independent of test temperature and is within the range in this study. At ambient temperature PCTFE specimens were more brittle. The end of the stress-strain curves occur around 25% strain.

The yield stress is between 70 MPa (tested at the strain rate of 4200 $s^{-1}$) and 100 MPa (tested at 233 $s^{-1}$) in PCTFE tests conducted at 50ºC. The specimen also goes though strain softening, after which it hardens and then softens for the second time before failure or a larger strain hardening and then failure. The highest fracture strain reached at 50ºC was 200 MPa which is almost double the yield stress of 98 MPa. The fracture stress at 50ºC, with strain rates lower than 3000 $s^{-1}$, happened near 25% strain. However, above this particular strain rate the material shows greater strain hardening as well as reaching 35% strain before failure.

For tests carried out at 100ºC, the yield stress (or rather the end of the elastic deformation) dropped between 44 MPa at 3225 $s^{-1}$ (and 4140 $s^{-1}$), and 96 MPa at 4950 $s^{-1}$. The specimen goes through a long strain softening, until up to 20% strain before a large strain hardening. All experiments have shown strain hardening at the end of the plastic flow deformation, with the strain hardening becoming greater at higher temperature experiments. The fracture strains at 100ºC can be divided into two groups. The first where after the strain softening the PCTFE specimen strain hardens slightly, reaching maximum stress no more than 30 MPa higher than yield stress. The second type of stress-strain curve found in this temperature experiences similar yield and strain softening, but then shows a dramatic strain hardening before the fracture of the specimen. The maximum stress reached with strain hardening in PCTFE at 100ºC

is 190 MPa, which in this case more than triples the yield stress at 44 MPa. At 100ºC, all PCTFE specimens reached above 25% strain before failure.

It is clear that the gradients of the stress-strain relation at the elastic region (before reaching yield point ) are lowering as the temperature increases, although there are limitations in the SHPB technique, and it is known that the specimen is not always in an equilibrium state before reaching the yield point. With the increase of specimen temperature the sample behaves in a more viscous manner. This effect can be confirmed with dynamic mechanical analysis results of PCTFE as well as with the previous work done by Brown et al. where PCTFE was tested at lower strain rates [**Brown/Rae/Orler 2006**]. Determining the yield point of the stress-strain curve is harder at 50ºC than at ambient temperature. This is also due to the slope of the elastic modulus. Also, as the sample is less brittle to start off with at 50ºC, the degree of transition between brittle and rubbery state lessens, showing a slow change in stress level rather than a sharp transition at yield point. At 100ºC, there is not a very clear-cut difference between yield and creep in the stress-strain curves. Where the PCTFE material is above its glass transition temperature at high strain rate, both creep and yield behaviour exists.

PCTFE specimens show lower transparency in both 50ºC and 100ºC tests. As is observed in the tested sample images of Figure 5.3 and Figure 5.4, the degree of optical transparency in a polymer depends on the amorphous structure, where the polymer chains are randomly orientated. The change of transparency in this case would suggest the specimen has gained enough energy to go though the phase transition and the polymer chains were freed to rearrange in some way. This is to be expected at a specimen temperature of 100ºC, as the polymer is in a rubbery state at this temperature and crystallisation fails upon the rearrangement of the polymer chains once cooled. However, at 50ºC, the specimen has not reached the glass transition temperature of PCTFE, even when the maximum temperatures rise during the compression at plastic flow is taken into consideration. Therefore it is the high strain rate impact which has onset the phase change in this case. In all cases, the end of the stress-strain curves shows the end of the experiment where the specimens were permanently deformed.

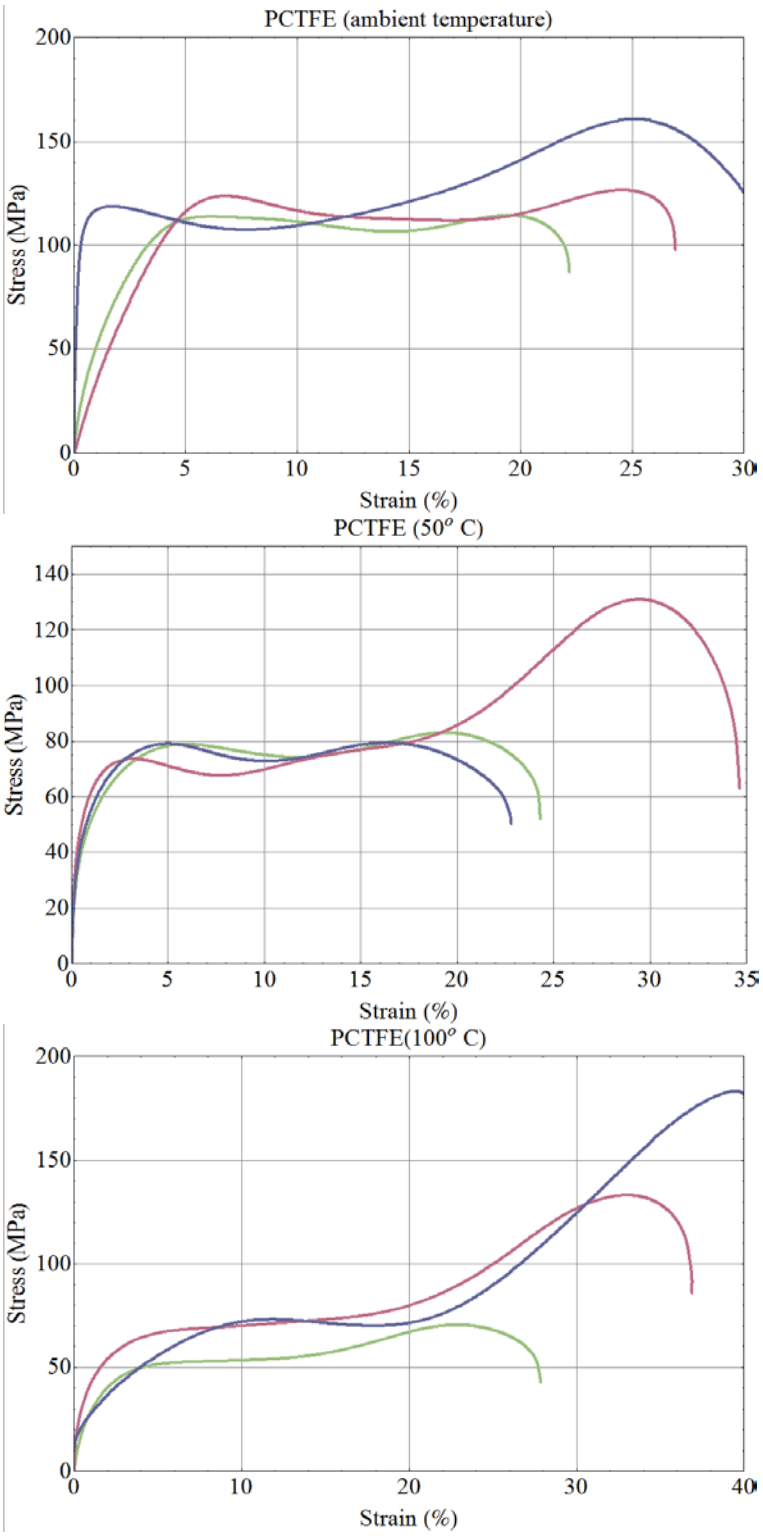


*Figure 5.5 Selection of PCTFE specimen stress-strain curves at ambient temperature, 50ºC and 100ºC. The curves show elastic deformation, yield point, plastic flow and strain hardening behaviour of the specimen response to high strain rate impact. The complete collection of PCTFE stress-strain curves can be found in Appendix D.*

### 5.1.2 Flow stress as a function of strain rate

The plastic flow stress of each high strain rate experiment that has been conducted at ambient temperature, 50ºC, and 100ºC has been plotted in Figure 5.6 against the rate of strain. The sensitivity of flow stress as a function of strain rate, depending on the specimen temperature, is shown. A range of strain in the plastic flow region of the stress-strain curve is chosen to monitor the plastic flow deformation as strain increases. The flow stress chosen for ambient temperature is at 5%, 10%, 15% and 20% strain. Most stress-strain curves found at this temperature terminated between 20% and 25% strain. The flow stress chosen for 50ºC and 100ºC experiments are at 10%, 15%, 20%, and 25% of strain. This is because the yield strain of some of the specimens exceeded 5% and the termination of the experiment usually extended beyond 25% strain. The most accurate flow stress to represent flow stress of PCTFE should be between 10% to 15% strain, where the flow stress is not fluctuating dramatically due to transition in the structure of the chains.

At ambient temperature, there is a clear point at 2690 $s^{-1}$where the flow stress jumped up 15 MPa at 10%, 35 MPa at 15% and 45 MPa at 20%. But for 50ºC and 100ºC, there is no apparent flow stress peak. Instead, a steep drop in flow stress is observed at 50ºC after 4100 $s^{-1}$. Also, a small possible peak between the values of 4100 $s^{-1}$ and 4500 $s^{-1}$ is observed at 100ºC.

For PCTFE specimens tested at 50ºC at strain rates above 3000 $s^{-1}$, large strain hardening occurred before failure (see Figure 5.5 for illustration). This strain hardening would also explain the large fluctuation of 25% flow stress seen at 100ºC (Figure 5.6iii).

As discussed in previous chapters, flow stress is linearly dependent on the strain rate at low rates of strain. High strain rate tests, however, have been found to be rate sensitive and display flow stress peaks. This effect is visible in PCTFE specimen at ambient temperature flow stress at 10%, 15% and 20% strain (Figure 5.6i).

Flow stresses below 20% strain for all three temperatures follow the same pattern in all PCTFE compression experiments. However, the function of flow stress at 25% strain against strain rate is less synchronised with the fitted lines of flow stresses at 5% - 15%.

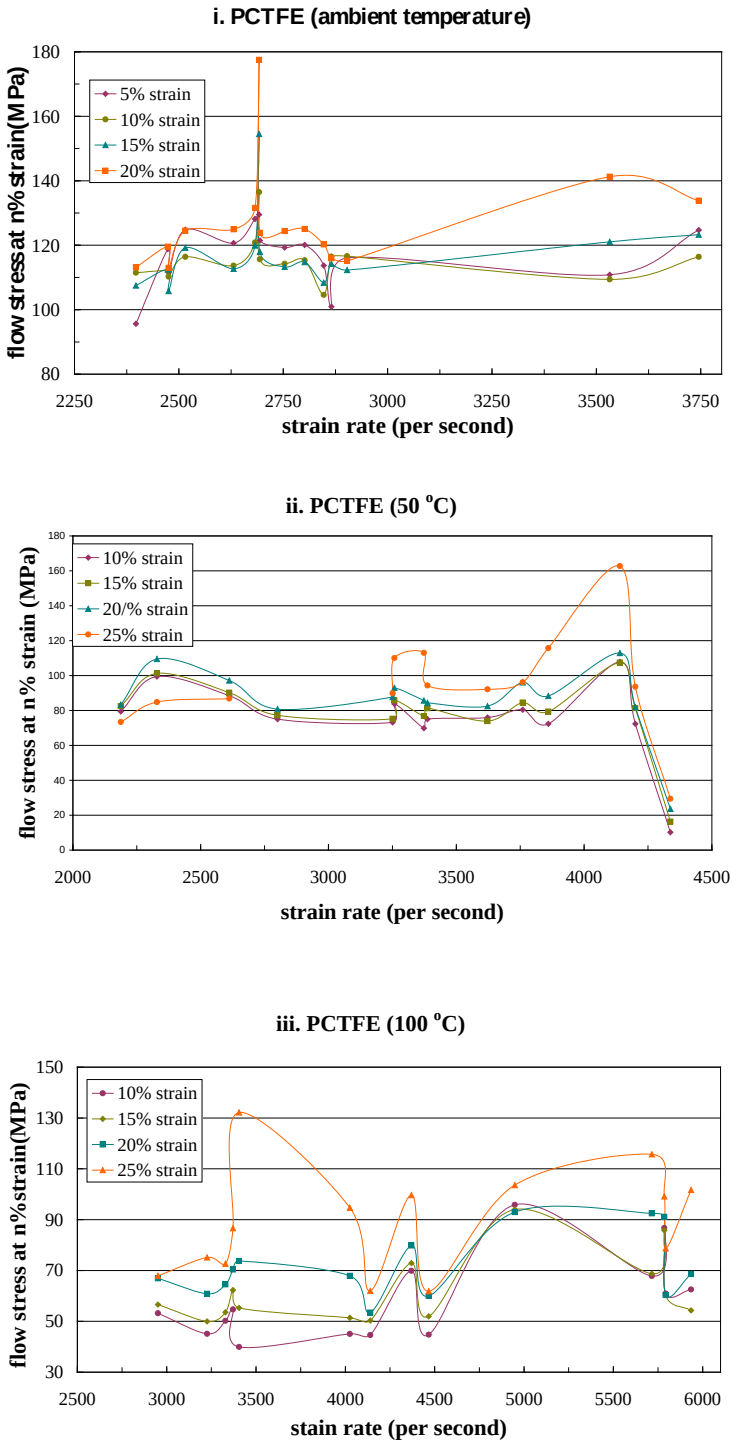


*Figure 5.6 Flow stresses as a function of strain rate, for PCTFE specimens tested in the SHPB. At (i) Ambient temperature experiments with flow stress at 5%, 10%, 15% and 20% strain, (ii) 50ºC and (iii) 100ºC experiments with flow stress taken at 10%, 15%, 20% and 25% strain. Flow stress peak is apparent at ambient temperature, but can not be detected at 50ºC and 100ºC.*

### 5.1.3 Heat transfer in flow stress

Temperature rise during the plastic flow in PCTFE specimens is shown in Figure 5.7, 5.8, and 5.9. The examples in the figures correspond to the specimens in Figure 5.2, 5.3, and 5.4. Temperature rise calculation is described in chapter two, section 2.4.

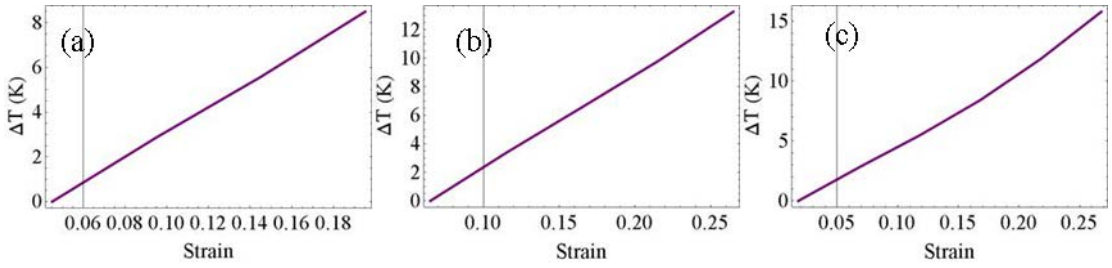


*Figure 5.7 Temperature rise in ambient temperature specimens during plastic flow. This is derived from the stress-strain curves obtained from PCTFE specimens to estimate the maximum rise in temperature at rates of (a) 2475 $s^{-1}$, (b) 2900 $s^{-1}$, and (c) 3530 $s^{-1}$.*

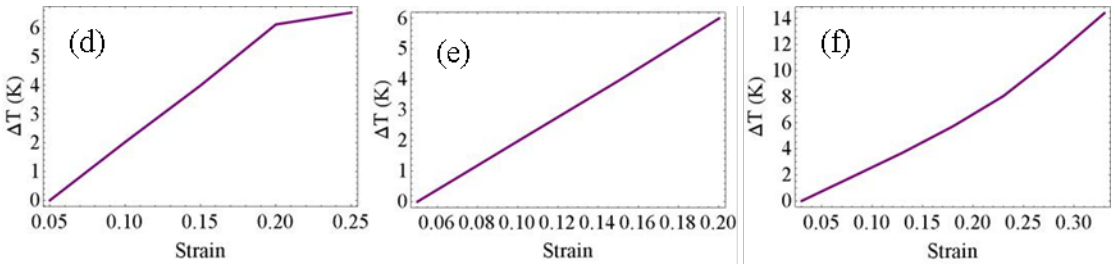


*Figure 5.8 Temperature rise in on the 50ºC specimens during plastic flow. This is derived from the stress-strain curves obtained from PCTFE specimens to estimate the maximum rise in temperature at rates of (d) 2800 $s^{-1}$, (e) 3370 $s^{-1}$, and (f) 3860 $s^{-1}$.*

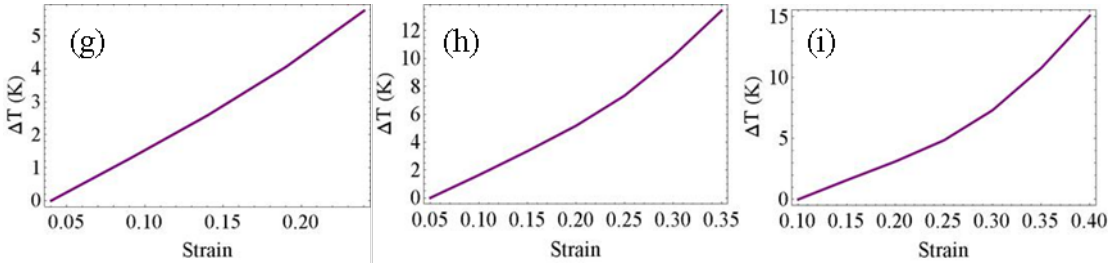


*Figure 5.9 Temperature rise in the 100ºC specimens during plastic flow. This is derived from the stress-strain curves obtained from PCTFE specimens to estimate the maximum rise in temperature at rates of (g) 2950 $s^{-1}$, (h) 4370 $s^{-1}$, and (i) 5795 $s^{-1}$.*

Specimens tested at ambient temperature, the temperature rise at 15% strain is around 6ºC at 2475 $s^{-1}$, 6.5ºC at 2900 $s^{-1}$, and 7.5ºC at 3530 $s^{-1}$. The rate of temperature rise is linear to the increase in strain. The average rate of temperature rise is 3ºC per 10% strain.

The specimens with test temperature at 50ºC, temperature rise calculated during the impact are 4.2ºC at 2800 $s^{-1}$, 3.8ºC at 3370 $s^{-1}$ and 4.5ºC at 3860 $s^{-1}$. The rate of temperature increase is still linear to the increase of strain at 2ºC per 10% strain. But at strain larger than 20%, the rate of temperature rise changes, in the incidence of Figure 5.8f the rate becomes 5ºC per 10% strain. The initial rate of increase in temperature is lower at 50ºC tests than those of ambient temperature tests. Hence the maximum total temperature rise in the PCTFE specimen, before failure, would be 65ºC.

For specimens test temperature at 100ºC, the calculated temperature rise is 2.8ºC at 2950 $s^{-1}$, 3ºC at 4370 $s^{-1}$ and 2ºC at 5795 $s^{-1}$. The temperature rise rate is linear to the increase of strain, consequently, the greater strain achieved higher compression strain rate of the experiment, producing large temperature rise in total. The rate of temperature rise is around 2.5ºC per 10% strain for specimens tested at 100ºC.

The relation of temperature rise and strain stays linear, but the gradient increases near 23% strain. This is demonstrated in Figure 5.8f, 5.9h and 5.9i where the change in gradient can be seen near 23% strain and also at 35% strain. This effect is not clear in specimens which failed near 25%.

### 5.1.4 DSC and DMA summary

The PCTFE test result from differential scanning calorimetry (DSC) technique was evaluated using the software provided by the manufacture. The net weight of the tested PCTFE sample was 16.0mg. The test temperature was between 0ºC and 250ºC, with the heating rate of 5ºC per minute. Three changes in the measured baseline were detected. The first was observed at 38ºC, this is the starting transition as demonstrated in Figure 4.1. The next positive change in the baseline is observed at 63ºC, this is an indication of a possible glass transition in the PCTFE sample.

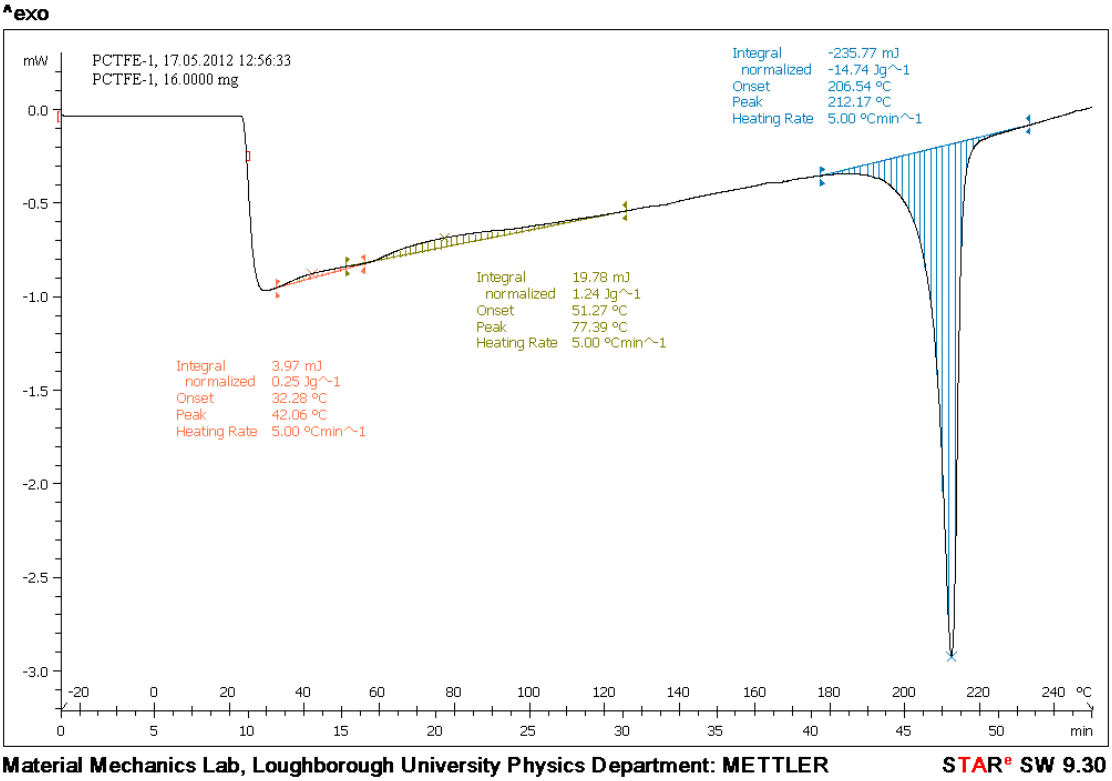


*Figure5.10 Thermal analysis using the differential scanning calorimeter tested on PCTFE sample at 5ºC per minute between 0ºC and 250ºC.*

The dynamic mechanical analysis of PCTFE sample was carried out between -50ºC and 150ºC at two different frequencies. The glass transition temperature according to the loss angle (the phase lag between the applied stress and the measured stress) is 109ºC at 1 Hz and 135ºC at 100 Hz. This is much higher than the glass transition measured by DSC and found in the literatures (chapter three, section 3.3). This could be due to the high increase of crystallinity of PCTFE samples with the increase of strain rate. The drop in PCTFE storage modulus shows that the elasticity of PCTFE decreased by 99% from -50ºC to 150ºC.

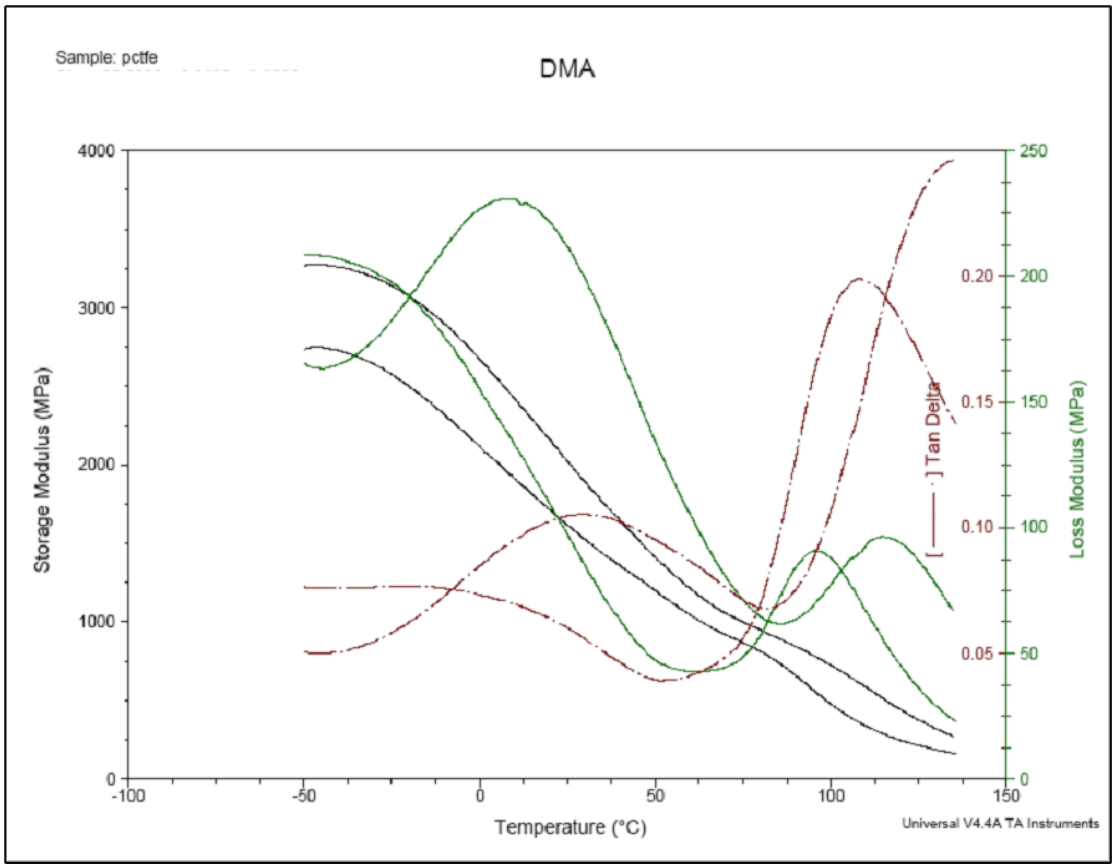


*Figure 5.11 A temperature sweep dynamic mechanical analysis from -50 ºC to 150 ºC on a PCTFE sample at frequencies of 1 Hz and 100 Hz. Using different initial static load and strain. Storage modulus (left), loss modulus (right) and loss angle is plotted against temperature. The glass transition temperature is measured at both frequencies.*

### 5.1.5 PCTFE results summary

A PCTFE sample was heated with constant temperature increase of 5ºC per minute using the differential scanning calorimeter. The heat flow is measured and plotted against temperature from 0ºC to 250ºC. Three transitions temperatures were found; $T_m$ = 214.14ºC, $T_g$ =77.39ºC, and $T_\gamma$ =42.06ºC.

Dynamic mechanical analysis was tested on PCTFE from -50ºC to 150ºC. The storage modulus shows smooth decreasing. The loss modulus at both 1 Hz and 100 Hz showed two peaks. Loss angle illustrated $T_g$ and $T_\gamma$. At 1 Hz, $T_g$ = 109ºC and $T_\gamma$ = -50ºC. And at 100 Hz, $T_g$ =135ºC and $T_\gamma$ =25ºC. $T_\gamma$ shifted by 50ºC and $T_g$ shifted by 24ºC.

High strain rate compression tests at ambient temperature were carried out between 2400 $s^{-1}$ and 3500 $s^{-1}$. The average yield stress was 120.5 MPa; the final

specimen strain was near 25% on average. A flow stress peak was found at the strain rate of 2680 $s^{-1}$. The maximum temperature rise during the plastic flow was 15ºC.

High strain rate compression tests at 50ºC were tested between 2185 $s^{-1}$ and 4340 $s^{-1}$. The average yield stress was 83.4 MPa; the final specimen strain was 25% for half of the specimen and 35% for the other half. No flow stress peak was found, but a drop at 4150 $s^{-1}$was observed. The maximum temperature rise during the plastic flow was 15ºC.

Also, high strain rate compression test at 100ºC were carried out at strain rates between 2950 $s^{-1}$ and 5795 $s^{-1}$. The average yield stress was 58.3 MPa, and the final specimen strain was between 30% and 40%. No flow stress peak was found. The maximum temperature rise during the plastic flow was 15ºC. All specimens were found to fail at this temperature.

## 5.2 PTFE results and analysis

The PTFE specimens tested at ambient temperature were at the strain rates from 1780 $s^{-1}$ to 4150 $s^{-1}$. The images of the specimens shown in the following are taken after the end of a test. In each the strain experienced are different. For example, in Figure 5.12c it is 30% which is higher than in Figure 5.12a at 25%. Below the strain rate of 2300 $s^{-1}$, the specimens responded to the stress by a homogenous deformation. An image example is shown in Figure 5.12a.

Between the strain-rates from 2300 $s^{-1}$ and 3000 $s^{-1}$ a network of deep fractures can be seen, while the specimens mainly survived in one piece. A demonstration of this is given in Figure 5.12b where the specimen was compressed at the stain rate of 2380 $s^{-1}$. The fracture cuts the specimen into many regions. However, the fractures branches into smaller fractures and do not cut the specimen apart. Beyond the strain rate of 3000 $s^{-1}$, the specimens reached ultimate mechanical failure. Illustrated in Figure5.12c is the PTFE granules from a specimen tested at 3745 $s^{-1}$. At 50ºC, PTFE was tested at the strain-rates of 1665 $s^{-1}$ to 4670 $s^{-1}$. PTFE specimens tested at the lower strain rate end deformed into a disc with curve edges. This is demonstrated in Figure 5.13d. The fracture of PTFE specimens began after the strain rates reached 1800 $s^{-1}$. An example of a fractured specimen is given in Figure 5.13e, with the size of the fragments measuring from 0.2 mm - 2.0 mm in length. At strain

rates above 3000 $s^{-1}$, a very thin layer of the specimen with irregular edges, as seen in Figure 5.15f, was found between the Hopkinson bars.

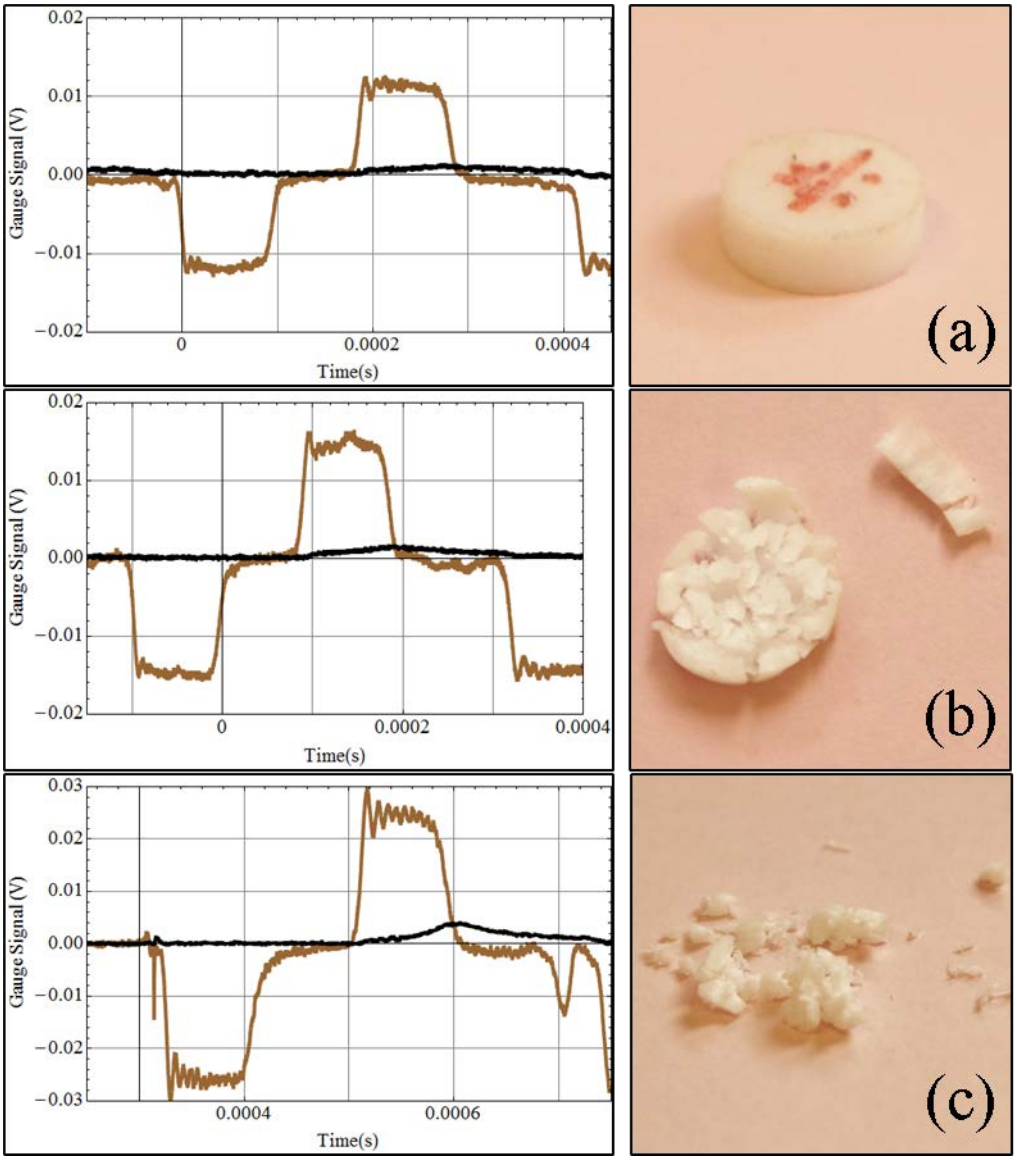


*Figure5.12 (Graph) Voltage change in strain gauge signals as a function of time. Brown line shows loading and reflecting signals and black line shows the transmitting signal from the impact. (Image) Corresponding image of the PTFE specimen after SHPB compression testing at ambient temperature under the strain rates of (a) 1780 $s^{-1}$, (b) 2380 $s^{-1}$, and (c) 3745 $s^{-1}$. Note that the deformed specimen in the image has gone though multiple loading, (i.e. Figure 5.1). Whereas, only the first set of reflecting and transmitting pluses are shown here.*

PTFE was also tested at the rate of strain between 2740 $s^{-1}$ and 4555 $s^{-1}$ at 100ºC. Figure 5.14g shows the specimen tested at a strain rate 2330 $s^{-1}$, where the specimen is seen to have deformed into fragments. Here the fragments are thin and stretched. This could be caused by multiple loading. The specimen was fractured into

granules and then the granules were compressed again resulting in thin fragments. All specimens tested at 100ºC were deformed into smaller pieces. The resulting granule size became smaller with the increase of strain rate. This is demonstrated by comparing Figure 5.14h and 5.14i. Eventually part of the specimen turned into power when tested above the strain rate of 3400 $s^{-1}$.

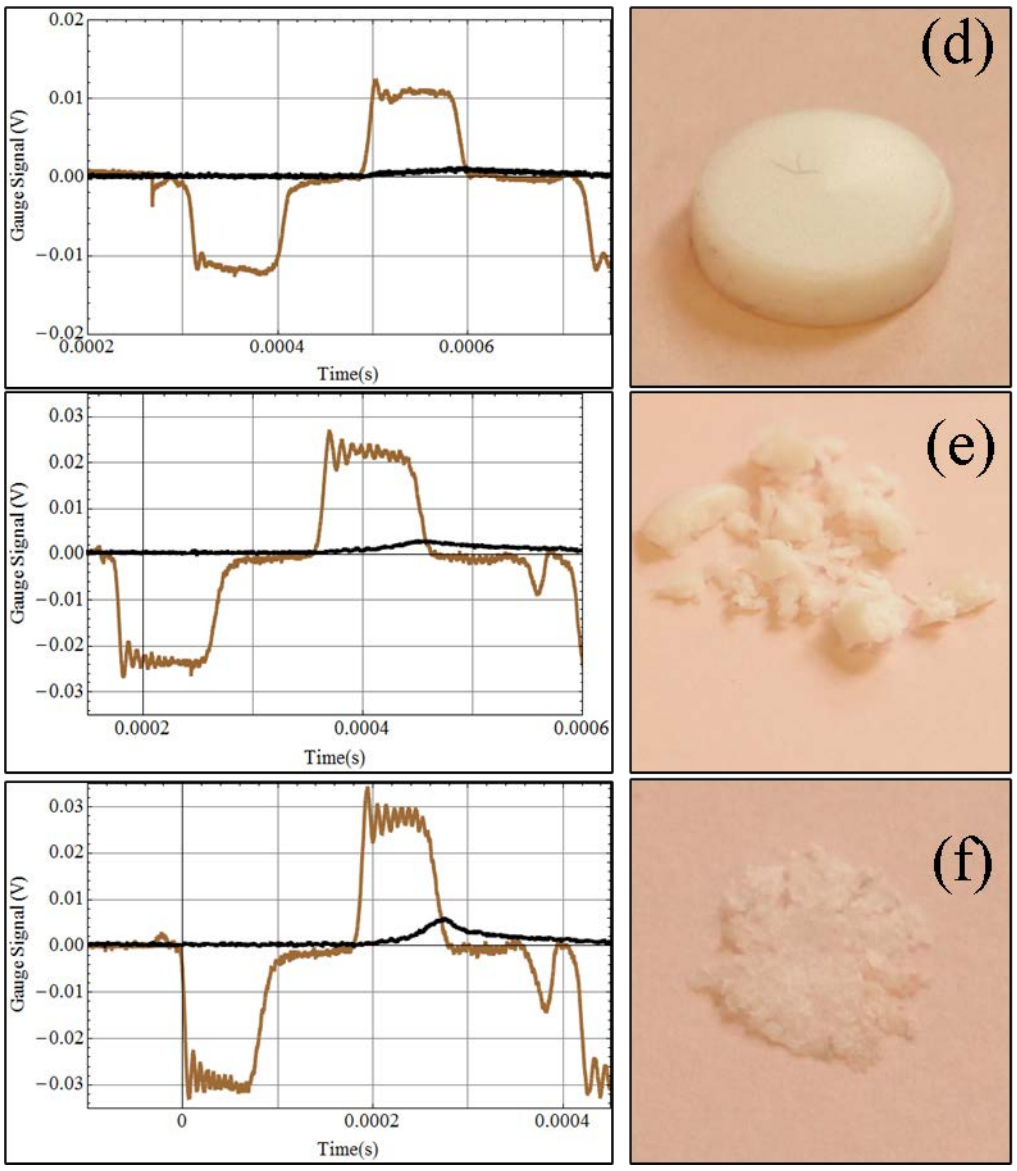


*Figure 5.13 (Graph) Voltage change in strain gauge signals as a function of time. Brown line shows loading and reflecting signals and black line shows the transmitting signal from the impact. (Image) Corresponding image of the PTFE specimen after SHPB compression testing at 50ºC under the strain rates of (d) 1665 $s^{-1}$, (e) 3345 $s^{-1}$, and (f) 4320 $s^{-1}$. Note that the deformed specimen in the image has gone through multiple loading, (i.e. Figure 5.1). Whereas, only the first set of reflecting and transmitting pluses are shown here.*

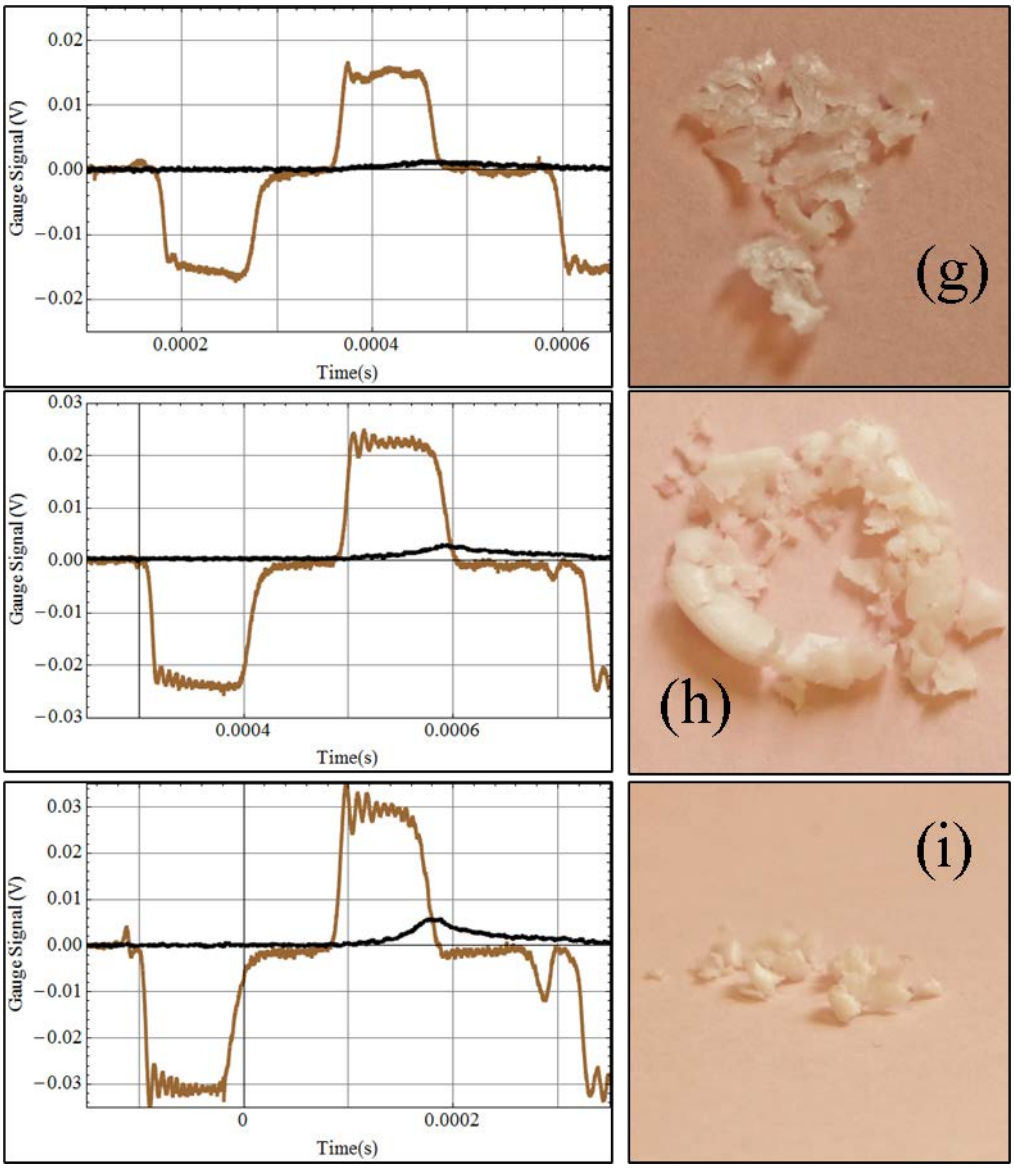


*Figure5.14 (Graph) Voltage change in strain gauge signals as a function of time. Brown line shows loading and reflecting signals and black line shows the transmitting signal from the impact. (Image) Corresponding image of the PTFE specimen after SHPB compression testing at 100ºC under the strain rates of (g) 2330 $s^{-1}$, (h) 3440 $s^{-1}$, and (i) 4460 $s^{-1}$. Note that the deformed specimen in the image has gone through multiple loading, (i.e. Figure 5.1). Whereas, only the first set of reflecting and transmitting pluses are shown here.*

### 5.2.1 Stress-strain curves

The stress-strain curves of the PTFE specimens are plotted in Appendix D. Ambient temperature, 50ºC and 100ºC in Figure C-4, C-5 and C-6 respectively. The stress-strain curves of the nine specimens shown in Figure 5.12, 5.13 and 5.14 can be found in Figure 5.15.

The SHPB test of ambient temperature PTFE specimens achieved the yield stress of 10.4 MPa when tested at 3240 $s^{-1}$ rate of strain, and the largest yield stress reached was 32.8 MPa at strain rate of 3775 $s^{-1}$. The average yield stress was 20.3 MPa, and the maximum stress reached was 95 MPa. The simple structure of the PTFE chain means there are less clusters of side-chain bonding producing low yield stress and small strain. The maximum strain of the elastic deformation of PTFE at ambient temperature is around 3% strain.

The ambient temperature PTFE specimen stress-strain curves are illustrated in Figure 5.15 and Figure C-14. Once the specimen yields, the sample continues to harden until specimen failure. The flow stress-strain curve is wavy, with two plateaus where the strain hardening slows down. Some specimens experience very large strain hardening after the second plateau before ultimate failure.

Specimens of PTFE tested at 50ºC yielded at a lower stress and strain compared to that at ambient temperature. The average yield stress was 14.7 MPa. The lowest yield stress occurred at 3550 $s^{-1}$, where the yield stress was at 6 MPa. And the maximum yield stress achieved was 39 MPa at 4670 $s^{-1}$. The stress-strain curves tested at 50ºC are similar to that of the ambient temperature. In the plastic region, the stress-strain curves show plateau regions in the continuity of strain hardening. Some specimens shows only one plateau, while most show two, and one showed three before reaching specimen failure.

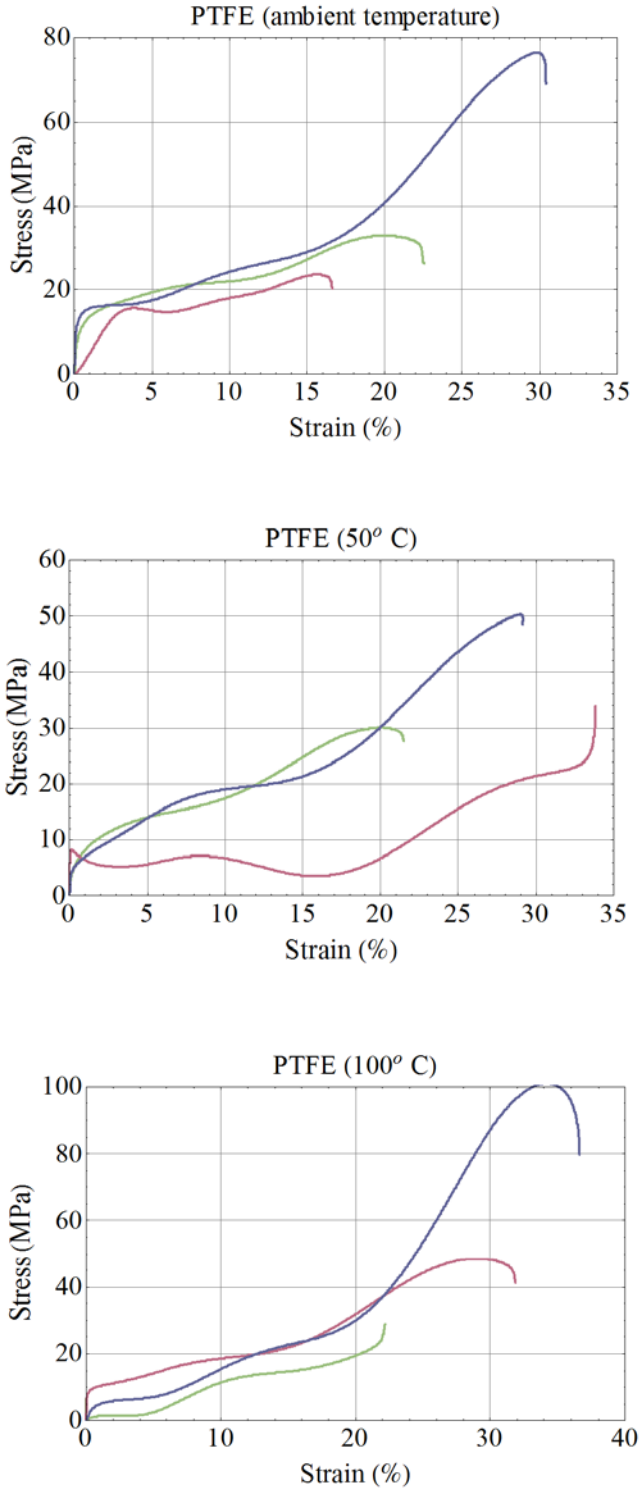


*Figure 5.15 Selection of PTFE specimen stress-strain curves at ambient temperature, 50 ºC and 100ºC. The yield point of PTFE is low. The plastic flow region in general shows strain hardening before failure of specimen. Complete collection of PTFE stress-strain curves can be found in Appendix D.*

It is not always possible to point out a practical yield point at 10% in PTFE specimens. The end of the small elastic region could be as low as 5MPa stress. This was detected at a strain rate of 2890 $s^{-1}$, and in some stress-strain curves the elastic deformation extends to a strain hardening, and the plot is more linear than a 'curve'. Mostly the stress-strain curve shows a very small region of elastic deformation, after which the strain softens, then hardens, and then softens again before a very large strain hardening. The amount of strain softening can vary by up to 8 MPa.

In all stress-strain curves, the more strain softens during deformation the higher stress is reached before failure. But what causes the strain softening after the elastic deformation and what determines the amount of strain softening is to be discussed.

### 5.2.2 Flow stress as a function of strain rate

The plastic flow stress of PTFE is plotted against the strain rate of the experiment at ambient temperature, 50ºC, and 100ºC in Figure 5.16. The aim is to find the dependence of the flow stress to strain rates, demonstrating the sensitivity of flow stress to strain rate. A range of strain at particular stress is chosen to represent flow stress. 5% strain is greater than the PTFE yield strain at around 3%. Above 20% strain, some specimens begin to fail, whereas, others experienced a dramatic increase in strain (the onset of the increase differs from specimen to specimen). Taking the two scenarios into consideration, stresses at 5%, 10%, 15% and 20% strain are used to determine flow stress of PTFE. Flow stresses of the same strain are connected into single plots to show how they develop against strain rate.

At ambient temperature the curves all follow the same trend, showing flow stress peak at 3100 $s^{-1}$. Flow stresses at 50ºC shows some fluctuation between strain rate of 3000 $s^{-1}$ and 4300 $s^{-1}$. The beginning of a peak is found at 4700 $s^{-1}$. Unfortunately, this was the highest strain rate reached. At 100ºC, flow stresses fluctuated though the whole range of strain rates tested (between 2740 $s^{-1}$ and 4555 $s^{-1}$). No clear flow stress peak can be observed.

An interesting phenomenon of a node is detected in the flow stresses of PTFE. At a particular strain rate, all flow stresses of different strain gives the same value. The node appeared at the strain rate of 2300 $s^{-1}$ at ambient temperature, 4300 $s^{-1}$ at 50ºC and 3970 $s^{-1}$ at 10 ºC.

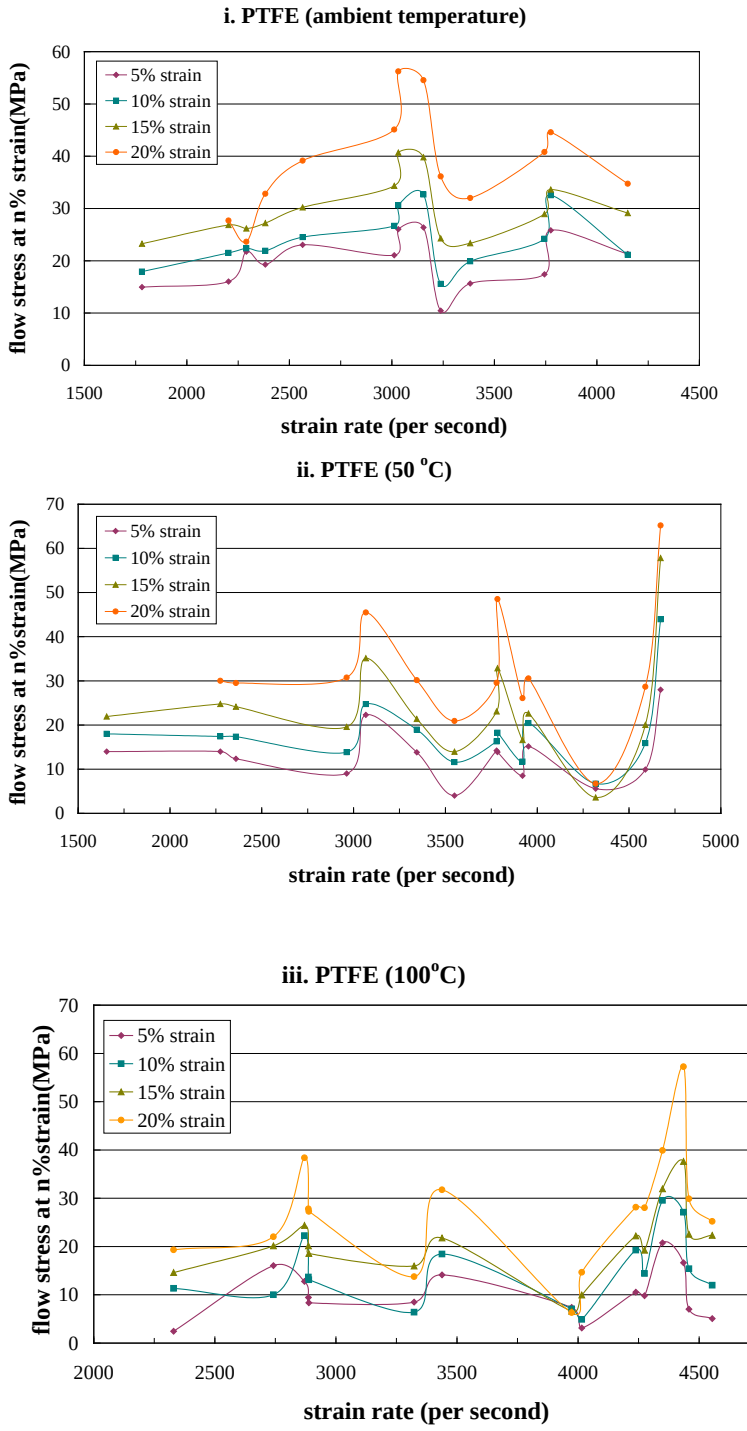


*Figure 5.16 Flow stresses (at 10%, 15%, 20% and 25% strain) as a function of strain rate, for PTFE specimens tested on the SHPB at ambient temperature, 50ºC and 100ºC. Flow stress peak is detected at 3100 $s^{-1}$ at ambient temperature, at 50ºC the beginning of a possible peak is detected at 4600 $s^{-1}$. And no peaks in flow stress can be found at 100ºC.*

### 5.2.3 Heat transfer in flow stress

The maximum temperature rise of PTFE during plastic deformation in the high strain rate experiments is the lowest of all four polymers. The temperature rise against strain plot is illustrated in Figure 5.17, 5.18 and 5.19, and the specimens are directly paired with the specimens in Figure 5.12, 5.13, and 5.14. Temperature rise calculations are described in chapter two, section 2.4.

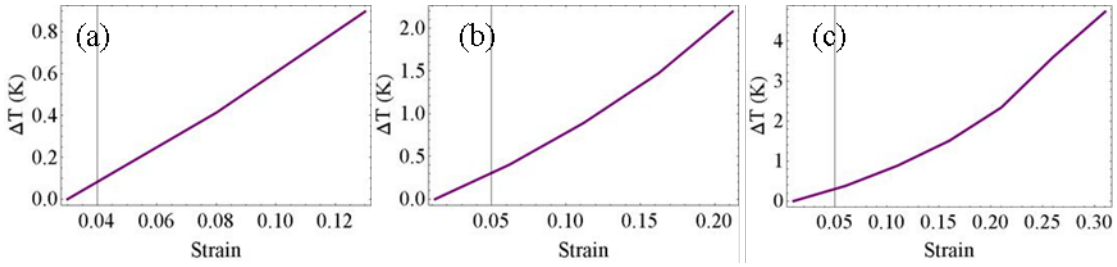


*Figure5.17 Temperature rise in the ambient temperature specimens during plastic flow. This is derived from the stress-strain curves obtained from PTFE specimens to estimate the maximum rise in temperature at rates of (a) 1780 $s^{-1}$, (b) 2380 $s^{-1}$, and (c) 3745 $s^{-1}$.*

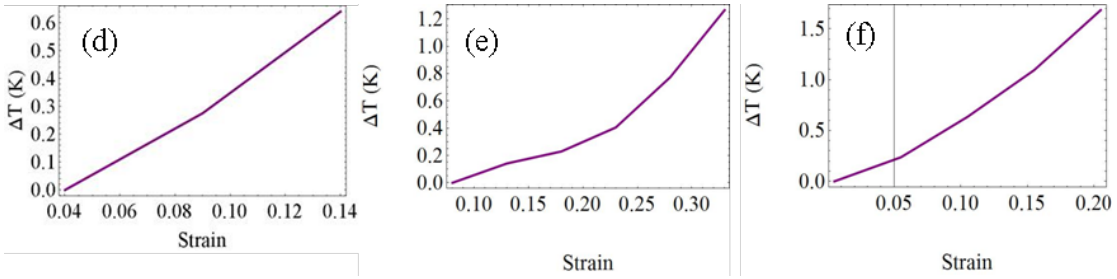


*Figure5.18 Temperature rise in the 50ºC specimens during plastic flow. This is derived from the stress-strain curves obtained from PTFE specimens to estimate the maximum rise in temperature at rates of (d) 1665 $s^{-1}$, (e) 3345 $s^{-1}$, and (f) 4320 $s^{-1}$.*

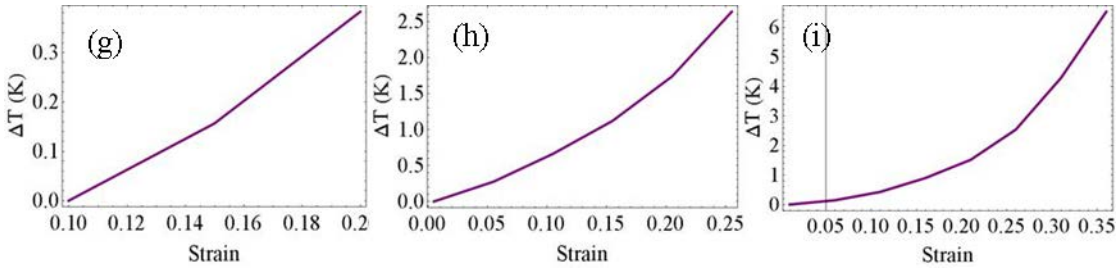


*Figure5.19 Temperature rise in the 100ºC specimens during plastic flow. This is derived from the stress-strain curves obtained from PTFE specimens to estimate the maximum rise in temperature at rates of (g) 2330 $s^{-1}$, (h) 3440 $s^{-1}$ and (i) 4460 $s^{-1}$.*

At ambient temperature tests in PTFE, the temperature rise during the impact test calculated at 10% strain is 0.6ºC at the strain rate of 1780 $s^{-1}$, 0.7ºC at 2380 $s^{-1}$, and 0.8ºC at 3745 $s^{-1}$. The rate of temperature rise is around 0.7ºC per 10% strain. The temperature rise in relation to strain is linear. Gradient change is detected in the specimen tested at the strain rate of 4320 $s^{-1}$, this is illustrated in Figure 5.17c at 22% strain.

Impact test conducted at 50ºC, the temperature rise at 10% strain is 0.35ºC at the strain rate of 1665 $s^{-1}$, 0.1ºC at 3345 $s^{-1}$, and 0.7ºC at 4320 $s^{-1}$. The rate of temperature rise is around 0.4ºC per 10% strain. The temperature rise in relation to strain is linear. Gradient change is detected in the specimens tested at the strain rate of 3345 $s^{-1}$; this is illustrated in Figure 5.18e at 18%, 23% and 29% strain.

For specimen test temperature at 100ºC, the temperature rise at 10% strain is 0.1ºC at the strain rate of 2330 $s^{-1}$, 0.7ºC at 3440 $s^{-1}$, and 0.5ºC at 4460 $s^{-1}$. The rate of temperature rise is around 0.4ºC per 10% strain. The temperature rise in relation to strain is linear. Gradient change is detected in the specimens tested at the strain rate of 3440 $s^{-1}$ and 4460 $s^{-1}$; this is illustrated in Figure.5.19h at 16%, and 20% strain, and in Figure 5.19i at 20%, 25%, and 30% strain.

Specimens where larger strain was achieved, the gradient change of the temperature rise becomes more obvious. This could be caused by the increase of strain during the compression. The specimen diameter/length ratio increases to a point where the inertia in the specimen causes strain hardening and larger temperature rise rate. Both by increasing strain rate and temperature will increase the specimen strain, and influence the gradient change of temperature increase.

### 5.2.4 DSC and DMA summary

The differential scanning calorimeter (DSC) testing result of PTFE is presented in Figure 5.20. The 22.5 mg PTFE sample was first cooled to 0ºC then heated at 5ºC per minute up to 150ºC. It was then cooled back to room temperature at the rate of 20ºC per minute. The grey dotted curve is the tested result and the purple solid line represents the PTFE sample without the influence of the pan and lid holding the sample.

Two changes in the baseline can be observed, the first is a drop with the peak at 18ºC. The second change is a positive step, which appeared at 12 minutes this

translates to at around 32ºC. This is the only transition we can see in the material using the DSC method (melting point of PTFE is 323 ºC). This would be the crystal-crystal mospheric change in the PTFE material discussed in section 3.2, Jordan et al. also reported the transition at 19ºC and 30ºC. [**Jorden et al. 2005**] The cooling rate was too fast, no clear transition can be found.

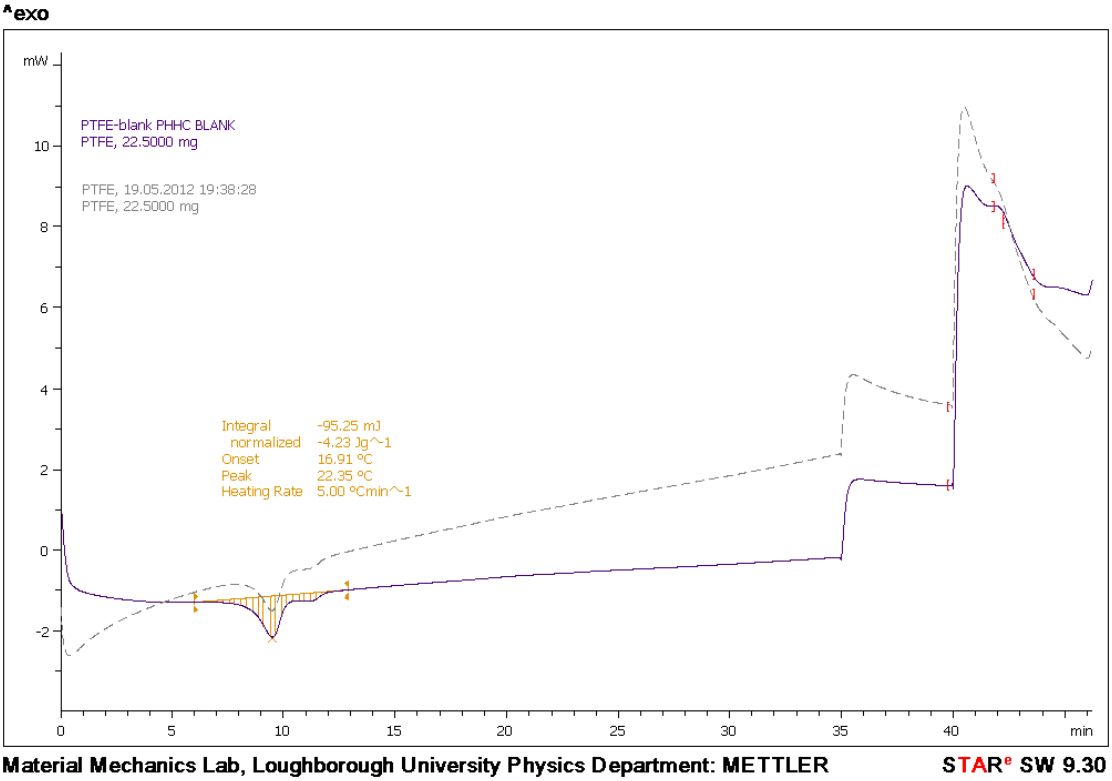


*Figure5.20 Thermal analysis using the differential scanning calorimeter tested on a PTFE sample. The sample was heated between 0ºC and 150ºC at the heating rate of 5ºC per minute, and then held at 150ºC for five minutes before cooling at the rate of 20ºC per minute.*

The dynamic mechanical analysis of PTFE sample was carried out between -50ºC and 150ºC at two different frequencies. A more detailed analysis of the storage and loss modulus along with the phase lag between applied and measured stress, the loss angle, are reported in chapter four, section 4.6.

The end of the storage modulus curve drops are more noticeable in the case of PTFE in comparison to PCTFE, these demonstrates there is more amorphous components in PTFE. The drops occurred at 45ºC of about 900 MPa at 1 Hz and near 55ºC for around 700 MPa at 100 Hz. These temperatures coincide well with the peaks found in the loss angle, with the loss angle peak at 100 Hz found slightly higher at 62ºC. The β-transition temperatures can be detected.

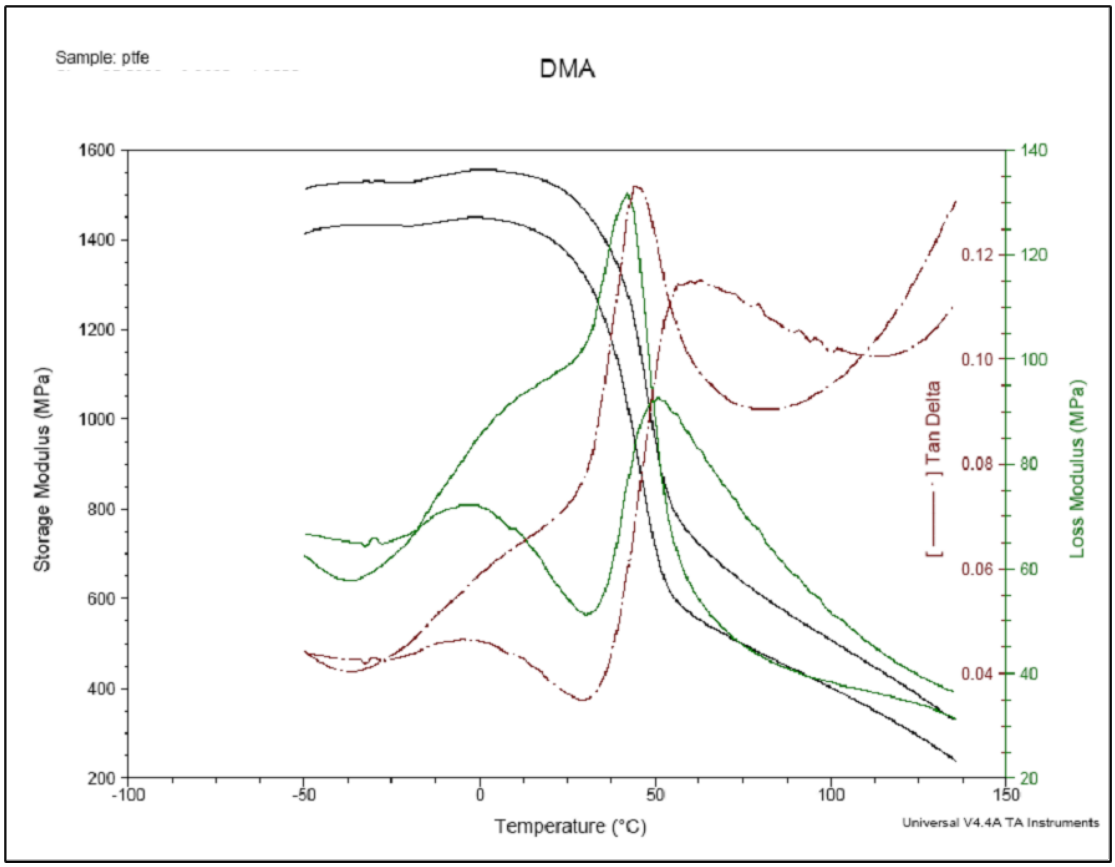


*Figure 5.21 A temperature sweep dynamic mechanical analysis from -50ºC to 150ºC on a PTFE sample at frequencies of 1 Hz and 100 Hz. Using different initial static load and strain. Storage modulus (left), loss modulus (right) and loss angle is plotted against temperature. The glass transition temperature is measured at both frequencies.*

## 5.2.5 PTFE results summary

A PTFE sample was heated with constant temperature increase of 5ºC per minute using the differential scanning calorimeter. The heat flow was measured and plotted against temperatures ranging from 0ºC to 150ºC. One transitions temperature is found at $T_g$ =38ºC.

Dynamic mechanical analysis was performed on PTFE from -50ºC to 150ºC. The storage modulus shows a sharp decrease. The loss modulus at 1 Hz showed two peaks, but at 100 Hz the two peaks merged and are partially overlapping. Tangent loss angle illustrates $T_g$. At 100 Hz, $T_g$ = 62ºC and at 1 Hz, $T_g$ = 45ºC. $T_g$ shifts 17ºC between the frequency change. High strain rate compression tests at ambient temperature were carried out between 2300 $s^{-1}$ and 3000 $s^{-1}$. The average yield stress was 20.3 MPa. The final specimen strain reached between 20%-30%. A flow stress

peak was found at the strain rate of 3100 $s^{-1}$. Maximum temperature rise during the plastic flow was 5ºC.

High strain rate compression tests at 50ºC were performed between 1665 $s^{-1}$ and 4670 $s^{-1}$. The average stress of yield was 14.7 MPa and the final specimen strain reached was between 25% - 35%. The beginning of a peak in flow stress is seen at 4700 $s^{-1}$. The maximum temperature rise during the plastic flow was 1.7ºC.

High strain rate compression tests at 100ºC were conducted between 2740 $s^{-1}$ and 4555 $s^{-1}$. The average stress of yield cannot be found because the yield point cannot be identified. The final specimen strain was between 30% and 40%. No flow stress peak was found. The maximum temperature rise during the plastic flow was 6.5ºC.

## 5.3 PVC results and analysis

At ambient temperature, PVC specimens were tested in the strain rate range of 2260 $s^{-1}$ to 5795 $s^{-1}$.

Fractures which outline the centre half of the specimen with more fracture which develops from this ring to the edge of the specimen is observed (i.e. Figure 5.22a) in all PVC specimens at the lower range of the strain rate. However, at higher strain rates from 3100 $s^{-1}$, the deformation is concentrated at the centre of the specimen as seen in Figure 5.22b, where the centre of the specimen (resembling a web with holes), also had a thin layer of powdered PVC is left on the bars. The centre of the specimen completely disappears by the point that strain rate reaches 5200 $s^{-1}$. Again a layer of powder was left on the bars after the impact. The specimen shown in Figure 5.22c also gave of a smell of burning after the impact.

PVC was tested in the strain range of 1840 $s^{-1}$ to 5412 $s^{-1}$ at 50ºC. At lower strain-rates, Figure 5.23d for example, the specimen deformed in a more viscous way without fracturing. The centre of the specimen concaved inwards, marking the inner area of which fails with increase of strain rate. It is of interest to note some experiments tested on high density polyethylene (HDPE) and low density polyethylene (LDPE) also shows a concave centre area under high strain compression tests. The ratio of the inner circle to the outer ring decreases with the increase of strain rate (The polymer structure of PVC is similar to PE with a chlorine atom substituting one of the four hydrogen.)

PVC was tested with in the strain range of 2555 $s^{-1}$ to 6187 $s^{-1}$ at 100ºC. The centres of the specimens have all failed, leaving the complete outer rings of the specimen. In Figure 5.24g, h and i, the PVC specimens shows elastic deformation on the outer ring of the specimen and inelastic deformation in the centre.

In Figure 5.23e the outer ring of the specimen tested at 4575 $s^{-1}$ shows inelastic deformation. The same can be found in Figure 5.24h and 5.24i specimens. The strain gauge signals of these three specimens gave much higher Pochhammer-Chree oscillations in the pulses; this could be the reason for the elastic deformation of the resulting specimens. And vice versa, the specimens that underwent a smoother loading pulse maintained the original shape of the specimen on the outer

ring almost like an elastic deformation, whereas the centre of the PVC specimens failed.

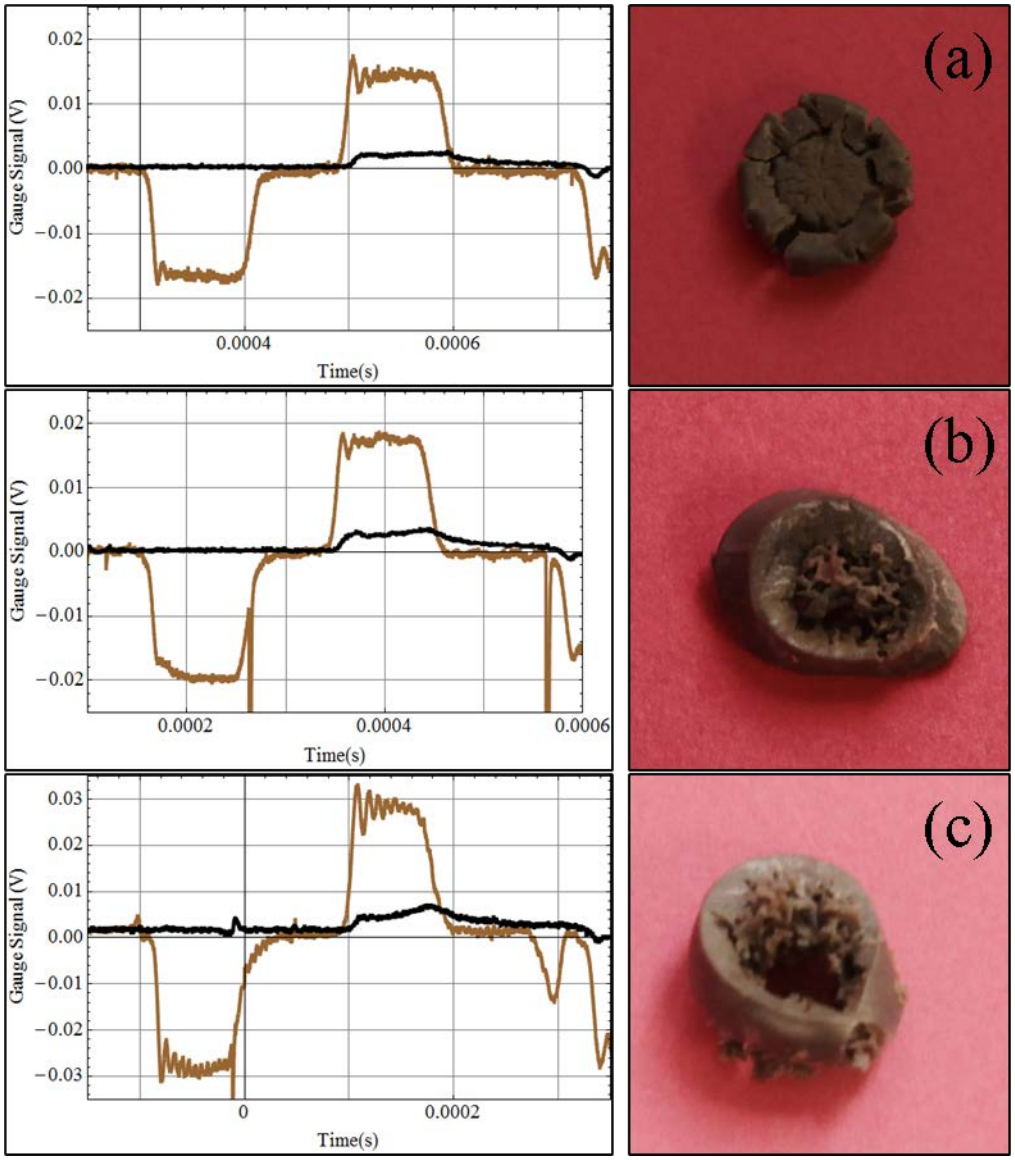


*Figure 5.22 (Graph) Voltage change in strain gauge signals as a function of time. Brown line shows loading and reflecting signals and black line shows the transmitting signal from the impact. (Image) Corresponding image of the PVC specimen after SHPB compression testing at ambient temperature under the strain rates of (a) 2840 $s^{-1}$, (b) 3445 $s^{-1}$, and (c) 5230 $s^{-1}$. Note that the deformed specimen in the image has gone though multiple loading, (i.e. Figure 5.1). Whereas, only the first set of reflecting and transmitting pluses are shown here.*

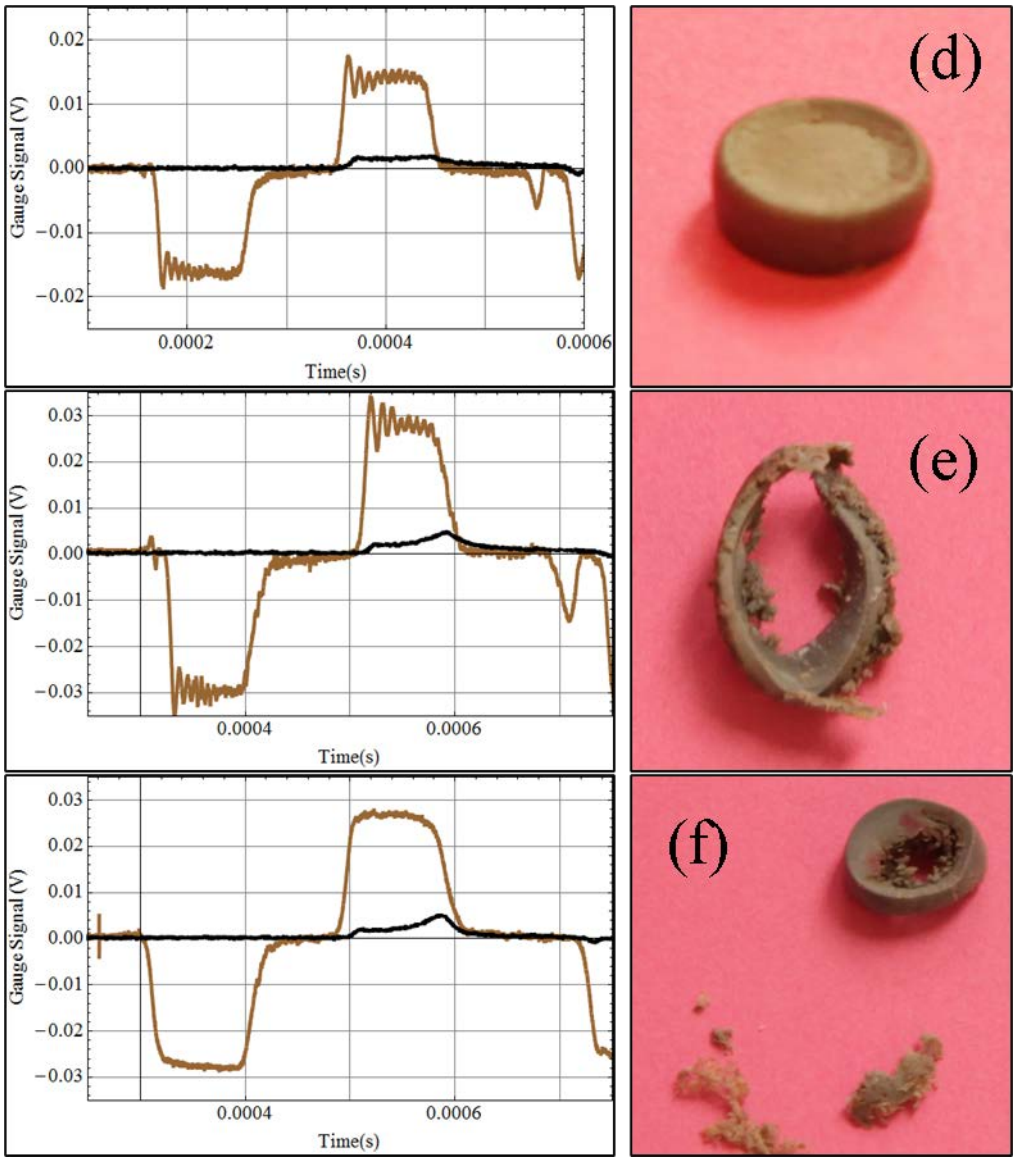


*Figure 5.23 (Graph) Voltage change in strain gauge signals as a function of time. Brown line shows loading and reflecting signals and black line shows the transmitting signal from the impact. (Image) Corresponding image of the PVC specimen after SHPB compression testing at 50ºC under the strain rates of (d) 2800 $s^{-1}$, (e) 4575 $s^{-1}$, and (f) 4760 $s^{-1}$. Note that the deformed specimen in the image has gone though multiple loading, (i.e. Figure 5.1). Whereas, only the first set of reflecting and transmitting pluses are shown here.*

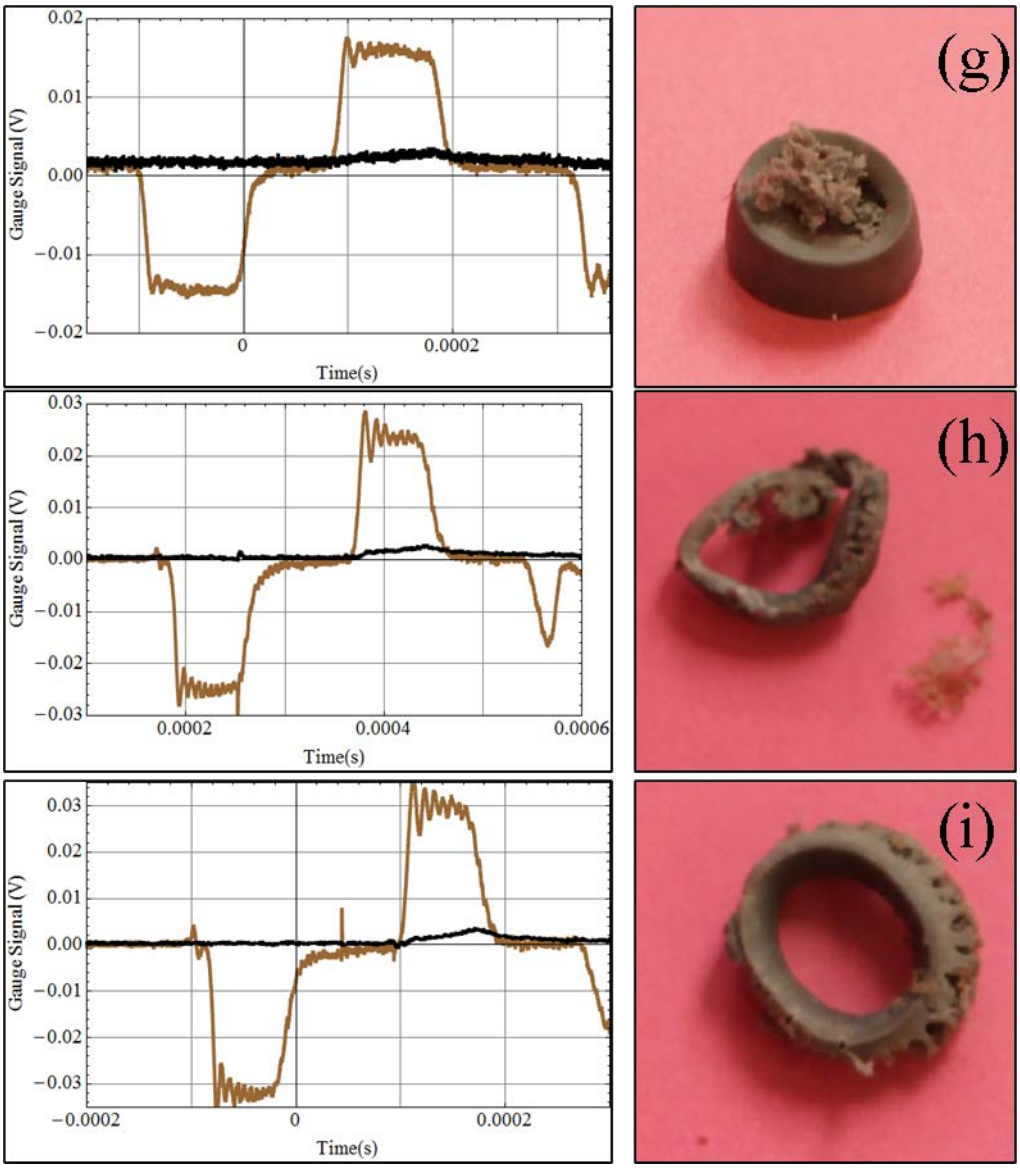


*Figure5.24 (Graph) Voltage change in strain gauge signals as a function of time. Brown line shows loading and reflecting signals and black line shows the transmitting signal from the impact. (Image) Corresponding image of the PVC specimen after SHPB compression testing at 100ºC under the strain rates of (g) 2860 $s^{-1}$, (h) 4540 $s^{-1}$, and (i) 5895 $s^{-1}$. Note that the deformed specimen in the image has gone though multiple loading, (i.e. Figure 5.1). Whereas, only the first set of reflecting and transmitting pluses are shown here.*

Observations made in the PVC experiments were that there are two scenarios to be found in ambient temperature PVC compression tests. The specimens' temperature was taken after impact. If the specimen shows lots of fractures then the temperatures of the specimen does not rise during the experiment, and vice versa the temperature of the specimen rises considerably after the experiment when the specimen seems to deform in a homogenous manner.

### 5.3.1 Stress-strain curves

The stress-strain curves achieved using the SHPB on PVC specimens are plotted in Appendix D. Ambient temperature, 50ºC and 100ºC in Figure D-7, D-8 and D-9 respectively. The stress-strain curves of the nine specimens shown in Figure 5.22, 5.23 and 5.24 can be found in Figure 5.25 in three plots; ambient temperature, 50ºC and 100ºC.

At ambient temperature, the lowest yielding point is at 81.3 MPa (this is achieved with a strain rate of 4340 $s^{-1}$) and the highest yield stress is 125.8 MPa at 5255 $s^{-1}$. The average yield stress is 101.3 MPa. The end of the elastic deformation is between 4% - 6% strain. And ultimate deformation is between 20% - 45% strain. The yield point is clearly seen in the stress-strain curves. The main part of the plastic flow region of the stress-strain rate curve is constant in stress before failure of the specimen. Specimens tested at higher strain rate also show strain hardening before failure.

At 50ºC, the lowest yielding point is at 62.3 MPa. This is achieved with a strain rate of 2800 $s^{-1}$ and the highest yield stress is 94 MPa at 5410 $s^{-1}$. This is not including the two stress-strain curves which yielded at a much higher stresses of 288 MPa and 266 MPa at strain rates of 3050 $s^{-1}$ and 3290 $s^{-1}$, respectively. The two stress-strain curves are illustrated in Figure D-8 (at 50ºC. The average yield stress was 79.7 MPa and the end of the elastic deformation was between 2% - 5% strain. Ultimate deformation was found to be between 20% - 45% strain. The specimen yields then experiences plastic flow without much change in stress, after which strain hardening can be found is most specimens. Strain hardening will be greater in the specimen before failure when the test strain rate is higher.

Stress-strain curves of experiments conducted at 100ºC are illustrated in Figure 5.25 and Figure D-9. The yield stress becomes lower as the temperature increases; the average yield stress is 47.5 MPa. The yield point is not so distinct. The elastic deformation at very high strain rates still shows brittleness where the specimen yields at less then 1% strain. However, some show rubbery characteristics where the specimen yields near 10% strain. The shape of the stress-strain curve is similar to that at ambient temperature and 50ºC.

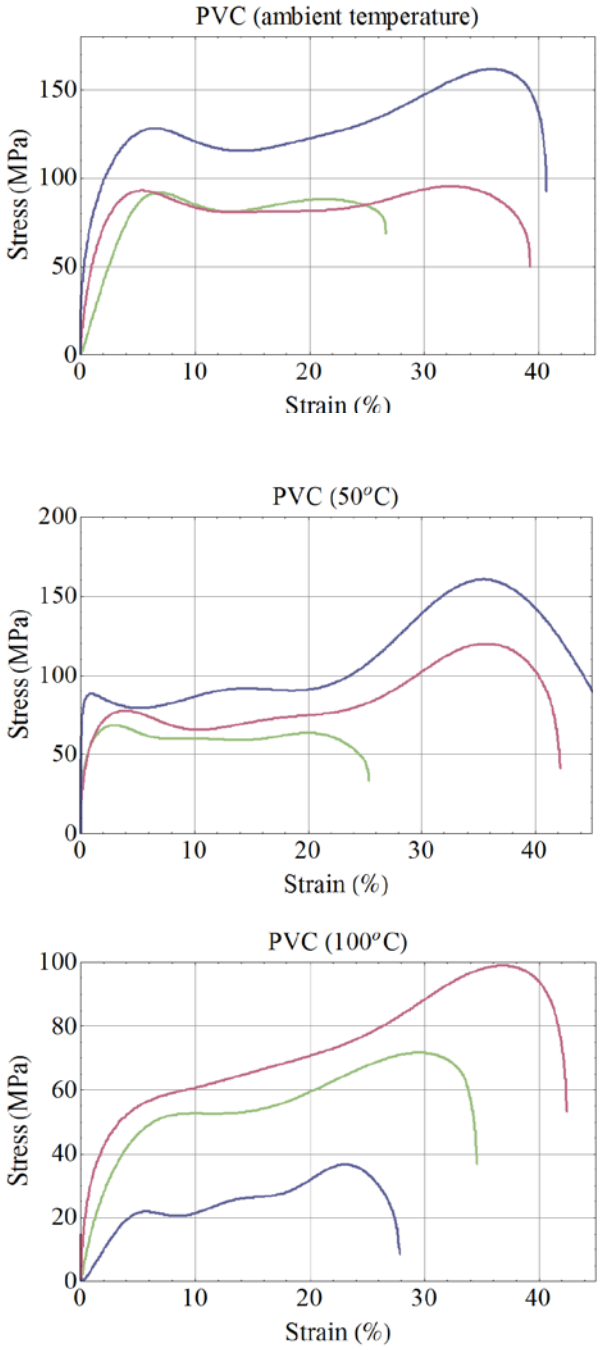


*Figure5.25 Selection of PVC specimen stress-strain curves at ambient temperature, 50ºC and 100ºC. The yield stress of PVC is largely reduced with increase in temperature. Strain softening is found after the yield point. Complete collection of PVC stress-strain curves can be found in Appendix D.*

## 5.3.2 Flow stress as a function of strain rate

The plastic flow stress of PVC is plotted against the strain rate at ambient temperature, 50ºC, and 100ºC in Figure 5.26. The aim is to find the dependence of the

flow stress to strain rates, demonstrating the sensitivity of flow stress to strain rate. A range of stress at a particular strain is chosen to represent flow stress. 10% stress is greater than the PVC yield strain of average 5% strain, however, the yield strain ranged from 1% up to 10% strain. Above 25% strain, some specimens begin to show failure, whereas, others experienced a dramatic increase in strain (the onset of the increase differs from specimen to specimen). Taking the two scenarios into consideration, stress at 10%, 15%, 20% and 25% strain is used to determine the flow stress of PVC. Flow stresses of the same strain were connected to show how it develops against strain rate.

At ambient temperature, flow stresses show a sharp peak at 3060 $s^{-1}$. At strain rates greater than 4000 $s^{-1}$, the material flow stresses generally increased with the increase in strain rate.

At 50ºC, two peaks are found at 3050 $s^{-1}$ and 3290 $s^{-1}$, with a drop in between the two points at 3125 $s^{-1}$. Again, after 4000 $s^{-1}$, the flow stresses increased as strain rate increased.

At 100ºC, one flow stress peak was found to occur at 5460 $s^{-1}$. At this temperature, the flow stress at 25% strain showed a very different pattern to flow stresses between 15% - 20% strain. This could be because of the wide yield strain range at 100ºC that occurred at 25% strain. In some PVC specimens the strain softening region of the stress-strain curve is still experienced at this temperature and strain, while other specimens are undergoing strain hardening. Flow stress at 25% strain at this temperature is not suitable for representing flow stress.

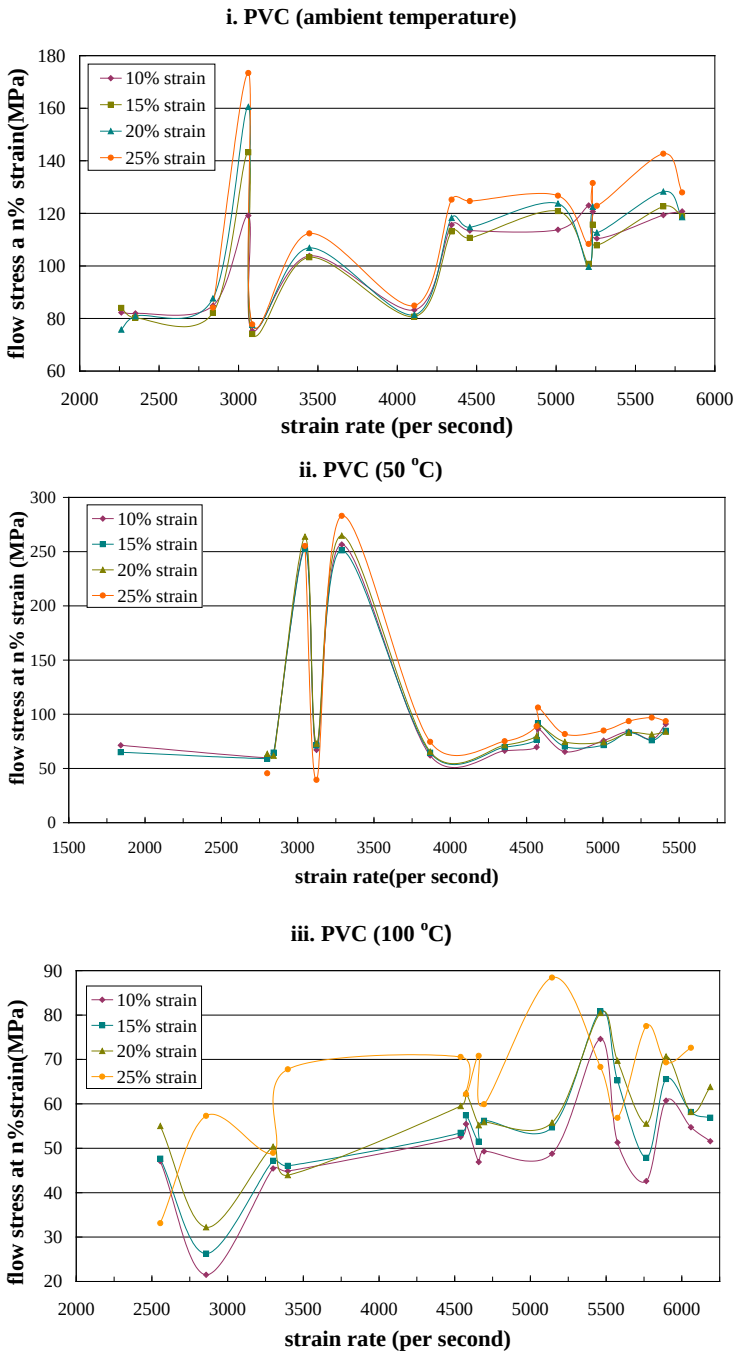


*Figure 5.26 Flow stresses (at 10%, 15%, 20% and 25% strain) as a function of strain rate, for PVC specimens tested on the SHPB at ambient temperature, 50ºC and 100ºC. Flow stress peak is detected at 3060 $s^{-1}$at ambient temperature, at 50ºC two peaks is detected at 3045 $s^{-1}$and 3290 $s^{-1}$. And a smaller peak is can be seen at 5460 $s^{-1}$ at 100ºC.*

### 5.3.3 Heat transfer in flow stress

The maximum heat created in the plastic flow region of the SHPB test was measured using the plastic flow area of the stress-strain curve. PVC shows the largest temperature rise in all four polymers tested. Examples of temperature rise (ΔT) plots are presented in Figure 5.27 for ambient temperature tests, Figure 5.28 for tests at 50ºC, and Figure 5.29 for tests done at 100ºC. The temperature rise calculations are described in chapter two, section 2.4.

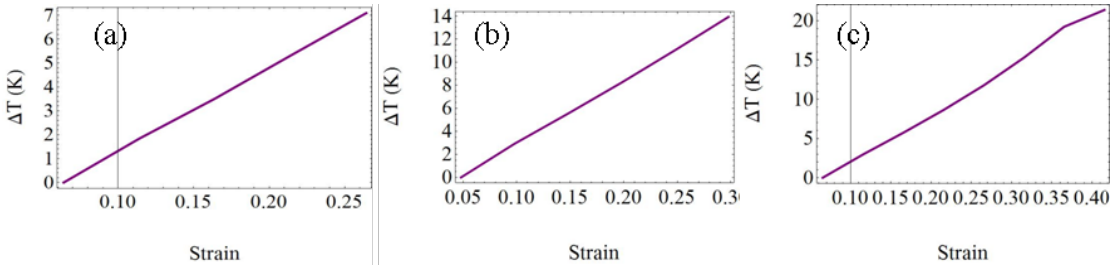


*Figure 5.27 Temperature rise in the ambient temperature specimen during plastic flow. This is derived from the stress-strain curves obtained from PVC specimens to estimate the maximum rise in temperature at rates of (a) 2840 $s^{-1}$, (b) 3445 $s^{-1}$, and (c) 5230 $s^{-1}$.*

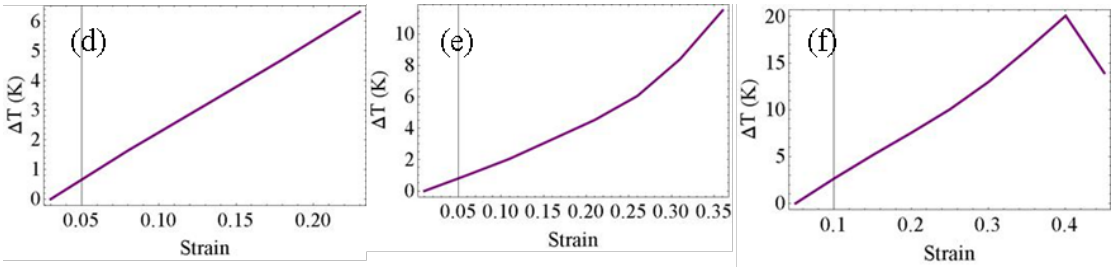


*Figure 5.28 Temperature rise in the 50ºC specimen during plastic flow. This is derived from the stress-strain curves obtained from PVC specimens to estimate the maximum rise in temperature at rates of (d) 2800 $s^{-1}$, (e) 4575 $s^{-1}$, and (f) 4760 $s^{-1}$.*

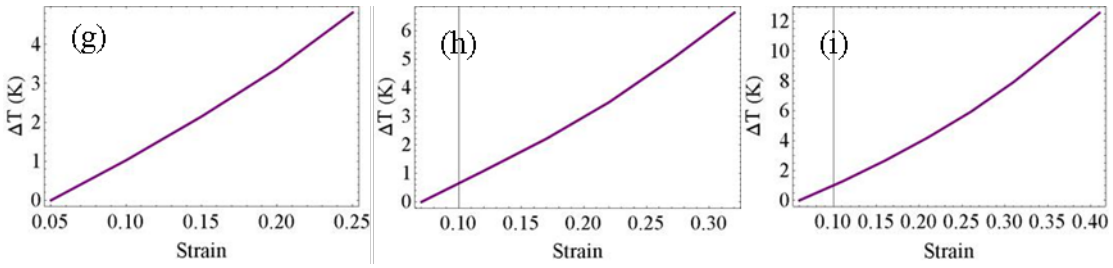


*Figure 5.29 Temperature rise in the 100ºC specimen during plastic flow. This is derived from the stress-strain curves obtained from PVC specimens to estimate the maximum rise in temperature at rates of (g) 2860 $s^{-1}$, (h) 4540 $s^{-1}$, and (i) 5895 $s^{-1}$.*

The calculated temperature rise at 15% strain in PVC specimens tested at ambient temperature at 2840 $s^{-1}$ was 3ºC and the rate change stayed the same till the specimen failed at 30% strain. Temperature rise was 5.5ºC for strain rate of 3445 $s^{-1}$, and at strain rate of 5230 $s^{-1}$ the temperature rise was 5ºC. All three ambient temperatures shows linear relation between temperature rise and increase of strain rate. Figure 5.26c shows a slight curvature after 30% strain.

Specimens tested at 50ºC the calculated temperature rises at 15% strain were a 4ºC increase for strain rate of 2800 $s^{-1}$, and 3ºC increases in temperature for 4575 $s^{-1}$ strain rate. In the sample tested at 4701 $s^{-1}$ in strain rate the temperature rise was calculated at 5ºC. The temperature rise against strain in Figure 5.28e shows rate changes at stain near 25% and again at 30%.

In 100ºC specimens tested, the temperature rise in the plastic region were 2.2ºC at 2860 $s^{-1}$ strain rate , 1.8ºC at 4540 $s^{-1}$ strain rate, and 2.5ºC at 5895 $s^{-1}$ strain rate. The temperature rise against strain in Figure 5.2h and 5.29i shows rate changes at stain near 25% and again at 30%.

### 5.3.4 DSC and DMA summary

The differential scanning calorimeter (DSC) testing result of PVC is presented in Figure 5.30. The 8.3mg PVC sample was first cooled to 0ºC then heated at 5ºC per minute up to 150ºC. It was then cooled back to room temperature at the rate of 20ºC per minute. The grey dotted curve is the tested result and the purple solid line represents the PTFE sample without the influence of the pan and lid holding the sample.

Four changes can be observed in the baseline one after another. The first is a drop with the peak at 66ºC. The second change is a drop at 77ºC, and the third at 93ºC followed by the last one at 103ºC. The largest change is the first one at 66ºC, this could be considered as the beginning of the glass transition in the specimen. The cooling rate was too fast to observe any transitions.

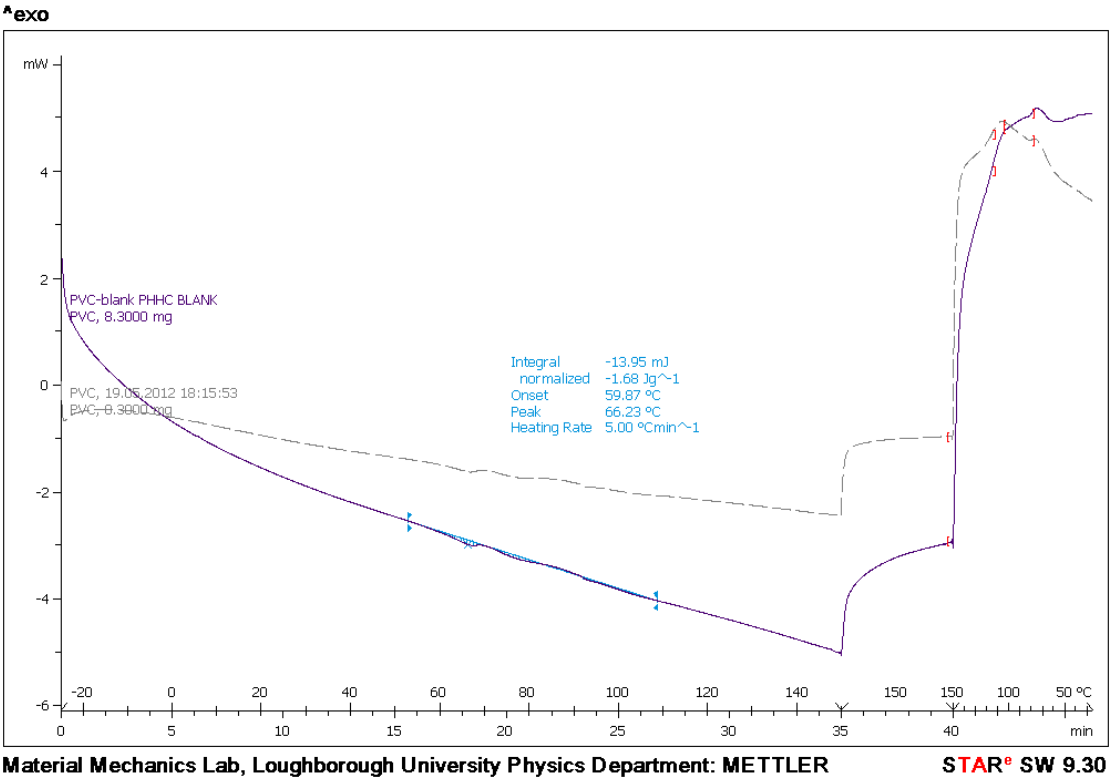


*Figure 5.30 Thermal analysis using the differential scanning calorimeter tested on a PVC sample. The sample was heated between 0ºC and 250ºC at the heating rate of 5ºC per minute, and then held at 250ºC for five minutes before cooling at the rate of 20ºC per minute.*

The dynamic mechanical analysis of PVC sample was carried out between -50ºC and 150ºC at two different frequencies. A more detailed analysis of the storage and loss modulus along with the phase lag between applied and measured stress, the loss angle, is reported in Chapter four, section 4.6.

The storage modulus curve drops at oscillation frequency of 1 Hz at 60ºC this extends to 100ºC. At oscillation frequency of 100 Hz, the glass transition began near 70ºC and extends to 110ºC. These temperatures coincide well with the peaks found in the loss angle, with the loss angle peak at 100 Hz found slightly higher at 109ºC, and at 1 Hz detected at 98ºC in PVC samples.

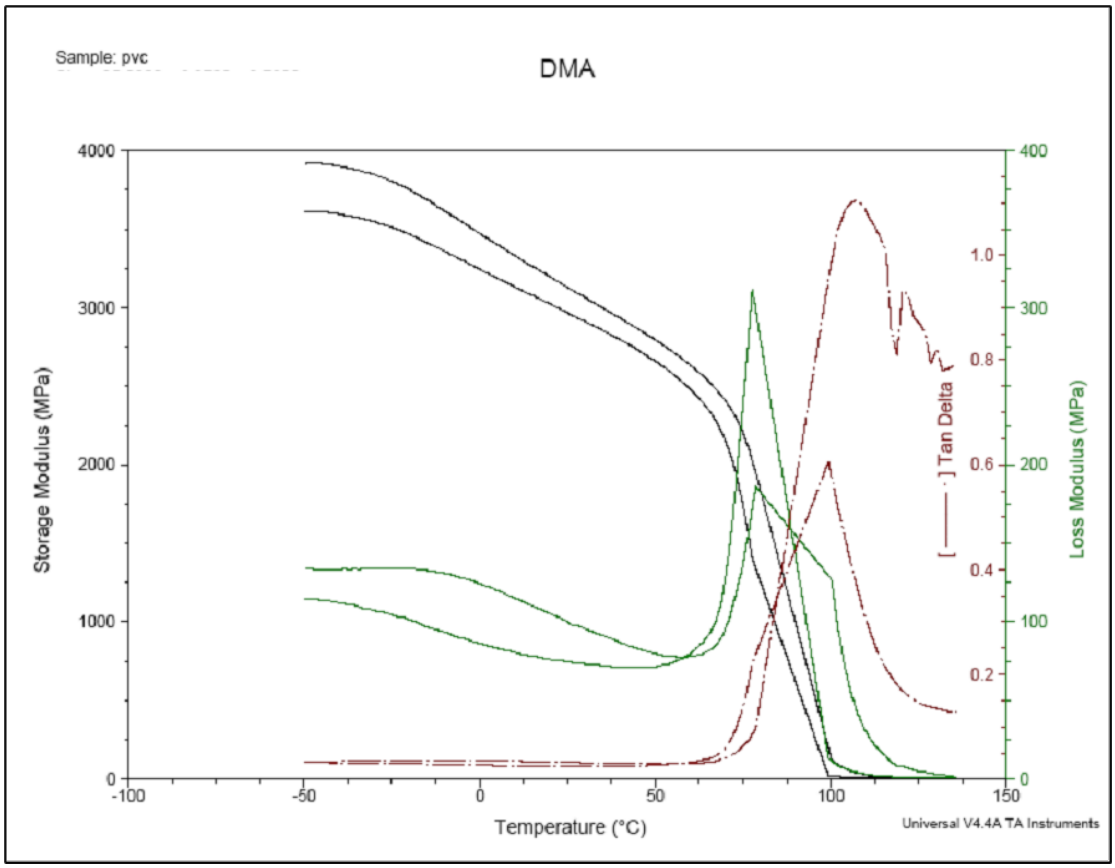


*Figure 5.31A temperature sweep dynamic mechanical analysis from -50ºC to 150ºC on a PVC sample at frequencies of 1 Hz and 100 Hz. Using different initial static load and strain. Storage modulus (left), loss modulus (right) and loss angle is plotted against temperature. The glass transition temperature is measured at both frequencies.*

## 5.3.5 PVC results summary

A PVC sample was heated with a constant temperature increase of 5ºC per minute using the differential scanning calorimeter. The heat flow is measured and plotted against temperature in the range from -20ºC to 150ºC. Four transitions in the range are seen close together at 66ºC, 77ºC, 93ºC, and 103ºC.

Dynamic mechanical analysis was carried out on PVC in the temperature range of -50ºC to 150ºC. The storage modulus shows sharp decrease in the range from 60ºC to 100ºC at 1 Hz, and 70ºC - 110ºC at 100 Hz. Loss angle peak illustrates $T_g$. At 100 Hz, $T_g$ =109ºC and at 1 Hz, $T_g$ = 98ºC. $T_g$ shifts 11ºC between the frequency changes.

High strain rate compression tests at ambient temperature were done at strain rates between 2260 $s^{-1}$ and 5790 $s^{-1}$. The average yield stress was 101.2 MPa and the

final specimen strain reached between 20% - 45%. A flow stress peak was found at the strain rate of 3060 $s^{-1}$. The maximum temperature rise during the plastic flow was 20ºC.

High strain rate compression testing at 50ºC was conducted between strain rates of 1840 $s^{-1}$ and 5410 $s^{-1}$. The average stress of yield is 80 MPa and the final specimen strain was reached between 25% - 35%. Two flow stress peaks are seen at 3050 $s^{-1}$ and 3290 $s^{-1}$. The maximum temperature rise during the plastic flow was 20ºC.

High strain rate compression tests at 100ºC were done between strain rates of 2555 $s^{-1}$ and 6190 $s^{-1}$. The average yield stress was 48 MPa. The final specimen strain was between 25% and 45%. A possible flow stress peak at 5460 $s^{-1}$ was witnessed. The maximum temperature rise during the plastic flow was 13ºC.

## 5.4 Overview of PMMA results and analysis

PMMA was the first polymer tested in this work and results are published in the paper included in Appendix C.

PMMA was tested at five different temperatures, ambient temperature (RT), 30ºC, 50ºC, 70ºC and 90ºC. Five sets of stress-strain rates curves are presented in Figure 5.32. The strain hardening and softening of PMMA stress-strain curves is less clear due to the brittleness of the material. Therefore, the yield stress of PMMA is difficult to determine, flow stress at 4% strain is chosen to represent flow stress. In general cases, 4% strain has passed yield point and the material has not deformed, however, in cases which this is not true the highest point of the stress-strain curve was chosen to represent flow stress.

Figure 5.32 also illustrates the samples response at RT and 30ºC, 50ºC, and 70ºC (image 5.32f, 5.32g, 5.32h and 5.32i, respectively). And the voltage-time plots of the impact related to these samples are presented in Figure 5.32j, 5.32k, 5.32l and 5.32m. There are obvious cracks and breakages at high strain rates ($2\times10^3$ $s^{-1}$).

PMMA under room temperature conditions is glassy and ductile, yet 70ºC and 90ºC heated samples had better impact resistance. From the appearances of the tested samples this is clearly demonstrated and is supported by the stress-strain curves. The flow stress as a function of strain rate is plotted in Figure 2 in Appendix C.

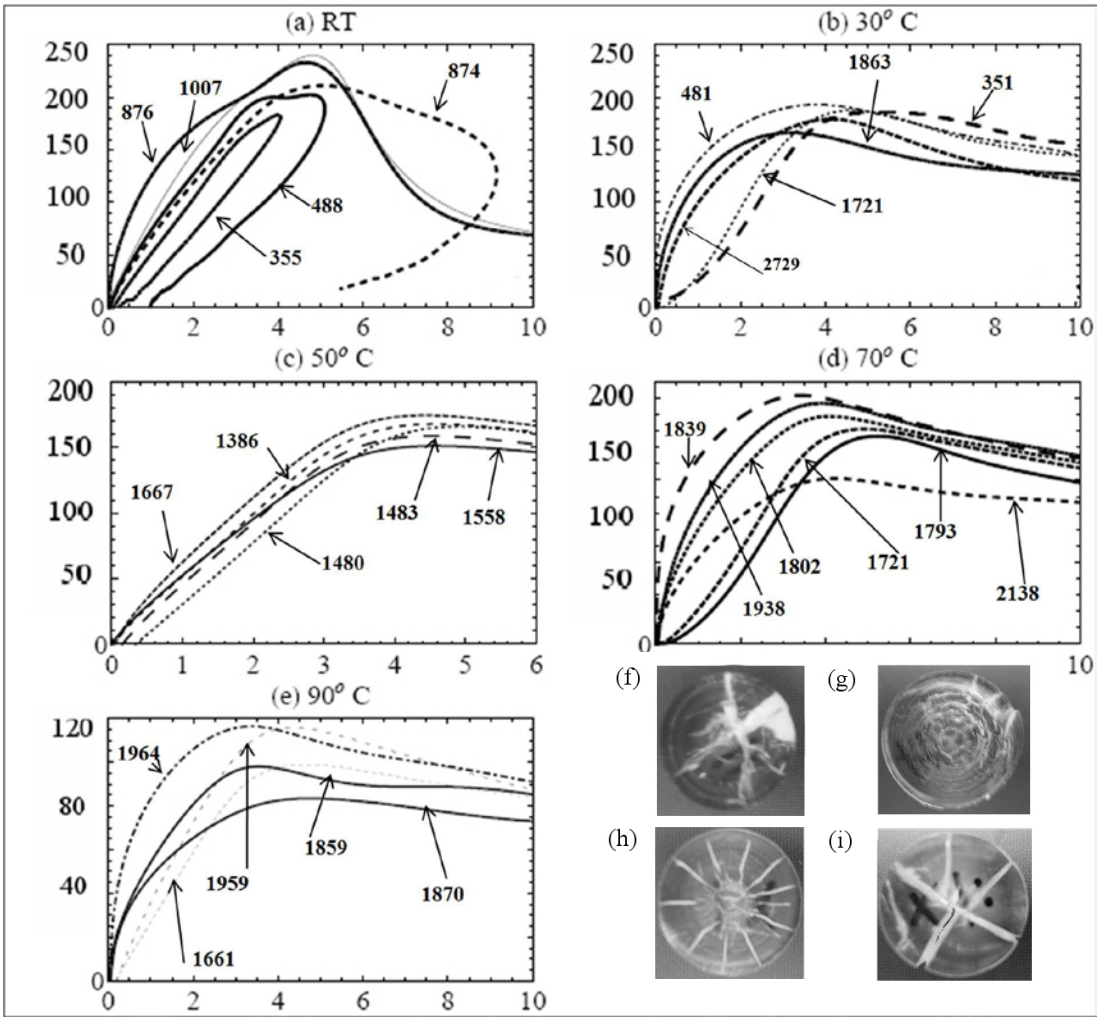


*Figure 5.32 PMMA True Stress(MPa) versus True Strain(%) curves at (a) room temperature, (b) 30°C, (c) 50°C, (d) 70°C and (e) 90°C over a range of high strain rates. Image (f) is a sample of the polymer is the sample having undergone testing at room temperature, (g) 30°C, (h) 50°C and (i) 70°C.*

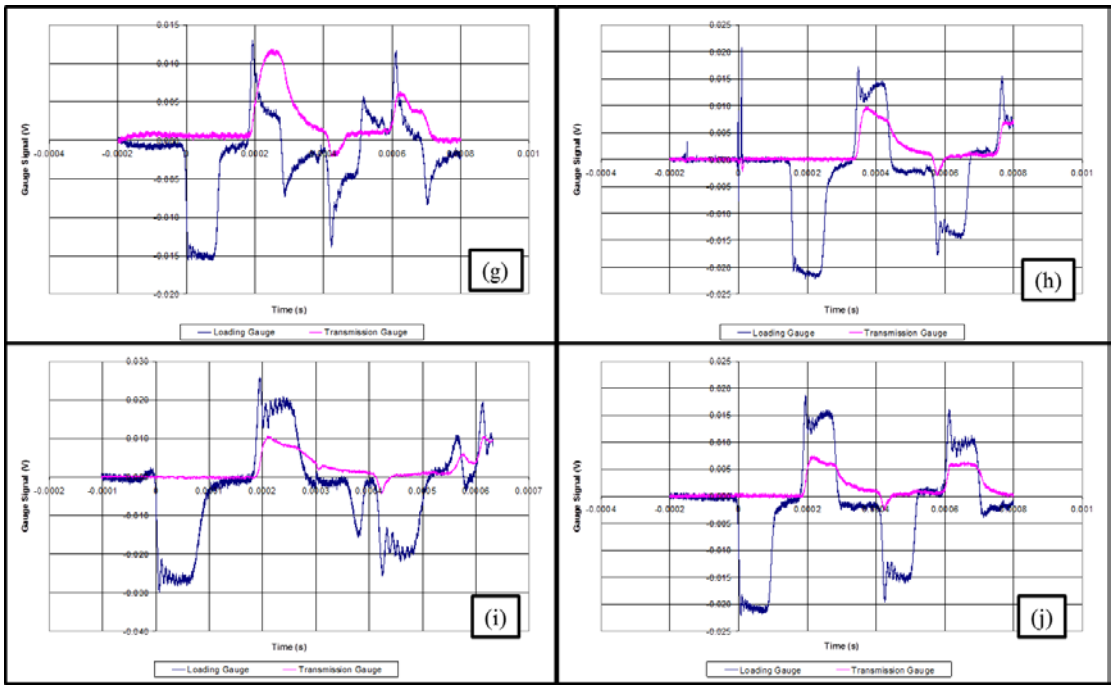


*Figure 5.33 Voltage change in strain gauge signals as a function of time. Blue lines show loading and reflecting signals and pink line shows the transmitting signal from the impact. The four graphs correspond to the image in Figure 5.32g, h, i and j.*

# Chapter Six

# Discussion and conclusion

## 6.1 Discussion

In this work we have studied the dynamic mechanical properties of four polymers at high strain rates range of $10^2$-$10^4$ $s^{-1}$. The relation of flow stress to strain and strain rate are elucidated by conducting SHPB experiments at a range of temperatures close to the glass transition temperatures. The primary objective was to identify the occurrence, or not, of flow stress peaks at high strain rates. It is suggested that the flow stress peaks are connected with the amorphous components in the polymers. The experiments were carried out at temperatures close to the glass transition temperature for the reason that it is the main characteristic of amorphous polymers. Flow stresses are considered over yield stress, due to the lack of consistency in identifying the experimental yield stress of some polymers. Several flow stress values at different strains are selected and compared. The assumption that the flow and yield stress values could be interchangeable will be examined. The high strain rate compression test is an adiabatic process. Therefore, temperature rises of the polymer specimens are calculated. The fracture and other deformations of the polymers are not observable during the impact experiments. However, the final specimens are photographed to give some understanding of polymer specimen deformation.

Some factors in the SHPB analysis which leads to inaccuracies in stress/strain results have been discussed in section 2.4. These factors include friction, polymer/bar interface area variation, inertia effects of specimens, mechanical noise interference, and axial alignment. These factors have been treated during the set-up and design of the experiment to minimise their effects.

The data analysis of errors for stress, strain, strain rate and temperature rise are calculated. The methodology of data analyses can be found in section 2.5 and the computer codes are presented in Appendix B. The main concern is the accuracy of

flow stress as this could determine the existence of the peaks found. The flow stress is determined by the stress-strain curve, for example if we were to work out the flow stress at 10% strain

The Young's moduli of the four polymers are calculated by finding the ratio of the axial stress to strain in the stress-strain plot shown in Figure 5.5, 5.15,and 5.25 for PCTFE, PTFE, PVC, respectively.

### 6.1.1 Glass transition temperature

The DSC and DMA technique were used to investigate the phase transitions of the four polymer samples. During the DSC test, the sample was kept at atmospheric pressure with a constant heating rate. The results represent the phase changes of the material without an additional load. The DMA method tested the polymer samples at two frequencies. The phase transitions found using different methods are given in Table 6-1, including glass transition from DSC method, DMA method at both frequencies of 1 Hz and 100 Hz, and the figures found from the literature (the references are in chapter three).

The glass transition temperature of PVC using the DMA method has been wrongly identified. This is because the temperature step size was too large, also because partial merge of β transition peak with the glass transition peak. Therefore the glass transition of PVC should be closer to 66 ºC.

| Polymers | DSC (ºC) | DMA at 1 Hz (ºC) | DMA at 100 Hz (ºC) | Literature (ºC) |
|---|---|---|---|---|
| PCTFE | 40 | 109 | 135 | 47-77 |
| PTFE | 38 | 45 | 62 | 27 |
| PVC | 66 | 98* | 109* | 71-80 |
| PMMA | 110 | 110 | 112 | 90-110 |

*Table 6-1 Comparisons of the glass transition temperatures (in Celsius) measured using the DSC, DMA and from the literature for the PCTFE, PTFE, PVC and PMMA samples.*

### 6.1.2 Flow stress versus yield stress

The strains at both flow stress and yield stress were calculated from each stress-strain curve found from PCTFE, PTFE, and PVC high strain rate tests. Then strain at yield stress is plotted against strain at flow stress to show possible correlations between flow and yield stress.

Flow stress at 15% strain is plotted against yield stress for room temperature, 50ºC and 100ºC specimens in the SHPB compression tests (Figure 6.1, 6.2 and 6.3) In general, the relation of flow and yield stresses is linear, with the stresses increasing with the decrease in temperature. In PCTFE specimens, the gradient of flow and yield stress ratios shows larger fluctuations in the 100ºC specimens. In PTFE specimens, the linearity of the flow and yield stresses is less apparent. First due to the lower yield/flow stress (the average yield of PTFE is 20 MPa, whereas it is 90 MPa in PCTFE). Secondly, the yield stress of PTFE covers a much wider range as the specimen is very soft at this temperature and the yield point is much harder to define. However, in PVC specimens most fluctuation of ratio of flow/yield stress was found at ambient temperature tests. PTFE is not as temperature sensitive as yield stress does not have a strong correlation to flow stress, which shows that PTFE is not as temperature sensitive compared to the other three materials.

In PCTFE and PVC specimens, both the yield and flow stresses dropped with the increase of temperature. It is the same in PTFE specimens other than at 100ºC.

The gradient of the yield stress against flow stress graphs shows the relation between temperature and strain rate, it is possible to work out the temperature shift to strain rates.

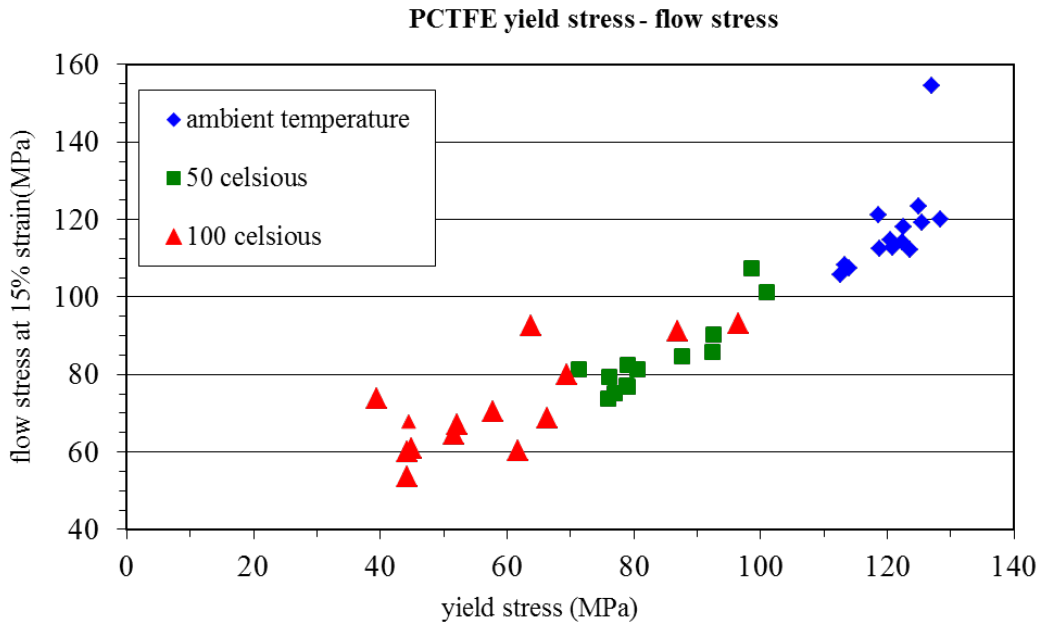


*Figure 6.1 PCTFE flow stress at 15% strain as a function of yield stress.*

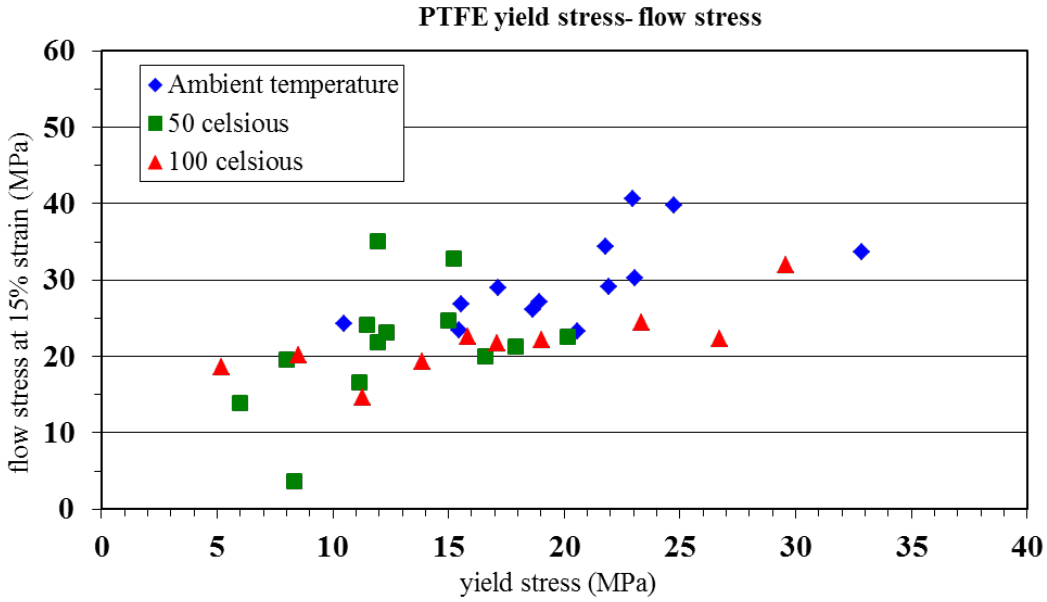


*Figure 6.2 PTFE flow stress at 15% strain as a function of yield stress.*

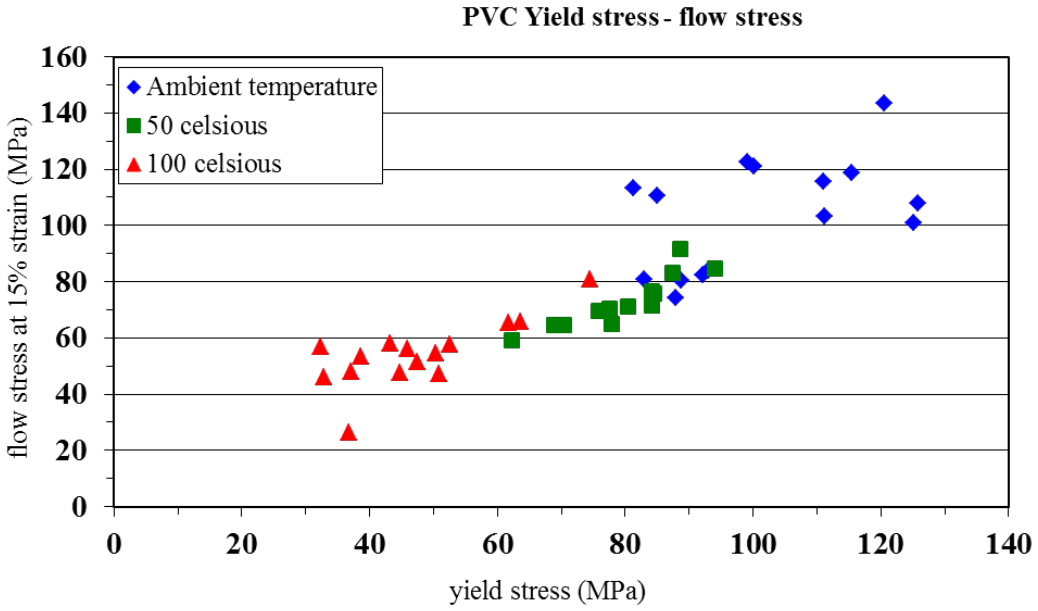


*Figure 6.3 PVC flow stress at 15% strain as a function of yield stress.*

### 6.1.3 Stress-strain curves

Most noticeable change in stress-strain curves of PCTFE is the increase of yield strain. During plastic flow the stress stays unchanged, after which two scenarios happen. First is the sample fails and stress drops before failure of sample, second is the stress dramatically increases which is seen in some samples at 50ºC and even more samples tested at 100ºC. In the second scenario the plastic flow stress fluctuates once and sometimes twice before the increase in stress, this could be because of internal temperature rise in the material which causes the final stress to increase. After the impact the temperature of the specimens increase beginning from the centre of the circle of the impact face, then it spreads in stages outwardly towards the edges. The fluctuations during plastic flow indicate the temperature rises in parts of the specimen. The calculations of the temperature increase in plastic flow (chapter five, section 5.1.3) also shows the change in temperature rise per unit strain. The modelling of the way the temperature increases in the disc sample at high strain rate impact testing are discussed further in section 6.1.5.

PTFE has a very low yield. However, with the increase of strain rate the material shows dramatic increase in final strain (before the failure of the sample). The stress increases during the plastic flow. The stress fluctuation during plastic flow can also be identified in this material at 100ºC tests. However, the fluctuation leads to

lower final stress (opposite of PCTFE). This could be due to phase changes in PTFE are much lower than PCTFE, see Table 6-1.

The most interesting point of the PVC stress-strain curves are that it is divided into two groups of higher and lower yield/flow stress. This is most apparent at 50ºC, but can also be found at ambient temperature and 100ºC. The two groups are not divided by the strain-rate. The modelling of high strain rate impact test is based on a PVC specimen to see if it is possible to understand why this is.

### 6.1.4 Flow stress as a function of strain rate

Flow stress of PCTFE specimens at 15% strain are plotted against strain rate in Figure 6.4. All three curves show a peak, the peaks broadens with the increase of temperature. The flow stress peaks shifts right in strain rate with increasing of temperature, as found in PMMA specimens. Figure 6.5 shows the flow peaks found in PTFE, again the flow peaks are found to shift higher in strain rate with the increase of temperature.

In the PVC specimens the flow peak can be seen at ambient temperature and very apparent at 50ºC, but cannot be found at 100ºC. The increase in the 50ºC flow peak could be that it is close to the glass transition temperature, and at 100ºC (pass the glass transition temperature) the flow stress peaks could not be found. In the case of PMMA, the flow stress peaks also became more apparent as the temperature approached the glass transition temperature. Other mechanical properties such as the formation of the adiabatic shear bands are also related to the glass transition temperature of the polymer [**Rittel/Wang/Merzer 2006**].

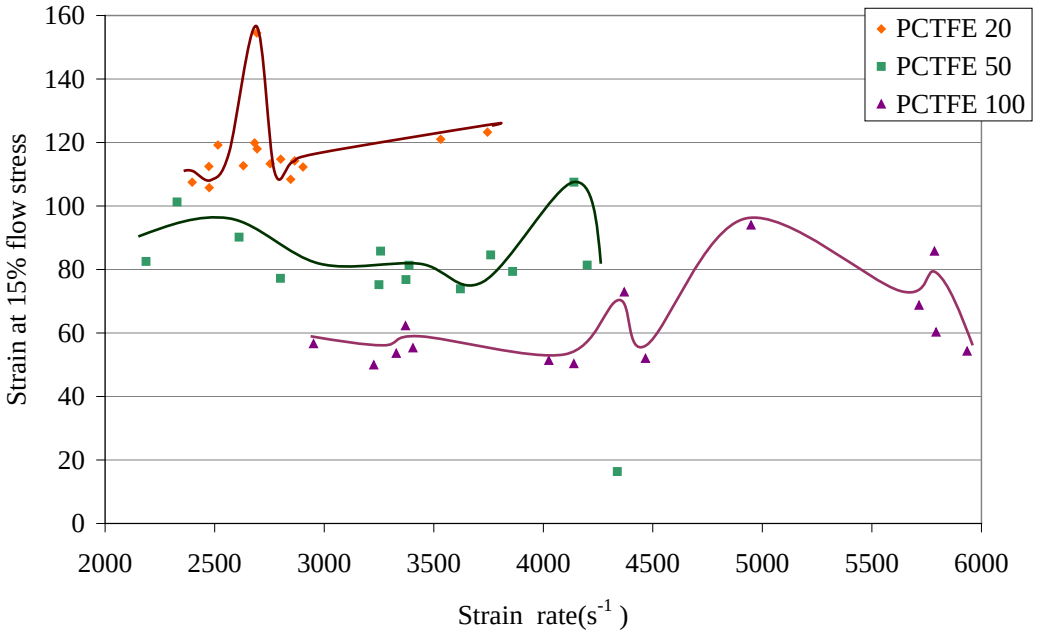


*Figure 6.4 Strain at 15% flow stress against strain rate in PCTFE specimens tested at ambient temperature, 50ºC and 100ºC.*

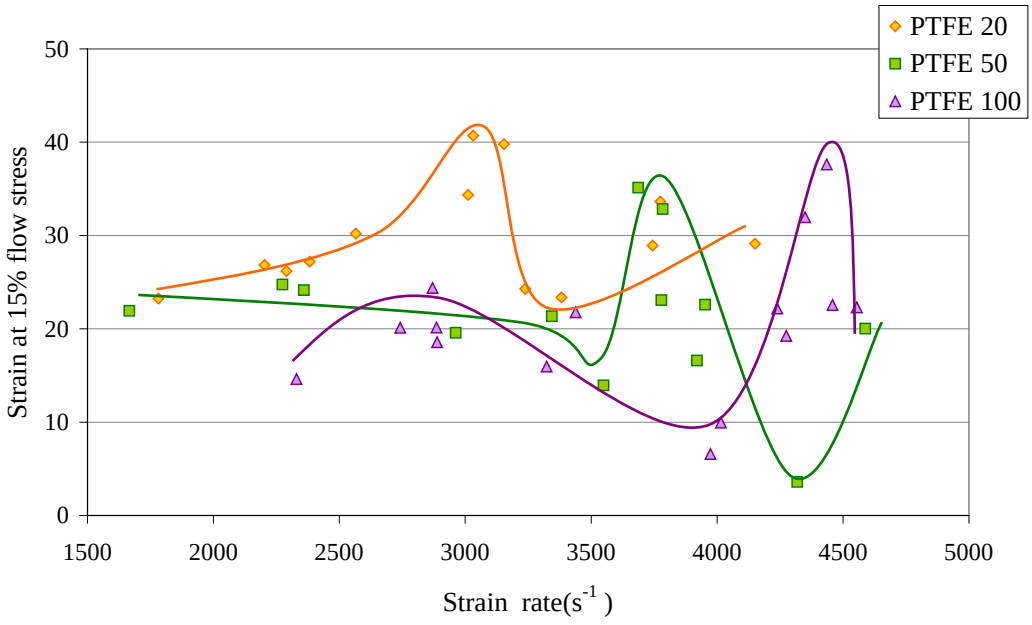


*Figure 6.5 Strain at 15% flow stress against strain rate in PTFE specimens tested at ambient temperature, 50ºC and 100ºC.*

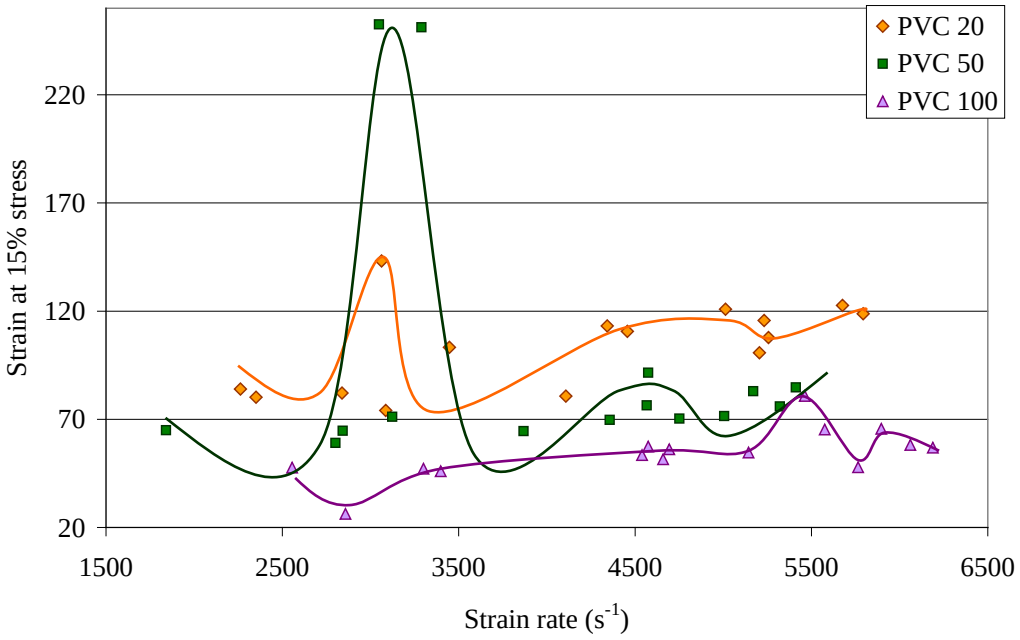


*Figure 6.6 Strain at 15% flow stress against strain rate in PVC specimens tested at ambient temperature, 50ºC and 100ºC.*

### 6.1.5 Modelling high strain rate compressed deformation of polymers

This thesis describes an investigation of the high strain-rate mechanical behaviour in compression of a number of polymeric materials. During the course of our investigations we found that there was a strong propensity for the cylindrical samples to deform into ring like structures. Of the polymers tested, this can be seen to be pronounced in PMMA but especially in PVC (see Figures 5.22-5.24). In these samples there is a high degree of irrecoverable deformation. The structures evidently become radically altered at a certain level of strain and temperature. Thus, in the following we include some of the on-going work on modelling the deformation phenomena. We focus on the energy due to deformation in the body of the samples, i.e. strain energy density. The strain energy density is the area under the stress-strain curves up until the end of plastic flow.


*Figure 6.7 The deformed PVC sample after testing in the split Hopkinson bar at a strain rate of 5895 $s^{-1}$ and with the sample preheated to 373 K. The image is also repeated from that of Figure 5.24(i).*

In this analysis we choose to delve into understanding the formation of the ring like structures that are obtained after testing at high strain-rates. We show the ring obtained after compression for a PVC sample at 373 K (more experimental information is found in Section 5.3 and Figure 5.24). We have simulated the formation of these ring structures in Comsol Multiphysics without the inclusion of inertial and frictional effects (two commonly cited sources of possible invalidity of Split Hopkinson bar tests [**Bauwen/Noskar 1985, Walley/Field/Pope/Safford 1991]**

using metallic striker bars upon polymeric samples). We calculated the force as a function of time at the interfaces between the split Hopkinson bars and the sample and found that it takes an almost Gaussian shape with maximum amplitude of around 5 kN. From the typical experimental data (e.g. reflecting, transmitting and incident pulses that are seen in Figure 5.24) generated from the strain gauge signals we find the contact force $P_1$ between the incident bar and the specimen and $P_2$ between the specimen and the transmission bar. The assumption of the split Hopkinson bar experiments is that $(\varepsilon_I + \varepsilon_R)/\varepsilon_T \approx 1$, meaning that the equilibrium state is achieved. We find that in using the steel bars of the Hopkinson setup, that suitable levels of lubrication, careful alignment of the bars and choice of sample size can all maintain the validity of the equilibrium state prerequisite. For the PVC sample in

Figure 6.7, the ratio of the incident and reflecting strains to the transmitting strain is given by $(\varepsilon_I + \varepsilon_R)/\varepsilon_T \approx 1.1$. This is found from comparing the areas under the transmitting, incident and reflecting pulses of the real experiment. With this in mind, we simulate the forces at the interfaces between the specimen and the bar with $P_2 = P_1 + \delta$, where $\delta$ is a deviation from equilibrium. In the following example for PVC, we take $\delta = 0.1P_1$. We follow this with an example with $\delta = 0$ for a PMMA specimen.

Figure 6.8 shows the forces that are applied between the bars and the sample. The loading is taken to be uniform across the faces of the samples. The simulations give some insights into the deformation in the bulk of the sample. In Figure 6.9a the strain energy density at the centre of the sample is shown. At about $17\mu s$ there is a massive spike in the strain energy within the volume. In Figure 6.9b the maximum dynamical strain energy throughout the entire sample can be seen. From the perspective of maximal strain energy in the volume one can see that the first spike in (a) is followed by a larger peak at about 60 μs. It is thought that this represents hot spots within the specimen interior and the onset of a phase transition that will ultimately result in the ring structure at the cessation of the compression test.

PVC is particularly prone to temperature effects and its structure begins to decompose at around 415 K. In Figure 6.9 the first peak occurs as a result of the maximum strain energy being highly localised right in the centre of the specimen. The three-dimensional simulations of the compression of the PVC sample show that the intensity of the strain energy follows a circular longitudinal distribution throughout the specimen. Figure 6.10 shows an ensemble of images at given times leading to the aforementioned peak in the strain energy density at the centre of the specimen. One can clearly see that at 17 μs the strain energy at this interior location is maximised with all the strain energy focused in a very small region at the very middle of the cross-section. Ultimately, at the end of the compression test the ring like geometry results and it is hypothesised that these interior rings of varying strain energy are the source of the decomposition of the sample. High-speed photography has often been applied to Hopkinson bar testing, for example to examine specimen deformation and indeed the work of Walley et al. also demonstrates the emergence of rings in a range of polymers (e.g. **Walley/Field/Pope/Safford 1991**). We have modelled the specimen as a viscoelastic material.

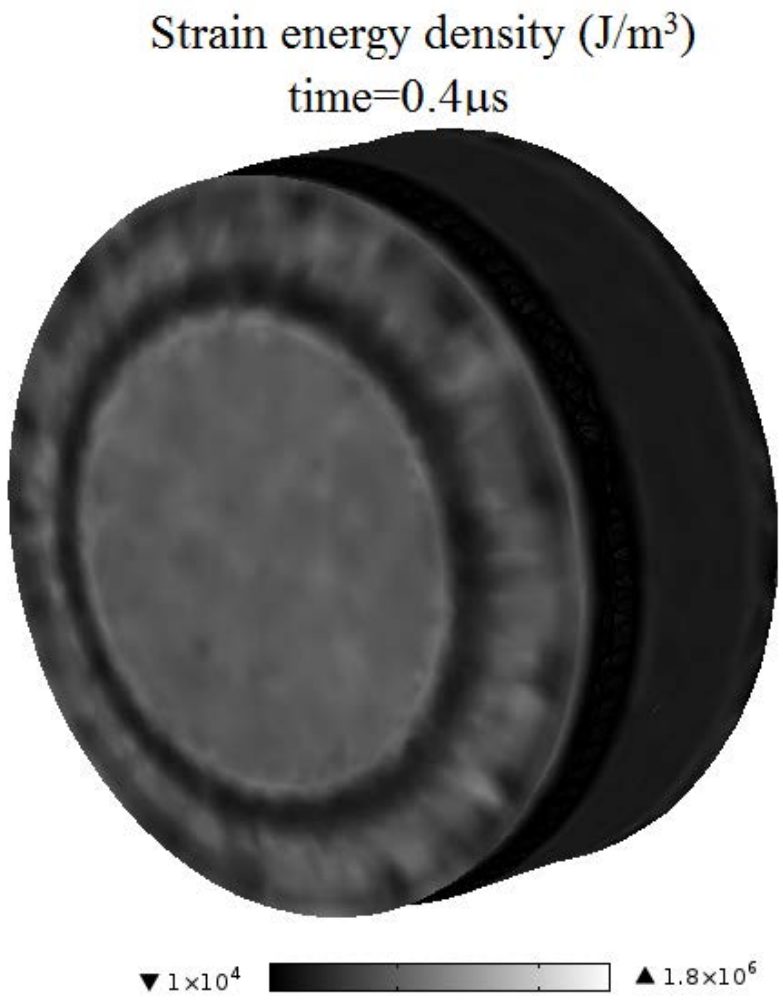


*Figure 6.8 The simulation of the PVC with initial conditions identical to that of the sample in Figure 6.7. The contact forces $P_1$ and $P_2$ are shown by the yellow arrows and are applied over the whole of each face of the sample. The sample is modelled undergoing a strain rate of 5895 $s^{-1}$ and with the sample heated to 373 K.*

These results are designed to show that the deformation and decomposition of the polymers in spit Hopkinson bar are predominantly down to the compression of the sample and not extraneous errors. The result is a deformation, in the cases highlighted here, whereby the centre of the samples disappears and the ring of PVC remains. This is shown below in Figure 6.10 in the image captured from the simulation. The decomposition of the matrix of the specimen in the simulations that may help gives insights into how the internal structure dynamically evolves. The impact initiates a compression wave in the polymer structure, see Figure 6.11.

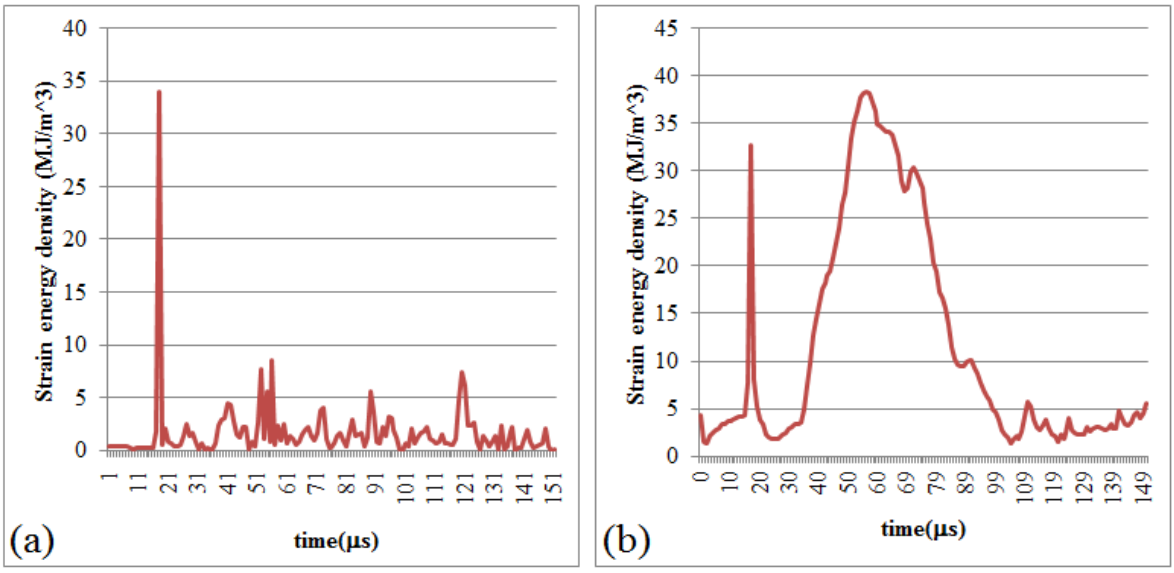


*Figure 6.9 (a) The simulated strain energy density as a function of time at the centre of the specimen of PVC that has been heated to 373 K. For the same simulation, (b) shows the maximum strain energy density in the entire specimen at each time increment.*

Our brief discussion of the modelling of the experimental deformations concludes with the results for PMMA. One will see that the compression wave creates a circular strain energy density in these numerical experiments too. Some illustrative examples are shown below in Figure 6.12.

Thus, the modelling of the polymers has been carried in order to alleviate doubts about the validity of the real experimental results that may arise due to the nature of the decomposition of the polymers. It has been shown that the strain energy density pulses through the sample in response to the compression wave in various circular intensities. The fact that the samples remain very symmetric after testing implies near perfect uniaxial loading.

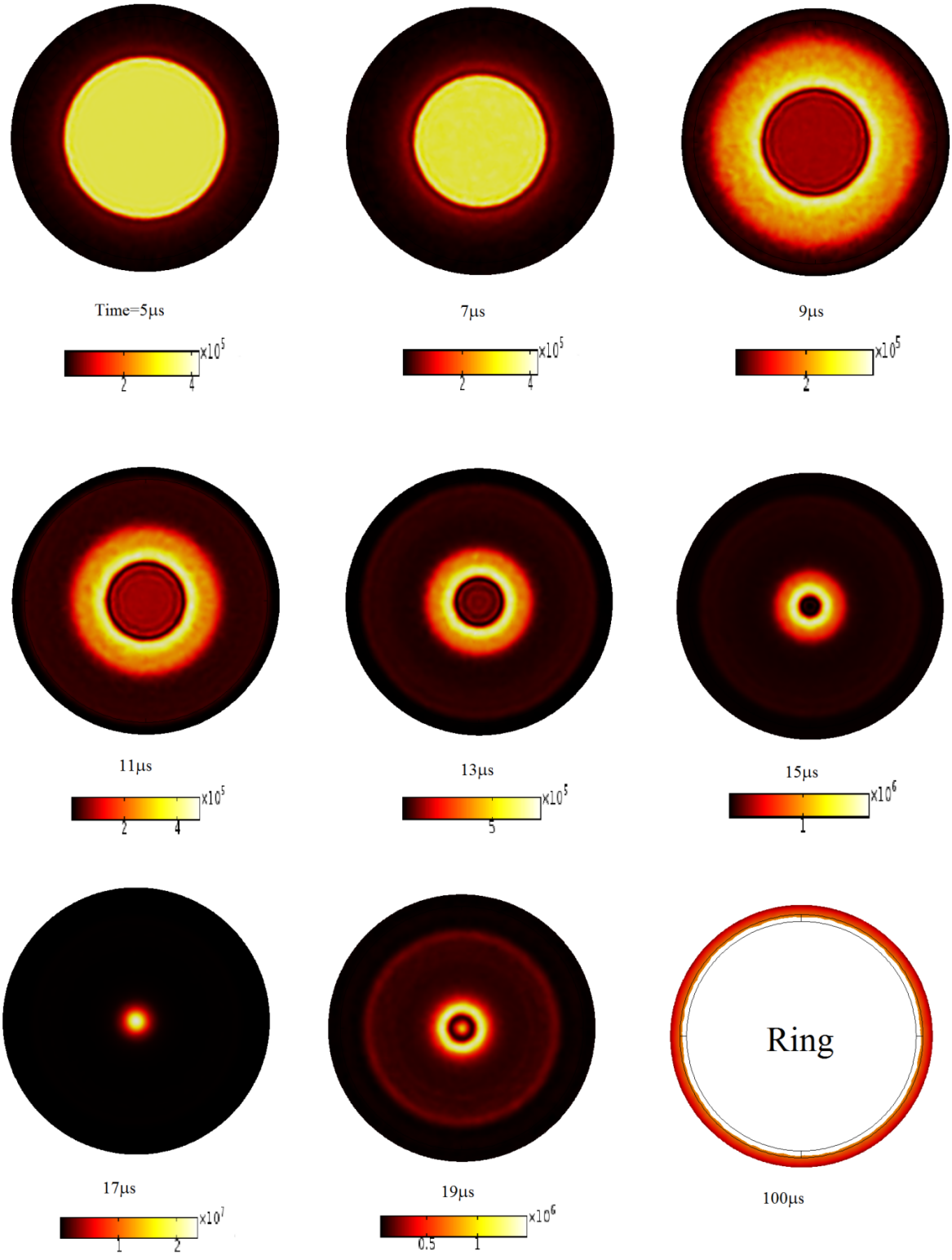


*Figure 6.10 The evolution of the strain energy in the centre of the specimen in the simulations is shown through the dissection of the specimen to give these cross-sectional images. The images are shown for* $t = 5 - 19\mu s$ *and finally the resulting ring structure at* $100\mu s$ *.*

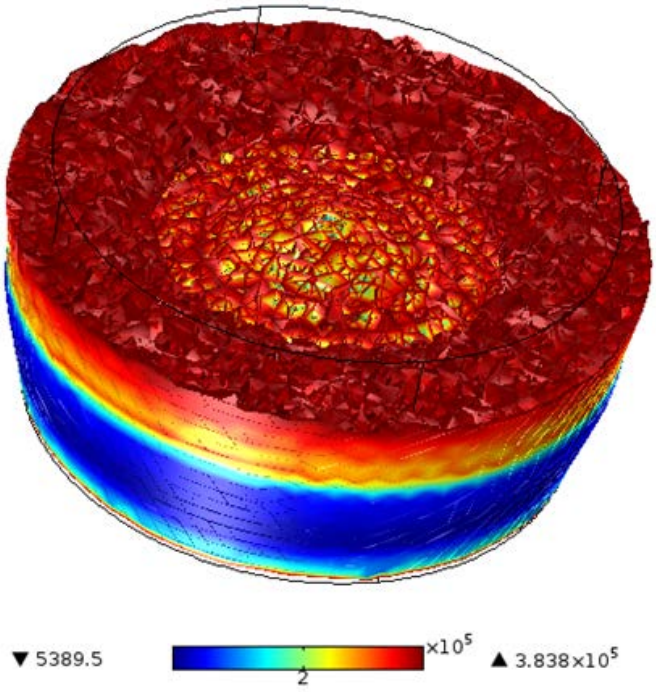


*Figure 6.11 The decomposition of the matrix of the specimen in the simulations that may help give insights into how the internal structure dynamically evolves. The impact initiates a compression wave in the polymer structure.*

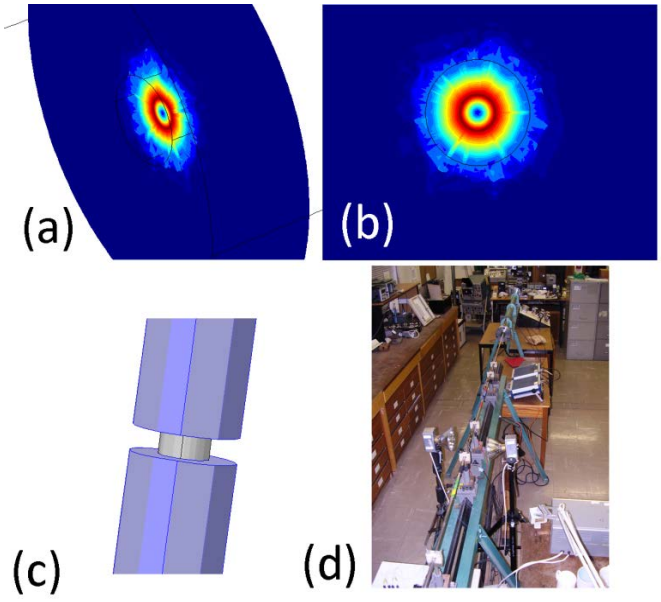


*Figure 6.12 In (a) and (b) typical strain energy density plots are shown to demonstrate the circular nature as the compression wave moves through the sample. (c) The simulated split Hopkinson bars. (d) The Loughborough University split Hopkinson bar apparatus.*

## 6.2 Conclusion

The mechanical properties of the four polymers (PCTFE, PTFE, PVC and PMMA) have been investigated at high strain rates. In all four polymers the flow stress peak has been identified at temperatures lower than the glass transition temperature.

- Evidence of flow stress peaks at high rates of strain is confirmed in this work. PCTFE, PTFE, PVC and PMMA all showed flow stress sensitivity at high strain rates between 2500 and 5000 $s^{-1}$ close to their glass transition temperature.
- The flow stress peaks in PCTFE , PTFE and PMMA showed a positive correlation between time and temperature where the peaks shifted with the increase of temperature. However, this was not found in PVC.
- Walley et al. [**Walley et al. 1994**] reported that PTFE is not sensitive to strain rate at low strain rates. In this work we found that PTFE at high strain rate is sensitive to strain rate but not temperature changes.
- Modelling of the experimental deformation of polymers has concluded that the circular structure seen on deformed specimens after both low and high strain rate compression tests are the strain energy density pulses though the disk specimen in response to the compression wave in various circular intensities.
- By plotting yield stress against flow stress, the positive correlations between the two values are clearly shown. PCTFE in Figure 6.1 and PVC in Figure 6.3 demonstrate that flow and yield stresses proportionally decrease with the increase of temperature. This was not observed in PTFE in Figure 6.2 at 100ºC.
- The glass transition temperature has been measured using different techniques. It is apparent that the glass transition temperature increases with the increasing rate of strain. However, it is not clear whether the relationship is linear when the materials are sensitive to strain rate at high rates of strain.
- The high strain rate failure of each material can be observed from the deformed specimen images shown in chapter five. At ambient temperature and 50ºC PCTFE, PTFE and PMMA are brittle and glass-like, and the polymer specimens fractured into crumbles of granulates. At 100ºC, PCTFE and PTFE

acted more rubber-like, where the fractured granulates mostly joined together. PMMA was still brittle at 100ºC.

- Deformations of PVC specimens were clearly divided between the inner circle and outer ring. The inner circle of the disk specimen easily fractured and temperature dramatically increased, whereas the outer rings of the PVC specimens still holds their shape, and are less deformed at high strain rates.
- The differential scanning calorimeter (DSC) PTFE results shows an endothermic phase change at 18 º C and an exothermic change at 32 º C where the material is known to show structural changes at molecular level. This could explain why the flow stress of PTFE is not found to be influenced by glass transition , as observed in other polymers in this work. It is reasonable to suggest that other secondary transitions could also have an influence on the sensitivity to flow stress peaks at high strain rates.
- By comparing the storage modulus to the flow stress peaks at ambient temperature, 50ºC, and 100ºC we conclude that if storage moduli are relatively small (i.e. PCTFE and PVC at 100ºC ), then flow stress peaks cannot be found at high strain rates.

# Appendices

# A The Eyring Theory

In the original paper by Eyring [**Eyring 1935**] on the activated complex in chemical reactions, the probability of the activated state is calculated using statistical physics. Eyring looked at the partition function through the use of quantum mechanics and developed the translational, rotational and vibrational forms of the equations. He then developed his rate dependent equations based upon these partition functions and the thermodynamical relationships for entropy, Gibbs free energy etc.

Eyring specified that the deformation of a polymer is a thermally activated rate process [**Eyring 1935, Eyring 1936**]. This involves the motion of parts of the molecular chains over potential barriers and represents non-linear viscoelastic behaviour (see Figure A-1). The parameters of interest in the Eyring model are those of activation energy and activation volume. These can possibly enlighten us as to the underlying molecular mechanisms in the materials. Eyring's 1935 paper [**Eyring 1935**] came at a time when quantum mechanics was relatively young and lots of older concepts were being generalised and modified to take into account areas where quantum effects cannot be ignored. An example is the Boltzmann distribution which was found to be a general form of Bose-Einstein or Fermi-Dirac distributions at elevated temperatures. In a similar vein, Eyring generalised the Arrhenius model based upon quantum mechanical principles. The Arrhenius and Eyring models describe the temperature dependence of a reaction rate (the Arrhenius equation being strictly applied to gases). Eyring's model can be used to study gas reactions, those of solutions and mixed phase reactions. The Eyring model is a theoretical model founded upon the transition state model [**Eyring/Lin/Lin 1980**]. The transition state model stipulates an approach that explains the temperature and concentration dependence of the rate law, e.g. $-rA=k[A][BC]=Aexp(-EA/RT)[A][BC]$. Within transition state theory an activated molecule forms between the stages of the reactant and the product.

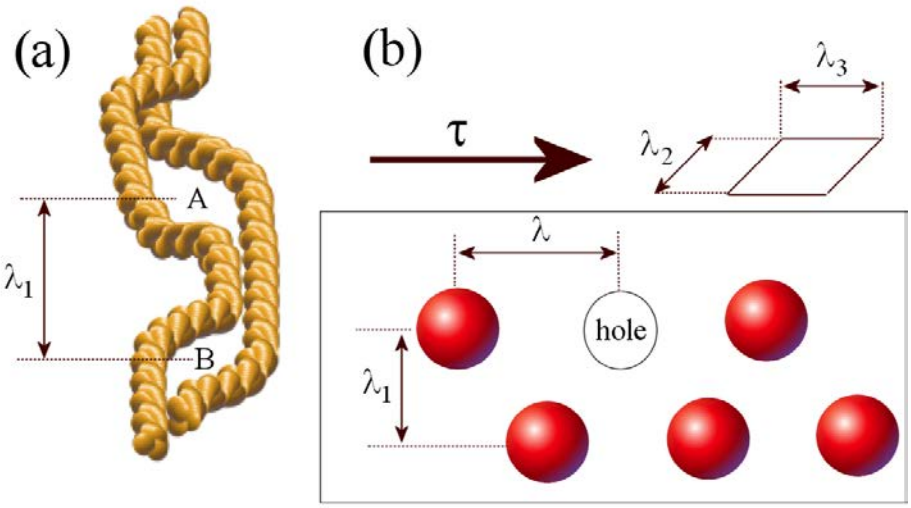


*Figure A-1: These are simplified representations of the vacancies that parts of the molecular chain can jump into in order to relax the stress in the system (adapted from [**Eyring 1935**]).*

When the shape of a polymer chain is altered the flow units exchange old neighbours for new ones. In fact even when there are no externally applied shear forces the same processes are going on. This can be seen in Figure A-2.

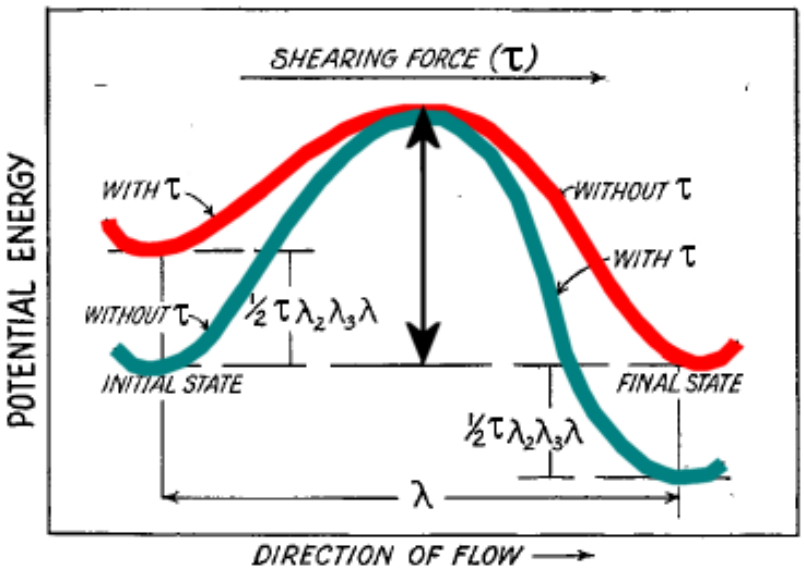


*Figure A-2: The applied stress will alter the potential energy landscape as illustrated above. The energy barrier at the inflexion point above must be overcome when flowing from one equilibrium position to the next [**Eyring 1935**].*

These processes increase and become unbalanced when there is an applied shearing force that adds additional stresses to the polymer. As seen in Figure A-1a,

the molecules movements occur in the locality of loose or empty spaces in the structure. In the figure these are depicted as vacancies A and B and it is assumed that they occur at equal spacings throughout the structure. The dimension of the flow, i.e. the distance between A and B is denoted by $\lambda 1$ and is in the direction of the applied force [**Eyring et al 1945**]. The shear force in a square centimetre of the polymer surface is $\tau$ and thus the force acting on a single flow unit is $\tau\lambda 2\lambda 3$. Here, $\lambda 2\lambda 3$ is the effective cross sectional area of the flow unit. This is normal to the direction of the flow. The force effectively speeds up the flow units. In Figure A-1a even if there is no force acting above A it is possible that the segment in the vicinity could move downwards k' times per second, with an equal number of movements in the upwards direction. In Figure A-1b the force $\tau\lambda 2\lambda 3$ performs along distance $\lambda$ doing a level of work equal to $\tau\lambda 2\lambda 3\lambda$. It is presumed that the unit, whilst proceeding in a forwards direction, will pass through a mid-point equal to $\lambda/2$ which marks a point of higher energy. This assumption is for a potential barrier that is completely symmetric. Therefore, the applied stress only adds work at a level $\tau\lambda 2\lambda 3\lambda/2$ towards the passage over the barrier. Logically, if the flow unit works against the applied force it will have to perform this same level of work against the applied stress. The flow unit will now move in the forwards direction in a manner that occurs $k'\exp[\tau\lambda 2\lambda 3\lambda/2KBT]$ times per second and $k'\exp[-\tau\lambda 2\lambda 3\lambda/2KBT]$ times per second in the opposite direction. Here k' is a specific rate constant. Therefore, the total number of forward movements per second of the flow unit is equal to

$$k'(\exp[\tau\lambda 2\lambda 3\lambda/2KBT]- k'\exp[-\tau\lambda 2\lambda 3\lambda/2KBT]) \quad (16)$$

Multiplying this by the distance $\lambda$ that the flow unit jumps gives the forward velocity of a flow unit:

$$\lambda k'\left(\exp\left[\tau\lambda_2\lambda_3\lambda/2K_BT\right]-\exp\left[-\tau\lambda_2\lambda_3\lambda/2K_BT\right]\right) \quad (17)$$

Now, by dividing through by the distance in the flow direction between points of flow, i.e. $\lambda_1$, the rate of strain is attained. Thus, the shear rate is

$$\dot{\gamma} = 2\frac{\lambda}{\lambda_1}k'\left(\exp\left[\tau\lambda_2\lambda_3\lambda/2K_BT\right]-\exp\left[-\tau\lambda_2\lambda_3\lambda/2K_BT\right]\right)$$
$$= 2\frac{\lambda}{\lambda_1}k'\sinh\left(\tau\lambda_2\lambda_3\lambda/2K_BT\right) \tag{18}$$

The volume of the hole swept out by the motion is given by $V_{hole} = \lambda_2\lambda_3\lambda$ and the volume of the molecule that is in action is $V_{molecule} = \lambda_1\lambda_2\lambda_3$ (See Figure A-1b). This leads to an equation for the rate of flow, i.e. strain rate that has the form

$$\dot{\gamma} = 2\frac{V_{hole}}{V_{molecule}}k'\sinh\left(\tau V_{hole}/2K_BT\right) \tag{19}$$

From the statistical thermodynamic theory of reaction rates the rate constant can be written in term of an activated Gibbs free energy $\Delta G^{\#}$ :

$$k' = \frac{K_BT}{h}\exp\left[-\Delta G^{\#}/RT\right] \tag{20}$$

where h is Planck's constant. This enables the strain rate to become,

$$\dot{\gamma} = 2\frac{V_{hole}}{V_{molecule}}\frac{K_BT}{h}\exp\left[\frac{-\Delta G^{\#}}{RT}\right]\sinh\left(\frac{\tau V_{hole}}{2K_BT}\right) \tag{21}$$

For high values of $\tau$, $\sinh\left(\frac{\tau V_{hole}}{2K_BT}\right) \approx \exp\left[\frac{\tau V_{hole}}{2K_BT}\right]/2$ the shear strain rate becomes,

$$\dot{\gamma} = \frac{V_{hole}}{V_{molecule}}\frac{K_BT}{h}\exp\left[\frac{-\Delta G^{\#}}{RT}\right]\exp\left[\frac{\tau V_{hole}}{2K_BT}\right] \tag{22}$$

Now, in order to use the above for uniaxial compression strain rates and stresses, the following identities are incorporated; $\tau = \sigma/2$ and $\dot{\gamma} = 3\dot{\varepsilon}/2$. This leads to,

$$\dot{\varepsilon} = \frac{2\lambda K_B T}{3\lambda_1 h} \exp\left[\frac{-\Delta G^{\#}}{RT}\right] \exp\left[\frac{\sigma}{4}\frac{V_{hole}}{K_B T}\right] \tag{23}$$

Taking the logarithm of each side then gives [**Swallowe 1999, 2003**],

$$\frac{\sigma}{T} = \frac{4K_B}{V_{hole}}\left(\ln\varepsilon - \ln\left(\frac{2}{3}\frac{\lambda}{\lambda_1}\frac{\dot{K_B T}}{h}\right) + \frac{\Delta G^{\#}}{RT}\right) \tag{24}$$

From thermodynamics,

$$\Delta G^{\#} = \Delta H^{\#} - T\Delta S^{\#} \tag{25}$$

Here $\Delta H^{\#}$ is the activation enthalpy and $\Delta S^{\#}$ is the activation entropy. The higher the amount of negative activation entropy that there is, the higher $\Delta G^{\#}$ will be. If $\Delta G^{\#}$ is less than zero then the reaction is spontaneous, whilst if it is greater than zero it is not. For the scenario where it is equal to zero the system is in equilibrium. Using the above form for $\Delta G^{\#}$ the equation becomes,

$$\frac{\sigma}{T} = \frac{4K_B}{V_{hole}}\left(\ln\varepsilon - \ln\left(\frac{2}{3}\frac{\lambda}{\lambda_1}\frac{\dot{K_B T}}{h}\right) + \frac{\Delta H^{\#}}{RT} - \frac{\Delta S^{\#}}{R}\right) \tag{26}$$

Incorporating the volumes related to the molecular movement and the vacancy it can be rewritten as

$$\frac{\sigma}{T} = \frac{4K_B}{V_{hole}}\left(\ln\varepsilon - \ln\left(\frac{2}{3}\frac{K_B T}{h}\right) - \ln\left(\frac{\dot{V}_{hole}}{V_{molecule}}\right) + \frac{\Delta H^{\#}}{RT} - \frac{\Delta S^{\#}}{R}\right) \tag{27}$$

This is a convenient form of the Eyring equation for analyses of polymer samples. The parameter $V_{hole}$ is also known as the activation volume and is related to the empty spaces found in a samples structure, i.e. the vacancies. These will vary in size but are assumed to be distributed evenly and to allow the polymer chain to slip.

# B. Data analysis program codes

1. Strain gauges signals

The strain gauge signals are collected from the Hopkinson bars, the incident and reflected signals in channel one of the oscilloscope and transmitted signal in channel two.

```
data1 =Import["PVC45-1.csv","csv"];
data2 = Import["PVC45-2.csv","csv"];
data3=Table[{data2[[n,1]],data2[[n,2]]/100},{n,1,Length[data2]}];
weighting1=Sum[data1[[n,2]],{n,1,100}]/100;
weighting2=Sum[data3[[n,2]],{n,1,100}]/100;
condition1=If[weighting1 □ 1,Abs[weighting1],-weighting1];
condition2=If[weighting2 □ 1,Abs[weighting2],-weighting2];
data4=Table[{data1[[n,1]],data1[[n,2]]+condition1},{n,1,Length[data1]}];
data5=Table[{data3[[n,1]],data3[[n,2]]+condition2},{n,1,Length[data3]}];

gsvst1=ListPlot[data4,Joined □ True,PlotStyle □ {Brown,Thickness[0.007]},FrameTicks □ {{-0.0002,0,0.0002,0.0004,0.0006,0.0008},Automatic,Automatic,Automatic},Frame □ True,FrameLabel □ {"Time(s)","Gauge Signal (V)"},GridLines □ Automatic,BaseStyle □{FontFamily □"Times",20}];
gsvst2=ListPlot[data5,Joined □ True,PlotStyle □ {Black,Thickness[0.007]},Frame □ True,DisplayFunction □ Identity,FrameLabel □ {"Time(s)","Gauge Signal (V)"},BaseStyle □{FontFamily □"Times",20}];
gtp=Show[gsvst1,gsvst2,PlotRange □ {{-0.00015,0.00035},{-0.02,0.02}},ImageSize □ 600]
```

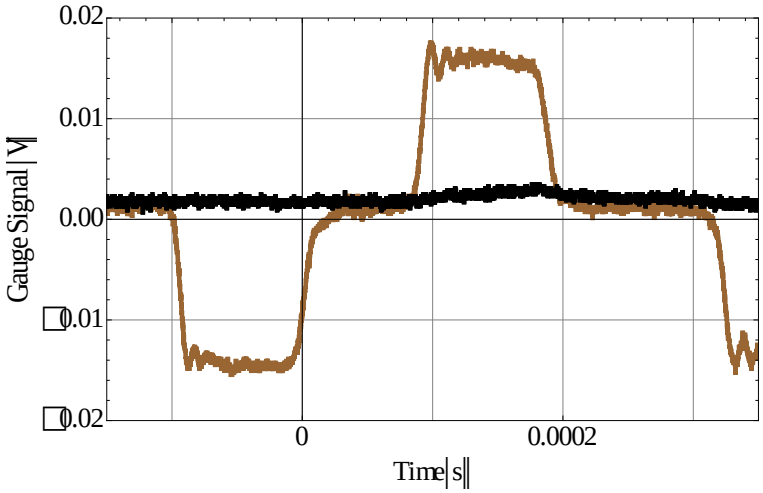


2. Stress and strain

The strain gauge signals are transferred to the Mathamatica program “Stress and strain” to calculate the stress and strain of the specimen against time, then the program plots the stress-strain curve shown in Appendix D.

```
(* Importing the data set *)

$BaseStyle={"TimesNewRoman",20};
data1 =Import["PTFE17-1.csv","csv"]//N;
data2 =Import["PTFE17-2.csv","csv"]//N;

(* Putting the data together *)
data3=Table[{data2[[n,1]],data2[[n,2]]/100},{n,1,Length[data2]}];

(* Adding weightings to the pulses *)
weighting1=Sum[data1[[n,2]],{n,1,100}]/100;
weighting2=Sum[data3[[n,2]],{n,1,100}]/100;
condition1=If[weighting1 □ 1,Abs[weighting1],-weighting1];
condition2=If[weighting2 □ 1,Abs[weighting2],-weighting2];
data4=Table[{data1[[n,1]],data1[[n,2]]+condition1},{n,1,Length[data1]}];
data5=Table[{data3[[n,1]],data3[[n,2]]+condition2},{n,1,Length[data3]}];
Clear[a1,a2]
a1:={};
a2:={};
```

```
ClickPane[Dynamic[Framed[gsvst1=ListPlot[data4,Joined □ True,PlotStyle □ {Hue[0.3],Thickness[0.007]},FrameTicks □ {{-0.0002,0,0.0002,0.0004,0.0006,0.0008},Automatic,Automatic,Automatic},PlotRange □ {{-0.0002,0.001},{-0.03,0.03}},Frame □ True,DisplayFunction □ Identity,FrameLabel □ {"Time(s)","Gauge Signal (V)"},GridLines □ Automatic,ImageSize □ 800,Epilog □ Point/@a1]]],AppendTo[a1,#1]&]
ClickPane[Dynamic[Framed[gsvst2=ListPlot[data5,Joined □ True,PlotStyle □ {Hue[0.6],Thickness[0.007]},PlotRange □ {{-0.0002,0.001},{-0.01,0.01}},Frame □ True,DisplayFunction □ Identity,FrameLabel □ {"Time(s)","Gauge Signal (V)"},GridLines □ Automatic,ImageSize □ 800,Epilog □ Point/@a2]]],AppendTo[a2,#1]&]

{x3,x4}={a1 □ 1,1\[RightDoubleBracket],a1 □ 2,1\[RightDoubleBracket]};

Clear[a3];
a3:={};
s:={};
fit2=Do[If[data4 □ n,1\[RightDoubleBracket]>x3&&data4 □ n,1\[RightDoubleBracket]<x4,AppendTo[s,{data4 □ n,1\[RightDoubleBracket],data4 □ n,2\[RightDoubleBracket]}]],{n,1,Length[data4]}]
Length[data4]
Length[s]
fitlist1=Partition[Flatten[s],2];
reflected=ListPlot[fitlist1,Joined □ True,Frame □ True,ImageSize □ 800,GridLines □{Automatic,{0}}];
powers:={};
tabx=Table[xn,{n,1,50}];
AppendTo[powers,{1,tabx}];
fitrange=Flatten[powers];
fittedR=Fit[s,fitrange,x];
```

```
fitplot2=Plot[fittedR,{x,x3,x4},PlotStyle □
{Hue[0.8`],Thickness[0.005]},GridLines □{Automatic,{0}}];

ClickPane[Dynamic[Framed[Show[reflected,fitplot2,Frame □
True,ImageSize □ 800,Epilog □ Point/@a3]]],AppendTo[a3,#1]&]

Clear[s]
{x3,x4}={a3 □ 1,1\[RightDoubleBracket],a3 □ 2,1\[RightDoubleBracket]};
nw2=-0.00;
s:={};
fit2=Do[If[data4 □ n,1\[RightDoubleBracket]>x3&&data4 □
n,1\[RightDoubleBracket]<x4,AppendTo[s,{data4 □ n,1\[RightDoubleBracket],data4
□ n,2\[RightDoubleBracket]}]],{n,1,Length[data4]}]
Length[data4]
Length[s]
fitlist1=Partition[Flatten[s],2];
reflected=ListPlot[fitlist1,Joined □ True,Frame □ True,ImageSize □
800,GridLines □{Automatic,{0}}];
powers:={};
tabx=Table[xn,{n,1,60}];
AppendTo[powers,{1,tabx}];
fitrange=Flatten[powers];
fittedR=Fit[s,fitrange,x]+nw2;
fitplot2=Plot[fittedR,{x,x3,x4},PlotStyle □
{Hue[0.8`],Thickness[0.005`]},GridLines □{Automatic,{0}}];
Show[reflected,fitplot2,Frame □ True,ImageSize □ 800]
```

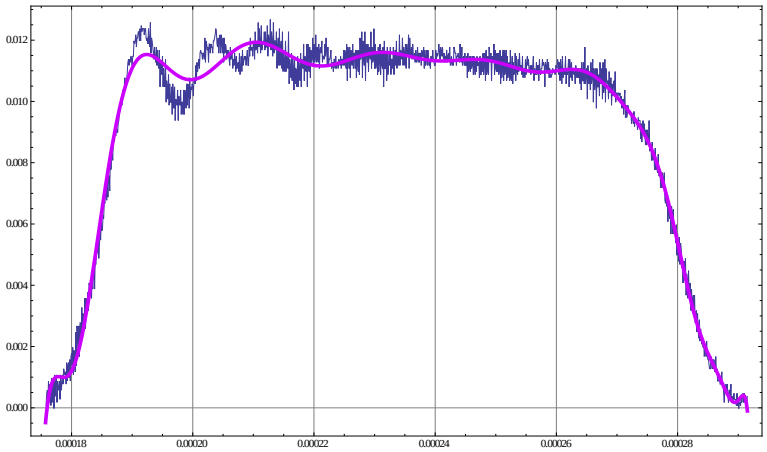


```
Clear[j,k];
Rb=2300//N;
Rs=480//N;
e=50//N;
F=2.14//N;
n=Rb/Rs//N;
co=4817.84//N;
lo=0.00404//N;
j:={};
k:={};
const1=(2 co)/lo//N;
const2=(n+1)2/(n e F)//N;
Do[especimen=const1  ;
AppendTo[j,{s[[m+1,1]]-
s[[1,1]],especimen*100}]//N;AppendTo[k,{s[[m+1,1]]-s[[1,1]],Abs[Log[1-
especimen/100]*100]}],{m,0,Length[s]-1,1}];//Timing

Clear[a4];
{x5,x6}={a2 □ 1,1\[RightDoubleBracket],a2 □ 2,1\[RightDoubleBracket]};
a4:={};
u:={};
fit2=Do[If[data5 □ n,1\[RightDoubleBracket]>x5&&data5 □
n,1\[RightDoubleBracket]<x6,AppendTo[u,{data5 □
```

```
n,1\[RightDoubleBracket],data5 □
n,2\[RightDoubleBracket]}]],{n,1,Length[data5]}];
        fitlist1=Partition[Flatten[u],2];
        transmitted=ListPlot[fitlist1,Joined □ True,Frame □ True,ImageSize □
800,GridLines □{Automatic,{0}}];
        powers:={};
        nw=0.000//N;
        tabx=Table[xn,{n,1,50}];
        AppendTo[powers,{1,tabx}];
        fitrange=Flatten[powers];
        fittedT=Fit[u,fitrange,x]-nw;
        fitplot3=Plot[fittedT,{x,x5,x6},PlotStyle □
{Hue[0.1`],Thickness[0.02`]},GridLines □{Automatic,{0}}];
        fitplot3nw=Plot[fittedT-nw,{x,x5,x6},PlotStyle □
{Hue[0.1`],Thickness[0.02`]},GridLines □{Automatic,{0}}];
        ClickPane[Dynamic[Framed[Show[transmitted,fitplot3,Frame □
True,ImageSize □ 800,Epilog □ Point/@a4]]],AppendTo[a4,#1]&]

        Clear[u]
        {x5,x6}={a4 □ 1,1\[RightDoubleBracket],a4 □ 2,1\[RightDoubleBracket]};

        u:={}
        fit2=Do[If[data5 □ n,1\[RightDoubleBracket]>x5&&data5 □
n,1\[RightDoubleBracket]<x6,AppendTo[u,{data5 □
n,1\[RightDoubleBracket],data5 □ n,2\[RightDoubleBracket]}]],{n,1,Length[data5]}]
        fitlist1=Partition[Flatten[u],2];
        transmitted=ListPlot[fitlist1,Joined □ True,Frame □ True,ImageSize □
800,GridLines □{Automatic,{0}}];
        powers:={};
        tabx=Table[xn,{n,1,50}];
        AppendTo[powers,{1,tabx}];
        fitrange=Flatten[powers];
```

fittedT=Fit[u,fitrange,x]-nw;

fitplot3=Plot[fittedT,{x,x5,x6},PlotStyle □ {Hue[0.1`],Thickness[0.02`]},GridLines □{Automatic,{0}}];

fitplot3nw=Plot[fittedT-nw,{x,x5,x6},PlotStyle □ {Hue[0.1`],Thickness[0.02`]},GridLines □{Automatic,{0}}];

Show[transmitted,fitplot3,Frame □ True,ImageSize □ 800]

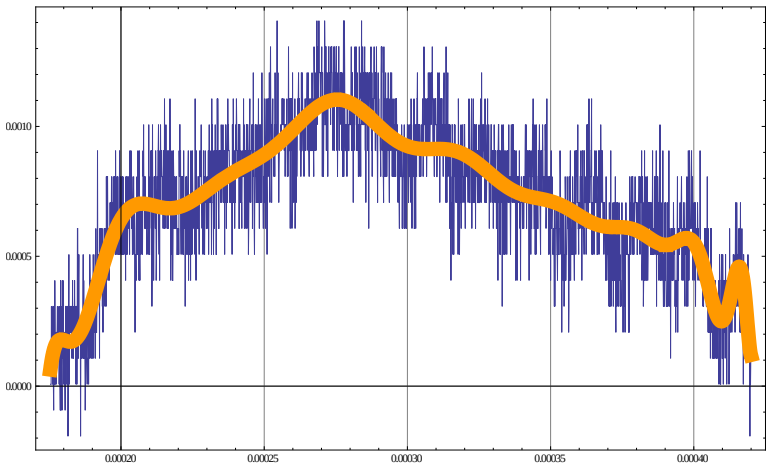


r:={};

w:={};

Eb=187*10^9//N;

Ab=Pi (2.54/400)^2//N;

As=Pi (0.00803/2)^2//N;

const3=(Eb Ab)/As (n+1)2/(n e F)//N;

Do[stressspecimen=const3 □ D fittedT□nw, x, □x //N;

AppendTo[r,{u[[m+1,1]]-u[[1,1]],stressspecimen}],{m,0,Length[k]-1}]//Timing

truestress=Table[r □ m,2\[RightDoubleBracket] (1-1/100 j □ m,2\[RightDoubleBracket]),{m,1,Length[r]}];

ressvrain=Table[{k □ m,2\[RightDoubleBracket] 100,truestress □ m\[RightDoubleBracket]},{m,1,Length[k]}];

lpr=ListPlot[ressvrain,Joined □ True,Frame □ True,PlotRange □ {{0,45},Automatic},ImageSize □ 300]

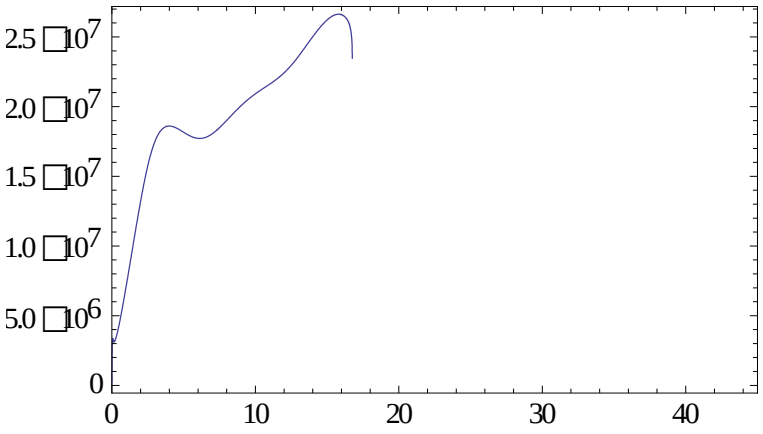


3. Flow stress

The stress strain curve is then imported into the next program to calculate the flow stress at different percentages of the plastic flow

i1=Import["PTFERT_17-2.csv","csv"];
Length[i1]

j1=Table[{i1[[n,1]]-0.15,(i1[[n,2]]/10^6)-3.1},{n,1,Length[i1]}];
(*j2=Table[j1[[n]],{n,1,30}];*)
j3=Table[j1[[n,1]],{n,1,Length[j1]}];
mj=Nearest[j3,5] ;(*The number in "Nearest" is the desired level of strain at which to find the yield point*)
Clear[yieldpt];
yieldpt:={};
Do[If[j3[[n]]□ mj[[1]],AppendTo[yieldpt,j1[[n]]]],{n,1,Length[j1]}];
yieldpt

lp1=ListPlot[j1,Frame □ True,PlotStyle □ {Purple,Thickness[0.008]},BaseStyle □ {FontFamily □ "TimesNewRoman",20},FrameLabel □ {"Strain (%)","Stress (MPa)",None,None},PlotLabel □ StringJoin[{"PTFE_17@ RT: Yield Point =

",ToString[{yieldpt[[1,1]],yieldpt[[1,2]]}]},ImageSize □ 800,Joined □ True,PlotRange □{{0,20},{0,30}}];

line1={{yieldpt[[1,1]],0},{yieldpt[[1,1]],0},Flatten[yieldpt]};
lp2=ListPlot[line1,Joined □ True,PlotStyle □ {Thickness[0.008],Dashed,Black}];

line2={{0,yieldpt[[1,2]]},{0,yieldpt[[1,2]]},Flatten[yieldpt]};
lp3=ListPlot[line2,Joined □ True,PlotStyle □ {Thickness[0.008],Dashed,Black}];
s1=Show[lp1,lp2,lp3]

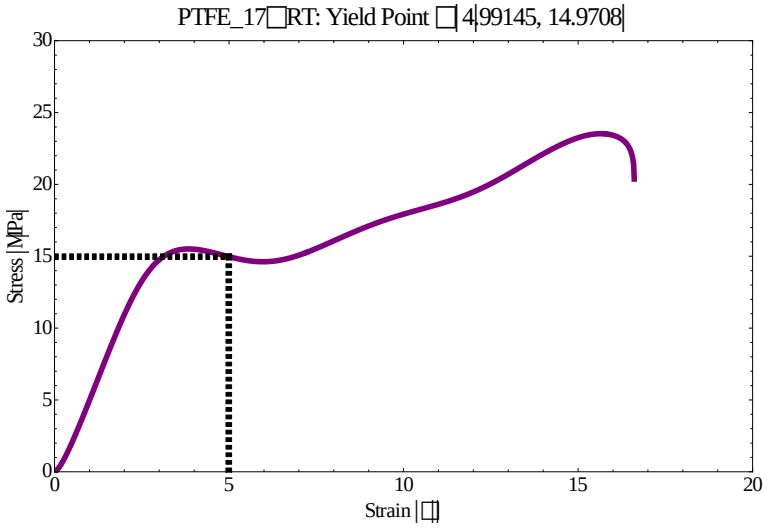


4. Yield stress

Yield stresses are determined by the first highest point in the stress strain curve.

i1=Import["PCTFE100_61.csv","csv"];
Length[i1]
j1=Table[{i1[[n,1]]-0.06,(i1[[n,2]]/10^6)+0.7},{n,1,Length[i1]}];
j2=Table[j1[[n]],{n,1,300}];
j3=Table[j2[[n,2]],{n,1,Length[j2]}];

```
mj=Max[j3];
yieldpt:={};
Do[If[j2[[n,2]]==mj,AppendTo[yieldpt,j2[[n]]]],{n,1,Length[j2]}];
yieldpt
lp1=ListPlot[j1,Frame □ True,PlotStyle □
{Purple,Thickness[0.008]},BaseStyle □ {FontFamily □
"TimesNewRoman",20},FrameLabel □ {"Strain (%)","Stress
(MPa)",None,None},PlotLabel □ StringJoin[{"PCTFE_61@ 100 degrees: Yield
Point = ",ToString[{yieldpt[[1,1]],yieldpt[[1,2]]}]}],ImageSize □ 800,Joined □
True,PlotRange □{{0,45},{0,180}}];

line1={{yieldpt[[1,1]],0},{yieldpt[[1,1]],0},Flatten[yieldpt]};
lp2=ListPlot[line1,Joined □ True,PlotStyle □
{Thickness[0.008],Dashed,Black}];
line2={{0,yieldpt[[1,2]]},{0,yieldpt[[1,2]]},Flatten[yieldpt]};
lp3=ListPlot[line2,Joined □ True,PlotStyle □
{Thickness[0.008],Dashed,Black}];
s1=Show[lp1,lp2,lp3]
```

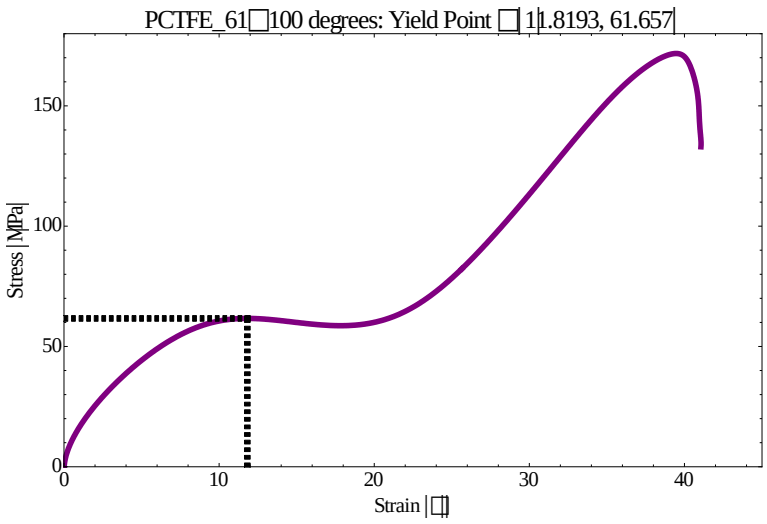


5. Strain rate

The true strain is plotted against time and the gradient is the strain rate of the experiment experienced by the specimen.

```
range=400
i1=Import["PVC50_21.csv","csv"];
j1=Table[{i1 □ n,1\[RightDoubleBracket]+0.0`,i1 □ n,2\[RightDoubleBracket]/106},{n,1,Length[i1]}];
time=N[Table[q/107,{q,0,Length[i1]-1}]];
stvt1=Table[{time □ n\[RightDoubleBracket] 106,i1 □ n,1\[RightDoubleBracket]},{n,1,Length[i1]}];
stvt2=Table[{time □ n\[RightDoubleBracket] 106,i1 □ n,1\[RightDoubleBracket]},{n,range,Length[i1]-range}];
strainvstime=Table[{time □ n\[RightDoubleBracket],1/100 i1 □ n,1\[RightDoubleBracket]},{n,1,Length[i1]}];
strainvstime2=Table[{time □ n\[RightDoubleBracket],1/100 i1 □ n,1\[RightDoubleBracket]},{n,range,Length[i1]-range}];
linearfit=Table[{time □ n\[RightDoubleBracket],1/100 i1 □ n,1\[RightDoubleBracket]},{n,range,Length[i1]-range}];
fline=Fit[strainvstime2,{1,x},x];
st1=ListPlot[stvt1,Frame □ True,PlotStyle □ {Hue[0.5507`],Thickness[0.02`]},FrameLabel □ {"Time ( □ s)","True Strain (%)","PVC50_21",None},ImageSize □ 400,Joined □ True,BaseStyle □{FontFamily □"TimesNewRoman",14}];
st2=ListPlot[stvt2,Frame □ True,PlotStyle □ {Hue[0.5507`],Thickness[0.02`]},FrameLabel □ {"Time ( □ s)","True Strain (%)","PVC50_21" fline,None},ImageSize □ 400,Joined □ True,BaseStyle □ {FontFamily □"TimesNewRoman",14}];
sh=Show[GraphicsGrid[{{st1},{st2}}],ImageSize □ 400]
```

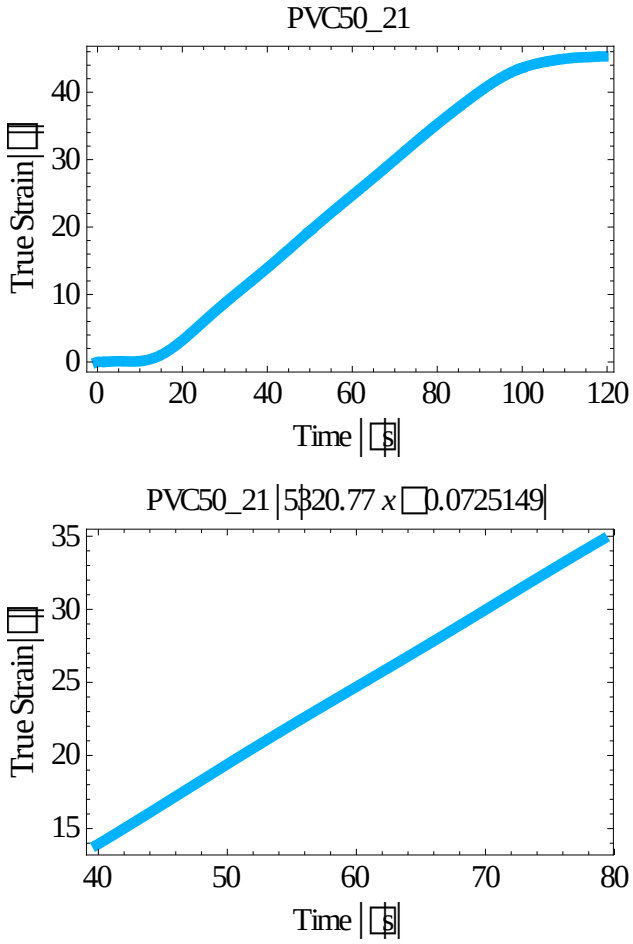


6. Temperature rise during plastic flow

First the yield point of the stress strain curve is given so that the plastic flow regain in the stress strain rate curve can be obtained. Then the specific heat, and the dimensions of the specimen are given to work out the temperature rise in the specimen.

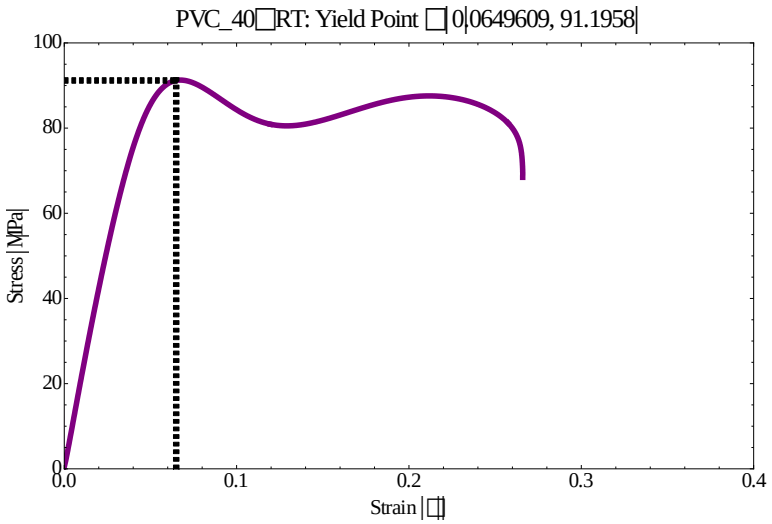

```
cp=1250;(*specific heat*)
radius=N[0.00825/2];
length=0.00412;
Volume=length Pi (radius^2);(*Volume of the sample*)
density=2200;
mass=Volume* density;
plasticrange=0.21;
deltaT=Table[{yq+n,((Volume/ mass)
Integrate[fittedT,{x,yq,yq+n}])/cp},{n,0,plasticrange,0.05}];(*Temperature change*)

s2=ListPlot[deltaT,Frame □ True,Joined □ True,PlotStyle □
{Purple,Thickness[0.008]},BaseStyle □ {FontFamily □
"TimesNewRoman",20},FrameLabel □{"Strain","□ T (K)",None,None}]
```

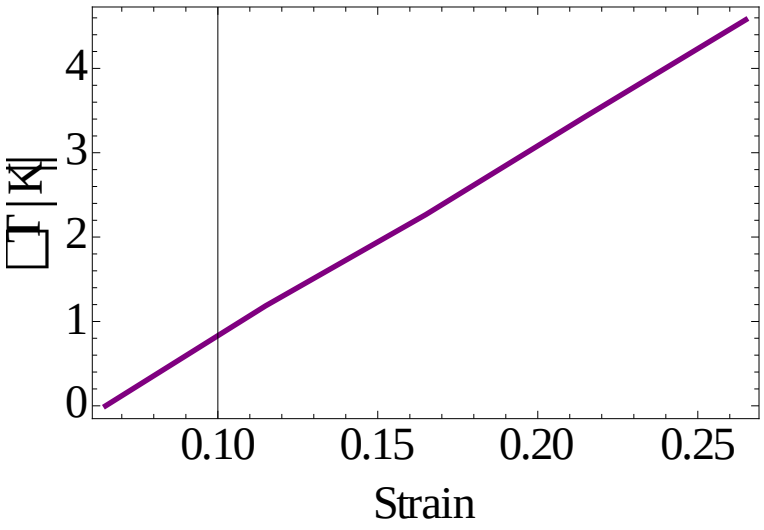

# C. Dymat 2009 conference paper and poster

*DYMAT 2009* (2009) 1443–1447

DOI: 10.1051/dymat/2009204

# Flow stress peaks at high strain rates in PMMA

H.H. Forrester and G.M. Swallowe

*Department of Physics, Loughborough University, Loughborough LE11 3TU, UK*

**Abstract.** The results of an investigation into the stress-strain behaviour of PMMA in the strain rate region of $10^2$ to $10^4\ s^{-1}$ over a range of temperatures from room temperature up to 90°C are reported. The investigation was carried out in an effort to detect the presence, or absence, of peaks in the flow stress – strain rate response. All tests were carried out in compression on a standard Hopkinson Bar system. Although not as clearly defined as the sharp peak in flow stress reported by previous workers in PEEK, there is good evidence of a peak in the flow stress in the strain rate range $10^2$ to $10^3$ which both narrows and moves to a higher strain rate as the temperature approaches the glass transition. Previously reported peaks in flow stress had only been observed in semi-crystalline polymers. The current observations in PMMA suggest that this may be a universal phenomenon. Preliminary work at similar strain rates and temperature ranges on PCTFE, show less conclusive indications of peaks in the flow stress at strain rates around $3 \times 10^3\ s^{-1}$.

## 1. INTRODUCTION

There have been many reports of a rapid increase in the flow stress of polymers when strain rates in the region of $10^2\ s^{-1}$ or higher are applied. Similar effects are observed in metals and are explained in terms of dislocation drag and associated mechanisms. An investigation by Walley and Field [1] into the behaviour of a range of polymers showed some materials having an increased flow stress and some with a decreased flow stress in the strain rate region of $\sim 10^3\ s^{-1}$. More recent work by Richeton et al. [2] and Sou et al. [3] show an increase in yield and flow stress at rates $\sim 10^3\ s^{-1}$ in poly(methy methacrylate), PMMA, but over rather limited strain rate and temperature ranges. A comprehensive room temperature investigation by Al-Maliky et al. on PEEK and Nylon [4] showed a rapid increase followed by a rapid decrease in flow stress over a narrow range of strain rates from $10^3$ to $10^4\ s^{-1}$. In general, most investigators only measure the mechanical properties at a very limited range of strain rates in the high rate region so there is the possibility that the conflicting results of some workers could be resolved by the fact that data in the high rate region is generally sparse and therefore the reported changes in flow stress may depend critically on exactly at which strain rate measurements were made. The results reported by Walley and Field [1] cover both semi-crystalline and amorphous polymers but, as far as the authors are aware, the only comprehensive investigations of possible peaks in the strain rate response have been on semi-crystalline polymers [4]. The primary purpose of the work reported here was to carry out a thermomechanical investigation of the behaviour of a fully amorphous polymer in the strain rate region where drops/rises in flow stress have been reported in order to investigate if the behaviour reported by Al-Maliky et al. in semi-crystalline materials is also observed in an amorphous material.

## 2. EXPERIMENTAL PROCEDURE

### 2.1 Materials

The primary material investigated was the amorphous polymer poly(methylmethacryalate), PMMA. Commercial rods of this polymer were purchased from Goodfellow Ltd, Cambridge, and

machined into cylinders of proportions: 10 mm diameter by 5 mm height or 6 mm diameter by 3 mm height depending on strain rate required for the test. The diameter/height ratio of 2/1 was kept constant in accordance with the recommendations of Cady et al. [5] to promote stress equilibrium and minimise barrelling in compressive tests.

### 2.2 Mechanical tests

All the samples were tested in compression using the Split-Hopkinson pressure bar (SHPB) system in the Physics department at Loughborough University, over a range of temperatures from room temperature (RT) to 90°C. The system incorporates a pre-loading bar which dampens high frequency oscillations on the stress pulse and is fully described in previous publications [6]. Prior to each test the sample was heated on a hot plate to the required temperature for at least 30 minutes and the two ends of the bars that would be in contact with the sample were heated for at least 30 minutes to the required temperature using a radiant heating system. Immediately prior to the test the completed sample/bar assembly was maintained at the required temperature for a further 10 minutes. The temperature was monitored using a thermocouple in contact with the sample. The samples were tested across a range of strain rates from $10^2$ to $10^4\ s^{-1}$. To reduce frictional effects the faces of the bars were lubricated using a PTFE spray.

Before analysis the raw data was smoothed by fitting a high order polynomial to the Hopkinson Bar pulses and adjusting the polynomial order until a close match between fit and raw data was achieved. Standard analysis was carried out on the fitted curves. This procedure effectively removed the high frequency noise in the data.

### 2.3 Thermal analysis

The thermal properties of the PMMA samples were characterised by differential scanning calorimetry (DSC) and dynamic mechanical thermal analysis (DMTA). DSC scans were conducted from $-30$°C to 130°C at 10°C/min using a Mettler TA3000 Thermal Analysis System. A TA Instruments 2980 DMA was used to perform DMTA on cylindrical bars of PMMA with length of 34.5 mm and diameter of 4.2 mm in the dual cantilever bending mode. Measurements were carried out at 0.1 and 100 Hz. The heating rate was set at 3°C/min and specimens were tested over the temperature range from $-30$ to 170°C, at which point the specimens were found to have become excessively softened. The storage and loss moduli were continuously recorded.

## 3. RESULTS AND DISCUSSION

### 3.1 Mechanical tests

#### *3.1.1 Stress-strain curves*

Five sets of stress-strain rates curves, at temperatures RT ($\sim$20°C), 30°C, 50°C, 70°C and 90°C were obtained. Selected samples of the resulting stress-strain curves are presented in Figure 1, the strain rates of each test is indicated in the Figure 1.

The yield strain of a PMMA stayed approximately constant, independent of temperature, whereas yield stress, as expected, was both temperature and strain rate dependent. Figure 1(f) to (i) illustrate recovered samples tested at various temperatures. There are obvious cracks and breakages in the RT samples and evidence of shear banding in the 30°C test – but at higher temperatures fracture, rather than shear banding, again becomes evident. Despite cracking the basic geometry of the sample remained intact under impact. At temperatures of 50°C and above

the total deformation before cracking increased with temperature. Other than the large cracks evident in Figure 1 the rest of the sample remained transparent.

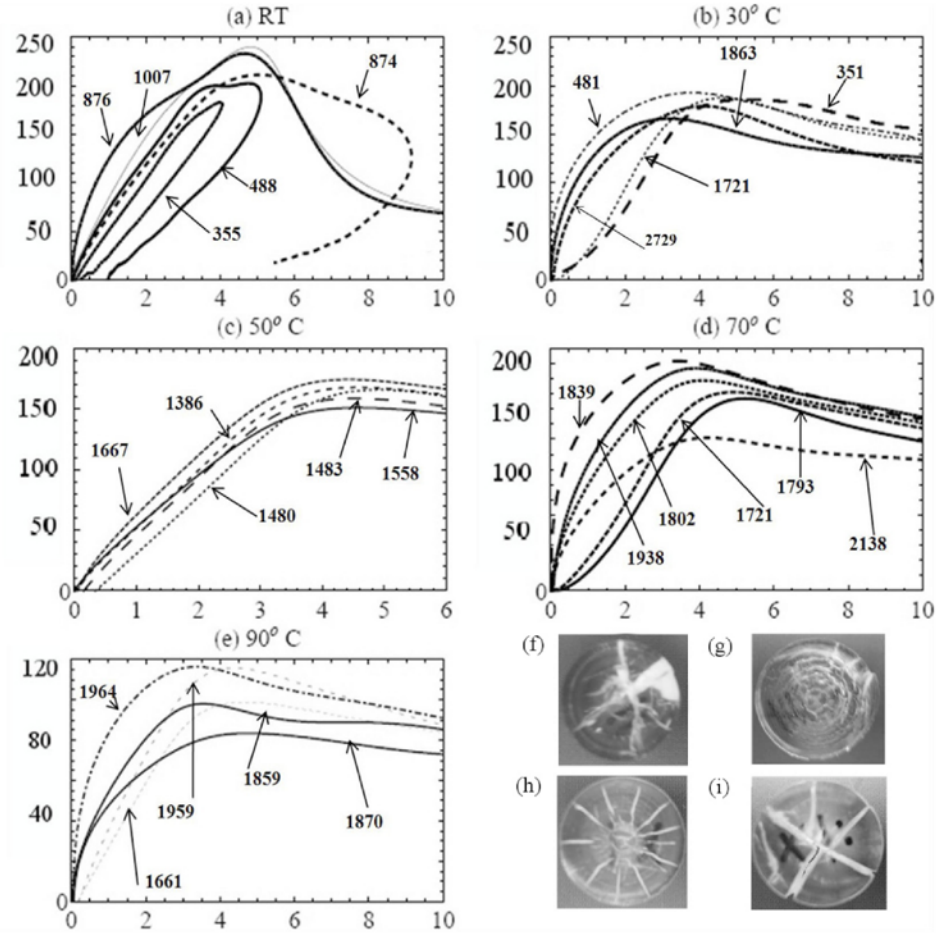


**Figure 1.** PMMA True Stress (MPa) versus True Strain (%) curves at (a) room temperature, (b) 30°C, (c) 50°C, (d) 70°C and (e) 90°C over a range of high strain rates. Image (f) is a sample of the polymer after testing at room temperature, (g) at 30°C, (h) at 50°C and (i) at 70°C.

### *3.1.2 Flow stress as a function of strain rate*

The flow stress of PMMA was determined from the data illustrated in Figure 1 by taking the stress reading at 4% strain from each sample tested. The results are illustrated in Figure 2. The accuracy in the flow stress is typically better than $\pm 10$ MPa as determined from the scatter of values from repeat measurements. PMMA samples tested at room temperature at strain rates over $1.2 \times 10^3\ s^{-1}$ shatter before yield so the RT data was limited to a maximum rate of $10^3\ s^{-1}$. No peak is evident at this temperature. There is some, rather inconclusive, hint of broad peaks at 30°C

and 50°C but the error in the results is such that this cannot be determined with any confidence. More conclusive peaks in flow stress-strain rate appear at 70°C and 90°C. There is good evidence of a peak in the flow stress in the strain rate range 1.7 to $2.0 \times 10^3$ which both narrows and moves to a higher strain rate as the temperature is increased.

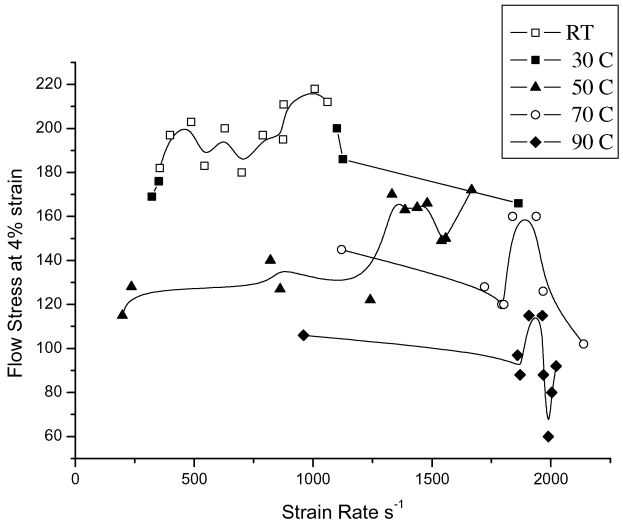


**Figure 2.** Flow stress at 4% strain as a function of compressive strain rate for PMMA over a range of temperatures. The spline fit lines are a guide to the eye.

### 3.2 Thermal analysis

Dynamic mechanical thermal analysis of PMMA was carried out at two frequencies, 0.1 Hz and 100 Hz and the results are illustrated in Figure 3. The rapid drop in the storage modulus and peak in Tan $\delta$ occurs at $\sim 110$°C which is taken to be the glass transition temperature (Tg). This was confirmed by the DSC data. The $\beta$ relaxation peaks are very broad and the maximum shifts from $\sim -10$°C at 0.1 Hz to $\sim 70$°C at 100 Hz. Because of the small displacements involved the strains imparted to the samples during DMTA are very small ($\sim 10^{-2}$), thus the strain rates at 0.1 Hz and 100 Hz are only $\sim 10^{-3}\,s^{-1}$ and $1\,s^{-1}$. From the change in position of the storage modulus a strain rate sensitivity for Tg of $\sim +2.5°$ per decade is evident.

## 4. PRELIMINARY WORK ON PTFE AND PCTFE

The semi-crystalline polymer polychorotrifluoroethylene (PCTFE), also purchased from Goodfellows Ltd., is under investigation at a range of compressive strain rates and temperatures from room temperature to 100°C. The glass transition temperature obtained by DSC for PCTFE was 52°C and the melting temperature 214°C. Initial results indicate that PCTFE shows evidence of peaks in the flow stress at strain rates of $\sim 3 \times 10^3\,s^{-1}$ at room temperature and $4 \times 10^3\,s^{-1}$ at 50°C. However, these initial results are not sufficiently conclusive to assert that a peak does exist. Investigations are continuing and full results will be presented at DYMAT 2009.

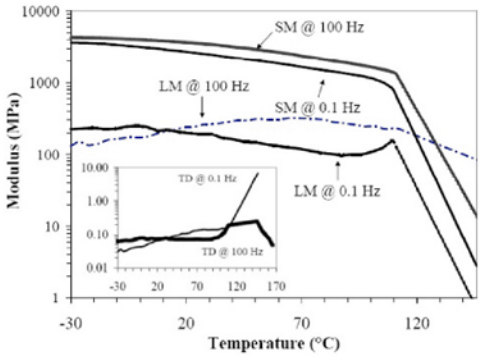


**Figure 3.** Temperature vs. Storage modulus (SM) and Lost modulus (LM) at 0.1 and 100 Hz. Tan delta as a function of temperature is the inset in the bottom left hand corner.

## 5. CONCLUSIONS

Although not as clear as the results of Al-Maliky [4] there is good evidence of a peak in the flow stress of PMMA at temperatures of 70°C and 90°C centred in the region of $1.6 \times 10^3\,s^{-1}$ to $2.0 \times 10^3\,s^{-1}$. The peaks both narrow and shift to higher strain rate as the temperature approaches the glass transition temperature. This observation suggests that this phenomenon could be a characteristic of amorphous regions and hence potentially be evident in all polymers both amorphous and semi-crystalline. In the present work on PMMA the peak only became evident when the ambient temperature was within 40° of Tg. The initial PCTFE data also indicates the formation of a peak at temperatures below and close to Tg. Higher temperature measurements are in progress. Previous observations [4] at room temperature were below Tg (Tg is 42°C for Nylon 66 and 143°C for PEEK), although the >100°C gap between measurement at Tg for PEEK is very large. Further investigation into this phenomenon is required.

## References

[1] Walley S.M and Field J.E., Dymat Journal, 1 (1994) 211.
[2] Richerton J., Ahzi S., Vecchio K.S., Jiang F.C. and Adharapurapu R.R., Intl. J. of Solids and Structures, 43 (2006), 2318-2335
[3] Suo T., Li Y., Liu Y., Key Engineering Materials, 340 (2007), 1079-1084
[4] Al-Maliky N., Fernandez J.O., Parry D.J. and Swallowe G.M., J. Mat. Sci., 17 (1998) 1141-1143
[5] Cady L.P., Blumenthal W.R., Gray III G.T., Idar D.J., J. de Physique IV, 110 (2003), 27-32
[6] Parry D.J., Walker A.G. and Dixon P.R., Meas. Sci. and Technol., 6 (1995), 443-446

# Flow Stress Peaks at High Strain Rates in PMMA


**H.H.Forrester, G.M.Swallowe**

Department of Physics, Loughborough University, Loughborough, LE11 3TU, UK


## Introduction

An investigation into the stress-strain behaviour of poly(methyl methacrylate), PMMA, in the strain rate region of $10^2$ to $10^4$ $s^{-1}$ over a range of temperatures are reported. This was carried out in an effort to detect the presence, or absence, of peaks in the flow stress – strain rate response.

In general, most investigators measure the mechanical properties at a very limited range of strain rates in the high rate region leading to some reporting increases and others decreases in flow stress.[1],[2],[3],[4] The conflicting results could be resolved if the reported changes in flow stress depend critically on exactly at which strain rate measurements were made.

## Experimental Methods

Commercial rods of PMMA were purchased from Goodfellow Ltd, Cambridge, and machined into cylinders of diameter/height ratio of 2/1 to promote stress equilibrium and minimise barrelling in compressive tests.[5]

Samples were tested in compression using the Split-Hopkinson pressure bar (SHPB) system at Loughborough University. The system incorporates a pre-loading bar which dampens high frequency oscillations on the stress pulse.[6]

Prior to each test, the samples were heated using a hot plate and the SHPB bars ends in contact were heated using a radiant heating system. Then the sample and bars were heated together till reaching equilibrium at required temperature. To reduce frictional effects the faces of the bars were lubricated using a PTFE spray.

## Results

Five sets of compression tests were carried out at room temperature (~20 $^0$C), 30 $^0$C, 50 $^0$C, 70 $^0$C and 90 $^0$C.

- The yield strain of PMMA stayed approximately constant, independent of temperature, whereas yield stress, as expected, was both temperature and strain rate dependent.
- There are obvious cracks and breakages in the RT samples and evidence of shear banding in the 30 $^0$C test – but at higher temperatures fracture, rather than shear banding.
- At 50$^0$C and above the total deformation before cracking increased with temperature.
- Despite cracking the basic geometry of the sample remained intact under impact.

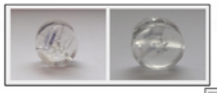

*PMMA samples tested at RT.*

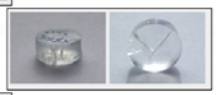

*PMMA samples tested at 30$^0$C.*

*PMMA samples tested at 50 $^0$C*

*PMMA samples tested at 70$^0$C*

*PMMA samples tested at 90 $^0$C*

### *Stress-strain curves*

Before analysis the raw data was smoothed by fitting a high order polynomial to the Hopkinson Bar pulses and adjusting the polynomial order until a close match between fit and raw data was achieved. Standard analysis was carried out on the fitted curves. This procedure effectively removed the high frequency noise in the data

Selected samples of the resulting stress-strain curves are presented in the figure below. The strain rates of each test is indicated by the appropriate curve.

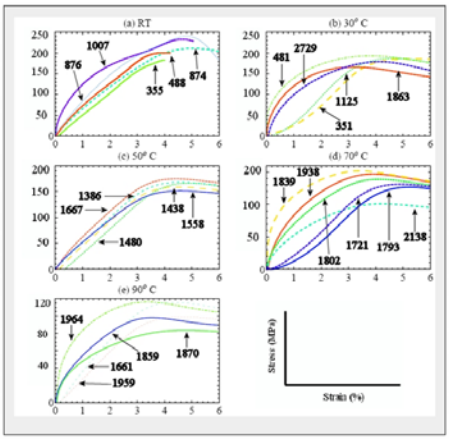


*PMMA True Stress versus True Strain curves at room temperature, 30, 50, 70 and 90 degrees over a range of high strain rates.*

## Analysis

### *Thermal Analysis*

The thermal properties of the PMMA samples were characterised by differential scanning calorimetry (DSC) and dynamic mechanical thermal analysis (DMTA) at 0.1Hz and 100Hz.

- The rapid drop in the storage modulus and peak in Tan $\delta$ occurs at ~ 110 $^0$C which is taken to be the glass transition temperature (Tg). This was confirmed by the DSC data.
- The $\beta$ relaxation peaks are very broad and the maximum shifts from ~ -10 $^0$C at 0.1 Hz to ~ 70 $^0$C at 100 Hz.
- Because of the small displacements involved the strains imparted to the samples during DMTA are very small (~ $10^{-2}$), thus the strain rates at 0.1 Hz and 100 Hz are only ~ $10^{-3}$ $s^{-1}$ and 1 $s^{-1}$.
- From the change in position of the storage modulus a strain rate sensitivity for Tg of ~ + 2.5$^0$ per decade is evident.

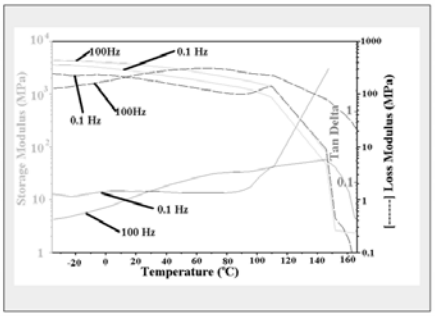


*Temperature vs. Storage modulus(SM) , Lost modulus(LM) and Tan $\delta$ at 0.1 and 100 Hz.*

### *Flow Stress as a function of Strain Rate*

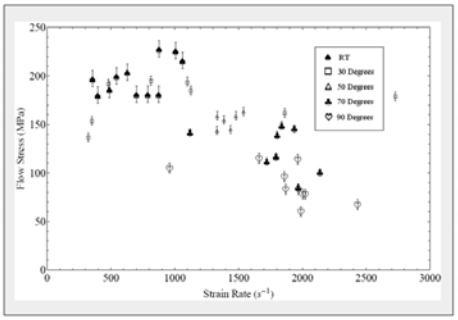


*Flow stress at 4% strain as a function of compressive strain rate for PMMA over a range of temperatures.*

The flow stress of PMMA was determined by taking the stress at 4% strain from each sample tested. The accuracy in the flow stress is typically better than ± 10MPa as determined from scattered values of repeat measurements.

- Room temperature PMMA samples tested at strain rates over 1.2 x $10^3$$s^{-1}$ shatter before yield so the RT data was limited to a maximum rate of $10^3$ $s^{-1}$. No peak is evident at this temperature.
- There is some hint of broad peaks at 30 $^0$C and 50 $^0$C but the error in the results is such that this cannot be determined with any confidence. More conclusive peaks in flow stress-strain rate appear at 70 $^0$C and 90 $^0$C.
- There is good evidence of a flow stress peak in the strain rate range 1.7 to 2.0 x $10^3$ which both narrows and moves to a higher strain rate as the temperature is increased.

### *Preliminary work on PCTFE*

Initial results indicate that PCTFE shows evidence of peaks in the flow stress at strain rates of ~ 3 x $10^3$$s^{-1}$ at room temperature and 4 x $10^3$$s^{-1}$ at 50°C.

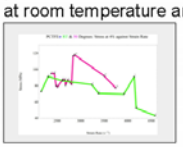

*Flow stress at 4% strain as a function of compressive strain rate for PCTFE at room temperature and 50 $^0$C.*

## Conclusion

There is good evidence of a peak in the flow stress of PMMA .

The peaks both narrow and shift to higher strain rate as the temperature approaches the glass transition temperature. This suggests the phenomenon could be a characteristic of amorphous regions and hence potentially be evident in all polymers both amorphous and semi-crystalline.

In the present work on PMMA the peak only became evident when the ambient temperature was within 40$^0$ of Tg. The initial PCTFE data also indicates the peak near to Tg. Higher temperature measurements are in progress. Previous observations for Nylon 66 and PEEK at room temperature were below Tg.

Further investigation into this phenomenon is required.

## References


[1] Walley S.M and Field J.E., Dymat Journal, **1** (1994) 211.
[2] Richerton J., Ahzi S., Vecchio K.S., Jiang F.C. and Adharapurapu R.R., Intl. J. of Solids and Structures, **43** (2006), 2318-2335
[3] Suo T., Li Y., Liu Y., Key Engineering Materials, **340** (2007), 1079-1084
[4] Al-Maliky N., Fernandez J.O., Parry D.J. and Swallowe G.M., J. Mat. Sci., **17** (1998) 1141-1143
[5] Cady L.P., Blumenthal W.R., Gray III G.T., Idar D.J., J. de Physique IV, 110 (2003), 27-32
[6] Parry D.J., Walker A.G. and Dixon P.R., Meas. Sci and Technol., **6** (1995), 443-446

# D. Complete stress-strain curves

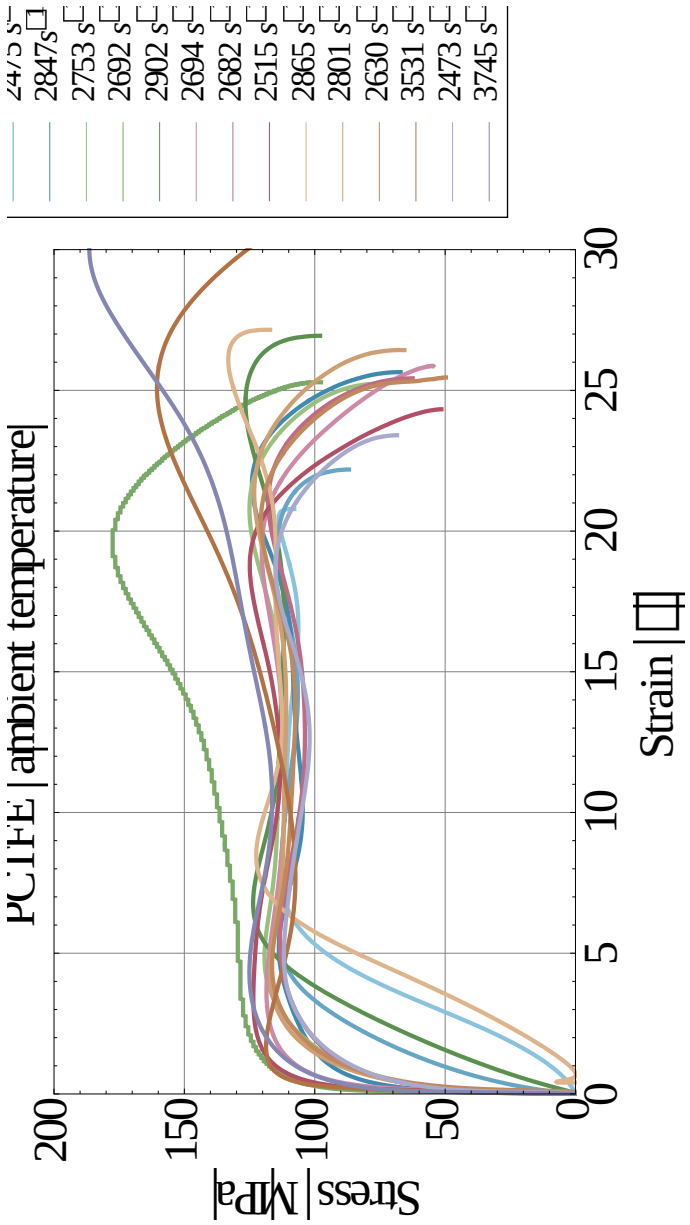


*Figure D.1 Complete collection of PCTFE specimen stress-strain curves at ambient temperature. The key on the right indicates the rate of strain achieved in each experiment.*

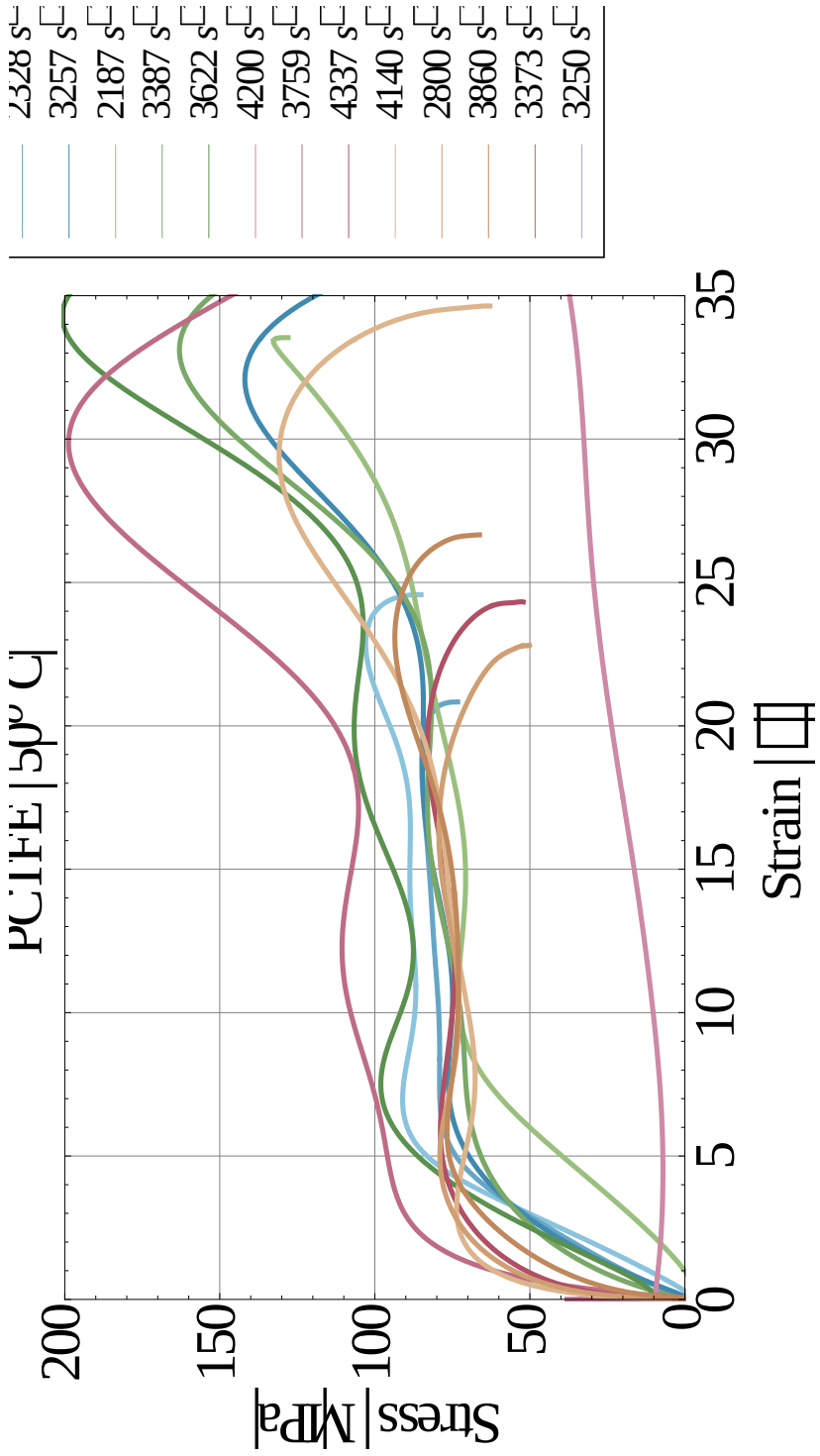


*Figure D.2 Complete collection of PCTFE specimen stress-strain curves at 50ºC. The key on the right indicates the rate of strain achieved in each experiment.*

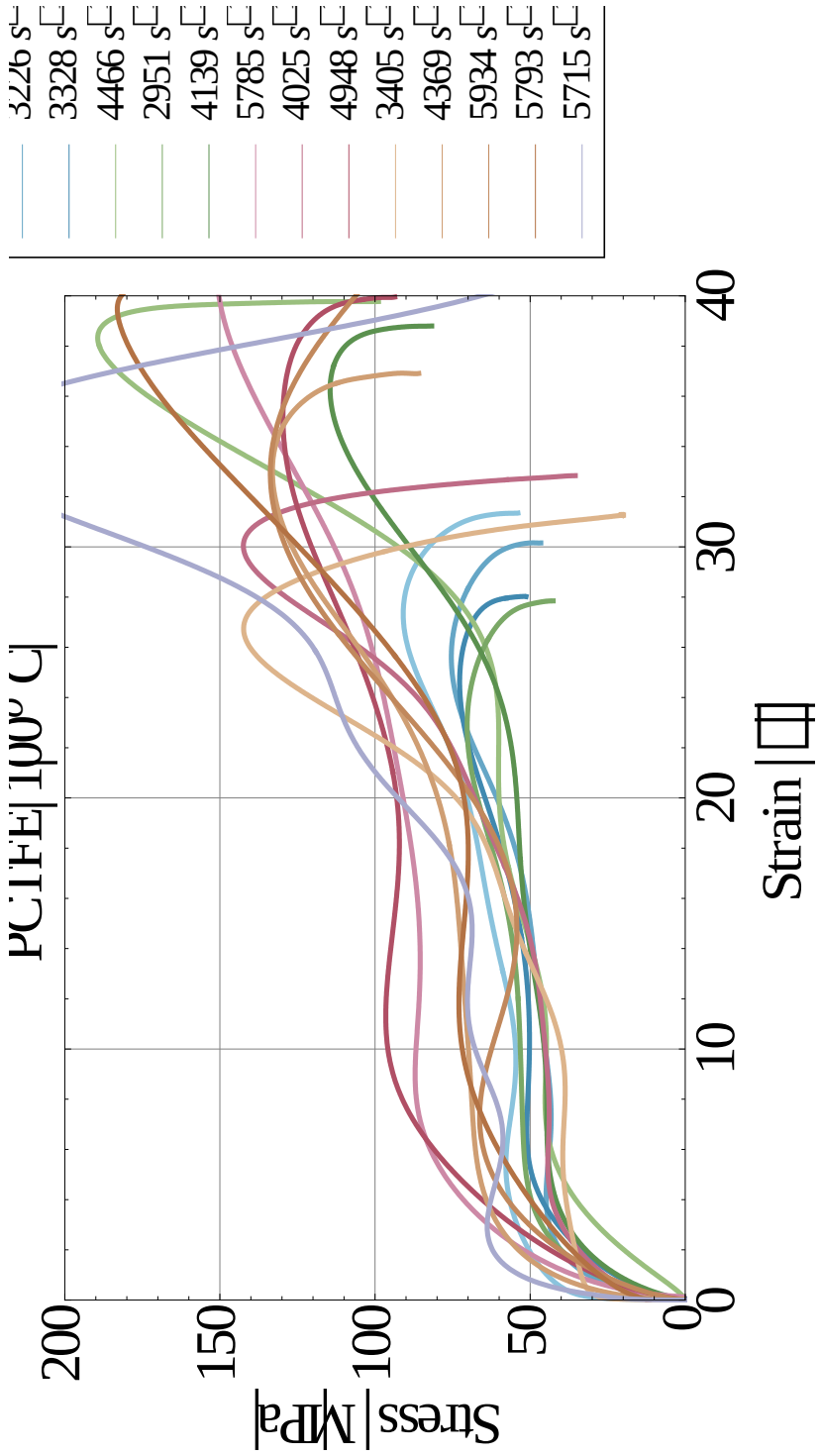


*Figure D.3 Complete collection of PCTFE specimen stress-strain curves at 100ºC. The key on the right indicates the rate of strain achieved in each experiment.*

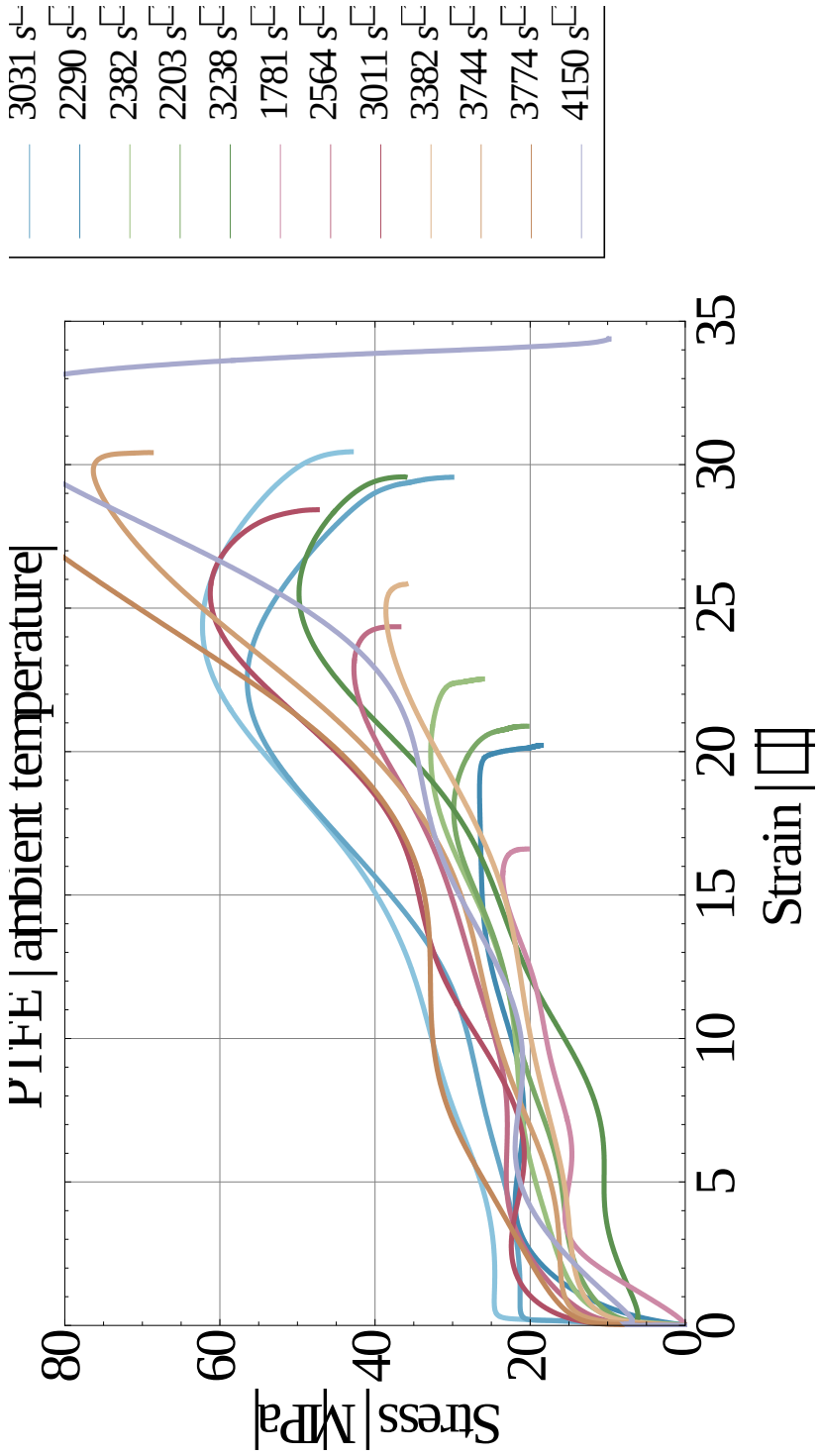


*Figure D.4 Complete collection of PTFE specimen stress-strain curves at ambient temperature. The key on the right indicates the rate of strain achieved in each experiment.*

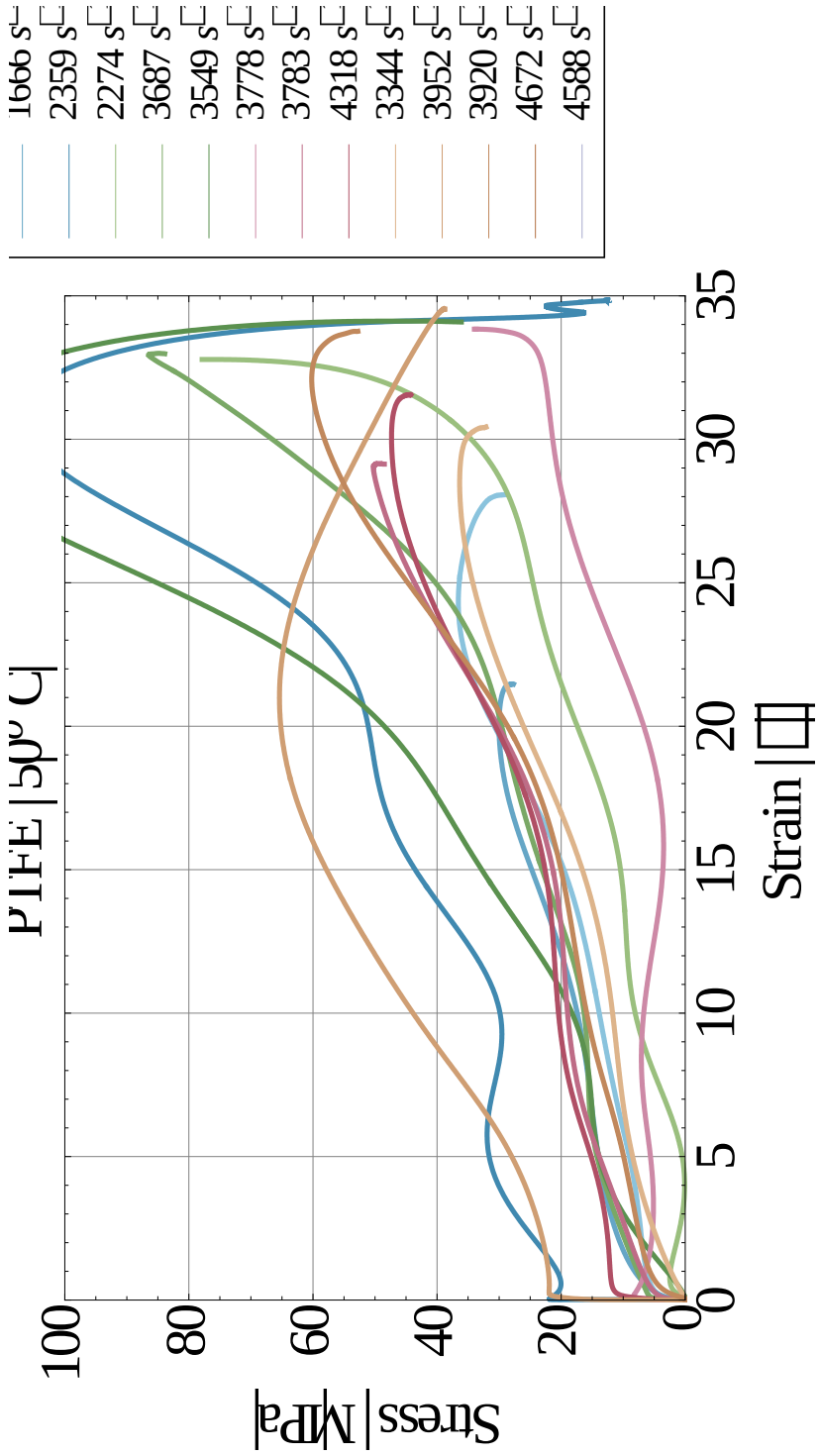


*Figure D.5 Complete collection of PTFE specimen stress-strain curves at 50ºC. The key on the right indicates the rate of strain achieved in each experiment.*

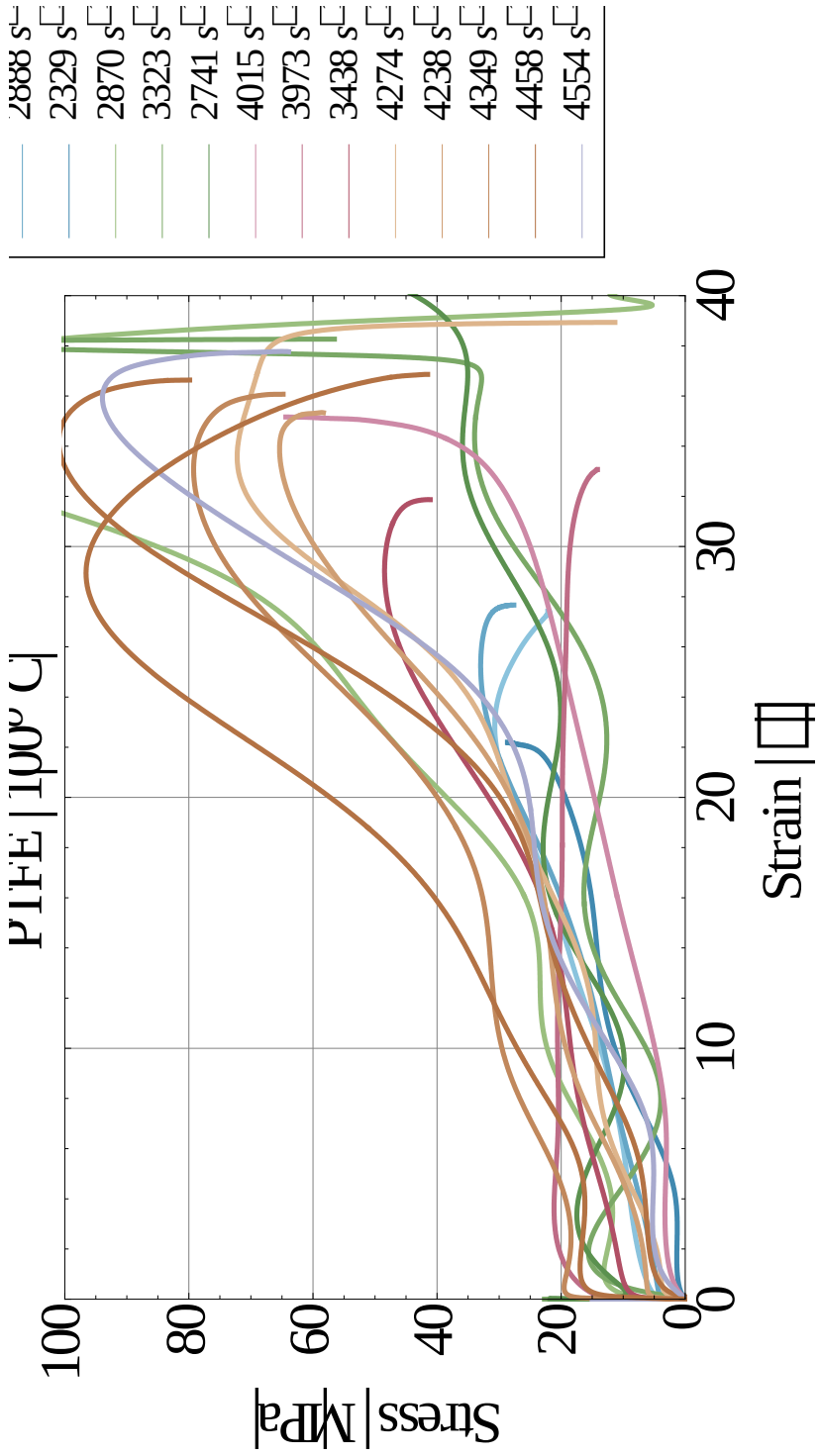


*Figure D.6 Complete collection of PTFE specimen stress-strain curves at 100ºC. The key on the right indicates the rate of strain achieved in each experiment.*

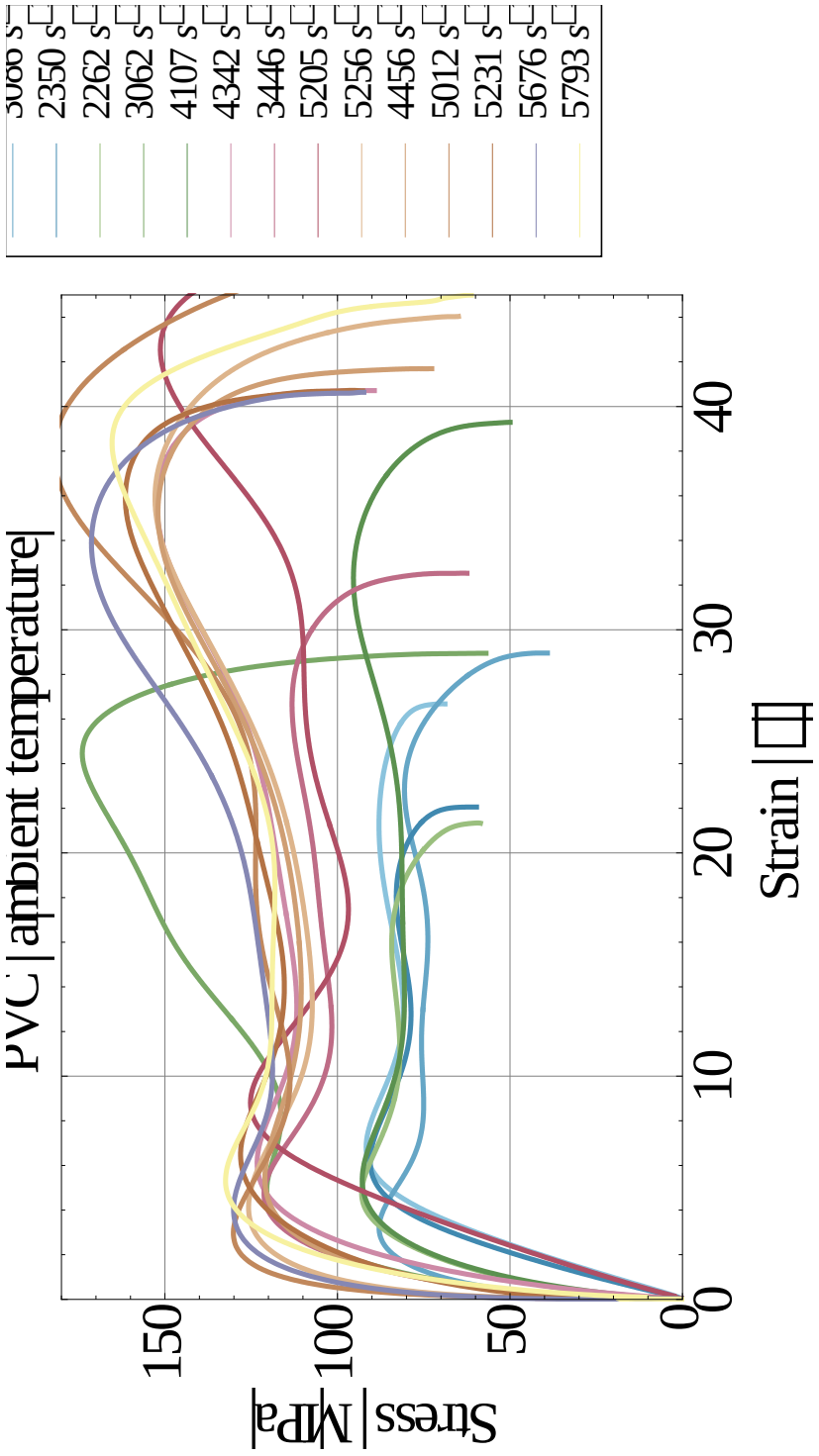


*Figure D.7 Complete collection of PVC specimen stress-strain curves at ambient temperature. The key on the right indicates the rate of strain achieved in each experiment.*

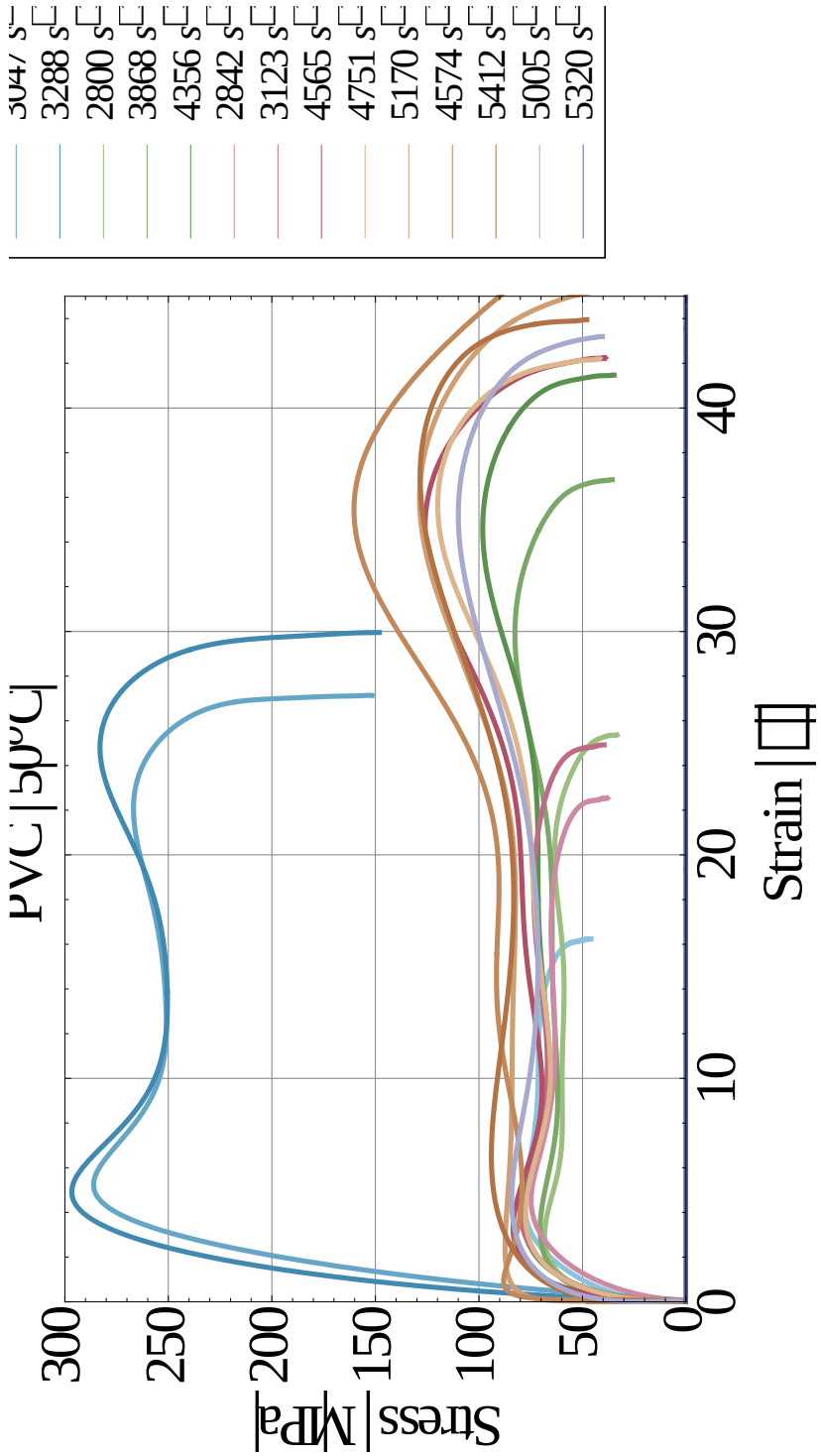


*Figure D.8 Complete collection of PVC specimen stress-strain curves at 50ºC. The key on the right indicates the rate of strain achieved in each experiment.*

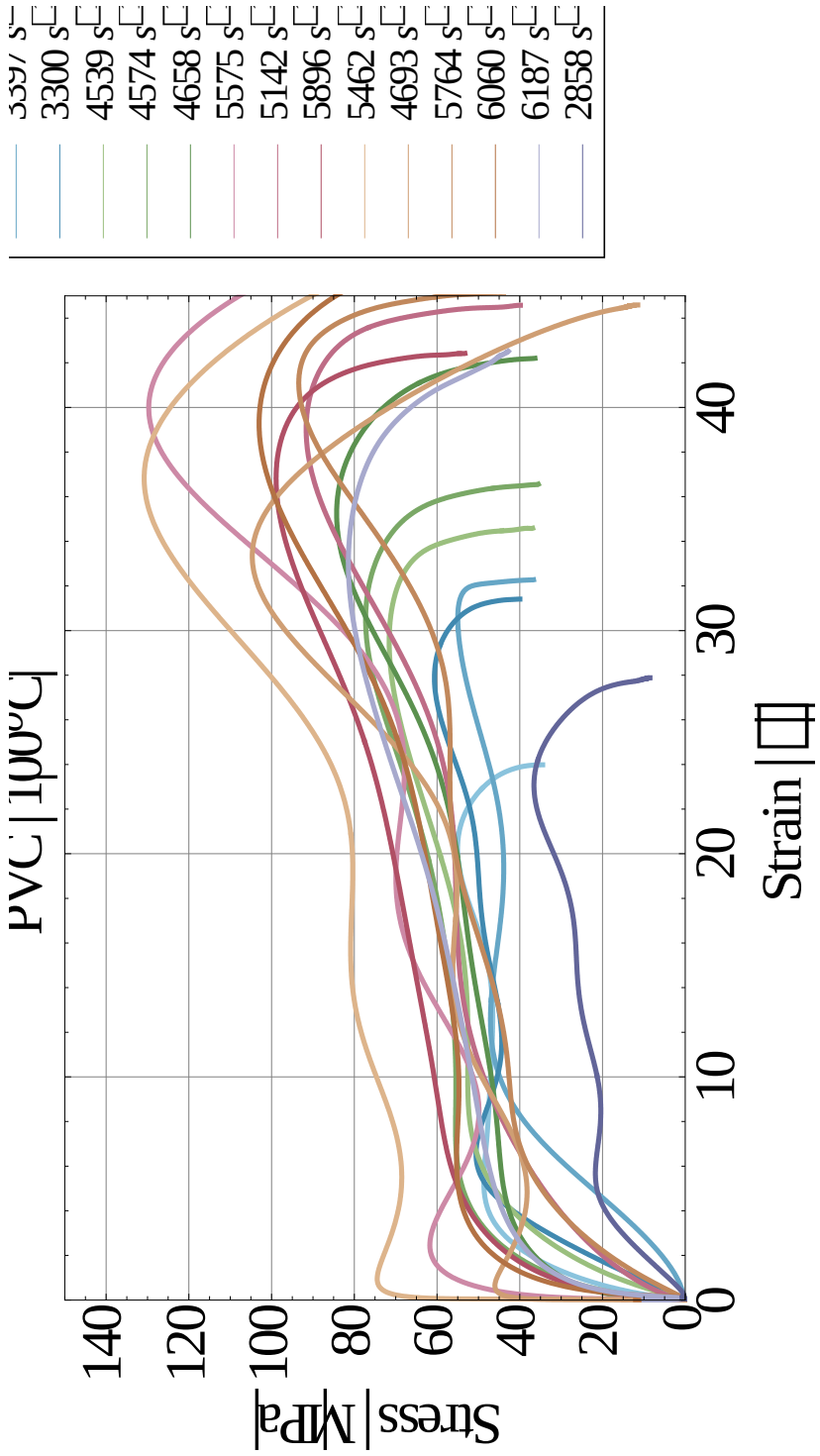


*Figure D.9 Complete collection of PVC specimen stress-strain curves at 100ºC. The key on the right indicates the rate of strain achieved in each experiment.*

# References

**Al-Maliky/Parry 1994,** Measurement of high strain rate properties of polymers using an expanding ring method *Journal De Physique IV* **4** C8-71

**Al-Maliky/Parry 1996** A freely expanding ring technique for measuring the tensile properties of polymers Meas. Sci. Technol. **7** 746-752

**Al-Maliky 1997**, *Strain rate behaviour of thermoplastic polymers* Ph.D. thesis Loughborough University

**Al-Maliky/Fernandez/Parry/Swallowe 1998**, *J. Mat. Sci*. 17 1141-43

**Bacon 1993**, Numerical prediction of the propagation of elastic waves in longitudinally impacted rods: Applications to Hopkinson testing *Int. J. Impact Eng*. **13** 527-539

**Bacon 1998**, An experimental method for considering dispersion and attenuation in a viscoelastic Hopkinson bar *Exp. Mech*. **38** 242-249

**Bauwens-Crowet 1973**, The compression yield behaviour of PMMA over a wide range of temperature and strain rates *J. Mater Sci.* **8** 968–79

**Bedford et al 1974**, The Phenomenon of Adiabatic Shear Deformation *J. Aust. Inst. Metals* **19** 61

**Bertholf/Karnes 1975**, Two-dimensional Analysis of the Split Hopkinson Pressure Bar System *Journal of the Mechanics and Physics of Solids* **23** 1-19

**Bios et al 2006** Material behaviour of polymers under impact loading *International Journal of Impact Engineering* **32** 725.

**Bowden/Field 1964**, The brittle fracture of solids by liquid impact, by solid impact and by shock *Proc. R Soc. Lond. A* **282** 331–52

**Bower 2002**, An Introduction to Polymer Physics ISBN:9780521637213

**Boyce/Arruda 1990**, An Experimental and Analytical Investigation of the Large Strain Compressive and Tensile Response of Glassy Polymers *Journal of Polymer Engineering and Science* **30** 1288-1298

**Briscoe/Hutchings 1976** *IM. Polymer* 17 1099–102

**Briscoe/Nosker 1984**, The influence of interfacial friction on the deformation of high density polyethylene in a split Hopkinson pressure bar *Wear* **95** 241-262

**Brown/Rae/ Orler 2006**, *Polymer* **47** (21) 7506-7518

**Chang/Bestul 1974**, *J. Chem. Thermodyn.* 6 325

**Chen/Lu/Cheng 2002**, *Polymer Testing* **21**(2) 113-121

**Davies 1948**, A critical study of the Hopkinson Pressure Bar *Philos. Trans. R. Soc. (London) A* **240** 375-457.

**Davies/Hunter 1963**, The Dynamic Compression Testing of Solids by the Method

of Split Hopkinson Pressure Bar (SHPB) *J. Mech. Phys. Solids* **11** 155–179

**Dawson/Swallowe/Xinwu 1991** Temperature rises during high rate deformation of polymers *Journal de Physique IV* C3-701

**Dioh et al 1994**, (**Dioh N N, Ivankovic A, Leevers P S and Williams J G**) Stress wave propagation effects in split Hopkinson pressure bar tests *Proc. R. Soc. Lond. A* **449** 187-204

**Ellwood/Griffiths/Parry 1982**, Material testing at high constant strain rates *Journal of Physics E: Scientific Instruments* **15(11)** 1169-72

**Engels et al 2010**, *J Mater Sci Mater Med* **21**(1) 89–97

**Escaig 1982**, In: Plastic Deformation of Amorphous and Semi-Crystalline Materials B. J. Escaig B J and G'sell C eds. Les Editions de Physique 187-225

**Eyring 1935**, The Activated Complex in Chemical Reactions *Journal of Chemical Physics* **3** 107

**Eyring 1936**, Viscosity, Plasticity, and Diffusion as Examples of Absolute Reaction Rates *Journal of Chemical Physics* **4** 283

**Eyring et al 1945**, Mechanical Properties of Textiles *Textile Research Journal* **15** 295

**Eyring/Lin/Lin 1980**, Basic Chemical Kinetics *John Wiley and Sons*

**Feck/Stronge/Liu 1990**, Proceedings of the Royal Society of London A **429(**1877) 459-479

**Feynman 1998**, Statistical Mechanics: A Set of Lectures Advanced Books Classics

**Field/Proud/Walley/Goldrein 2001,** Review of experimental techniques for high rate deformation and shock studies *In:* **Nowacki W K and Klepaczko *J R*** ed. *New Experimental Methods in Material Dynamics and Impact* Institute of Fundamental Technological Research, Polish Academy of Sciences, Warsaw 109-178

**Field/Proud/Walley/Goldrein/Siviour 2004,** Review of experimental techniques for high rate deformation and shock studies *International Journal of Impact Engineering* **30** 725-775

**Follansbee/Kocks 1988**, *Acta metal* 36 (I) 81-93

**Forrester/Swallowe 2009**, Flow stress peaks at high strain rates in PMMA *DYMAT 2009* **2** 9th International Conference on the Mechanical and Physical Behaviour of Materials under Dynamic Loading 1443–1447

**Gama/Lopatnikov/Gillespie Jr. 2004,** Hopkinson bar experimental technique: A critical review *Appl. Mech. Rev.* **57(4)** 223-249

**Gorham 1989**, Specimen inertia in high strain-rate compression *J. Phys. D: Appl. Phys.* **22** 1888-1893

**Gourdin/Lassila 1996**, Proceedings of the TMS Annual Meeting, Anaheim, CA 59

**Gray III 2000**, Classic Split-Hopkinson Pressure Bar Testing In: *ASM Handbook* ASM International **8** 462-476

**Griffiths/Martin 1974**, A study of the dynamic behaviour of a carbon-fibre composite using the split Hopkinson pressure bar *J. Phys. D: Appl. Phys.* **7** 2329-41

**Hamdan/Swallowe 1996** Crystallinity in PEEK and PEK after mechanical testing and its dependence on strain rate and temperature *Journal of Polymer Science B: Polymer Physics* **34** 699-705

**Hochstetter et al 2003**, *Tribology International* **36** 973–985

**Hoffman 1952**, *J. Am. Chem. Soc.* **74** 1696

**Hohne 2002**, *Polymer* **43** 4689–4698

**Hopkinson J 1872a**, *Proc Proc. Manchest. Liter.* Philos. Soc. **11** 40-45

**Hopkinson J 1872b**, *Proc. Manchest. Liter*. Philos. Soc. **11** 119-121

**Hopkinson B 1905**, *Phil. Trans. R. Soc. Lond* A**213** 437-456

**Hopkinson B 1914**, *Phil. Trans. R. Soc. Lond* A213 (1914) 437-456.

**Houlsby/Puzrin 2006**, Principles of Hyperelasticity *Springer*

**Jordan et al 2007** Compressive properties of extruded polytetrafluoroethylene *Polymer* **48** 4184

**Khanna/Kumar 1991**, *Polymer* **32** (11) 2010-13

**Kolsky/Shi 1958**, Fractures produced by stress pulses in glass-like solids *Proc Phys Soc Lond* **72** 447–53

**Kolsky 1959** Fractures produced by stress waves In: **Averbach B L, Felbeck D K, Hahn G T, Thomas D A,** ed. *Fracture*. Wiley 281–96

**Kolsky 1963** *Stress Waves in Solids* (Dover, New York)

**Kandasamy/Brar 1994**, Flow stress and material model study at high strain rate and low temperature *In*: **S.C. Schmidt, J.W. Shaner, G.A. Samara and M. Ross** ed. *High Pressure Science and Technology* New York, American Institute of Physics 1031-1034

**Lindholm 1964**, Some Experiments with the Split-Hopkinson Pressure Bar *Journal of the Mechanics and Physics of Solid* **12** 317

**Lu/Li 2010**, Dynamic behaviour of polymers at high strain-rates based on split Hopkinson pressure bar tests, *International Journal of Impact Engineering*

**Massey 1921**, The Flow of Metal During Forging *Proc. Manchester Assoc* Engineers 21-26

**McCrum/Buckley/Bucknall 2003**, *Principles of Polymer Engineering* Oxford Science Publications ISBN 0-19-856526-7

**Mencik 1973**, *J. Polym. Sci.* Polym. Phys. Ed. **11** 1585

**Mulliken/Boyce 2006a**, Mechanics of the rate-dependent elastic-plastic deformation of glassy polymers from low to high strain rates. *International Journal of Solids and Structures* 43 **5** 1331–1356

**Mulliken/Boyce 2006b**. Mechanics of high-rate deformation of amorphous polymers *13th International Conference on Deformation, Yield, and Fracture of Polymers* Rolduc Abbey, Kerkrade Netherlands 10–13

**Murthy/Grubb 2002**, *J. Polym. Sci*. Polym. Phys **40** 691-705

**Parry/Stewardson/Ahmad 1988,** Measurements of high strain rate properties of materials using an exploding wire technique *Journal de Physique* C3-689

**Parry/Dixon/Hodson/Al-Maliky 1994,** Stress equilibrium effects within Hopkinson bar specimens *Journal de Physique* IV **4** C8-107

**Parry/Griffiths 1979** A compact gas gun for materials testing *Journal of Physics E: Scientific Instruments* **12 (1)** 56-58

**Parry/Walker/Dixon 1995**, Hopkinson bar pulse Smoothing *Measurement Science & Technology* **6(5)** 443-6

**Parry 1997**, *J. PHYS IV FRANCE* 7, colloque C3, Supplement au *Journal de Physique 111*

**Pruden 2012**, , PhD thesis, Loughborough University

**Pollak/Talkner 2005**, *Reaction rate theory: What it was, where it is today, and where it is going?* , Chaos, **15** 026116

**Privalko 1998**, *J. Mater. Ed*. **20** 57

**Rae/Dattelbaum 2004**, *Polymer* **45** 7615–7625

**Ramesh 2008**, High strain rate and impact experiments, *Springer Handbook of Experimental Solid Mechanics* 929-960

**Rand 1967**, *An analysis of the split Hopkinson pressure bar* PhD thesis University of Maryland

**Recht 1963**, Catastrophic Thermoplastic Shear *J. Appi. Mech* 63-WA-67, November 1-5

**Rittel 2000a,** An inve,stigation of the heat generated during cyclic loading of two glassy polymers. Part I: Experimental *Mechanics of Materials* **32** 131-147

**Rittel 2000b,** An investigation of the heat generated during cyclic loading of two glassy polymers. Part II: Thermal analysis *Mechanics of Materials* **32** 149-159

**Rittel/Wang/Merzer 2006**, Adiabatic shear failure and dynamic stored energy of cold work. *Phys Rev Lett* **96** 075502

**Samanta 1971**, Dynamic Deformation of Aluminum and Copper at Elevated Temperatures *Journal of the Mechanics and Physics of Solids* **19** 117-124.

**Siviour/Walley/Proud/Field 2005,** The high strain rate compressive behaviour of polycarbonate and polyvinylidene difluoride *Polymer* **46** 12546-555

**Siviour 2009** A measurement of wave propagation in the split Hopkinson pressure bar *Meas. Sci. Technol.* **20** 065702

**Sizek/Gray III 1993**, Deformation of polycrystalline $Ni_3Al$ at high strain rates and elevated temperatures *Acta. Metall. Mater* **41** 1855-60**Song/Chen 2005**, Latin American Journal of Solids and Structures 2 (2005)

**Song/Chen 2005,** Split Hopkinson pressure bar techniques for characterizing soft materials *Latin American Journal of Solids and Structures* **2** 113-152

**Swallowe/Field 1982**, The ignition of a thin layer of explosive by impact; the effect of polymer particles *Proc. R. Soc. Lond. A* **379** 389–408

**Swallowe/Field/Hutchinson 1986**, Impact experiments on thin layers of polymers and intermediate explosives In: Y.M. Gupta Ed. *Shock Waves in Condensed Matter* New York SpringerUS 891–898

**Swallowe et al 1997(Swallowe G M, Fernandez J O and Hamdan S)**, Crystallinity increases in semi crystalline polymers during high rate testing *J. Phys. IV France* **7** 453

**Swallowe (editor) 1999**, *Mechanical Properties and Testing of Polymers: an A-Z Reference* Volume 3 of polymer science and technology series Springer

**Swallowe/Lee 2003** A study of the mechanical properties of PMMA and PS at strain rates of $10^{-4}$ to $10^{3}$ over the temperature range 293-363 K *J. Phys IV France* **110** 33

**Trautmann et al 2005(Trautmann A, Siviour C R, Walley S M and Field J E)**, Lubrication of polycarbonate at cryogenic temperatures in the split Hopkinson **pressure bar** ***International Journal of Impact Engineering*** **31 523–544**

**van Melick et al 2003**, *Polymer* **44** 2493–2502

**Walley/Field/Swallowe/Mentha 1985,** The response of various polymers to uniaxial compressive loading at very high rate of strain *Journal de Physique* **C5**-607

**Walley/Field 1987**, The erosion and deformation of polyethylene by solid-particle impact. *Phil. Trans R Soc. Lond. A* **321** 277–303

**Walley/Field/Pope/Safford 1989,** A study of the rapid deformation behaviour of a range of polymers *Phil. Trans. R. Soc. Lond. A* **328** 1-33

**Walley/Field/Pope/Safford 1991**, The rapid deformation of various polymers *J. Phys. III France* **1** 1889-1925

**Walley/Field 1994**, Dymat Strain rate sensitivity of polymers in compression from low to high rates *Dymat Journal* **1**(3) 211-227

**Walley/Xing/Field 1995**, Mechanical properties of three transparent polymers in compression at a very high rate of strain In: Williams JG, Pavan A, ed. *Impact and dynamic fracture of polymers and composites* 289–303

**Walley 2000a** Hokinson bar testing at non-ambient temperatures *Proc. 6th Int. Conf. on Mechanical and physical behaviour of materials under dynamic loading: DYMAT Krako´w, Poland, September* pp.67–94 Institute of Fundamental Technological Research

**Walley/Proud/Rea/Field 2000b** Comparison of two methods of measuring the rapid temperature rises in split Hopkinson bar specimens *Review of Scientific Instruments* **71**(4) 1766-71

**Walley/Balzer/Proud/Field 2000c,** Response of thermites to dynamic high pressure and shear *Proc. R. Soc. Lond. A* **456** 1483-1503

**Ward/Sweeney 2004**, *An Introduction to the Mechanical Properties of Solid Polymers* Wiley 2nd Edition ISBN: 9780471496267

**Wilkes 2005 (Wilkes C E, Summers J W, Daniels C A and Berard M T***PVC Handbook* Hanser Verlag ISBN: 1569903794

**Williams et al 1955**, The temperature dependence of mechanical and electrical relaxations in polymers *J. Amer. Chem. Soc*. **59** 95

**Yang/Shim 2005** An analysis of stress uniformity in split Hopkinson bar test specimens *International Journal of Impact Engineering* **31** (2) 129-150

**Zerilli 2004**, Dislocation Mechanics-Based Constitutive Equations *Metallurgical and Material Transactions A* **35**A 2547

**Zerilli/Armstrong 2007**, A constitutive equation for the dynamic deformation behaviour of polymers *Journal of Material Science* **42** 4562-74